Mechanobiology of Cardiac Disease and Fibrosis: a Novel Role for Cadherin-11

By

Alison Koelle Schroer

Dissertation
Submitted to the Faculty of the
Graduate School of Vanderbilt University
in partial fulfillment of the requirements
for the degree of

DOCTOR OF PHILOSOPHY
in

Biomedical Engineering
December, 2016
Nashville, Tennessee

Approved:

W. David Merryman, Ph.D.

John Wikswo, Ph.D.

Michael Miga, Ph.D.

Jeffrey Davidson, Ph.D.

Antonis Hatzopoulos, Ph.D.

Copyright © 2016 by Alison K Schroer
All Rights Reserved

ACKNOWLEDGEMENTS

The heart has its reasons, of which reason knows nothing - Pascal

I must acknowledge my coauthors on the manuscripts which have been adapted and included in this dissertation. First and foremost, my advisor Dave Merryman. Also Larisa Rhyzhova, Cyndi Clark, Hind Lal, Qinkun Zhang, Tom Force, John Wikswo, Veniamin Sidorov, Matthew Shotwell, Annabelle Manalo, and David Bader. I would also acknowledge Josh Bender and Claire Lafferty, undergraduate research assistants who assisted in the collection of some of the data included in this work. I would also like to acknowledge Meghan Bowler, Mark Vander Roest, Caleb Snider, Allison Price, and Jeffrey Davidson for their editorial comments on the work included in this dissertation.

I would like to acknowledge my funding sources, especially the NSF and the AHA. Also, the ever wonderful Merryman Lab, members both past and present, who have been my comrades and friends throughout the last five years. Finally, I must acknowledge my family, my friends, and my God, without whom I never could have done all this.

Keep your heart with all vigilance, for from it flow the springs of life.

- Proverbs 4:23

TABLE OF CONTENTS

Page

ACKNOWLEDGEMENTS iii

LIST OF TABLES vi

LIST OF FIGURES vii

CHAPTER

1. Introduction and Motivation 1

2. Background: Myocardial Development and Disease 8

Mechanobiology of cardiac development 8
Cellular players in fibrotic cardiac disease, parallels with valve disease 10
Etiology of cardiac fibrotic disease 15

3. Background: Fibroblast Mechanobiology 21

Myofibroblast differentiation in response to mechanical stress 21
Integrins sense mechanical signals from the ECM 28
Cadherins sense intercellular forces 33

4. Aim 1: Elucidating Mechanosensitive Signaling Crosstalk in Fibroblasts 39

Introduction 39
Methods 45
Results 47
Discussion 56

5. Aim 2: Cadherin-11 Exacerbates Tissue Remodeling after Myocardial Infarction 62

Introduction 62
Methods 63
Results 71
Discussion 93

6. Aim 3: Quantifying Cardiomyocyte Mechanics 105

Introduction to cardiomyocytes and motivation for study 105
CENP-F mutation alters cardiac cell structure and mechanics 106
Introduction to engineered cardiac tissue constructs 113
Methods of I-wire development and analysis 116
Results of I-wire analysis 123
Disscussion 131

7. Impact and Future Directions 137

Summary and impact of results 137
Future directions 144

APPENDIX

A. Model of Myofibroblast Differentiation 148

B. Model Derivation for I-wire 166

REFERENCES 180

LIST OF TABLES

Table Page

1.1 Vocabulary and Abbreviations 7

3.1 Summary of integrin isoform expression in normal function and disease 27

3.2 Summary of cadherin isoform expression in normal function and disease 27

5.1 qPCR primers 70

6.1 Model variables 120

6.2 Passive mechanic metrics for control and isoproterenol-treated ECTCs 124

LIST OF FIGURES

Figure Page

1.1 Graphical overview of dissertation topic and aims 5

2.1 Interplay between ECM stiffness and fibroblast phenotypes 10

2.2 Relevance of adhesion mechanobiology to fibrotic heart disease 14

2.3 Schematic of the stages in healing after myocardial infarction 19

3.1 Mechano-sensitive mechanisms of myofibroblast differentiation 23

3.2 Crosstalk between growth factor and adhesion protein signaling 32

4.1 Src and p38 are necessary for TGF-β1 induced myofibroblast differentiation 42

4.2 Relevant signaling network 43

4.3 α-SMA is oppositely regulated by TGF-β1 and FGF2 through focal adhesion proteins and p38 and ERK dependent mechanisms 49

4.4 Different dynamic activation profiles for activation of ERK and p38 51

4.5 α-SMA and cadherin-11 are not necessarily coexpressed 53

4.6 α-SMA and cadherin-11 are sensitive to stiffness and the presence of FAK 55

4.7 Expression of myofibroblast markers after treatment with TGF-β1 and FGF2 with GSK-3β inhibition 56

5.1 Cadherin-11 is expressed after myocardial infarction 73

5.2 Cadherin-11 null hearts respond differently after MI 75

5.3 Cadherin-11 blocking antibody treatment improves outcomes after MI 77

5.4 SYN0012 reduces infarct remodeling and myofibroblast differentiation. 79

5.5 SYN0012 effect on CF contractility 80

5.6 Reduction of IL-6 observed 3 days post-MI *in vivo* with SYN0012 treatment 82

5.7 Reduction of F4/80 observed 3 days post-MI *in vivo* with SYN0012 treatment 82

5.8 Transcriptional changes of inflammatory proteins after MI 84

5.9 Transcriptional changes of pro-fibrotic proteins after MI..... 85

5.10 Transcriptional changes of pro-angiogenic proteins after MI 87

5.11 Co-culture of macrophages and fibroblasts increase expression of IL-6 and MMP13 89

5.12 Co-culture effects on other aspects of inflammatory/remodeling cascade 90

5.13 Transcriptional changes of markers of macrophage polarization 92

5.14 Proposed cellular mechanisms of cadherin-11 in macrophages and fibroblasts . 101

5.15 Summary of results 103

6.1 Quantification of sarcomere length..... 108

6.2 Quantification of adherens junction β-catenin 109

6.3 Quantification of cardiac cell stiffness 111

6.4 Quantification of cardiac fibroblast stiffness 112

6.5 Platform description and model schematic..... 118

6.6 Passive and developed forces in constructs are affected by pharmacological perturbations 125

6.7 Predicted active force in ECTCs..... 127

6.8 Simulation of active contraction using construct action potential..... 129

6.9 Shortening construct to predict length-related effects 131

7.1 Graphical summary of dissertation topic and aims..... 143

CHAPTER 1

INTRODUCTION AND MOTIVATION

Cardiac disease is implicated in one in four deaths in the United States and is the leading cause of death world-wide. Myocardial infarction (MI) alone afflicts close to 1.5 million Americans annually [1]. Regardless of specific cause, cardiac disease manifests as significant loss of heart function following maladaptive tissue remodeling that alters the mechanical properties and function of the heart. Many forms of cardiac disease are characterized by fibrosis, a broad disease classifier marked by extracellular matrix (ECM) accumulation, tissue stiffening, and loss of function. Tissue remodeling, including fibrosis, is a cell-mediated process that dynamically changes the mechanical properties of the heart and has important implications to the progression of disease and patient outcomes.

Many proposed pharmacological solutions have not translated well from experimental settings to clinical practice, failing to achieve the successful outcomes predicted from experimental tests [2]–[4]. Most of these treatments target chemical signaling pathways to regulate cell behavior. ACE inhibitors, β-blockers, and statins have shown some success alleviating the symptoms and slowing the progression of heart failure, but they can do little to restore functional heart tissue [5]. Recent experiments with stem cells have shown promising results, but they are limited by an incomplete understanding of the dynamic chemical and mechanical environment of a healing infarct and its effect on cellular interactions and differentiation during myocardial

remodeling [6–9]. Traditional biological studies often fail to consider the role of mechanical cues on cellular phenotype and function. To develop better therapies, we need to develop a better understanding of how the various cells in the heart respond to and alter their mechanical environment of the heart during normal function and disease.

The heart is a complex organ comprised of several specialized cell types that work in concert during normal development and function, but also differentiate and interact in distinct ways during the progression of cardiac disease [10]. Cardiomyocytes (CMs) are the cellular effectors of contraction, generating the large forces which drive the essential pumping function of the heart. Specialized intracellular structures within the CMs and linkages between the CMs and a well-maintained cardiac ECM are required for these forces to propagate appropriately [11], [12]. The cells responsible for the maintenance of the ECM are cardiac fibroblasts (CFs), the next most prevalent cell type in healthy adult hearts [13]. During both development and fibrotic remodeling, these cells are activated to the myofibroblast (MyoFB) phenotype, characterized by increased ECM production and restructuring. Endothelial cells (ECs) line the vascular network oxygenating cardiac tissue, and can be an additional source of MyoFBs during disease [14]. Finally, inflammatory cells, including macrophages (MΦs), are often recruited and activated to affect tissue breakdown and initiate fibrotic remodeling during disease [15], [16]. The cellular populations and phenotypes present in the heart change dramatically during the transition from healthy to diseased tissue, especially after an acute event such as a MI. These cells interact with one another and drastically alter the chemical and mechanical microenvironment, all of which is constantly contracting and

relaxing. Understanding cellular phenotypes in this dynamic mechanical and cellular environment is crucial for developing better therapies for heart disease.

There is a growing appreciation in the field for the importance of mechanical context when studying cardiac cell behavior. All of these cell types are sensitive to changes in their mechanical environment, and their ability to sense and respond to mechanical forces determines both normal development and the progression of disease [11], [15], [17]–[19]. Mechanobiology is the study of the cellular response to altered mechanical inputs, which are often sensed through cellular adhesion to both the surrounding ECM and neighboring cells. Two key families of proteins which mediate cellular adhesions and transduction of mechanical signals are integrins and cadherins [20]. Integrins form adhesions with the ECM and trigger intracellular signaling cascades and cellular responses to changes in substrate stiffness and ECM composition. These adhesions also allow for transmission of intracellular force generated by the cellular cytoskeleton to the ECM [21], [22]. Cadherins mechanically link neighboring cells and can transmit intracellular forces between cells. They have also more recently been revealed to play a role in transduction of mechanical cues into intracellular signals. Cadherin-11 is a specialized cadherin expressed by MyoFBs, along with other cell types, that has been shown to contribute to the progression of fibrotic disease in several tissues, including the lungs and cardiac valves, but has never been studied in the context of myocardial remodeling [23]–[25].

Between the diversity of cellular populations and biological processes, as well the dynamic mechanical context, myocardial remodeling has a high degree of complexity. Biomedical engineering as a discipline is particularly well suited to tackle the question of

how mechanics affects cellular response during myocardial fibrosis. Engineering approaches including multiscale system analysis and quantitative assessment of mechanical forces and properties can be used to clarify specific cellular mechanisms within this complex problem. Traditional 2-D cell culture on tissue culture plastic or glass allows for rapid and reproducible study of intracellular signaling, but it is relatively poorly suited for studying the effect of mechanical environment and structure on cell function. In the highly dynamic mechanical environment of the heart, this limitation is particularly significant. Animal models, primarily mice, have long been used to study the organ level changes in function and signaling with a functional combination of these varied cell types; however, it can be difficult to tease out the effect of specific cell types and mechanisms in a whole organ context. Novel *in vitro* constructs have been developed by biomedical engineers which can be effectively used to bridge the gap between 2D cell culture and *in vivo* studies. Various 3-D scaffolds and biomimetic devices allow for study of cardiac cell growth, differentiation, and dysfunction in a more physiologically and mechanically relevant controlled systems [26]. Biomedical engineers are well situated to engage with this complexity and draw out biological insights. My position in the Merryman Mechanobiology Laboratory has allowed me to draw on a vast body of work in the study of fibroblast mechanobiology in the heart valve and translate it to studying mechanobiology in the myocardium.

My doctoral work has aimed to gain a more complete understanding of the interactions between cardiac cells and their environment in the remodeling myocardium (**Figure 1.1**). The complex question of the role of mechanics and mechanosensing in fibrotic myocardial remodeling was addressed through three specific aims to gain a

better understanding of particular cellular contexts. The first portion of this work focuses on CFs and a subset of the intracellular signaling downstream of growth factors and integrins which regulates the transition from the quiescent to active MyoFB phenotype. Next I expanded my focus to the general population of non-CM cells and their interactions in the process of healing after MI. The second section focuses on cadherin-11, a protein that sits at the intersection of mechanosensing, transmission of intercellular forces, MyoFB differentiation, and fibrotic cardiac remodeling. Finally, I address CMs, the primary source of heart contraction, and describe a set of tools and analyses that allow for improved characterization of cellular structure, function, and interactions in both healthy and diseased hearts.

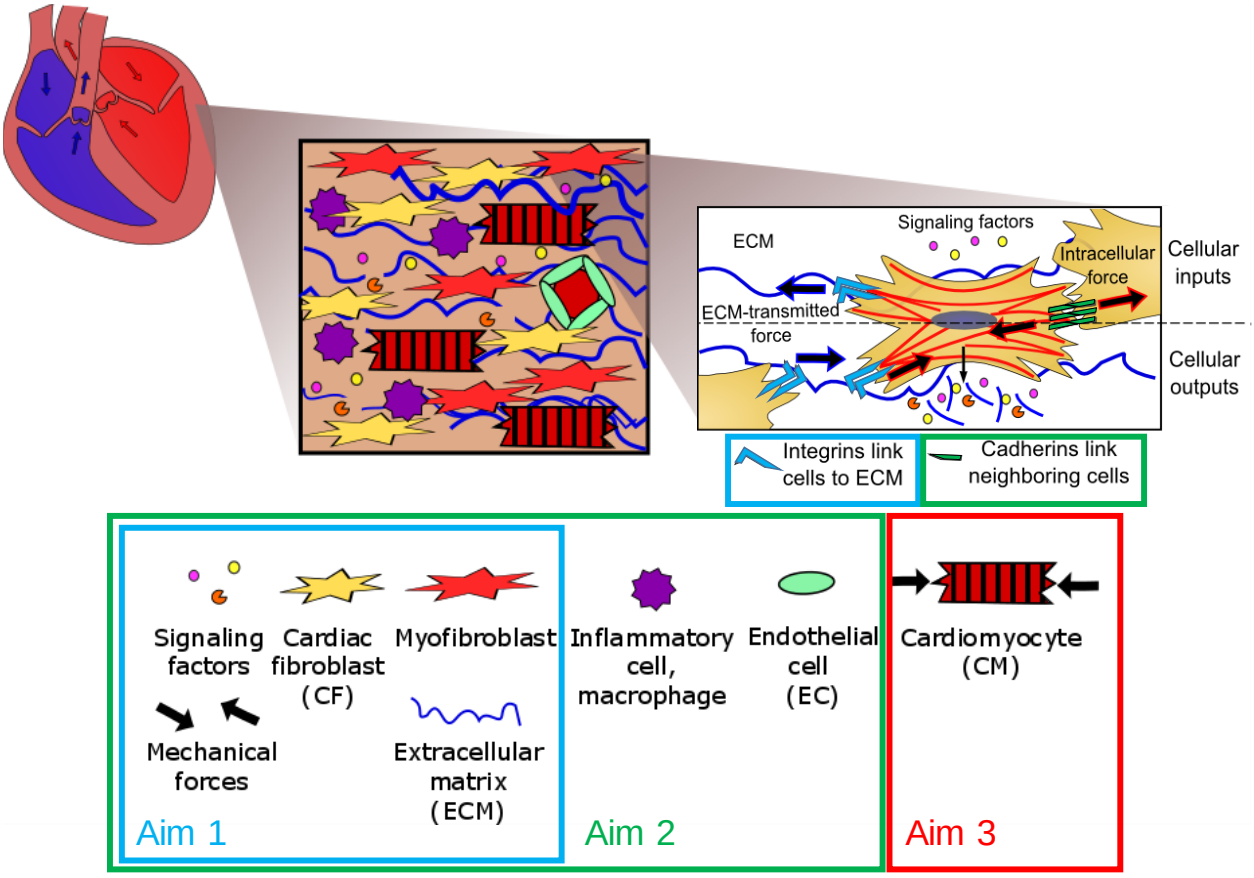

Figure 1.1 Graphical overview of dissertation topic and aims

The work will address three specific aims:

1. Elucidate the crosstalk between growth factor signaling and integrin sensing of substrate stiffness in the regulation of fibroblast phenotype
2. Determine the role of cadherin-11 in remodeling after myocardial infarction
3. Develop tools to quantify CM mechanics in normal function and disease

To begin, a detailed background on cardiac development, disease, and fibroblast mechanobiology is provided. Each specific aim is then considered separately with each section offering a focused introduction and set of research methods that were used to complete the study. A combination of computational, biological, and engineered tools were used to investigate cardiac mechanobiology with a deeper appreciation for the role of mechanics and mechanosensing in multiple cellular contexts. Finally, a discussion of the complete dissertation is presented to highlight the potential impact of the results. This dissertation summarizes my findings on the role of mechanotransduction through integrins and cadherins, particularly cadherin-11, to regulate mechanically-induced differentiation and fibrosis in the context of cardiac disease.

Table 1.1. Vocabulary and Abbreviations

Category	Term or Abbreviation	Definition
General terms	LV	Left ventricle
	MI	Myocardial infarction
	AV	Aortic valve
	BZ	Border zone
	IN	Infarct region
	ECM	Extracellular matrix
	EMT/EndMT	Epithelial/endothelial to mesenchymal transition
Cells	MEF	Mouse embryonic fibroblast
	CF	Cardiac fibroblast
	MyoFB	Myofibroblast – activated fibroblast involved in tissue remodeling
	CM	Cardiomyocyte – heart muscle cells
	EC	Endothelial cell – lining of vascular system
	MΦ	Macrophage – inflammatory cells
	AVIC	Aortic valve interstitial cell – involved in valve ECM maintenance
Marker of fibroblast phenotype	α-SMA	α smooth muscle actin – contractile cytoskeletal protein
	cadherin-11	Cadherin-11 – strong cell-cell adhesion molecule
	Col-1	Collagen-1 – most common ECM component of fibrotic tissue
Markers of MΦ phenotye	F4/80	MΦ marker
	CD14	Cell surface marker protein – indicates M1, inflammatory phenotype
	Mnr1	Mannose receptor 1 – indicates M2, reparative phenotype
	Arg1	Arginase 1 – indicates M2, reparative phenotype
Secreted growth factor or inflammatory agent	TGF-β1	Transforming growth factor β1 – promotes MyoFB differentiation
	FGF	Fibroblast growth factor – reverses MyoFB differentiation
	VEGF	Vascular endothelial growth factor – promotes angiogenesis
	IL-1	Interleukin-1 – proinflammatory cytokine
	IL-6	Interleukin-6 – proinflammatory cytokine
	MMP13	Matrix metalloproteinase 13 – breaks down collagen-1
	MMP3	Matrix metalloproteinase 3 – breaks down ECM and activates MMP1
Cellular signaling proteins and terms	FA	Focal adhesions – link integrins to cytoskeleton
	AJ	Adheren junction – link cadherins to cytoskeleton
	FAK	Focal adhesion kinase
	Src	Tyrosine kinase found at FAs
	MAPK	Mitogen activated protein kinase
	p38	MAPK downstream of TGF-β1
	ERK	Extracellular regulated kinase – MAPK involved in many pathways
	β-catenin	Component of AJ and involved in Wnt signaling
	GSK-3β	Glycogen synthase kinase 3β – involved in Wnt signaling
Assays and techniques	ELISA	Enzyme-linked immunosorbent assay
	Western blot	Assay for quantifying protein expression
	RT qPCR	Reverse Transcription quantitative polymerase chain reaction
	IHC	Immuno-histochemistry
	AFM	Atomic force microscopy
	Gel assay	Free floating collagen gels with embedded cells to measure contractility
	ECTC	Engineered cardiac tissue construct
	I-wire	ECTC developed at VIIBRE

CHAPTER 2

BACKGROUND: MYOCARDIAL DEVELOPMENT AND DISEASE

Text for Chapter 2 adapted in part from:

[7] Schroer, A.K. and W.D. Merryman, *Mechanobiology of myofibroblast adhesion in fibrotic cardiac disease.* J Cell Sci, 2015. **128**: p. 1865-1875.

Mechanobiology of myocardial development

A human heart will beat around two and a half billion times in the average lifetime. Given the high mechanical demands on the heart, it is perhaps not surprising that it is so prone to failure. To power the circulatory system and perfuse blood throughout the body, the heart uses concerted contraction of thick muscular walls called the myocardium that require constant perfusion of oxygenated blood. These walls form the four main chambers of the heart and are separated from each other and the outflowing vasculature by thin flexible valves. The structures of both the valves and the myocardium are formed early in development and rely on precise timing of cytokine signaling and mechanotransduction to induce proper cell alignment and vascularization [13], [27]. Development of the heart begins as a muscular tube lined internally with endocardial cells. Heart valves are formed by the differentiation of endocardial cells through endothelial-to-mesenchymal transformation (EndMT) into mesenchymal cells, which can migrate into a mixture of ECM known as the cardiac jelly. This cellular transformation requires the active contraction of the developing myocardium to fully

occur [28]–[30]. These transformed endocardial cells become the valve interstitial cells (VICs) in adult valves and are necessary for developing the initial structure of the valve and maintaining that structure through adulthood. A similar mechanism accounts for the origin of CFs in the myocardium. CFs are derived primarily from the proepicardial organ, a cluster of epithelial-like cells that migrate to cover the developing heart and form the mature epicardium. A significant portion of these cells undergo epithelial to mesenchymal transition (EMT) in response to TGF-β1 signaling to gain a more migratory, fibroblast-like phenotype and invade into the myocardium [31], [32]. These cells are believed to be the origin of vascular smooth muscle cells, vascular ECs, and resident CFs. During development, CFs differentiate into active MyoFBs - producing fibrillar collagen and organizing a 3-D network for myocardium development and maturation. These MyoFBs express contractile α-smooth muscle actin (α-SMA), can apply forces to both the developing myocytes and collagen framework, and are responsible for the laminar structure and fibrous alignment of the myocardium. Tissue remodeling by MyoFBs during development causes a significant increase in myocardial stiffness, in preparation for the mechanical demands of active circulation (**Figure 2.1**). From mid-development to birth, the stiffness of mouse ventricle increases from 12 to 39 kPa, according to atomic force microscopy (AFM) measurements [33]. At the end of development, CFs surround and run parallel to myocytes throughout the myocardium, and are generally maintained in a quiescent state (**Figure 2.1**), producing ECM proteins and matrix metalloproteinases (MMPs) in a tightly regulated balance to maintain a stable mechanical environment [34], [35]. However, in the case of cardiac disease,

physiological stress can trigger the reactivation of fibroblasts into MyoFBs and begin the chronic process of tissue remodeling.

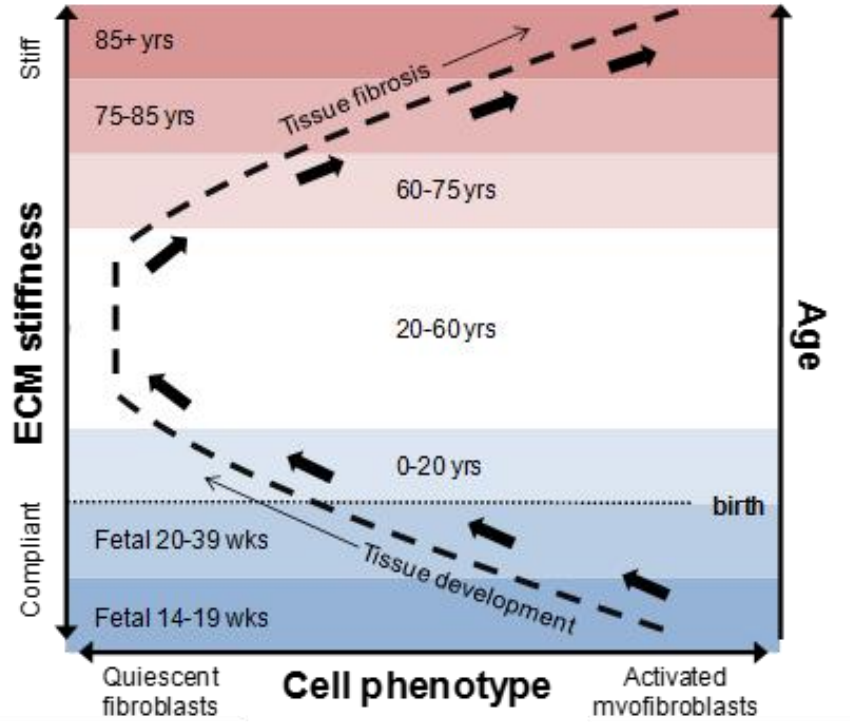

Figure 2.1 Interplay between ECM stiffness and fibroblast phenotypes. (Figure adapted from Merryman et. al [36])

Cellular players in fibrotic cardiac disease, parallels with valve disease

While they have significant differences in composition and function, there are some important mechanistic similarities between the myocardium and the heart valves. Both are highly mechanically active tissues susceptible to fibrotic remodeling and progressive disease. With the Merryman Laboratory's extensive expertise in studying valve disease, I was able to translate recent advances in the field of valve mechanobiology to the study of myocardial fibrosis. Proper function of cardiac

structures is dependent on their active and passive mechanical properties, and alteration of these properties is a hallmark of fibrotic cardiac disease. In both tissues, inflammation and fibrosis drive extensive tissue remodeling that significantly impairs cardiac function (**Figure 2.2A**). Inflammation triggers ECM degradation and the release of profibrotic factors, such as angiotensin II (AngII), transforming growth factor β1 (TGF-β1), and fibroblast growth factor (FGF2), that promote accumulation of ECM and fibrosis of the valves and myocardium [37], [38]. However, drugs targeting these pathways have had limited success, which has been attributed to their failure to address the concurrent mechanical signals that play a critical role in the initiation and progression of disease [4]. Increased local tissue strains and stresses increase the risk of developing fibrotic disease by altering the phenotype of cardiac cells, which contributes to maladaptive tissue remodeling [15], [39], [40]. Therefore, determining how various cardiac cells respond to a changing chemical and mechanical environment will aid our understanding of heart disease development and potentially uncover novel therapeutic targets (**Figure 2.2A**).

Inflammatory cells, including neutrophils and MΦs, are the first responders after acute injury and often act as chronic drivers of inflammation and remodeling during different types of cardiac disease. ECs are ubiquitous throughout the heart, forming the cellular coat of the valve, the heart chambers, and the dense vascular bed required for proper myocardial oxygenation. VICs and CFs are primarily responsible for maintaining the ECM, a key structural framework for the tissue. The primary cellular source of mechanical signals in the heart are the cardiomyocytes (CMs), which use complex intracellular structure and intercellular junctions to contract as a unit and effectively

pump blood. All of these cell types are present in both healthy and diseased tissues, and their interactions, both through chemical signaling and more direct mechanical linkages, are integral to the process of fibrotic tissue remodeling. These signals, both chemical and mechanical, can alter cell activation and phenotype, which are key components of the remodeling process.

Mechanically-induced signaling promotes MyoFB differentiation in VICs and CFs, resulting in cells that exhibit increased contractility and increased secretion of growth factors and ECM proteins (**Figure 2.2B**) [41]–[43]. MyoFBs are identified by their expression of α-smooth muscle actin (α-SMA), a specialized cytoskeletal protein that allows for enhanced generation of cellular force [44]. All adherent cells interact with the local ECM and sense tissue forces through transmembrane ECM receptors called integrins. Upon adhesion to the ECM, integrins recruit intracellular proteins to form a focal adhesion (FA), which links integrins to the actin cytoskeleton and initiates force-dependent signaling [45], [46]. In addition to force transduction from the ECM to the cells, integrins also regulate force transmission from intracellular stress fibers to the local microenvironment [47].

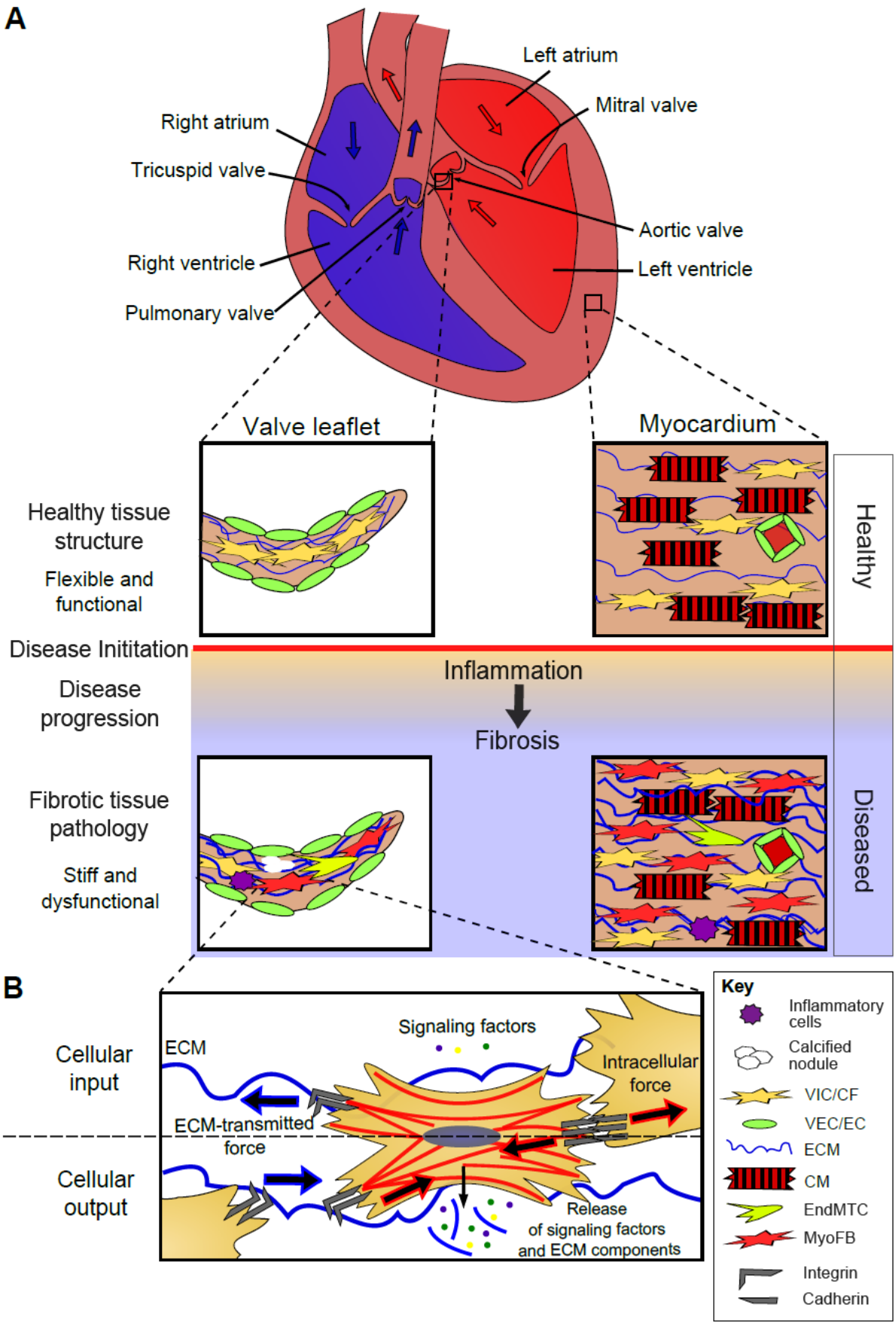
A
Left atrium
Mitral valve
Right atrium
Tricuspid valve
Aortic valve
Right ventricle
Left ventricle
Pulmonary valve
Valve leaflet
Myocardium
Healthy tissue structure
Flexible and functional
Healthy
Disease Inititation
Disease progression
Inflammation
Fibrosis
Fibrotic tissue pathology
Stiff and dysfunctional
Diseased
B
Cellular input
Cellular output
ECM
Signaling factors
Intracellular force
ECM-transmitted force
Release of signaling factors and ECM components
Key
Inflammatory cells
Calcified nodule
VIC/CF
VEC/EC
ECM
CM
EndMTC
MyoFB
Integrin
Cadherin

Figure 2.2: Relevance of adhesion mechanobiology to fibrotic heart disease. Fibrotic disease affects both heart valves and heart myocardium and is characterized by changes in the mechanical properties of the ECM and the cellular phenotypes present in the tissue. Healthy valves have primarily quiescent fibroblast-like cells called valvular interstitial cells (VICs) that are embedded in a stable, organized ECM and surrounded by a single layer of valvular endothelial cells (VECs). Similarly, healthy myocardium contains cardiomyocytes (CMs), cardiac fibroblasts (CFs), and endothelial cell-(EC) lined blood vessels embedded in stable ECM. Disease can be initiated by acute or chronic cardiac conditions. Inflammation initiates ECM breakdown and accumulation of inflammatory cells (ICs), fibroblast-like cells, and endothelial-to-mesenchymal-transformed cells (EndMTCs). Inflammation can transition into fibrosis, which is characterized by accumulation of stiff ECM and a large number of myofibroblasts (MyoFBs) that are derived from VICs, CFs, and EndMTCs. MyoFBs are particularly relevant to disease because they are able to initiate ECM remodeling and intercellular signaling pathways. The MyoFB phenotype is promoted by combined inputs of mechanical and chemical signals, which are transduced through integrins and cadherins, and signaling factor receptors, respectively. Increased expression of α-SMA in MyoFBs stabilizes and further activates integrins and cadherins; this increases intracellular force generation and actively remodels the ECM. MyoFBs also express ECM and growth factors, which not only affect themselves but also neighboring cells. (Figure adapted from Schroer et al [19])

Intercellular forces are also transmitted between neighboring cells through adherens junctions (AJs), which contain calcium-dependent adhesion proteins called cadherins. Classical cadherins form homotypic bonds to neighboring cells and mechanically link the cytoskeletal elements of both cells. Different cadherins are found in various cell types, and major shifts in cell phenotype are often accompanied by a corresponding shift in cadherin expression. For example, cadherin-2 is typically expressed in CMs and quiescent fibroblasts, whereas cadherin-11 is highly expressed in MyoFBs [44], [48]–[50]. Cadherin-11 forms significantly stronger bonds than cadherin-2 and is thus able to transmit increased levels of intercellular tension generated by α-SMA in MyoFBs [44], [51]. Recent studies have revealed novel signaling roles for cadherins in addition to their structural function [52], [53]. Signaling effectors downstream of cadherins, including β-catenin, undergo significant crosstalk with cytokine and integrin signaling in the regulation of MyoFB differentiation and function [54]–[56].

Etiology of fibrotic cardiac disease

Fibrotic disease affects both the valves and the myocardium and is characterized by significant changes in tissue composition and biochemical signaling, which in turn affect cell behavior and accelerate progression of disease (**Figure 2.1A**). Several cardiac conditions with large clinical impacts are perpetuated by active remodeling of the ECM by VICs in valves and by CFs in the myocardium.

Heart valve disease

Valve diseases affect over six million Americans and are associated with changes in mechanical properties of the leaflets that impair normal blood flow through the heart.[1] The etiologies of these conditions are often linked to altered mechanical loading (e.g. hypertension, ventricular remodeling, bicuspid aortic valve mutation), and in all cases tissue remodeling is perpetuated by sustained inflammatory and fibrotic responses, which trigger ECM degradation and accumulation, respectively [57], [58]. The mitral and aortic valves on the left side of the heart are most susceptible to disease, which manifests most often as regurgitant flow or stenosis [1]. Regurgitant mitral valve disease has the highest prevalence (1.7% of adults), but aortic valve disorders are associated with higher mortality, especially when calcification and stenosis of the valve is evident [1]. The mitral valve is particularly susceptible to tissue weakening in a process known as myxomatous remodeling, whereas the aortic valve is susceptible to tissue stiffening in response to fibrosis and sclerotic remodeling [59], [60]. Myxomatous remodeling is characterized by increased expression of TGF-β1, matrix

metalloproteinases (MMPs), and a variety of ECM components and results in valve billowing and regurgitant blood flow [59], [61], [62]. Calcific aortic valve disease (CAVD), a stenotic disease often necessitating valve replacement, is characterized by increased TGF-β1 and collagen expression and the development of calcified nodules, resulting in a stiff, partially occluded, stenotic valve [63], [64]. These pathologic alterations to the mechanical properties of the tissue are primarily mediated by VICs, a heterogeneous population of fibroblast-like cells that differentiate into active MyoFBs in response to fibrotic signaling factors and mechanical cues (**Figure 2.1**) [65].

Cardiac fibrosis

Cardiac fibrosis is a hallmark of heart failure, and results in an increased passive stiffness of the heart wall, diastolic dysfunction, and poor long-term prognosis [61–64]. Many chronic cardiovascular conditions, including valve disease and hypertension can cause pressure overload in the ventricles, which subsequently develop hypertrophy and fibrosis [61,65]. Another common initiator of cardiac fibrosis is scar formation after MI, which affects over one million Americans annually [1]. MI occurs when an occluded coronary artery causes ischemic cell death in a region of the myocardium. In both chronic conditions and MI, inflammatory cytokines induce tissue remodeling and degradation of ECM in the myocardium [71], [72]. The loss of ECM can result in a temporary decrease in the passive wall stiffness and increase in diastolic strains in the infarct region, which increase the chance of myocardial wall rupture [12], [73]. Deposition of *de novo* ECM is necessary to maintain structural integrity and requires the switch from inflammatory to profibrotic signaling factors [4]. In both chronic and acute myocardial remodeling, AngII inhibits the degradation of collagen-1 and promotes the

expression of FGF2 and TGF-β1, which in turn promote fibroblast growth and collagen production in the diseased myocardium [34], [70], [74], [75]. TGF-β1 inhibits inflammation and promotes the differentiation of fibroblasts into MyoFBs and the accumulation of dense ECM in the myocardial interstitium [76]. This increases stress on the remaining contractile myocardium, resulting in further adverse remodeling and fibrosis largely mediated by CFs that have differentiated into active MyoFBs (**Figure 2.1A**) [77].

Myocardial infarction

The same signaling modalities that contribute to the gradual progression of cardiac decline in cardiac fibrosis are drastically dysregulated after acute MI. MI causes an immediate and extensive myocardial injury, requiring a dramatic cellular response and significant tissue remodeling. Hypoxia in the environment triggers the release of more cytokines and increases fibroblast sensitivity to other available cytokines [78]. Repair of MI entails the formation of a large collagen scar, which significantly impairs cardiac function and often results in cardiac fibrosis, dilated cardiomyopathy, or secondary MI.

There are four partially overlapping phases to healing after MI that are regulated by an array of cytokines and cellular responses (**Figure 2.3**). The first phase is an inflammatory response characterized by expression of pro-inflammatory cytokines and recruitment of leukocytes within 24 hours after MI. The immune cells and resident fibroblasts produce proinflammatory cytokines like tumor necrosis factor α (TNFα) and interleukin 1 (IL-1) to recruit MΦs, which proceed to phagocytose cellular debris and release more cytokines and MMPs to clear the necrotic tissue and debris from the area.

These inflammatory cytokines also stimulate the release of MMPs by fibroblasts in the wound area. IL-1 and hypoxia are known to stimulate CF release of MMP1, which is responsible for degrading collagen-1 [34]. The wound size expands beyond its initial borders as MyoFBs and MΦs produce MMPs and other proteases to breakdown damaged ECM and allow for increased cell migration. At this point, there is an influx of fibroblasts from non-infarct areas of the myocardium and from differentiated bone-marrow derived cells and endothelial derived cells [79], [80]. The resulting increase in cellular density is known as the granulation phase (days three to seven post MI) and is characterized by high levels of cytokine signaling, specifically AngII, FGF2, TGF-β1, and vascular endothelial growth factor (VEGF) to promote matrix remodeling and angiogenesis [34], [81]–[83]. AngII suppresses expression of MMP1, and TGF-β1 suppresses inflammatory cytokines to end the controlled destruction of inflammation and allow for *de novo* accumulation of ECM in the infarct area. A combined treatment of angiotensin converting enzyme (ACE) inhibitors and AngII type 1 antagonist (ARB) was shown to reduce TGF-β1 and collagen expression and inflammatory cell infiltration in rat hearts, but without reduction in infarct size [84]. Finally, one to two weeks after initial infarct many of the invaded cells in the granulation tissue undergo apoptosis and only a small population of MyoFBs and blood vessels persist in a collagen-rich initial scar. Over the following weeks, MyoFBs produce more collagen and contract the collagen scar in a TGF-β1-mediated process of fibrosis. Each of these phases performs an essential function for surviving significant myocardial damage, but results in the formation of a collagen scar. Disruption of these phases can prevent adequate scar formation to resist dilated cardiomyopathy or rupture [4].

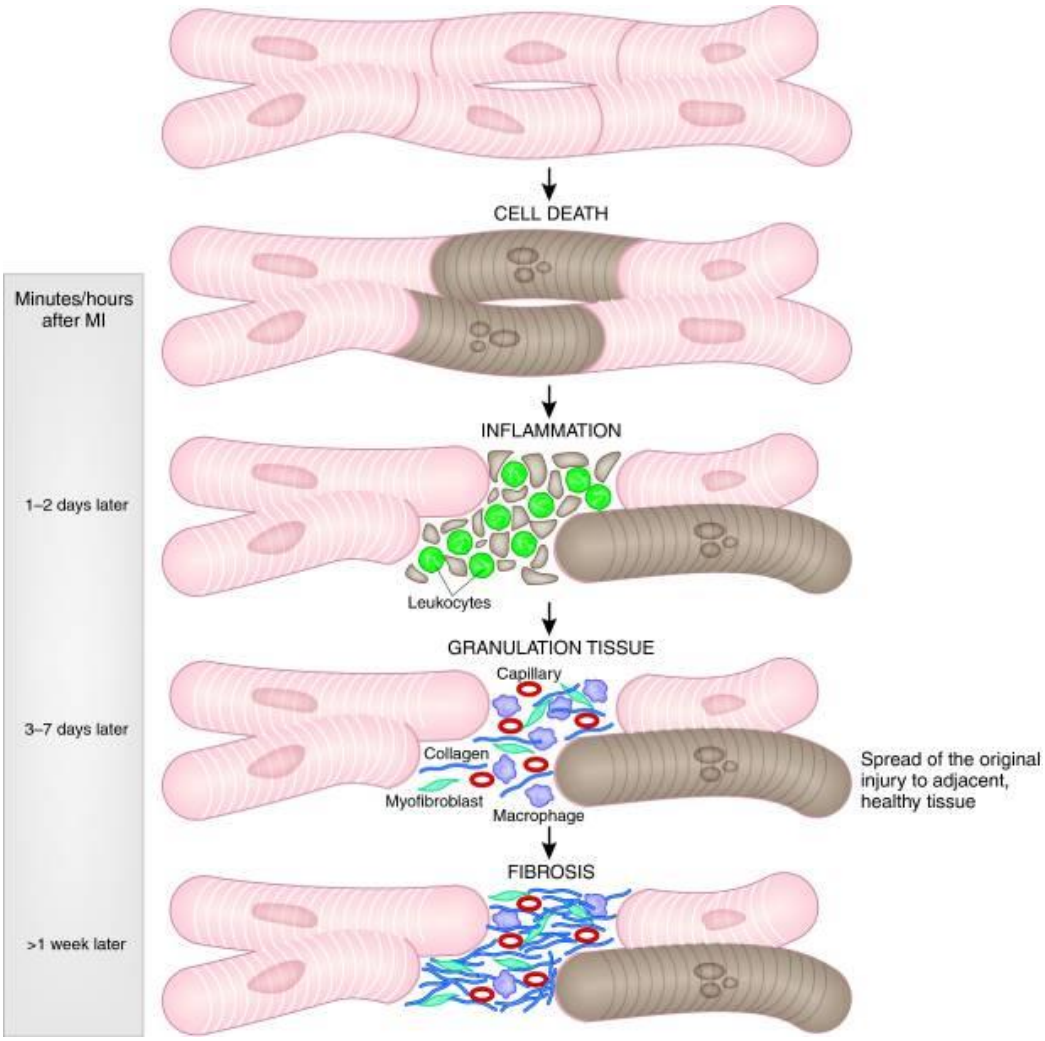

Figure 2.3. Schematic of the stages in healing after myocardial infarction Following initial cell death, the infiltration of leukocytes marks the start of inflammation response, which clears debris and makes way for new tissue formation during the granulation phase. A large population of MyoFBs participates in producing pro-fibrotic signals that ultimately result in the formation of a stiff collagen scar. (Adapted from Boudoulos et. al, 2009 [79])

The scar formed after MI is significantly stiffer than the surrounding tissue; the resulting reduced contractile capacity and increased mechanical resistance puts stress on the remaining myocardium. This stress often leads to adaptive remodeling, generally characterized by dilated cardiomyopathy or cardiac hypertrophy and fibrosis. The mechanisms controlling dilated cardiomyopathy are not fully understood, but some evidence points to extended inflammation and ECM break down. TGF-β1 is crucial in suppressing inflammation signals after initial clearance of debris, and its expression must be maintained at least until the end of inflammation [37]. However, excessive TGF-β1 signaling has been implicated in the other commonly observed example of maladaptive remodeling. Cardiac hypertrophy and fibrosis and scarring after MI are examples of fibrotic diseases with a large effect on our population. Both are characterized by an accumulation of ECM proteins, notably type-1 collagen, and a loss of tissue compliance, which can severely impair organ function [63]. In both cases, reduced electrical conductivity of the scar increases the risk for arrhythmia and sudden cardiac death [85]. Understanding the processes by which MyoFB activation occurs and is regulated is especially crucial to understanding the progression of infarct expansion and fibrotic remodeling after MI.

CHAPTER 3

BACKGROUND: FIBROBLAST MECHANOBIOLOGY

Text adapted from

[7] Schroer, A.K. and W.D. Merryman, *Mechanobiology of myofibroblast adhesion in fibrotic cardiac disease.* J Cell Sci, 2015. **128**: p. 1865-1875.

MyoFB differentiation in response to mechanical stress

In healthy tissue, quiescent fibroblasts maintain tissue homeostasis by a controlled and balanced release of ECM proteins and proteases [80]. However, these fibroblasts transition to an active MyoFB phenotype during injury or disease in response to the synergistic contributions of growth factor signaling (primarily TGF-β1) and mechanical cues (**Figure 3.1**) [79–81]. In reality, this differentiation occurs along a spectrum, often with at least one intermediate state often described as a protomyofibroblast, which has some features of MyoFBs, but is still highly migratory, characterized by expression of Fibronectin EDA and lack of α-SMA [88]. Decreasing substrate stiffness and treatment of MyoFBs with FGF2 have been shown to reverse MyoFB differentiation and promote the quiescent fibroblast phenotype *in vitro* [82, 83, 84]. However, the increased mechanical stimulation during fibrosis may prevent such a dedifferentiation and could be responsible for the long-term persistence of MyoFBs that are observed in disease. The three main mechano-sensitive mechanisms of cellular

differentiation that give rise to MyoFBs in the heart during disease initiation are described below (**Figure 3.1**).

Endothelial to mesenchymal transition

ECs directly contribute to tissue remodeling by differentiating into fibroblast-like cells in response to chemical and mechanical signals through EndMT (**Figure 3.1A**). These cells lose their endothelial cell-cell adhesions, including cadherin-5 (also known as vascular-endothelial (VE)-cadherin), and express migratory, mesenchymal cell markers, including cadherin-2, MMP-2 and α-SMA [32]. A similar mechanism is responsible for the origin of both VICs and CFs during development and is enhanced by active contraction of the myocardium and surrounding matrix [25, 28]. Inflammation and TGF-β1 signaling both promote EndMT in valve ECs during the initiation of valve disease [29,85]. EndMT also accounts for approximately 25% of the α-SMA-positive, MyoFB-like cells that are found in the myocardium after infarction; this transition is dependent on canonical Wnt signaling, a pathway that also promotes fibrosis in concert with TGF-β1 [86, 87]. These cells participate in ECM remodeling during the transition from inflammation to fibrosis, but future work is needed to completely characterize this cell population and its contribution to disease manifestation.

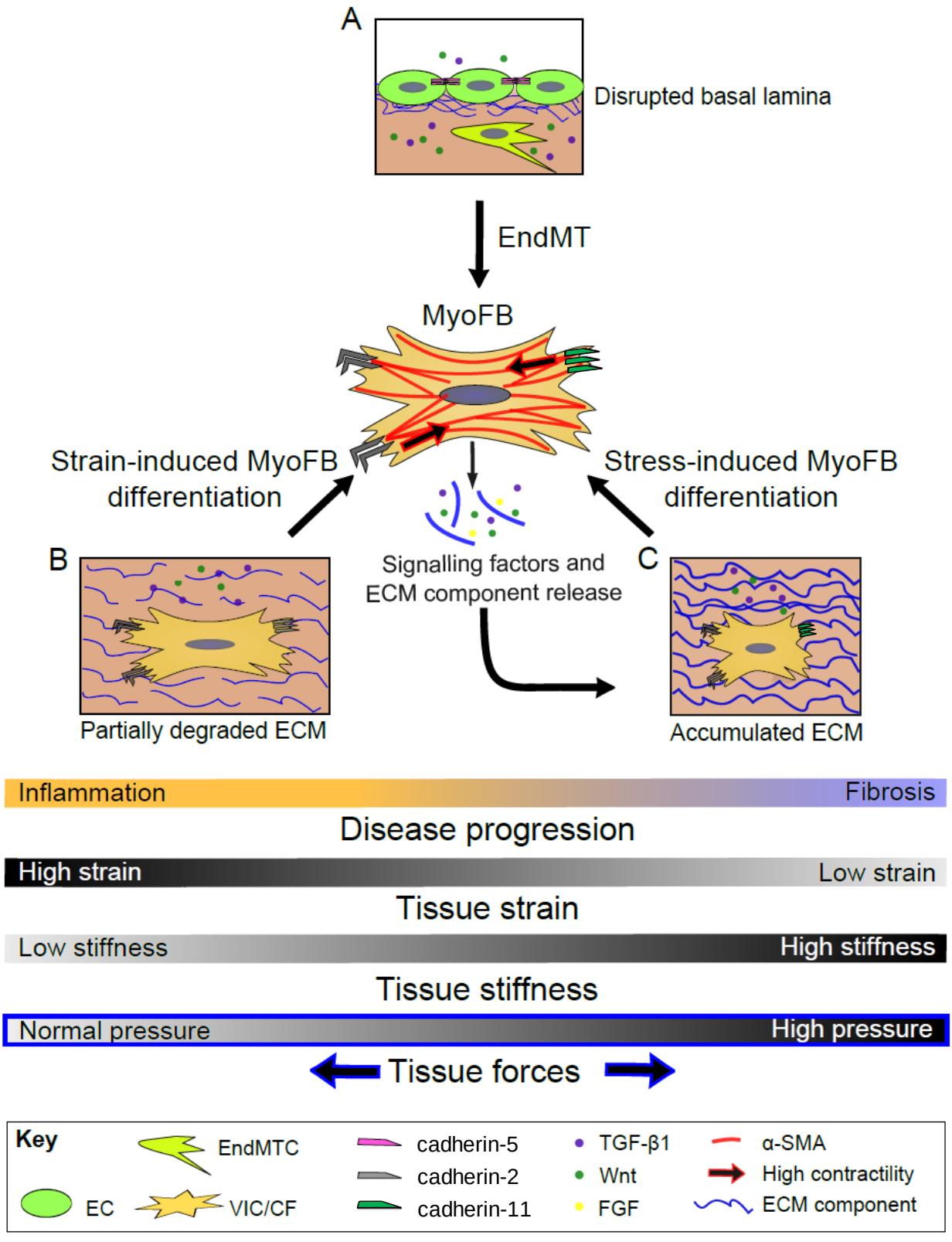
A
Disrupted basal lamina
EndMT
MyoFB
Strain-induced MyoFB differentiation
Stress-induced MyoFB differentiation
B
C
Signalling factors and ECM component release
Partially degraded ECM
Accumulated ECM
Inflammation
Fibrosis
Disease progression
High strain
Low strain
Tissue strain
Low stiffness
High stiffness
Tissue stiffness
Normal pressure
High pressure
Tissue forces
Key
EndMTC
EC
VIC/CF
cadherin-5
cadherin-2
cadherin-11
TGF-β1
Wnt
FGF
α-SMA
High contractility
ECM component

Figure 3.1. Mechano-sensitive mechanisms of MyoFB differentiation. MyoFBs play a central role in fibrotic disease progression in the heart because of their roles in cellular force generation and transmission, intercellular signaling, and ECM remodeling. One important mechanism yielding MyoFBs is endothelial-to-mesenchymal transformation (EndMT) (A), by which endothelial cells (ECs) lose their endothelial markers (including VE-cadherin) and become migratory and contractile. Valvular interstitial cells (VICs) and cardiac fibroblasts (CFs) can differentiate into MyoFB in response to high mechanical strain (B), which is often experienced during inflammation with the degradation of initial ECM and a corresponding decrease in tissue stiffness. Quiescent VICs and CFs can also differentiate into MyoFBs in response to high mechanical stress (C), caused by both increased tissue stiffness and increased tissue forces. MyoFBs increase the overall stress in the environment by producing excess ECM and contracting existing ECM through increased cellular contractility. MyoFBs also release profibrotic signaling factors, including TGF-β1 and Wnt, which promote further MyoFB differentiation and tissue stiffening. This forms a positive feedback loop leading to progressively worsening fibrosis. Tissue stiffening also often leads to compensatory increases in ventricular pressure, which increases the applied tissue forces and reinforces this positive feedback loop. (Figure replicated from Schroer et al [19]).

Strain-induced MyoFB differentiation

Another well-established mechanism for MyoFB differentiation that is relevant to the progression of cardiac disease is the differentiation of quiescent VICs and CFs in response to high strains (**Figure 3.1B**). Pressure overload increases strains in the valves and myocardium, and the initiation of inflammation causes a breakdown of ECM, which can further increase local strains. *Ex vivo* aortic valves that are exposed to pathologic strain (15-20% of original length) expressed more matrix metalloproteinases (MMP1, -2, and -9) and collagen-I than valves that are exposed to physiologic valve strains (10%) [93]. MMPs and other proteases are also expressed by MyoFBs in infarct regions to breakdown any damaged ECM and allow for increased fibroblast migration into the infarct region [14], [75], [94]. The resulting decrease in stiffness would lead to higher strain when subject to mechanical loading, which is especially relevant at the border between the infarct tissue and the remaining contractile myocardium. CFs proliferate and express increased levels of α-SMA and MMP-2 *in vitro* after exposure to approximately physiological cyclic strain between 5 and 15 % [95]. In addition, expression of MMPs and α-SMA increases the ability of CFs to migrate through and

contract 3-D substrates [96]. High local strain may also signal the transition from inflammation to fibrosis. In response to increased cyclic strain, aortic VICs (AVICs) express reduced levels of inflammatory markers and increased levels of profibrotic factors including TGF-β1 [97]. Furthermore, strain can activate latent TGF-β1 that is sequestered in the ECM [98], [99]. Strain and TGF-β1 together enhance MyoFB differentiation and cell contractility and increase the formation of calcified nodules by AVICs in dynamic culture [86], [100], [101]. This increase in calcific nodule formation is dependent on the establishment and intercellular transmission of cellular tension by α-SMA and cadherin-11, respectively [51], [101].

Stress-induced MyoFB differentiation

A third mechanical trigger for MyoFB differentiation is increased mechanical stress (**Figure 3.1C**). *In vitro*, increased substrate stiffness promotes MyoFB differentiation in AVICs, leading to increased calcific nodule formation, α-SMA expression, and expression of TGF-β receptor type 1 [83, 95, 96]. On stiff 2D substrates, CFs exhibit an increase in the expression of α-SMA, TGF-β1, and collagen-1 [96–98]. MyoFBs generate increased intracellular tension to balance the increase in extracellular tension they experience on stiffer substrates, and can then use this tension to remodel their local microenvironment [105]. After cells have increased their intracellular tension, the surrounding ECM becomes more taut, compact, and stiff, which can in turn promote the differentiation of nearby fibroblasts and perpetuate disease progression [104].

Besides their active role in ECM modification after differentiation into MyoFBs, CFs can alter myocardial structure by affecting the behavior and function of CMs. Direct

intercellular contacts between CFs and CMs *in vitro* decrease the contraction velocity of CMs and increase the expression of inflammatory cytokines therein [12]. CF-induced changes in ECM stiffness and composition can also promote CM hypertrophy [106]. Finally, the release of profibrotic factors, such as TGF-β1, AngII, and FGF2 by CFs have all been shown to promote CM hypertrophy, which leads to a thickening of the muscular walls that are then able to generate stronger contractions and enhance mechanotransductive signaling throughout the heart [107]. These tissue-level forces are transmitted to the different cardiac cells through the cardiac ECM and through intercellular adhesions between them. In the following sections, we highlight recent research that has provided new insights into the molecular mechanisms by which mechanical signals are transduced from the cellular microenvironment in order to elicit these tissue-level changes.

Mechano-sensitive adhesion proteins, including integrins and cadherins, transduce mechanical signals between cells and their microenvironment and can stimulate cellular responses including cell growth and differentiation. Both integrins and cadherins are large families of proteins, and expression of specific isoforms within these families is associated with cell phenotype changes and disease progression (**Table 3.1-2**). The following sections will summarize the integrin and cadherin isoforms that are upregulated in fibrotic disease in the heart and discuss the mechanosensitive signaling pathways they initiate.

Table 3.1. Summary of integrin isoform expression in normal function and disease

Tissue	Integrin type	ECM Binding Partner	ECM Expression		References
			Normal	Diseased	
Valves	α2β1	Collagen-1	Arranged circumferentially, primarily in the fibrosa layer	Increased, disorganized expression throughout valve	[81]
	α1β1	Collagens IV and VI	Basal lamina of endothelium and fibrosa	Increased expression throughout valve	[39]
	α3β1	Collagens IV and VI	Basal lamina of endothelium and fibrosa	Increased expression throughout valve	[82]
	α5β1	Fibronectin	Limited expression in basal lamina	Increased expression throughout valve	[83]
	αvβ3	RGD	Minimal expression and exposure	Primarily exposed and expressed in areas of MyoFB differentiation	[84]
Myocardium	α2β1	Collagen-1	Organized network surrounding CMs and CF	Major component of scar after MI and general cardiac fibrosis	[85]
	α1β1	Collagen-1	Organized network surrounding CMs and CF	Major component of scar after MI and general cardiac fibrosis	[85]
	α5β1	Fibronectin	Limited expression in basal lamina	Increased throughout the myocardium	[85]
	α7β1	Laminin	Expressed throughout the myocardium	Increased throughout the myocardium	[85]
	β1	Fibronectin/ collagen	Organized network surrounding CMs and CF	Increased throughout the myocardium	[86]
	α8β1	RGD	Organized network surrounding CMs and CF	Increased collagen and fibronectin throughout myocardium	[87]
	αvβ3	RGD	Organized network surrounding CMs and CF	Increased collagen and fibronectin throughout myocardium	[88, 89]

Table 3.2. Summary of cadherin isoform expression in normal function and disease

Tissue	Cadherin Expression		Cell Type	Mechanotransductive effect	References
	Normal	Diseased			
Valves	cadherin-2	cadherin-11	AVIC	Increased cell tension, calcific nodule formation	[28]
	cadherin-5	cadherin-2	VEC	EndMT, migratory, α-SMA positive cell	[90]
Myocardium	cadherin-2	cadherin-11	CF	unknown	[91]
	cadherin-2	cadherin-2	CM	reduced cell contraction	[91]
	cadherin-5	cadherin-2	EC	EndMT, migratory, α-SMA positive cell	[1]

Integrins sense mechanical signals from the ECM

Integrins are a diverse class of ECM receptors comprised of heterodimers of α and β subunits that determine ECM binding specificity and intracellular signal transduction. Upon ECM engagement, integrins recruit FA proteins that mechanically link the cytoskeleton to the ECM, mediating a force balance between stress fibers and ECM fibrils and initiating downstream signaling pathways. This signaling is sensitive to ECM composition, stiffness, and applied strains and regulates cell phenotype, which in turn affects ECM synthesis and integrin expression throughout the progression of disease.

The β1 subunit is part of most collagen-binding integrins in the heart and can induce force-dependent cellular responses, including cell growth and MyoFB differentiation through activation of FAK, ERK, p38 and other mitogen activated kinases (MAPKs) and their downstream signaling cascades. The exact functional effects depend

on the cell type and the local microenvironment. For example, CM-specific deletion of β1-mediated adhesion results in cardiac fibrosis and heart failure in response to pressure overload by disrupting CM membrane integrity and contractile function [108]. A recent study investigating cardiac fibrosis in an aortic constriction model showed a correlation between β1 integrin persistance and the severity of cardiac fibrosis and remodeling, in the context of depleted disintegrin and metalloproteinase ADAM17 expression [109]. In addition, α7β1 integrin, a laminin receptor, has also been shown to have a protective effect in CMs that are exposed to ischemic stress [110]. Removal of the β1 integrin-associated mechanosensitive protein melusin alters signaling through ERK and glycogen synthase kinase 3β (GSK-3β) and leads to dilated cardiomyopathy and fibrosis in response to pressure overload in the heart [111]. These studies highlight that β1 integrin helps to protect CMs from adverse effects of the mechanical strains they experience.

Another β1-containing integrin that protects cardiac cells against fibrosis is α2β1 integrin, the primary receptor for collagen-1, which forms the largest fraction of healthy ECM in both valves and the myocardium [112], [113]. Fibrillar collagen-1 networks are maintained in a tightly regulated homeostasis that has been shown to be dependent on α2β1 integrin-mediated adhesion in fibroblasts [114]. Consequently, blocking α2β1 adhesion causes a build-up of ECM in the skin and in collagen gel lattices, which is prevented by α2β1-induced release of the collagen-1 protease MMP-13 [114]–[117].

However, while α2β1 integrin inhibits fibrosis in healthy tissues, other β1 integrins promote MyoFB differentiation and fibrosis. For instance, α1β1 has been shown to promote both inflammation and MyoFB differentiation in adult connective tissue [110,

111]. In addition, α3β1 integrin promotes EndMT and MyoFB differentiation in fibrotic lungs and mediates crosstalk between factors involved in TGF-β1- and Wnt-associated signaling [120]. These integrins are expressed in the heart and bind to non-fibrillar collagens IV and VI, which are upregulated during valve disease and myocardial fibrosis [61], [121], [122]. Another β1 integrin that has been linked to cardiac fibrotic disease is α5β1 integrin, the classic fibronectin receptor. Expression of α5β1 is increased in fibrotic myocardium, and signaling downstream of α5β1 promotes the expression of additional fibronectin in an example of positive feedback [99], [123]. Secretion of fibronectin contributes to further MyoFB differentiation by initiating signaling through FAK that facilitates the formation of new integrin adhesions and increases matrix stiffness (**Figure 3.1C**). Fibronectin-induced signaling promotes MyoFB differentiation and MMP release by fibroblasts in 3-D *in vitro* systems, but these effects are reduced or reversed by the addition of collagen-1 to the matrix [124], [125]. Another fibronectin-binding integrin, α8β1, is specifically enhanced in MyoFBs in fibrotic hearts [126]. Overall, β1 integrin expression is increased in fibrotic and hypertrophic hearts, and, moreover, fibroblast-specific deletion of β1 integrin causes insufficient wound healing and reduced MyoFB differentiation in a dermal model [115], [127], [128]. Taken together, these data suggest that, despite their protective effect on CMs, β1 integrins exert a pro-fibrotic effect in heart fibroblasts during disease.

Another important integrin type that has been directly linked to mechanotransduction and MyoFB differentiation are the β3 integrins [129]. β3 integrins recognize the RGD peptide sequence that is found in fibronectin, collagen, and vitronectin, and they are highly expressed during development and disease [130]. In

accordance with this, AVICs cultured on RGD-coated substrates express increased levels of MyoFB markers and of αvβ3 integrins and are more prone to calcification [131], [132]. Furthermore, β3 integrin expression in the heart is significantly increased after MI, and expression of β3 integrins in CFs is necessary for the accumulation of collagen and fibronectin in response to pressure overload [130], [133]. This effect is likely mediated by the FA component talin, which links integrins to the cytoskeleton and is required for αvβ3 integrin-mediated mechanotransduction [129]. The talin1 isoform is expressed in the heart during development and disease, and its deletion prevents pressure-induced hypertrophy and fibrosis in the myocardium by altering signaling through p38, ERK, protein kinase B (Akt), and GSK-3β [134]. All of these kinases are involved in TGF-β1-induced MyoFB differentiation and promote the expression of α-SMA and increased intracellular tension. Furthermore, β3 integrin engagement with ECM proteins enhances TGF-β1 signaling through Src and p38 to further promote the expression of α-SMA and of β3 integrins, thereby forming another positive feedback loop [135].

The convergence on TGF-β1 signaling is but one example of the significant crosstalk between integrin and growth factor signaling that is involved in the regulation of MyoFB differentiation in the heart (**Figure 3.2**) [92]. Non-canonical TGF-β1 signaling through Src and p38 promotes the production of α-SMA in AVICs by the transcription factors myocardin related transcription factor (MRTF) and serum response factor (SRF) [136]–[138]. FGF2 signaling through FAK and ERK has been shown to prevent MyoFB differentiation in MEFs and to reverse TGF-β1-mediated expression of α-SMA [139], [89], [140], [141]. Src and FAK are directly activated by β3 and β1 integrins,

respectively, and the effects of the adhesions they mediate on MyoFB differentiation is mirrored in this crosstalk (**Figure 3.2**). Compounding this crosstalk, integrin signaling also regulates the expression and activation of growth factors. For example, β1 integrins regulate the expression of the angiotensinogen gene in CFs through p38 signaling in response to mechanical stretch. This effect is mediated by activation of Rac1 and inhibition of RhoA, intracellular kinases involved in cytoskeletal organization and contraction [142].

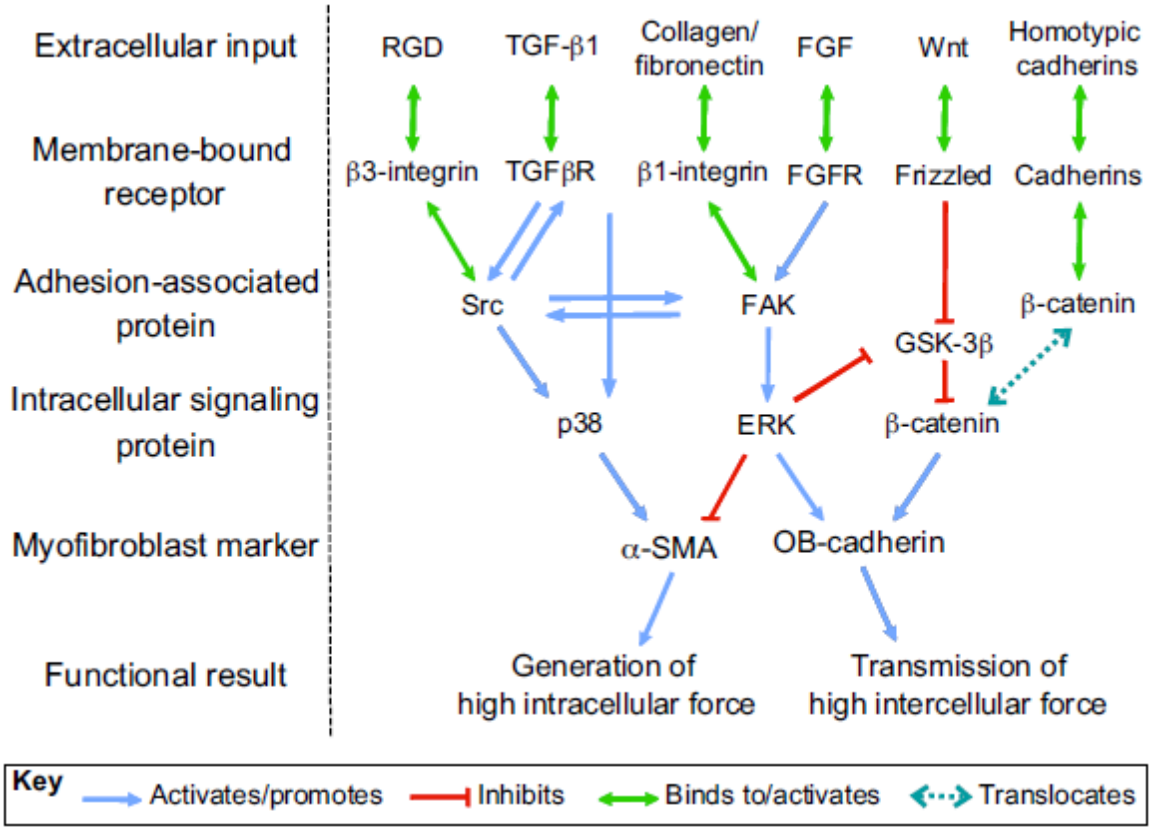

Figure 3.2. Crosstalk between growth factor and adhesion protein signaling. Illustrated here are the intracellular signaling pathways and crosstalk between integrin, growth factor and cadherin signaling. β3 integrin signals through the same intracelullar pathways as TGF-β1 increasing α-SMA expression and cellular contractility. β1 integrin shares pathways with both TGF-β1 and FGF2, which may in part explain its context-dependent effects on MyoFB differentiation. Cadherins regulate the availability of β-catenin to participate in Wnt signaling, a pathway that promotes cadherin switching and fibrosis. Both integrins and cadherins mechanically link the ECM and the actin cytoskeleton and are sensitive to increases in applied force from extracellular or intracellular sources; therefore, increased expression of α-SMA in MyoFBs

forms a positive feedback loop to further promote adhesion stability and associated signaling pathways. Figure replicated from Schroer et al [19]).

In addition to such ‘outside-in’ signaling, integrins can also participate in ‘inside-out’ signaling, by which FA proteins can modify the intracellular domain of integrin subunits to activate them, resulting in stronger adhesions to the ECM [143], [144]. Vinculin is a force-sensitive FA protein that is recruited to FAs in a tension-dependent manner, and has been shown to strengthen and stabilize the FA when held under high tension, allowing for greater transmission of force [145]–[147]. Active vinculin can also recruit FA proteins including FAK to potentiate further signaling [146], [148]. Intracellular force generated by actin stress fibers can be transmitted through these adhesions to the ECM to alter its organization. Certain growth factors, including TGF-β1, are secreted into the ECM in an inactive form, but αvβ3 integrins can activate such latent TGF-β1 via ECM tension, thereby further promoting MyoFB differentiation and fibrosis [98], [99].

MyoFB differentiation results in an increase in α-SMA stress fibers, which can strengthen and increase the activation of integrins in FAs, forming a positive mechanical feedback loop. The resulting increase in cellular tension can then be transmitted to neighboring cells through cadherin-rich AJs as discussed below.

Cadherins sense intercellular forces

Cadherins mediate mechanically-induced signaling between cells through AJs, which link cadherins to the cytoskeleton, as described in a recent review [52]. Differential cadherin expression is a major feature of cell differentiation and function

during disease and this ‘cadherin switching’ is mediated in part by signaling downstream of cadherins (**Table 3.2**). β-catenin is present in AJs and is intimately involved in crosstalk between cadherins, canonical Wnt, and TGF-β1 signaling (**Figure 3.2**). Molecular signaling or mechanical perturbations that disrupt cadherin-cadherin interactions between cells have been shown to release β-catenin into the cytoplasm where it acts in concert with growth factor signaling to promote a mesenchymal cell phenotype [49]. For example, exposure to oscillatory fluid flow triggers a cadherin-2-mediated release of β-catenin and a subsequent osteogenic differentiation in stem cells [149]. Typically, free cytoplasmic β-catenin is rapidly marked for degradation by GSK-3β; however, inhibition of GSK-3β by activation of TGF-β1, ERK, or Wnt allows for an accumulation of β-catenin in the cytoplasm and its subsequent translocation to the nucleus where it activates its target genes [56], [150]. In addition to signaling though β-catenin, several recent studies have characterized a force-dependent interaction between vinculin and α-catenin, another protein linking AJs to the cytoskeleton [151]–[154]. Vinculin is recruited to AJs in a force-dependent manner by α-catenin, which results in strengthening of the adhesion and increased cell contractility [53], [151]. This result indicates that integrins and cadherins might share a common mechano-sensitive mechanism, in which vinculin-induced stabilization of either FAs or AJs affects downstream signaling pathways. p120-catenin is also involved in stabilizing AJs and increases activation of Rac1 when bound to either N- or Cadherin-11, leading to increased expression of mesenchymal cadherins [155], [156].

Cadherin-2 (N-cadherin) is the classical cell-cell adhesion protein that is expressed by quiescent fibroblasts and CMs in the heart. Cadherin-2 expression and

localization at cell-cell contacts is associated with increased stability of β-catenin and decreased expression of α-SMA [54]. CFs form Cadherin-2-mediated interactions with CMs, which influences CM structure and contractility during development, normal function and disease [157]–[159]. In a recent study, cadherin-2 bonds between CFs and CMs were shown to dynamically deform CM membranes in response to MyoFB contraction and induce a measurable slowing of CM conduction velocity [50]. This study demonstrates a mechanical signal from MyoFBs that affects the electrophysiology of CMs, and may contribute to risk of arrhythmia and other cardiovascular conditions associated with low conduction velocity [160].

While quiescent AVICs and CFs express cadherin-2, during injury and disease these cells differentiate into MyoFBs characterized by expression of cadherin-11. Cadherin-11 (also known as OB-cadherin) was first described in 1994 in the context of osteogenesis and bone development, but recent work has shown its importance in a range of tissues [161]. Over 100 papers have been published in the past few years that examine the role of cadherin-11 in cancer and fibroblast-mediated disease. In the context of cancer, cadherin-11 expression is associated with increased migration and metastasis, especially metastasis to bone [162]. As cell differentiation and migration in cancer and inflammatory disease show some similarities, cadherin-11 has been proposed as a common possible therapeutic target for both types of disease [163]. Cadherin-11 plays an important role in inflammation in the context of rheumatoid arthritis; it stimulates synovial fibroblasts to release proinflammatory cytokines upon cadherin engagement [19, 155]. Celecoxib, a pharmacological inhibitor of cyclooxygenase-2 that inhibits inflammation during rheumatoid arthritis, has been

shown to bind to cadherin-11 [163]. Inflammation often leads to fibrosis, which is mediated by activated MyoFBs. In this context, cadherin-11 has been implicated in the progression of dermal and pulmonary fibrosis and suggested to promote MyoFB differentiation through interactions with β-catenin [25], [164]. In accordance with this, injection of a function-blocking antibody against cadherin-11 improves bleomycin-induced dermal and pulmonary fibrosis, but its effect has not yet been investigated in other organ systems [21,157]. Taken together, these studies indicate that cadherin-11 is a promising target in the field of fibrotic disease.

During MyoFB differentiation, TGF-β1 signaling induces an increase in cadherin-11 concurrently with a decrease in the expression of cadherin-2 [44]. Within cell-cell adhesions, cadherin-11 is able to withstand significantly higher forces than cadherin-2, which allows for stronger matrix contraction and the transmission of higher intercellular tension [44], [51], [165]. Cadherin-11 has been found to localize at focal adhesions and promote cell-substrate adhesion [166]. Cadherin-11 is highly expressed in diseased heart valves in both VECs and VICs and has been implicated in the development of calcified nodules in the aortic valve in CAVD through increased transmission of intercellular force [51], [167]–[169]. It is also expressed in CFs, but the functional significance of this expression in the context of cardiac fibrosis and wound healing has not been studied. Given the known roles of cadherin-11 in inflammation and fibrosis in joint connective tissue and lungs, it is likely that cadherin-11 also has an important role in myocardial remodeling [23], [25].

In addition to functional mechanical roles, cadherin-11 can also potentiate downstream signals to control cell behavior. Although the downstream signaling of

cadherin-11 is still relatively uncharacterized, recent studies show a significant crosstalk with MyoFB regulatory signals. For instance, it was found that cadherin-11 engagement promotes smooth muscle cell differentiation through TGFβRII-mediated pathways and increases the expression of α-SMA and cadherin-11 through SRF activation [169]. Similarly, blocking cadherin-11 or cadherin-2 engagement reduces the expression of MyoFB markers in diseased dermal fibroblasts, which express higher basal levels of cadherin-11 and α-SMA compared to healthy fibroblasts [170]. Cadherin-11 overexpression in fibroblasts has also been shown to increase expression of Wnt and β-catenin, increase activation of ERK and Akt, and promote cadherin-2 expression [171]. These studies indicate that cadherin-11 expression and engagement promotes MyoFB differentiation and increase α-SMA expression. This increase in α-SMA stress fibers, in turn, contributes to the strengthening and further stabilization of cadherin-11 junctions, allowing for enhanced force transmission [44]. However, it is not clear how increased tension at cadherin-11 junctions effects signaling through catenins and downstream MAPKs. Furthermore, α-SMA and cadherin-11 are not always co-expressed or co-regulated. For example, increased binding on cadherin-11-coated surfaces has been shown to inhibit α-SMA expression in porcine AVICs and knockdown of cadherin-11 has been shown to increase α-SMA expression [167]. Future studies are needed to clarify the interplay between cadherin-11 mechanotransduction and MyoFB differentiation.

To conclude, there are mechanistic similarities between fibrotic disease progression in the heart wall and valves that can inform future studies of disease. Namely, in both myocardium and valve tissue, there is an increase in active MyoFBs that remodel ECM and alter cardiac mechanics and function. These cells are sensitive

to mechanical signals that are transduced largely through integrins and cadherins. Integrins react to the composition and mechanics of the microenvironment of a cell and can promote cell differentiation in a context-dependent manner. MyoFB differentiation potentiated by integrin and cadherin signaling can contribute to further ECM remodeling and tissue stiffening, which in turn enhances mechanotransductive signaling in nearby cells (**Figure 3.1**). Such a system of positive feedback loops can then perpetuate the progression of fibrotic disease. Prolonged inflammatory responses further compound the problem by initiating and propagating ECM remodeling. Both integrin- and cadherin-11-mediated signaling have been implicated in inflammation, and strategies aimed at blocking the functions of these adhesion molecules have shown preliminary success in limiting inflammation-triggered maladaptive remodeling [23]–[25], [118]. The overlapping and integrated networks of chemical and mechanical signals that regulate fibrotic heart disease progression will continue to make the development of promising therapies a challenge. Nevertheless, the crucial role of cadherins and integrins in both chemical and mechanical signaling makes them excellent potential targets for therapy and future study [20].

CHAPTER 4

AIM 1: ELUCIDATING MECHANOSENSITIVE SIGNALING CROSSTALK IN FIBROBLASTS

Text for Chapter 4 taken in part from:

[139] **Schroer, A.K**., Rhyzova, L.M., Merryman, W. D., *Network Modeling Approach to Predict Myofibroblast Differentiation.* Cellular and Molecular Bioengineering, 2014. **7**(3): p. 446-459.

Introduction

Fibroblast cells play a key role in producing and maintaining connective tissue throughout the body. The ability of these cells to differentiate into active MyoFBs is important during development and wound healing, but prolonged MyoFB activation can lead to overproduction of ECM proteins and stiffening of the surrounding tissue. This stiffening can cause heightened differentiation of neighboring fibroblasts through force transduction pathways and can lead to detrimental fibrotic pathologies in many organ systems [172]. One hallmark of the MyoFB phenotype is the production of α-SMA stress fibers, which transmit intracellular forces and increase the contractility of the cells and surrounding tissue [88], [173]. Clarifying the inputs and intracellular mechanisms that govern MyoFB differentiation will provide insights into the pathophysiology of many fibrotic diseases.

Mechanical stress and TGF-β1 are known to promote the MyoFB phenotype [88] and FGF2 has been shown to oppose TGF-β1 signaling and promote the quiescent fibroblast phenotype [83], [100], [140], but the intracellular effectors of these environmental cues have significant crosstalk [174], [175]. Cells can experience mechanical tension and substrate rigidity through integrins: transmembrane proteins that transduce forces from the ECM to intracellular structures like FAs and stress fibers. Different isoforms of integrin subunits are activated to transmit mechanical signals by specific ECM proteins. Integrins with β3 subunits are activated by fibronectin and transmit mechanical signals through the tyrosine kinase Src [129], [176]. Together, Src and β3 integrin enhance TGF-β1 non-canonical signaling to p38 [177], [178]. β1 integrin subunits activate focal adhesion kinase (FAK) in a stiffness dependent manner [179]. Src and FAK are important in the formation and maintenance of FAs and are known to form a complex and activate each other's kinase activity to enhance downstream signaling [176], [180].

Both integrin signaling and cadherin regulation have significant interaction with TGF-β1 signaling pathways. TGF-β1 is a major promoter of the MyoFB phenotype that is known to play a role in cardiac fibrosis. TGF-β1 is a key mediator of the hypertrophic and dilative ventricular remodeling and is released by cardiac fibroblasts and myocytes with pressure overload and infarction and in response to AngII expression [181], [182]. TGF-β1 also plays a crucial role in ending inflammation and beginning wound strengthening by repressing inflammatory signals and promoting accumulation of ECM by inhibiting proteases [182]. Canonical TGF-β1 signaling through TGF-β receptors and Smads 2 and 3 is required for many of these mechanisms. A recent study investigating

reperfusion MI in mice lacking Smad3 demonstrated that canonical TGF-β1 signaling through Smad3 increases collagen expression and inhibits fibroblast proliferation [170]. However, inhibition of Smad function did not prevent TGF-β1 induced α-SMA expression, indicating an important role for non-canonical signaling [137]. Non-canonical TGF-β1 signaling through Src and p38 has been implicated in the regulation of contractile α-SMA production. TGF-β1 binding to its type 1 receptor activates Src, which in turn phosphorylates tyrosine 294 on TGFβ receptor 2 (TβR2), leading to p38 phosphorylation [177]. This signaling is crucial for MyoFB differentiation of AVICs and other fibroblast cell types [136], [137]. Mouse embryonic fibroblasts that cannot express Src family kinases (SYF-/-) express significantly fewer MyoFB markers than their wild type counterparts (MEF+/+) (**Figure 4.1A**). MAPK p38 is also critically important for MyoFB differentiation [137], [183]. Inhibiting p38 effectively blocks TGF-β1 induced MyoFB differentiation, but does not interfere with canonical Smad signaling indicated by PAI-1 expression (**Figure 4.1B**). PAI-1 reduces protease activity in the local microenvironment and can allow for accumulation of ECM. Within the nucleus, transcription factors myocardin related transcription factor (MRTF) and serum response factor (SRF) (downstream of Src and p38, respectively) are required for the transcription of α-SMA and other markers of contractile MyoFBs [138].

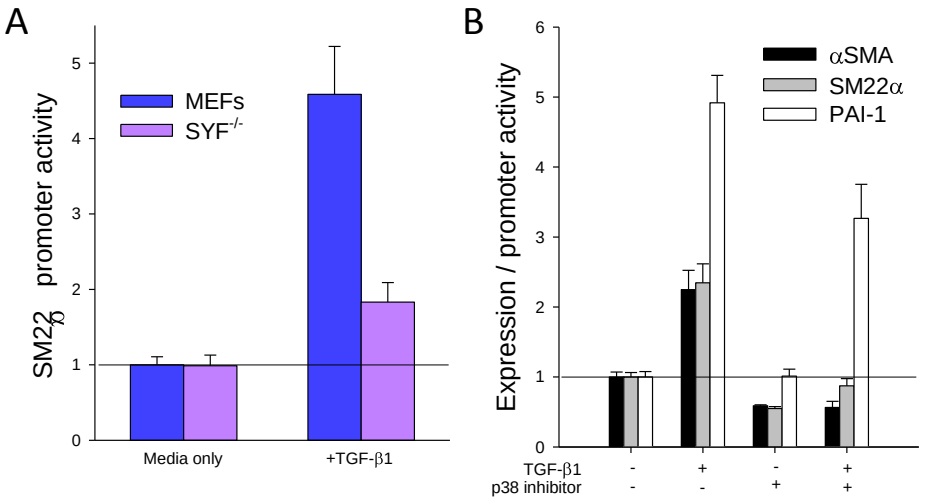

Figure 4.1. Src and p38 are necessary for TGF-β1 induced MyoFB differentiation Deletion of Src family kinase in SYF-/- MEFs prevents TGF-β1 induced increase of a MyoFB marker (A). TGF-β1 induced upregulation of MyoFB markers α-SMA and SM22α, but not PAI-1, are prevented by p38 inhibition (B). (Figure adapted from Hutcheson et al. 2012 [137])

FGF2 is another factor that is critical for development and can have a potent effect on fibroblast phenotype that is upregulated in the heart after MI [74]. In addition to promoting proliferation, FGF2 signaling to ERK has been shown to prevent MyoFB differentiation in MEFs and reverse TGF-β1 induced α-SMA expression [89], [140], [141]. Kawai-Kowasa et al. demonstrated that expression of the transcription factor SRF is crucial for α-SMA expression, but its function is blocked by phosphorylated ERK after FGF2 treatment [140]. Greenberg et al. found that this effect is modulated by FAK and does not occur in FAK-/- cells [89]. FGF2 is also known to activate p38, a crucial player in TGF-β1 induced α-SMA expression [184]. In the context of the heart, FGF2 is released in response to AngII signaling and induces CM hypertrophy while stabilizing gap junction coupling in CMs [181]. It has been reported to have a cardioprotective effect during healing after MI, allowing for scar deposition and contraction, stimulating CM hypertrophy, and promoting angiogenesis [10], [74], [107]. With such a striking

effect on cardiac outcomes, it is perhaps surprising that the mechanisms for FGF2 action on CFs are relatively poorly understood. There have been no studies investigating the role of FGF2 in regulating cadherin-11 expression or signaling, despite the growth factor's known roles in regulating MyoFB differentiation and cardiac remodeling.

In a simplified scheme of α-SMA production (**Figure 4.2**), signaling through integrins and growth factors appears to converge at the intracellular level on two particular kinases, p38 and ERK. TGF-β1 signaling and β1 integrin signaling both activate p38, which has been shown to promote the MyoFB phenotype [42], [185]. Conversely, ERK is required for FGF2 induction of the quiescent fibroblast phenotype [141], [186], [187] . FAK serves as a docking site for Src and enhances Src activation and signaling to p38 [136], while transducing signals from integrins and FGF2 to enhance ERK activation and limit α-SMA production [89], [188]. FGF2 and TGF-β1 stimulate both p38 and ERK; however, they are known to lead to divergent outcomes [140], [189]. The complex and dynamic interactions of these signaling pathways complicates the regulation of fibroblast differentiation.

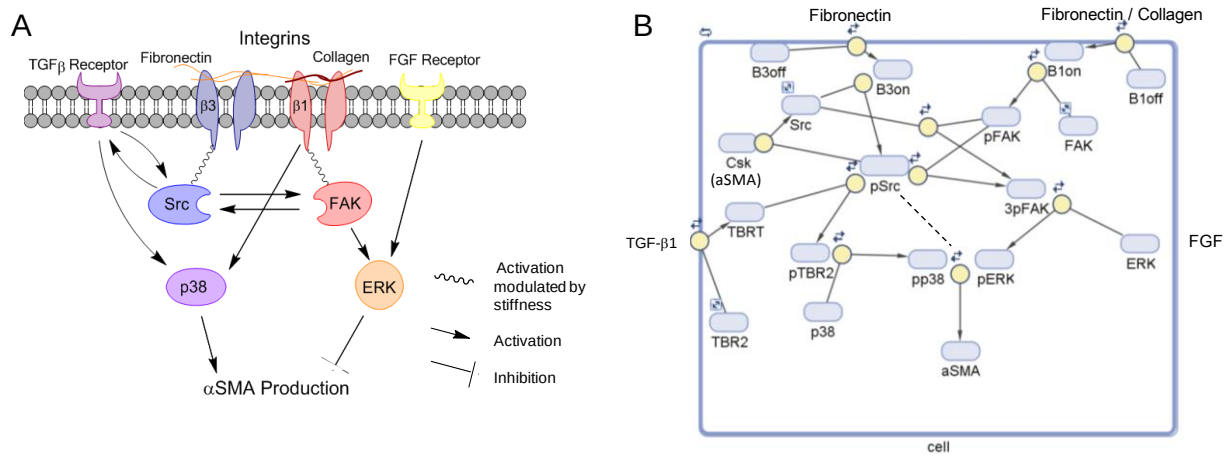

Figure 4.2. Relevant signaling network. The cartoon depicts the major pathways of MyoFB regulation and convergence on p38 and ERK kinases (A). Degradation and interactions details are not shown for the

sake of clarity. The schematic shows the model protein species and reactions (B). Proximity to the yellow node indicates that the rate of the reaction depends on the activation of the upstream protein species. The dashed line represents the contribution of Src. Figure replicated from Schroer et al [139].

Computational models of cell signaling networks have been developed and used in many biological systems to clarify complex interactions, especially when intracellular activation states are difficult to quantify [190]. Some models have been developed for subsets of this system to clarify specific mechanisms, but do little to address network effects and responses [191]–[193]. Modeling biological networks is challenging because of the high number of interactions, the range of relevant time scales, and the difficulty of acquiring quantitative data of intracellular kinetics. Despite these hurdles, many model strategies have been developed and successfully implemented in similar network settings [190]. A model developed by Janes et al. integrates complex cytokine signals to predict apoptosis, and they countered these difficulties by focusing on data-derived models [194]. Further analysis of the same model indicated that the dynamic range of a given intracellular signaling event is more important for system function than the signal strength, which lessens the need to define system components with absolute protein numbers or concentrations [195].

The goals of this aim are to clarify the roles of FAK and Src in linking integrin and cytokine signaling, and characterize the signaling profiles of TGF-β1 and FGF2 through p38 and ERK in the regulation of α-SMA and cadherin-11 expression. These experiments were used to develop a quantitative model to evaluate and compare potential mechanisms for protein interactions in the regulation of α-SMA expression, that is described in detail in APPENDIX A. Known TGF-β1, FGF2, and integrin signaling

to p38 and ERK through Src and FAK from previously reported literature informed the development of an ODE based model of fibroblast differentiation in different chemical and mechanical environments. The model was refined by fitting to experimental results for α-SMA production and dynamic phosphorylation events. We further compared the expression of cadherin-11 in these same conditions to gain a better understanding of MyoFB heterogeneity and regulation.

Methods

Cell Culture

Wild type mouse embryonic fibroblasts (MEF+/+), MEFs lacking Src, Yes and Fyn (SYF-/-), and MEFs lacking FAK (FAK-/-) [196] were used in this study. Cells were cultured in DMEM supplemented with 10% FBS, 1% antibiotic-antimicrobial and 1% non-essential amino acids. Unless otherwise noted, cells were plated at a density of 8000 cells/cm^2 on tissue culture plastic (TCP) and kept in serum free conditions during treatment with 1 ng/ml TGF-β1, 10 ng/ml FGF2 or 20mM LiCl.

PDMS for stiffness studies

Polydimethylsiloxane (PDMS) (Sylgard 184 from Dow Corning) culture surfaces were made with 10:1:0, 10:1:5, and 20:1:2 ratios of silicone-elastomer base to elastomer curing reagent to silicone oil as previously described [197], [198]. Bulk stiffness of these formulations was measured to be 2.1, 0.9 and 0.24 MPa, respectively [198]. The dishes were then sterilized under UV light for 40 minutes and coated with human full-length fibronectin in filtered carbonate-bicarbonate buffer overnight to ensure proper cell adhesion.

Immunohistochemistry

Coverslips were coated in human full-length fibronectin by overnight incubation in a 50 μg/ml solution in sterile carbonate-bicarbonate buffer and rinsed in PBS before addition of cells. After 24 hours of treatment, cells were fixed with 4% paraformaldehyde and permeabilized in 0.4% triton for 10 minutes, blocked in 1% BSA for 1 hour, and stained with a Cy3 conjugated monoclonal α-SMA antibody (Sigma) or an antibody against cadherin-11 (Invitrogen). Cadherin-11 primary was diluted 1:100 in 1% BSA and incubated overnight at 4˚ C. An antirabbit secondary conjugated to a far red fluorophore and the α-SMA antibody were both diluted 1:300 in 1% BSA and incubated at room temperature for 1 hour. Slides were mounted in Prolong Gold with DAPI mounting media to stain the nuclei and imaged at 20x magnification.

Quantification of α-SMA production by indirect ELISA

Indirect ELISA assays with α-SMA polyclonal antibody (Abcam) were used to quantify α-SMA expression after 24 hours in serum free conditions as previously described [137]. Briefly, cells were lysed in Cell lytic M media and diluted to a common concentration. Samples were incubated on 96 well plates in a blocking solution of 5% milk overnight at room temperature, incubated with an antibody against α-SMA, an antirabbit secondary conjugated to HRP, then incubated the Sure blue ELISA reagent, with thorough PBS washes between each step.

Quantification of MAPK activation and CDH11 expression by western blot

Western blots were used to study dynamics of MAPK activation in MEF+/+ and FAK-/- cells as previously described [137]. Briefly, cells were serum starved for 3-4

hours before treatment, and were lysed and diluted to equal protein concentration in RIPA buffer supplemented with protease and phosphatase inhibitors. Relative p38 and ERK phosphorylation was quantified by densitometry analysis and normalized to a loading control (β-actin, total ERK, or total p38) (Cell Signaling Technologies) and then to the average MEF+/+ no treatment case within each time point for each experiment.

Statistical analysis

For all experiments measuring outputs across a range of cell types and treatments, a two-way ANOVA was run within each time point to determine significant effects of cell type and treatment, and interactions between the two. The Holms-Sidak method and individual student t-tests with an overall significance level of 0.05 were used for multiple comparisons within cell-type and treatment groups. One-way ANOVA was used for dose response experiments that were limited to one cell type. Non-parametric tests (ANOVA on ranks or rank sum tests) were used if the samples failed the Shapiro-Wilks normality test or had unequal variance ($p < 0.05$).

Results

Removing focal adhesion kinase proteins and growth factor treatments altered α-SMA

Immortalized cell lines generated with genetic deletions certain proteins can be a powerful tool to probe intracellular signaling. In these experiments we found that MEFs with genetically deleted focal adhesion proteins expressed significantly different levels of α-SMA in serum free conditions when compared to wild type cells (**Figure 4.3A**). SYF-/- cells expressed significantly less α-SMA than MEF+/+ cells in all treatment groups (**Figure 4.3A**), expressing less than 20% of the α-SMA expressed in MEF+/+

cells. Furthermore, there was no significant difference between treatment groups within the SYF-/-. FAK-/- cells expressed significantly more α-SMA than MEF+/+ cells regardless of treatment, and both growth factors caused a significant effect relative to untreated FAK-/- cells (**Figure 4.3A**).

Our next experiment clarified the relationship between growth factor concentration, equilibrium p38 and ERK phosphorylation and α-SMA expression in MEF+/+ cells. At 24 hours, there is no significant change in pp38 with treatment with 1 or 10 ng/mL FGF2 (despite early dynamic signaling changes), but there is a significant log-linear increase proportional to TGF-β1 concentration (**Figure 4.3B**). There is significant ERK phosphorylation after a 24 hour treatment with TGF-β1 that is independent of TGF-β1 concentration. There is also a significant increase in ERK activation with FGF2 treatment, which is highly dependent on FGF2 concentration (**Figure 4.3C**). Finally, these data show divergent regulation of α-SMA by FGF2 and TGF-β1, despite acting through common intracellular mediators (**Figure 4.3D**). Both TGF-β1 and FGF2 play important roles in remodeling after MI, so their interaction and crosstalk deserves significant consideration in the context of myocardial remodeling. The demonstrated cardioprotective effects of FGF2 signaling observed in cardiac disease may be due in part to the suppression of highly contractile α-SMA expression MyoFBs [74].

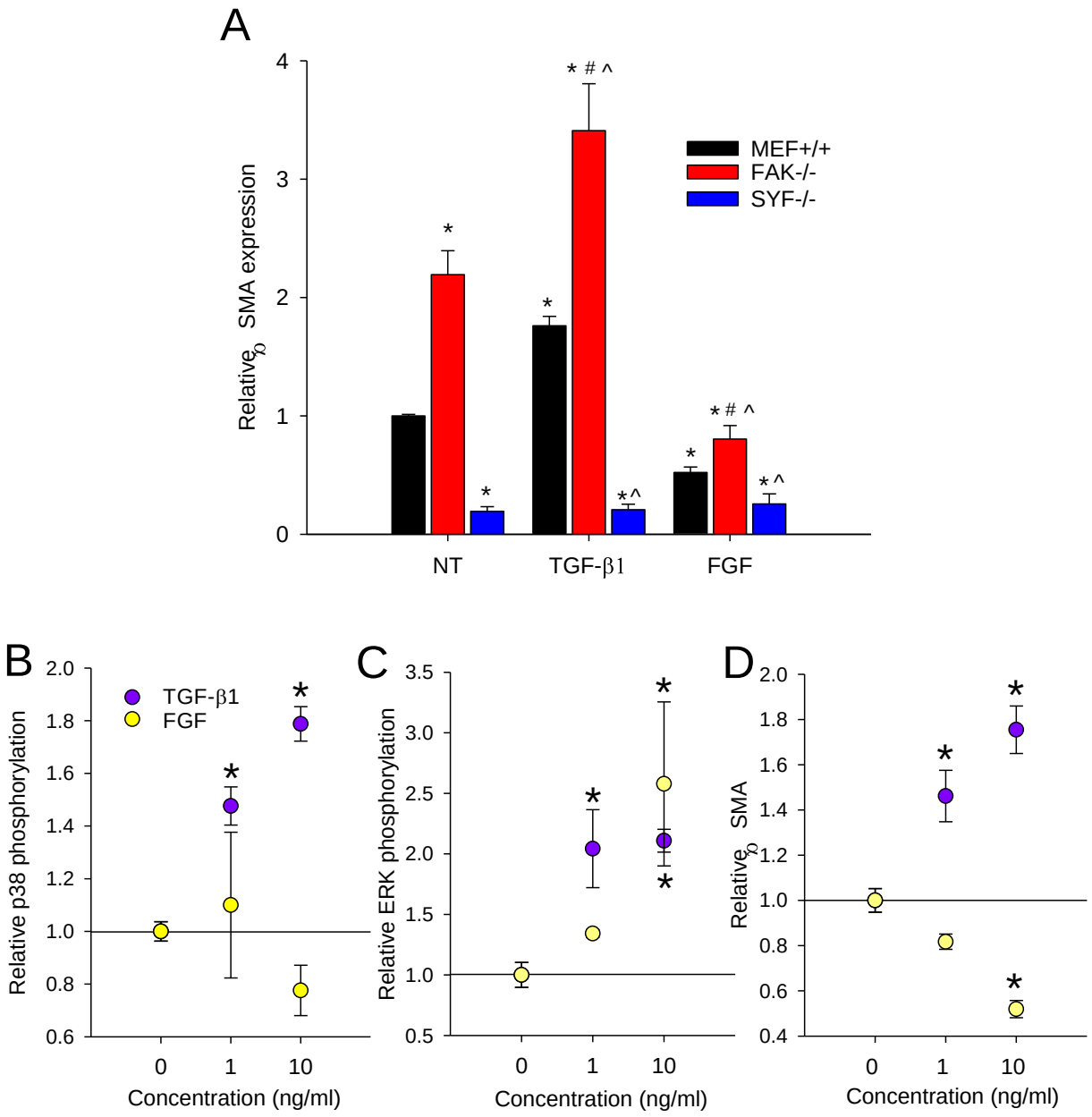

Figure 4.3. α-SMA is oppositely regulated by TGF-β1 and FGF2 through FA proteins and p38 and ERK dependent mechanisms. (A) α-SMA measured by ELISA after 24 hours of culture in serum free media, 1ng/ml TGF-β1, or 10ng/ml FGF2. All FAK-/- and SYF-/- were all significantly different from the wild type MEFs ($p < 0.01$). (B-D) A set of experiments to determine concentration dependent changes to p38 and ERK activation and α-SMA expression in response to TGF-β1 and FGF2. p38 (B) and ERK (C) phosphorylation determined by densitometry of western blots and α-SMA (D) expression determined by indirect ELISA. * denotes a significant difference between the NT and TGF-β1 treated MEFs ($p < 0.05$). # denotes significant difference from the FAK-/- NT group. ^ denotes significant difference from the MEF+/+ sample under a given treatment. (Figure adapted from Schroer et al. 2014 [139])

TGF-β1 and FGF2 induce MAPK phosphorylation with different dynamic profiles

Next we measured and compare the dynamic activation profiles of both p38 and ERK in MEF+/+ and FAK-/- cells. Western blot data showed significant and sustained p38 phosphorylation in response to TGF-β1 that peaked at 1 hour in both MEF+/+ and FAK-/- cells and remained significantly enhanced ($p = 0.017$) after 24 hours treatment (**Figure 4.4A-C**). While the shape of this activation was consistent between cell types, the peak magnitude in the FAK-/- cells was significantly lower ($p = 0.007$). Steady state p38 phosphorylation at 24 hours was also significantly lower in FAK-/- cells relative to MEF+/+ cells ($p = 0.046$). In the same set of experiments, FGF2 induced a rapid increase in p38 phosphorylation that attenuated to less than 1.5 fold of the non-treated group within one hour. FGF2 induced a dramatic increase in ERK phosphorylation in both cell types in five minutes that persisted for at least three hours (**Figure 4.4D-E**) and was still significantly elevated at 24 hours (**Figure 4.4F**). TGF-β1 induced a slight significant increase at 30 minutes that faded to insignificance within one hour. However, both cell types showed significantly enhanced ERK phosphorylation at 24 hours after treatment with TGF-β1 (**Figure 4.4F**).

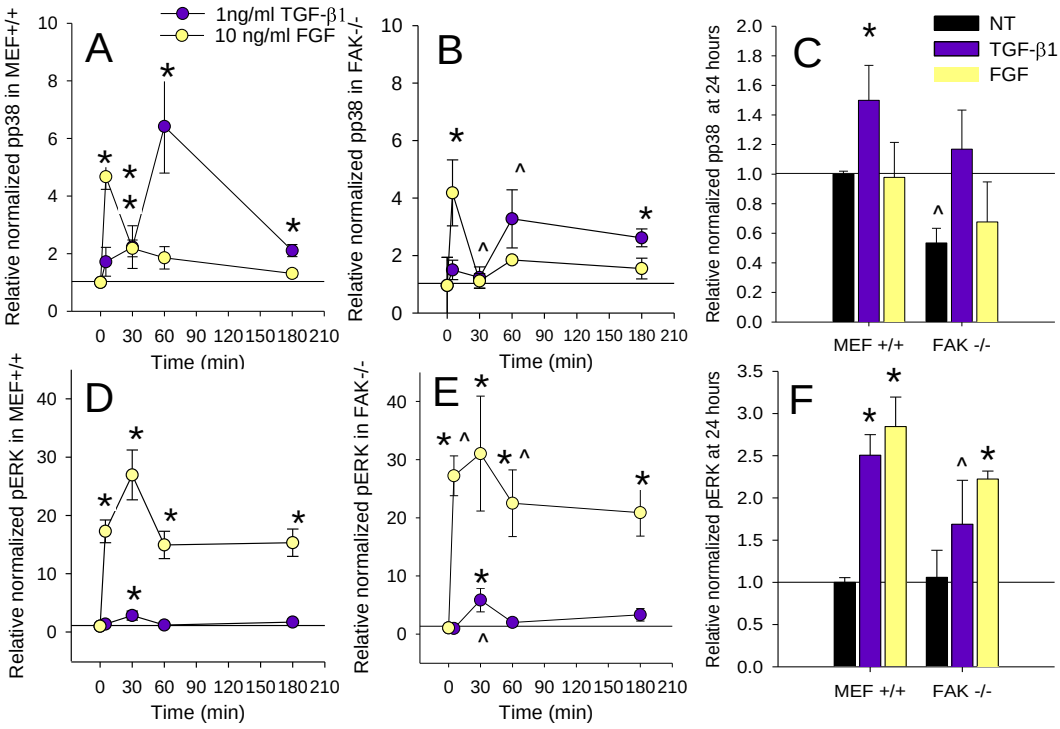

Figure 4.4. Different dynamic activation profiles for activation of ERK and p38. Averaged results of western blot densitometry analysis for pp38 (A-C) and ERK (D-F) activation over a three hour time course in MEF+/+ (A,D) and FAK -/- (B,E) cells treated with 1ng/ml TGF-β1 or 10 ng/ml FGF2. Average p38 and ERK activity after 24 hours of treatment (C,F). * indicates significant difference ($p < 0.05$) from average no treatment within cell type and time course. ^ indicates significant difference ($p < 0.05$) from the MEF+/+ sample within treatment and time point. G-L are the model output values for the same quantities at the same time points. (Figure adapted from Schroer et al. 2014 [139])

These experiments informed the development of an ODE based signaling model for α-SMA regulation via TGF-β1, FGF2 and integrin signaling through the network depicted in **Figure 4.2** [115]. The model was able to match relative α-SMA production in MEF+/+ and FAK-/- cells with and without TGF-β1 and FGF2 treatment. It was also able to predict MEF+/+ expression of α-SMA on PDMS with and without these growth factor treatments. Sensitivity analysis of the model correctly predicted increased sensitivity to growth factors in the absence of FAK.

We then expanded our focus on MyoFB differentiation to include cadherin-11. We observed a profound reduction in cadherin-11 expression in response to FGF2 treatment in both the immunostaining and western blot results (**Figure 4.5**) that represents a novel and potentially significant finding in the field of MyoFB regulation. We found that cadherin-11 was regulated in parallel to α-SMA by TGF-β1 and FGF2, but FAK-/- cells expressed significantly less cadherin-11 than their wild type counterparts (**Figure 4.5A-B**). SYF-/- cells expressed significantly less cadherin-11 than FAK-/- cells (data not shown), indicating that Src family kinase signaling is critical for expression of both cadherin-11 and α-SMA. The inverse response of cadherin-11 and α-SMA to the absence of FAK suggests that the two markers of MyoFBs are regulated through different, FAK-dependent mechanisms. Immunostaining of MEFs on fibronectin coated coverslips confirms that α-SMA and cadherin-11 are not always co-expressed within individual cells (**Figure 4.5C**, white arrows). This imbalance could affect the ability of MyoFBs in the heart to transmit forces to their neighbors and the microenvironment. We also observe what appears to be cadherin-11 staining inside the FAK-/- cells, which may indicate an inability to effectively traffic this protein to the membrane (**Figure 4.5C**, yellow arrows).

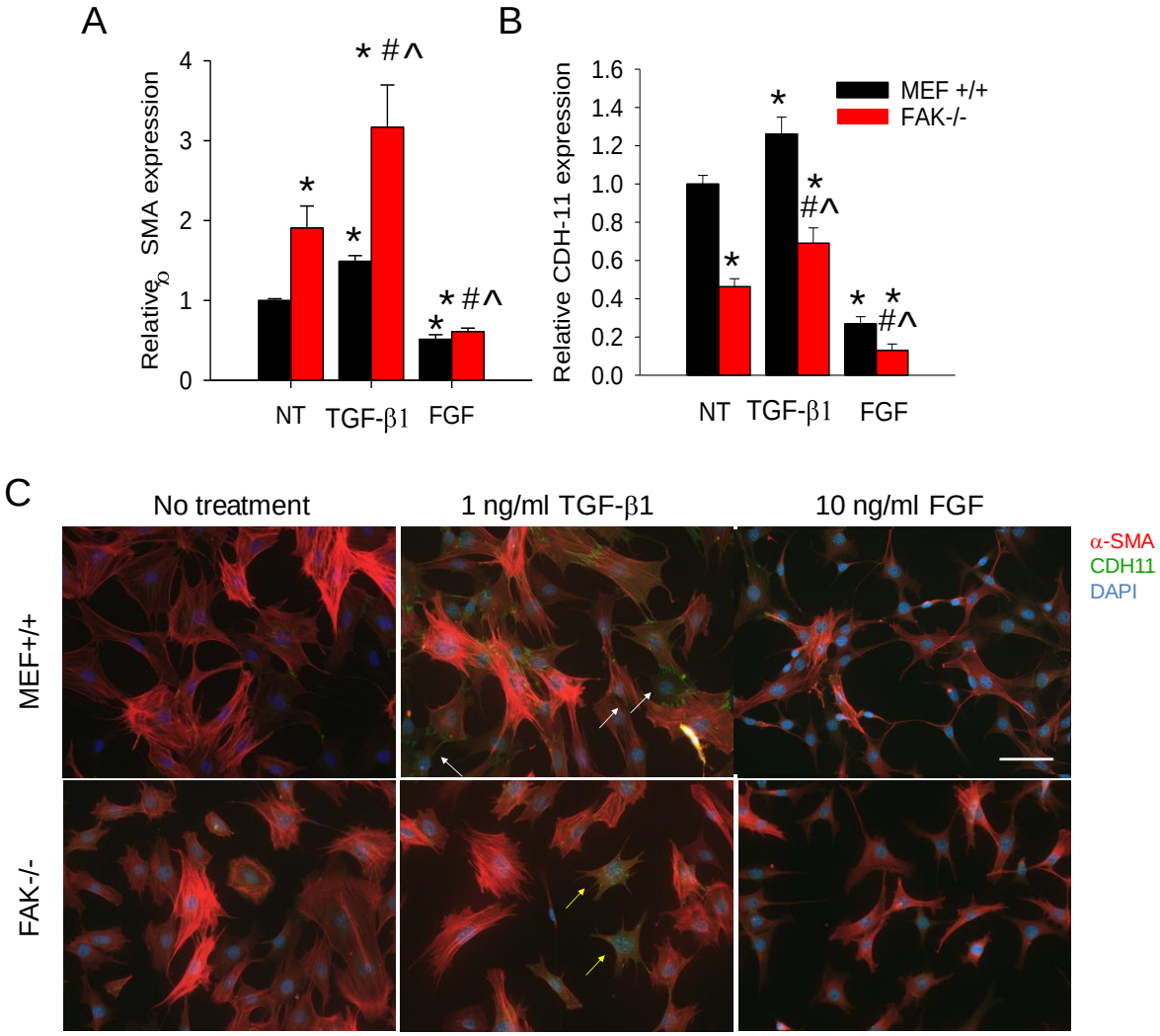

Figure 4.5. α-SMA and cadherin-11 (CDH11) are not necessarily coexpressed. α-SMA (A) and **c**adherin-11 (B) expression as measured via western blot, normalized to β-actin loading controls. TGF-β1 and FGF2 treated samples are significantly different from not treated controls and FAK-/- samples are significantly lower than MEF+/+ ($p < 0.05$). (C) Immunoflourescence of WT and FAK-/- MEFs plated on fibronectin coated coverslips and treated with 1ng/ml TGF-β1 or 10 ng/ml FGF2 for 24 hours. α-SMA is shown in red, cadherin-11 is shown in green, and nuclear stain is depicted as blue. Images taken at 20X magnification. White arrows indicate α-SMA-negative, cadherin-11 positive cells and yellow arrows indicate apparent transport defects in FAK-/- cells.

In addition to quantifying the effect of cytokine dose and FA protein removal, we wanted to assess the effect of mechanical stiffness on α-SMA and cadherin-11 expression. PDMS plates of stiffnesses ranging from 230 kPa to 2.1 MPa were made and coated with full length fibronectin. Cells seeded on this substrate should develop robust FAs containing activated β1 and β3 integrins. We hypothesized that these FAs would signal through Src and FAK in a stiffness dependent manner. After 24 hours of serum starvation, cells were lysed and prepped for indirect ELISA quantification of α-SMA production or western blot for cadherin-11 expression (**Figure 4.6**). We found a statistically significant interaction between cell type and substrate stiffness ($p = 0.009$). α-SMA production was significantly reduced when cells were cultured on PDMS, with the lowest α-SMA expression corresponding to a PDMS stiffness of 900 kPa. There was no significant difference between α-SMA expression on fibronectin coated TCP and uncoated TCP in either cell type. α-SMA in FAK-/- cells is significantly higher than in MEF+/+ ($p < 0.001$) on TCP (stiffness = 3E6 kPa) but is not statistically different at lower stiffness, indicating that the regulation of α-SMA in FAK-/- cells is more sensitive to changes in stiffness than in MEF+/+ cells. Cadherin-11 expression was significantly lower in FAK-/- cells across all stiffnesses and is less sensitive to changes in stiffness than α-SMA (Figure 4.6B). We did observe a significant decrease in cadherin-11 expression from TCP to 10:1 PDMS in MEF+/+ cells. The apparent importance of FAK in both α-SMA and cadherin-11 regulation points to an important regulatory role for ERK. Inhibition of ERK has been shown to increase α-SMA and prevent TGF-β1 induced cadherin-11 expression in porcine AVICs, but recent work in our lab suggests a more complex role for ERK that overlaps with the GSK-3β pathway [51]. These data

confirm that mechanotransduction through integrins plays a significant role in the regulation of MyoFB differentiation through integrins and FAK.

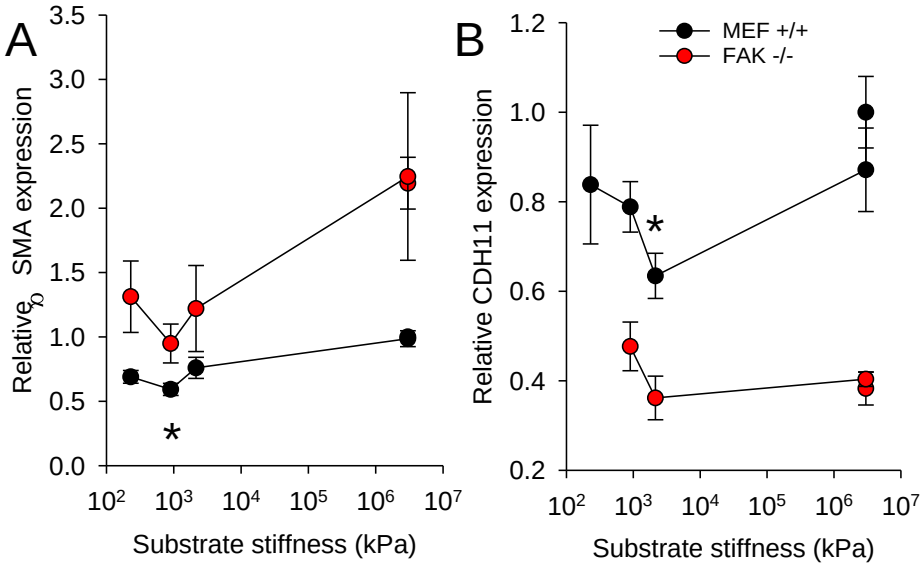

Figure 4.6. α-SMA and cadherin-11 are sensitive to stiffness and the presence of FAK. WT and FAK-/- MEFs were seeded on fibronectin coated PDMS of varying stiffnesses and α-SMA and cadherin-11 expression was determined by ELISA and western blot, respectively. * indicates significant differences from TCP. (Figure adapted from Schroer et al. 2014 [139])

We performed preliminary experiments probing canonical Wnt signaling with the GSK-3β inhibitor LiCl at a concentration of 20 mM in complete media. Western blot analysis confirmed a significant increase in phosphorylation of GSK-3β after 24 hours of LiCl treatment. In MEFs we observed a substantial increase in both cadherin-11 expression and α-SMA with LiCl alone. We further observed significant reduction of TGF-β1 induced cadherin-11 expression with LiCl treatment. LiCl did not seem to affect TGF-β1 induced increase in α-SMA expression, but did partially recover the FGF-induced decrease in both cadherin-11 and α-SMA (**Figure 4.7**).

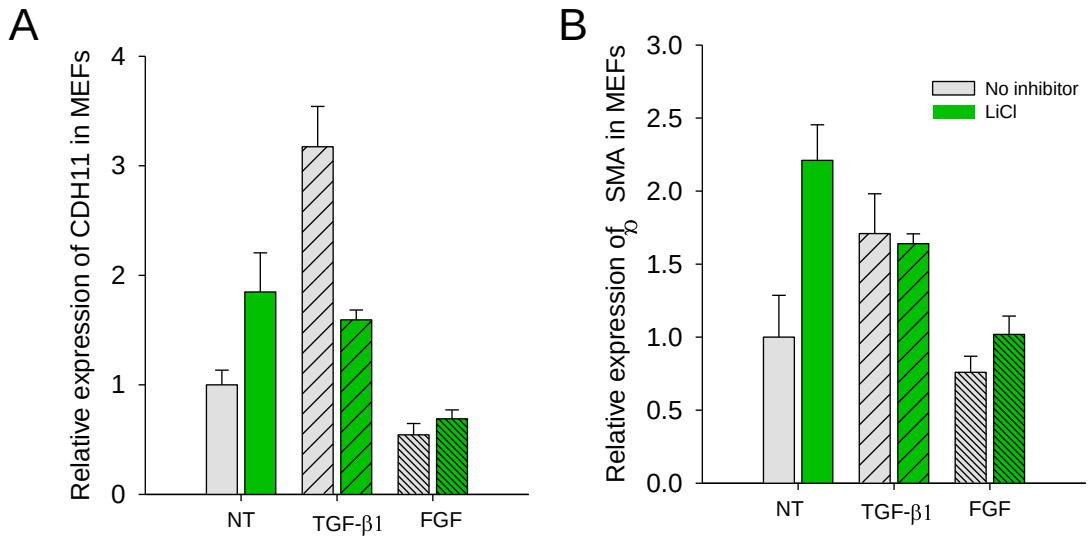

Figure 4.7. Expression of MyoFB markers after treatment with TGF-β1 and FGF2 with GSK-3β inhibition. Cadherin-11 and α-SMA expression determined by western blot. Data normalized to α-tubulin loading control.

Discussion

Using genetically modified MEFs, we have highlighted the importance of Src family kinases and FAK in the regulation of MyoFB differentiation. Our results demonstrate a profound inhibitory effect of removing Src, Yes, and Fyn on α-SMA production and stress fiber assembly. Densitometry of western blots revealed comparable levels of p38 and ERK phosphorylation in SYF-/- cells relative to MEF+/+ cells (data not shown), so the effect is likely operating through a different mechanism. It is likely that signaling downstream of Cas and other Src substrates is necessary for proper α-SMA synthesis. TGF-β1 signals to TGF-β activated kinase 1 and subsequent α-SMA production is significantly reduced with Src inhibition and the removal of FAK

[199]. This result is consistent with recent reports of Src's prominent role in non-canonical TGF-β1 signaling in the context of MyoFB differentiation [137].

Interestingly, the absence of FAK, a protein that is known to enhance Src activation and signal to p38, caused a significant increase in α-SMA. Given its complex role in multiple signaling cascades, it is not surprising that reports of the effect of FAK on MyoFB differentiation vary. Blocking FAK expression in cardiac fibroblasts with siRNA has been shown to decrease force induced α-SMA promoter activity [188]. Furthermore, it has been reported that α-SMA production in serum free conditions and after TGF-β1 treatment are higher in FAK expressing MEFs compared with FAK-/- counterparts [200]. Alternatively, others have reported that FAK is involved in FGF2 signaling to ERK in response to FGF2 cells, and FAK-/- cells contain enhanced α-SMA accumulation and persistence after treatment with FGF2 [89], [140]. Reduced basal ERK phosphorylation in FAK-/- cells has also been reported, and a model proposed for FGF2 signaling to ERK requiring FAK [89]. This informed the development of our model and is consistent with the decreased initial ERK phosphorylation and increased α-SMA that our model predicted. Additionally, we found that FGF2 was able to induce significant ERK phosphorylation and lower α-SMA in the absence of FAK, which indicates that FAK is not required for FGF2 and ERK based inhibition of α-SMA.

Surprisingly, our time course results show that ERK phosphorylation in non-treated FAK-/- cells is not significantly different from MEF+/+ at 24 hours and is significantly higher at 30 minutes. Sensitivity analysis of the model predicted that FAK-/- cells would be more sensitive to changes in TGF-β1 and FGF2. Our experimental results seem to confirm that FAK-/- cells have a higher sensitivity to environmental

perturbations when the media is changed at the start of the time course. ERK's specific role in α-SMA regulation has also presented in multiple perspectives. Some have argued that ERK is necessary for TGF-β1 induced activation [200], [201], while others proposed a largely inhibitory role [85], [89], [140], [202] . Several groups have shown that MEK1/2 inhibition significantly increases α-SMA expression in fibroblast-like cells [51], [203] [46, 109]. One of the goals achieved in this project was to investigate the possibility of matching the observed upregulation of ERK by TGF-β1 and FGF2 in a model with a relatively straightforward α-SMA regulatory scheme inversely proportional to pERK.

Another main goal of this project was to clarify the interactions between growth factor and integrin signaling in the regulation of MyoFB differentiation. We first showed that decreasing substrate stiffness can significantly lower the expression of α-SMA in MEFs through a fibronectin-integrin interaction that is significantly altered in FAK-/- cells (**Figure 4.6**). Sensitivity analysis of our network model predicted that FAK-/- cells would be more sensitive to changes in stiffness, which we observed in the experimental data (**Figure 4.6A**). The relationship between α-SMA and stiffness has been shown previously and is correlated with changes in p38 activation [42]. Both β1 and β3 integrins have been shown to have mechanosensitive capabilities and are involved in outside-in signaling to intracellular kinases like FAK and Src [129], [179]. β3 integrins are known to interact with TGF-β1 signaling to Src and p38 [204] and are a likely target for further insights.

All of the work reported in Schroer et al. 2014 ([139]) used relative α-SMA expression as a metric of MyoFB differentiation. While it is a key and widely recognized

marker of the MyoFB phenotype, it is not the only indicator of an active fibroblast. Expression of ECM protiens, including collagen-1 and fibronectin EDA, and the cell-cell adhesion protein cadherin-11 are also important markers of an activated fibroblast [44], [88]. Understanding the heterogeneity within fibroblast/MyoFB population can be especially important to understand the function of CFs after MI [13].

We also observed that while cadherin-11 expression in MEFs changes similarly to α-SMA in response to both TGF-β1 and FGF2, its expression is inversely affected by the absence of FAK. This further confirms a critical regulatory role for FAK in controlling the MyoFB phenotype. We also observed a decrease in cadherin-11 expression with on 900 kPa PDMS relative to plastic, though there was no significant change in FAK-/- cells. Interestingly, in both MEF+/+ and FAK-/- cells, cadherin-11 expression appears to be trending upwards on softer PDMS samples. It is possible that fibroblast populations on softer, more physiologically relevant, substrates have more innate heterogeneity of phenotype and protein expression. While an increase in cadherin-11 after TGF-β1 treatment has been well established, a corresponding reduction after treatment with FGF has not been reported. The fact that cadherin-11 expression was drastically decreased by FGF2 is consistent with a key function to promote quiescence in fibroblasts, but the mechanism of this effect is still largely undefined.

Our first step to determining a potential mechanism, we observed a reversal of both TGF-β1 and FGF2 effects' on cadherin-11 expression with the inhibition of GSK-3β. These results suggest that GSK-3β also has a significant role in regulating MyoFB differentiation and influences TGF-β1 and FGF2 signaling. GSK-3β has been reported to regulate cadherin-11 expression [205] and is known to play important roles in healing

after MI [206]. The Wnt pathway has significant crosstalk with TGF-β1 in the progression of fibrosis and plays important roles in the origin of MyoFBs after MI [14]. By signaling through β-catenin, it also has some natural cross-talk with signaling downstream of cadherins, including cadherin-11 [48]. Signaling downstream of cadherin-11 has also been reported to act through p38 and ERK specifically [207]. Future studies are needed to elucidate signaling downstream of cadherin-11.

There are several important limitations to the conclusions of this work that must be acknowledged. While they can be a powerful tool, cell-lines with a permanent deletion of signaling proteins often compensate by altering expression of other related proteins, which can have confounding effects on signaling studies. Repetition of these studies using an inducible knock-down cell line, siRNA, or a small molecule inhibitor would help to support the postulated mechanisms and confirm acute effects on signaling and myofibroblast regulation. Future studies could also probe the phosphorylation of both Src and FAK over the time course of activation and in response to the various conditions mentioned. Direct integrin blocking with a blocking antibody or knock-down with siRNA, would give more fine detail into the roles of specific integrin subtypes on intracellular signaling. The range of stiffnesses used in this study was intended to span from measured fibrotic tissue stiffness to traditional cell culture plastic [198]. The stiffness of 900 kPa approximately matches the stiffness of the Flexcell plates used in the Merryman lab to probe the effect of active strain on cellular phenotype. Healthy cardiac tissue is generally much softer, between 10 and 50 kPa depending on the measurement modality, so while the PDMS substrates are certainly softer than tissue culture plastic, they are not in a physiologic range. Furthermore, all of

these experiments were performed on 2D culture, which promotes adhesion formation very different from the adhesions formed in 3D environments [45].

Our results indicate that Src family kinases are crucial for α-SMA synthesis in fibroblasts and demonstrate that FAK plays an important role in integrating signals for the regulation of α-SMA and cadherin-11 production during MyoFB differentiation. They also confirm significant interaction between growth factor and integrin signaling through the MAPKs p38 and ERK. Finally, they suggest that cadherin-11 may have a critical role in both MyoFB function and regulation. Cadherin-11 expression is increased by TGF-β1 signaling and sensitive to changes in substrate stiffness, both of which are relevant in healing after MI.

CHAPTER 5

AIM 2: CADHERIN-11 EXACERBATES TISSUE REMODELING AFTER MYOCARDIAL INFARCTION

Text for Chapter 5 adapted in part from:

[208] **Schroer, A.K.**, Clark, C., Zhang, Q., Sanders, L.H., Hatzopoulos, A.K., Lal, H., Force, T., Merryman, W.D., *Cadherin-11 exacerbates inflammation and maladaptive remodeling after myocardial infarction.* Circulation Research, 2016. **(submitted)**.

Introduction

Over one million Americans experience a myocardial infarction (MI) every year, and the resultant cardiac remodeling significantly reduces function and increases risk of subsequent infarctions and heart failure. The process of infarct healing requires complex interactions between resident and recruited cells that must coordinate the clearance of damaged tissue and replacement with a stable and robust collagen scar to prevent cardiac rupture. However, excess repair activity can ultimately lead to expansion of the infarct area and worsened cardiac function.

Developing treatment strategies for MI is made particularly challenging by the precise and necessary timing of both chemical signals and cellular activity. Many treatments targeting specific growth factor cascades have failed to maintain the delicate balance between necessary and excessive inflammation and fibrosis. Furthermore, broad target treatments can often have adverse side effects on the surviving

cardiomyocytes (CMs), causing additional loss of contractile potential [209]. An ideal therapy for MI would reduce without completely blocking both the initial inflammatory response and later progression of fibrosis.

One protein whose role in other inflammatory and fibrotic cell processes has recently been described is cadherin-11 (CDH11), a cell-cell adhesion protein expressed by activated fibroblast-like cells in multiple inflammatory and fibrotic disease models. Cadherin-11 has recently been shown to play key roles in the progression of both arthritis and pulmonary fibrosis, but its function in infarct healing has not been studied [25], [210].

Cadherin-11 engagement promotes the expression of the inflammatory cytokine IL-6 as well as profibrotic signaling factors and MyoFB markers in joints, lungs, and heart valves [23], [51], [163], [210]. Established inflammation-induced fibrosis in the lungs has been reversed by treatment with functional blocking antibody against cadherin-11 [25]. Mechanosensitive signaling through cadherin-11 affects both inflammation and fibrosis, two key phases of remodeling after MI, but the details of this signaling are still poorly understood. The objective of this work is to clarify the role and function of cadherin-11 in the dynamic chemical and mechanical context of myocardial remodeling. We hypothesize that preventing cadherin-11 adhesion in CFs will reduce inflammation-driven infarct expansion and fibrotic scar formation after MI and improve cardiac outcomes.

Methods

Mice

Vanderbilt University biomedical research programs are supported by a comprehensive Animal Care and Use Program (ACUP) that has been fully accredited by AAALAC since 12/1967 (PHS Animal Welfare Assurance No. A3722-01). All animal procedures were performed in accordance with the Vanderbilt IACUC approved protocol M/15/126. Cadherin-11 transgenic mice [209] were given to us by collaborators. These mice were maintained on a C57BL/6J background, and both CDH11-/- and WT littermates were used for experiments. C57BL/6J male mice (Jackson Labs) were purchased between 12 and 16 weeks of age for MI surgeries. All mice were given pre and post-op analgesic of 5mg/kg ketoprofen every 24 hours for 72 hours. For the antibody treatment study, mice were administered an intraperitoneal (IP) injection every four days beginning one day after surgery, consisting of 10mg/kg of a functional blocking antibody against cadherin-11 (SYN0012) or an isotype control antibody (IgG2a) dissolved in sterile saline. The last treatment was given on day 17 after infarct.

Quantification of heart function and size by echocardiography

Ejection fraction and LV volume were measured from m-mode images of the short axis of hearts captured on the Vevo 2100 system. At least 6 independent measures of LV diameter and wall thickness were used for each mouse for each time point. Ejection fraction and LV Volume were calculated from the measured LV inner diameter at diastole and systole.

Measurements were made before surgery, and at seven, twenty-one, and fifty-six days after surgery. Mice whose ejection fraction was reduced by less than 5% or greater than 60% were excluded from subsequent analysis to ensure that all mice included had reasonably consistent, intermediate to large infarcts that had not

progressed to complete heart failure. Mice were euthanized in a CO_2 chamber in accordance with university guidelines at three, seven, twenty-one and fifty-six days after infarct.

Identification of non-CM cell types by flow cytometry

Relative contributions of different cell types were measured by flow cytometry [13]. Hearts were isolated from animals at three or seven days after sham or MI surgeries and immediately placed in a solution of ice cold 5% FBS in PBS. The atria were removed and the ventricle tissue was minced and stored on ice. Two mLs of digest solution comprised of 10 mg/ml of type II collagenase in dispase was added to each sample, and then incubated at 37 degrees for seven minutes. The digested sample was filtered through a 100 μm cell strainer and resultant cells were washed in 50 mLs of ice cold PBS, and refiltered through a 70 μm cell strainer. Red blood cells were lysed with Gey's solution and cells were washed again in PBS and counted to measure the total number of viable, non-CM cells. 500 thousand cells were then taken from each sample, suspended in DAPI to identify dead cells, blocked with Fc antibody, and then stained for Ter119 (eBioscience), CD45 (BD Bioscience), CD31 (Biolegend), and CD11b (Tonbo biosciences).

Windowing based on size, shape and negative staining for DAPI and Ter119 was used to identify viable single cells. Further windowing based on full panel minus one stained controls, was used to identify distinct cell populations relevant to our study. We identified leukocytes ($CD45^{high)}$, inflammatory monocytes ($CD45/CD11b^{high}$), endothelial cells ($CD31^{high}$,$CD45/CD11b^{low}$), fibrocytes ($CD31/CD45^{low}$,$CD11b^{high}$), and fibroblasts ($CD31/CD45/CD11b^{low}$).

Cryosectioning and trichrome stain/histological assessment

Hearts were dissected into PBS, weighed, and then submerged briefly in a KCl solution to relax the CMs. They were then sliced in half in the transverse plane (orthogonal to the long axis of the heart) and mounted in OCT media and frozen. They were subsequently cryosectioned into 10 μm thin sections and stored at -20C. A selection of the slides were stained with Masson's trichrome (sigma) according to the manufacturers instruction to identify regions of healthy myocardium (red/pink), ECM (blue), and cell nuclei (black). Before staining, sections were thawed, the OCT media was dissolved in PBS, and the sections were fixed in Bouin's fluid. To quantify scar length and thickness, we measured the fractional length and average radial thickness of 4 sections each at least 300 μm distant from each other.

Immunohistochemistry

Non-conjugated antibodies (CDH11, CD45, IL-6) were incubated on the sample overnight at 4 degrees at a 1:100 dilution in 1% BSA, then rinsed with PBS and incubated with fluorescently tagged secondary antibodies for 1 hour at a 1:300 dilution in 1% BSA. The rest of the antibodies were directly conjugated and were incubated on the sample at a 1:100 dilution in 1% BSA for 1 hour at room temperature. Slides were mounted in prolong gold with DAPI mounting media to stain the nuclei and imaged on an Olympus scope.

AFM

After thawing frozen sections and dissolving the OCT in PBS, tissue sections were blocked in 10% FBS for 20 minutes, and stained for α-SMA (sigma) or a Hoest

nuclear stain (invitrogen) for 20 minutes. This staining allows for visualization of the infarct while scanning, which is performed in PBS (Online Figure II). We used a Biocatalyst AFM developed by Bruker to measure topography and stiffness of 10x10 μm areas within the infarct (at least 5 per mouse from at least 2 sections). We used a blunted pyramidal tip specifically developed for soft biological samples (MLCT-Bio) and the peak force quantitative nanomechanical mapping scanning mode that provides robust measurement of topography and elastic modulus. Each day before scanning samples, the spring constant and deflection sensitivity of the probe was calculated, and the system was calibrated on a 40 kPa polyacrylamide gel.

Quantification of α-SMA protein by western blot

Protein was isolated from the organic phase of the TRIZOL samples according to manufacturers' instructions and equal amounts of protein for each sample were run on an 8% polyacrylamide gel to separate by size. After transferring and blocking, α-SMA and the loading control α-tubulin was identified with fluorescently tagged antibodies and scanned on a LICOR scanner. Densitometry analysis was performed in the image studio software, and α-SMA signal was normalized to alpha tubulin.

Cell isolation and culture

To complement and inform our *in vivo* studies, we isolated cardiac fibroblasts [211] and intraperitoneal MΦs from mice. CFs were isolated from WT and CDH11-/- mice that had been bred with the immorto mouse line, so that cells from littermate controls could be cultured for longer. Hearts were isolated from 8 week old mice, minced, and digested in 2% collagenase solution supplemented with trypsin for the last

10 minutes of a 40 minute digest. CFs were then rinsed and plated on gelatin coated plates, and cultured in DMEM supplemented with 10% FBS, 1% penicillin/strep, and gamma interferon at 33 degrees to maintain the immortalized phenotype. Cells were replated in DMEM supplemented with 10% FBS and 1% penicillin/strep and grown at 37 degrees for 48 hours to deactivate the immortalized gene.

MΦ exfiltration was stimulated by IP injection of 1mL of 4% thioglycollate media three days before isolation. Mice were sacrificed and the interperitoneal cavity flushed with 10 mLs of cold RPMI media to collect the cells. After washing in cold PBS, cells were plated in RPMI media supplemented with 10% FBS on tissue culture plastic and allowed to adhere for 1 hour. Non-adherent cells were then rinsed away, and the remaining cells should all be MΦs [212].

Gel contraction assay

CFs were diluted to a final concentration of 250k cells/mL in a 1.28 mg/ml collagen solution derived from PureCol (Advanced Biomatrix) to a final concentration of 250 thousand cells/ml and were poured into a Teflon ring in a suspension well. After polymerizing for 1 hour, media was added to flood the well and release the gels from both the bottom of the well and the Teflon ring. The gels were imaged immediately after release and at different times over the next 48 hours, and the area of the gels measured and normalized to the original area of the gel. For comparison of IgG2a and SYN0012, antibody was added to the cell/gel mixture before pouring for a final concentration of 20 μg/ml, and media added to the well also contained 10 μg/ml of antibody.

I-wire contraction assay and measurement

CFs were diluted in an identical collagen solution as the one used in the floating gel assay and added to a PDMS channel about 10 mm in length with wires crossing through the channel near the ends (more information about I-wire platform can be found in Chapter 6). After polymerizing for 1 hour, media was added. Over the course of a week, the fibroblasts contract the matrix to form a linearized construct supported by wires on each end, but suspended in media along the length of the channel. After 7 days (changing media every 2 days), a calibrated probe was used to measure the passive tension in the construct in response to increasing extension. Stage displacement drives the probe into the construct, applying a transverse force and resulting in simultaneous probe deflection and construct stretch. Deflection of the probe was measured and used to calculate the stretch and tension in the construct, and a quadratic fit was used to calculate the predicted intrinsic stress present in the construct as formed.

qPCR

For assessment of *in vivo* transcription, hearts were isolated under RNAse-free conditions and immediately flash frozen until the time of analysis. Samples were subsequently thawed and lysed in TRIZOL, with chloroform induced phase separation to isolate mRNA according to manufacturers' instruction. cDNA was synthesized using the Superscript IV kit (Invitrogen) from 500 ng of mRNA. Real time qPCR was performed to amplify specific targets from the cDNA by mixing it with SYBR green master mix (BIO-RAD) and primer sets (**Table 5.1**). The BIO-RAD CFX96 C1000 system was used to quantify relative transcription. For all of the *in vivo* results we

averaged the three- and seven-day sham values these and normalized all post-MI samples to this value.

Table 5.1 qPCR primers

Target	Forward	Reverse
GapDH	ATGACAATGAATACGGCTACAG	TCTCTTGCTCAGTGTCCTTG
cTnT	AGGAGCTGATTTCCCTCAAAG	TTTCCTTCTCCCGCTCATTG
Cdh11 exon12	TCACTATCAAAGTCTGTGGCTG	CAAACAGCACAACGATGACC
IL-6	CAAAGCCAGAGTCCTTCAGAG	GTCCTTAGCCACTCCTTCTG
F4/80	ACC ACA ATA CCT ACA TGC ACC	AAG CAG GCG AGG AAA AGA TAG
IL-1β	TCCTGTGTAATGAAAGACGGC	ACTCCACTTTGCTCTTGACTTC
TNFα	AGACCCTCACACTCAGATCA	TGTCTTTGAGATCCATGCCG
MMP13	GATTATCCCCGCCTCATAGAAG	TCTCACAATGCGATTACTCCAG
MMP3	CAGGAAGATAGCTGAGGACTTTC	GGTCAAATTCCAACTGCGAAG
TGF-β1	CCTGGGTTGGAAGTGGATC	TTGGTTGTAGAGGGCAAGG
α-SMA	GAGAAGCCCAGCCAGTCG	CTCTTGCTCTGGGCTTCA
collagen 1	CACCCTCAAGAGCCTGAGTC	GTTCGGGCTGATGTACCAGT
FGF2	GGAGTTGTGTCTATCAAGGGAG	TGCCCAGTTCGTTTCAGTG
VEGFa-1	AAAGCCAGCACATAGGAGAG	CGAGTCTGTGTTTTTGCAGG
Flk1	TGCGGGCTCCTGACTACACTAC	TTCCCAAATGCTCCACCAACTCTG
Mrc1	ATGGATGTTGATGGCTACTGG	TTCTGACTCTGGACACTTGC
Cd14	CCTTTCTCGGAGCCTATCTG	CAACTTTCCTCGTCTAGCTCG
Arg1	AAGAATGGAAGAGTCAGTGTGG	GGGAGTGTTGATGTCAGTGTG

Quantification of IL-6 production by indirect ELISA

Fifty thousand CFs were plated in a 12 well plate, allowed to adhere for 20 min, and then supplemented with media containing between 0 and fifty thousand MΦs, for a final volume of 1.3 mLs per well. We tested the interaction of cells (including MΦs alone) without antibody treatment, and then specifically compared CFs and a range of co-culture with IgG2a or SYN0012. These samples were incubated with antibody for 15 minutes before plating. After 48 hours in culture, conditioned media was removed from wells and IL-6 expression over this period was measured with a Duoset mouse IL-6

ELISA (R&D Systems). After boiling, 100 μl of each samples were added to the prepared ELISA plate, and the IL-6 expression was measured in duplicate and compared against a provided standard.

Statistical analysis

For all experiments measuring outputs across a range of time points and treatments, a two-way ANOVA was run to determine significant effects of time and treatment, and interactions between the two. The Holms-Sidak method and individual student t-tests with an overall significance level of 0.05 were used for multiple comparisons within cell-type and treatment groups. Non-parametric tests (ANOVA on ranks or rank sum tests) were used if the samples failed the Shapiro-Wilks normality test or had unequal variance ($p < 0.05$). F-tests were run on median stiffness values to compare variances of tissue stiffness.

Results

Establishing relevance of cadherin-11 after MI

The first step in our investigative process was to determine if, when, and where cadherin-11 is expressed after MI. We first confirmed that CM have significantly less transcription of cadherin-11 relative to non-CMs (**Figure 5.1A**). This confirms what had been reported in the literature, that CMs do not express cadherin-11 [50], and led us to focus subsequent experiments on the non-CM cellular population. We next established relevance of cadherin-11 to healing after MI by assessing transcription of cadherin-11 after MI, which rose to the highest fold change we observed in the course of these

experiments with a significant, 10-fold increase above sham control hearts at day seven after infarct (**Figure 5.1B**). While we did not measure cadherin-11 in untreated mice at 21 days, mice treated with either IgG2a or SYN0012 had similar fold-increase in cadherin-11 transcription relative to sham at day 7, and both groups' transcription dropped notably between day 7 and day 21 (Figure 5.9B), from roughly 7-fold to 3-fold. Having determined when cadherin-11 transcription is upregulated, we wanted to confirm literature reports of the rough make-up of non-CM cell populations in the heart after MI, especially at days 3 and 7 after MI. As expected, the total non-cardiomyocyte cell population increased significantly after MI (**Figure 5.1C**), consisting of a large population of inflammatory monocytes $(CD45/CD11b)^{high}$ at day three, which had significantly shrunk by day seven after MI. There was also a significant increase in fibroblasts $(CD45/CD31/CD11b)^{low}$ cells at three days, which had not significantly decreased by day 7. Co-staining of a 7-day post-MI heart revealed significant cadherin-11 staining in MΦs (CD45+ and F4/80+), endothelial cells (CD31+ and CD45-), smooth muscle cells and MyoFBs (α-SMA+) (**Figure 5.1D)**, indicating that all three of these cell types may be playing a role in the dynamic process of healing after infarct. With a peak in cadherin-11 transcription at day 7, when inflammation has largely subsided, it seems likely that MyoFBs are important cadherin-11 expressers.

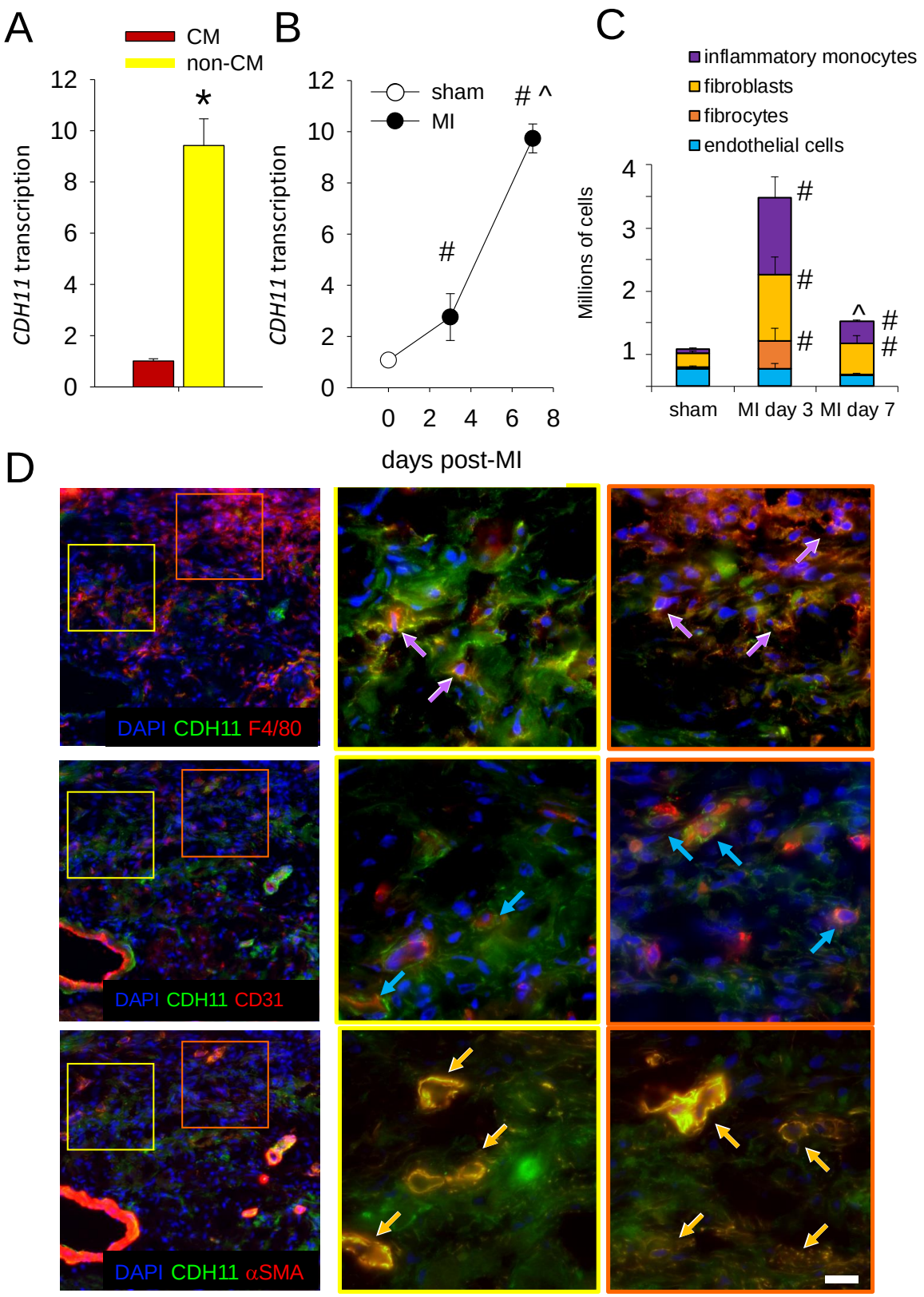
A
CM
non-CM
*
CDH11 transcription
12
10
8
6
4
2
0
B
sham
MI
^
#
CDH11 transcription
days post-MI
0 2 4 6 8
C
inflammatory monocytes
fibroblasts
fibrocytes
endothelial cells
Millions of cells
sham
MI day 3
MI day 7
D
DAPI CDH11 F4/80
DAPI CDH11 CD31
DAPI CDH11 αSMA

Figure 5.1 Cadherin-11 is expressed after myocardial infarction. Cadherin-11 (CDH11) transcription was significantly higher in the non-cardiomyocyte (non-CM) cell population relative to cardiomyocytes (CM) (* indicates $p < 0.05$) (**A**). Transcription of cadherin-11 was significantly increased (# indicates $p < 0.05$ relative to sham) at both three and seven days following MI (**B**), and was significantly higher at seven days than three days (^ indicates $p < 0.05$ difference between days). The noncardiomyocyte (non-CM) cell population changed after MI (**C**) as measured by flow cytometry. There was a significant increase in the number of inflammatory monocytes (CD45+/CD11b+), and fibroblasts (CD45-/CD31-/CD11b-) at both time points, no change in the number of endothelial cells (CD45-/CD31+), and a significant decrease in resident MΦs from day three to day seven after MI. n = 3 mice per group. Immunostaining confirmed the presence of cadherin-11 expressing MΦs, endothelial cells, and MyoFBs in the infarct region seven days after MI (D). Arrows indicate the location of the cells in magnified callouts.

Comparison of WT and CDH11-/- animals

We next measured the effect of MI in WT vs. cadherin-11 null (CDH11-/-) animals and observed significant improvement of both ejection fraction and systolic LV volume in CDH11-/- animals relative to WT at seven days, but these differences did not persist to day twenty-one (**Figure 5.2A-B**). Immunostaining confirmed the presence of cadherin-11 in the infarct of the WT mice at twenty-one days after infarct (**Figure 5.2C**), and trichrome images suggest that the collagen in the infarct at twenty-one days is less compacted in the CDH11-/- animals (**Figure 5.2D**). Finally, a collagen gel contraction assay revealed a significant reduction in contractility of CDH11-/- CFs (**Figure 5.2E**), which has been reported [167]. This results confirm a functional role for cadherin-11 in the process of myocardial remodeling after MI. However, a global knockout can have subtle, negative effects on heart structure that may explain the transience of the beneficial effect. In any case, since there is no known clinical link between cadherin-11 mutations and human disease, we transitioned to studying a more clinically relevant strategy targeting cadherin-11 adhesion after MI.

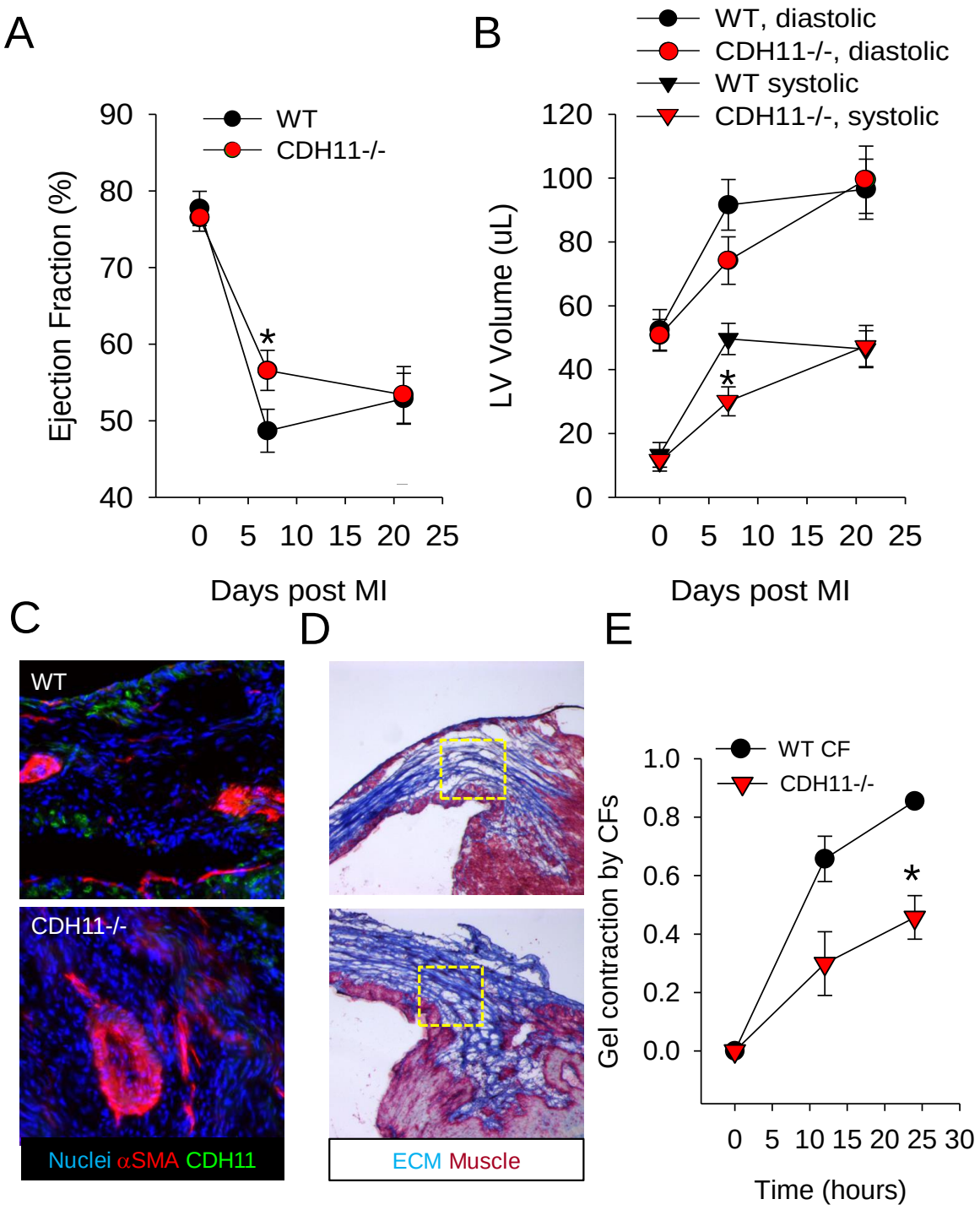

Figure 5.2 Cadherin-11 null (CDH11-/-) hearts respond differently to MI. Comparison between wild type (WT) and CDH11-/- mice ejection fraction (A) and LV volume (B) as measured by echocardiogram following infarct. n ≥ 3 mice per group. Immunostaining of MyoFB markers in the infarct at twenty-one days (C) and trichrome images of the infarct (yellow dashed area indicates approximate area of images in C) to visualize scar thickness (D). Results of gel contraction assay using WT or CDH11-/- cardiac fibroblasts embedded in a floating collagen gel (E). n = 3 gels. * indicates $p < 0.05$ relative to WT.

Comparison of function with IgG2a or cadherin-11 blocking antibody (SYN0012)

Treatment with a blocking antibody against cadherin-11 has been shown to have beneficial effects in the case of both rheumatoid arthritis and pulmonary fibrosis, which supported the hypothesis that a similar strategy would prove efficacious after MI. Having identified injury-induced cadherin-11 expression in multiple non-CM cell types after MI, we moved on to test a cadherin-11 blocking antibody (SYN0012) treatment. We observed a small increase in survival ($p = 0.16$) (**Figure 5.3A**) and an increasingly improved ejection fraction (**Figure 5.3B**) in the SYN0012 treated group relative to controls over the entire time of the experiment (eight weeks). Furthermore, significantly increasing dilation of the left ventricle observed in the IgG2a treated mice was curtailed in the animals receiving the blocking antibody, resulting in improved, reduced ventricle volume at twenty-one and fifty-six days post-MI, in both diastole (**Figure 5.3C**) and systole (**Figure 5.3D**). These results were very exciting, supporting the hypothesized role of cadherin-11 as a regulator of both inflammation and fibrosis and further its suitability as a therapeutic target.

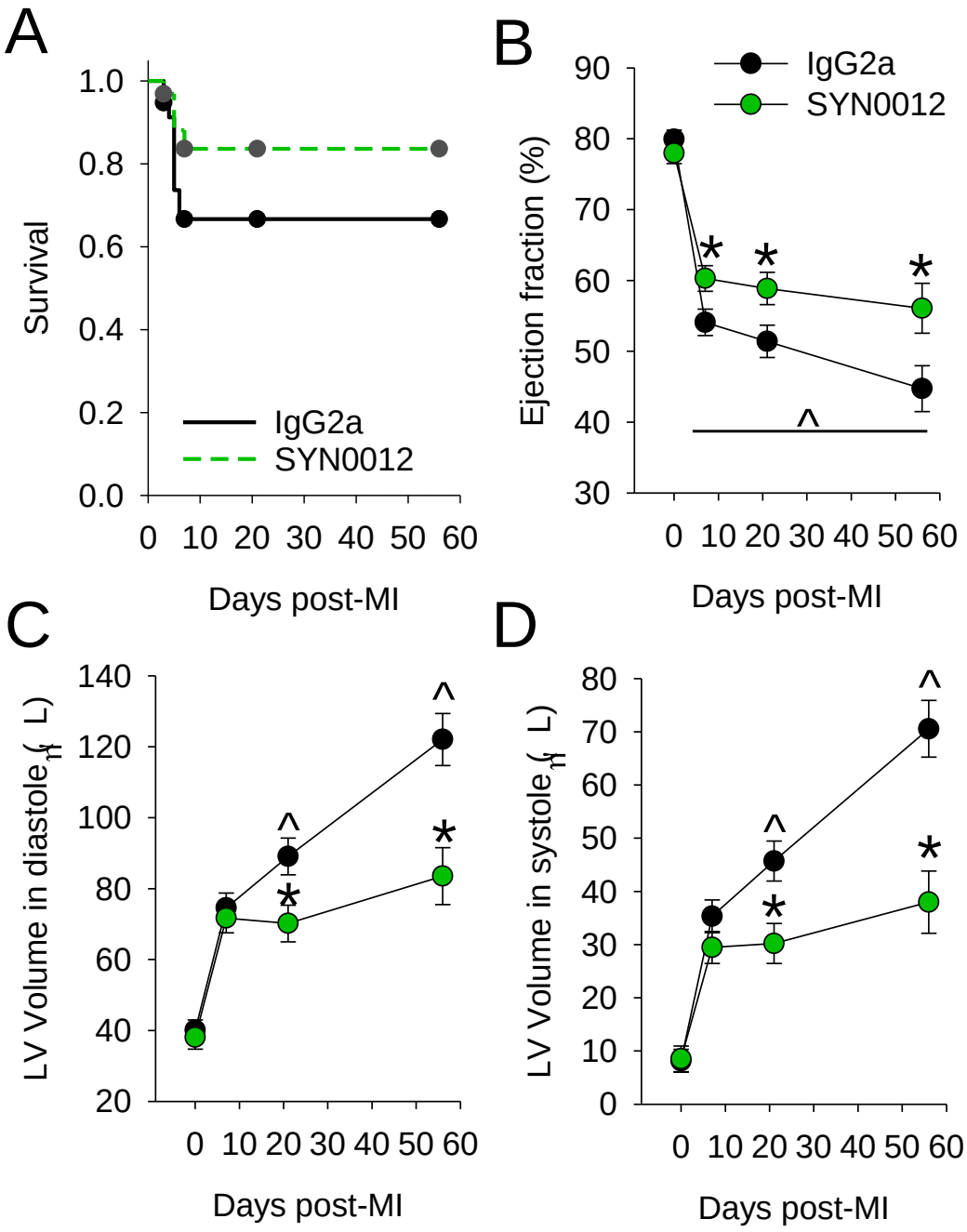

Figure 5.3 Cadherin-11 blocking antibody treatment improves outcomes after MI. Mice were treated with cadherin-11 blocking antibody (SYN0012) or isotype control (IgG2a) for twenty-one days beginning 1 day after infarct. Fewer animals receiving SYN0012 treatment compared with IgG2a ($p = 0.16$) died in response to the large infarct (A). $n \geq 33$ mice per group initially. While ejection fraction (B) and left ventricular volume (C,D) was significantly changed from baseline in all groups, treated animals had significantly improved ejection fraction and reduced LV expansion compared to controls (* indicates $p < 0.05$ difference between treatments). $n \geq 8$ mice. Furthermore, the significant change over time observed in control animals (^ indicates $p < 0.05$ difference between timepoints) was prevented by treatment.

Comparison of remodeling with IgG2a or cadherin-11 blocking antibody (SYN0012)

We further assessed tissue properties with AFM and measured a significant decrease relative to sham animals in infarct tissue stiffness at seven days in both groups (**Figure 5.4A**). The mean and median stiffness measurements were lower in the IgG2a treated animals compared to the SYN0012 stiffness at day seven, and the variability was significantly less than both sham and SYN0012 animals. However, by day twenty-one, both groups stiffened significantly, their mean and median stiffness rising above the sham myocardial stiffness. The range of measured stiffnesses in the IgG2a treated hearts exceeded the time-matched SYN0012 group, especially at 56 days-post MI. These results suggest that during the first week after infarct, more tissue breakdown (and subsequent softening) occurs in the IgG2a treated hearts compared to SYN0012. Between week one and three, both groups appear to experience similar stiffening with the creation of a collagen scar, but there is more heterogeneity in the properties of the scar in the control group. Histologic assessment revealed that scars in SYN0012-treated animals spanned a lesser fraction of the circumference of the left ventricle at both twenty-one and fifty-six days after MI and were thicker in the radial direction (**Figure 5.4B-D**). Western blots also revealed a decrease in α-SMA expression at twenty-one days after infarct (**Figure 5.4E**). These findings indicate that infarct expansion due to inflammation and myofibroblast-driven scar compaction and remodeling were both reduced by SYN0012 treatment.

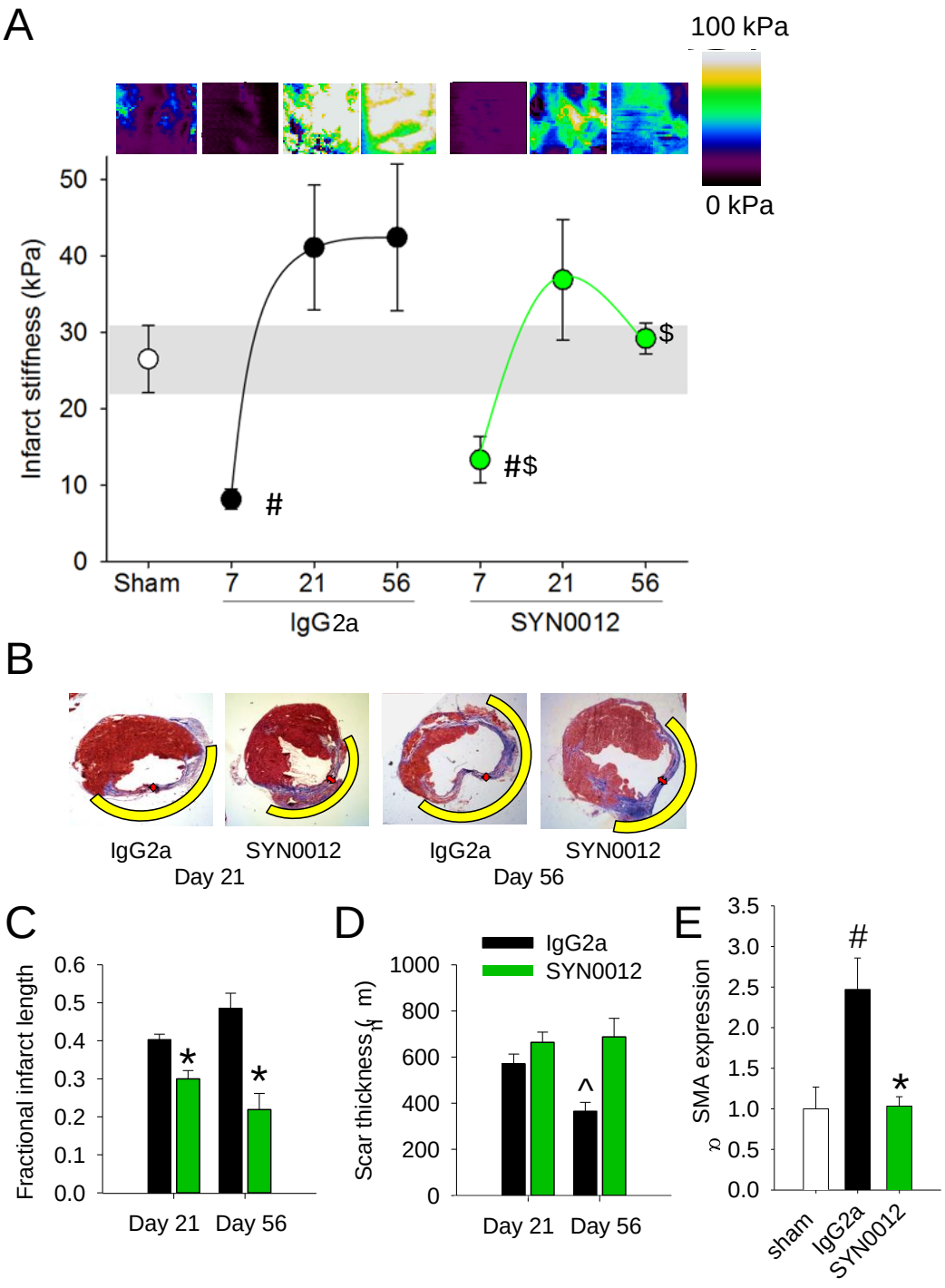

Figure 5.4 SYN0012 reduces infarct remodeling and MyoFB differentiation. Atomic force microscopy was used to measure median stiffness of 10x10 μm regions throughout the infarct over time. Colormaps of representative scans are depicted above the corresponding plot of average median stiffness (A). Representative trichrome sections (B) used to quantify the relative length of the infarct (C) and the scar thickness (D). Western blot revealed that α-SMA was significantly reduced at twenty-one days after infarct in the treated animals (E). # indicates $p < 0.05$ relative to sham, ($ indicates $p < 0.05$ relative to variance of IgG2a, * indicates $p < 0.05$ between treatment, ^ indicates $p < 0.05$ relative to previous timepoint. $n \geq 3$

CF contractility with IgG2a or cadherin-11 blocking antibody (SYN0012)

We next wanted to determine whether CF contractility was similarly affected by blocking cadherin-11 engagement as by removal of cadherin-11. A gel contraction assay (n=3) showed no difference in bulk gel contraction between IgG2a treated and SYN0012 treated CFs (**Figure 5.5A**). There was also no change in lateral compaction in the I-wire construct mold, but assessment of the intrinsic stress developed in the construct after seven days using a parabolic fit to the passive elasticity/stress curve (**Figure 5.5B**) revealed a significant decrease in intrinsic stress developed under linearized tension in the SYN0012 treated samples (**Figure 5.5C**). These findings highlight a functional difference between a genetic knock-down and blocking antibody treatment.

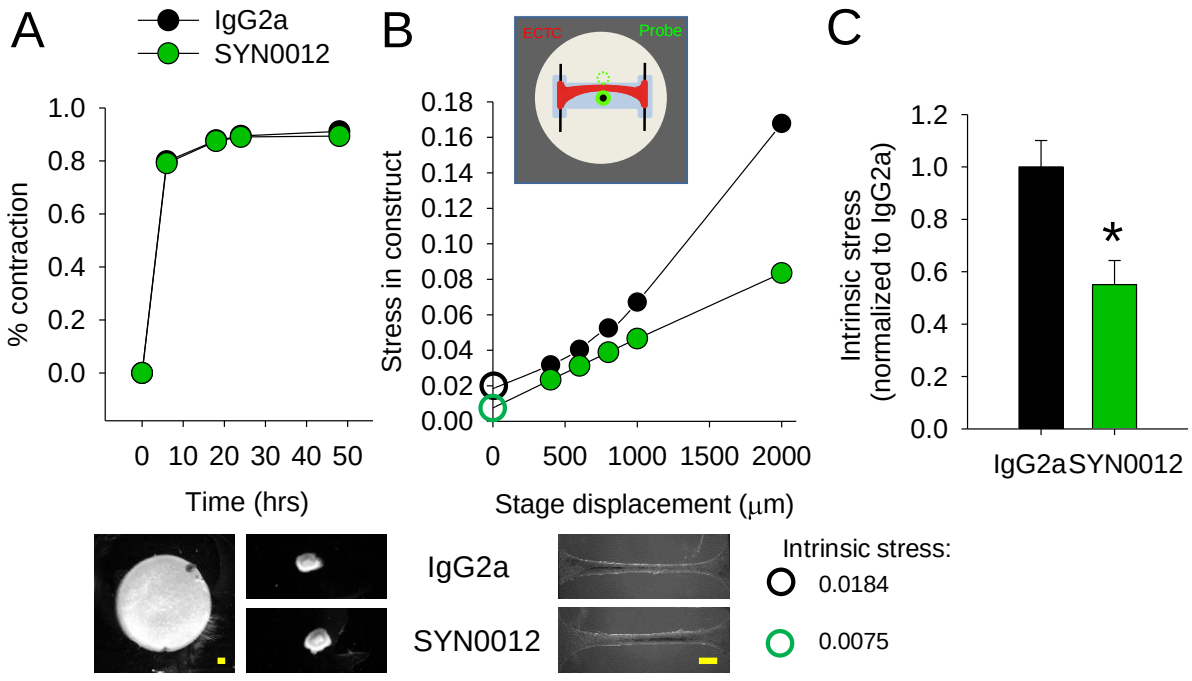

Figure 5.5 SYN0012 effect on CF contractility. Results of collagen gel contraction assay (A) with representative images of gels at 0 and 48 hours. Schematic of I-wire construct system inset above stress/displacement curves in I-wire construct from representative constructs (B) with intrinsic stress (arbitrarty units) marked by open circles. Yellow scale bar represents about 1 mm in image callouts below

graphs. Average relative intrinsic stress from I-wire constructs (n = 3) (C). * indicates significant difference ($p > 0.05$) between IgG2a and SYN0012 samples.

IL-6 expression with IgG2a or cadherin-11 blocking antibody (SYN0012)

While cadherin-11 transcription peaked at day 7 after infarct, the fact that there were significant differences in function at day 7 indicates that the treatment is having some sort of effect on the cells of the heart within the first week, during the inflammatory and granulation phases. To determine the cellular changes that mediated these changes in dynamic tissue remodeling, we evaluated transcriptional changes of a variety of inflammatory and fibrotic markers over the time course of experiment. We observed a decrease in transcription of IL-6, a pro-inflammatory cytokine, in the antibody treated group three days post-MI (**Figure 5.6A**). This reduction seems to occur primarily in the non-CM cells of the infarct, a mixed population of inflammatory cells, endothelial cells and myofibroblasts (**Figure 5.6B**). Pronounced IL-6 expression can still be seen in the CMs of the BZ in both groups, as compared to low IL-6 expression in the distant myocardium.

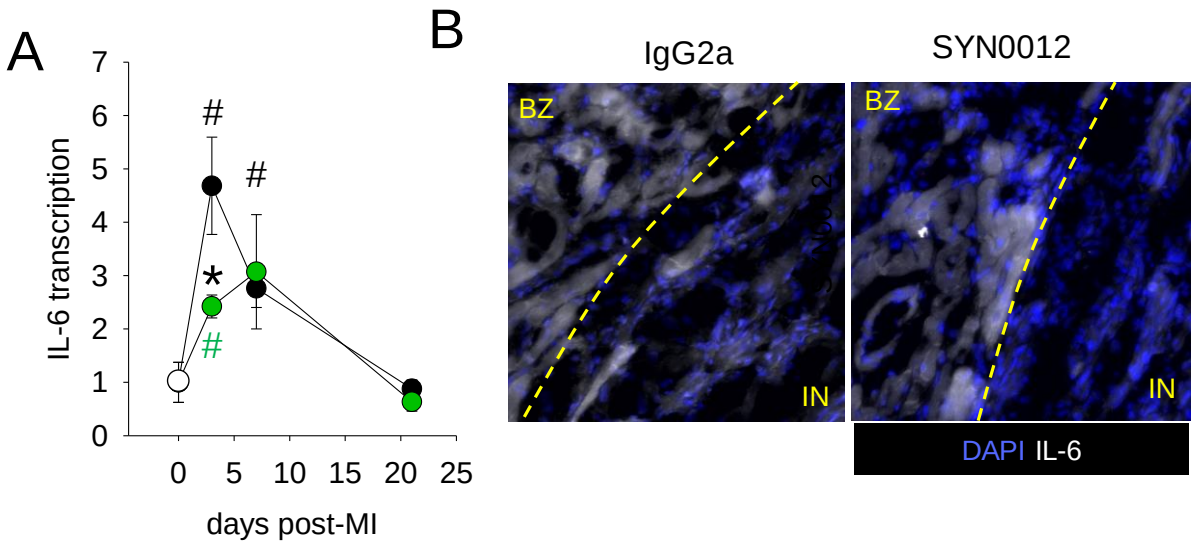

Figure 5.6 Reduction of IL-6 observed three days post-MI *in vivo* with SYN0012 treatment. Transcription of IL-6 after MI relative to sham. # indicates significant ($p > 0.05$) difference from sham, and * indicates significant difference ($p > 0.05$) between IgG2a and SYN0012 samples. Immunostaining for IL-6 three days after infarct at the border zone (BZ) and transition to the infarct (IN).

Macrophage alterations with IgG2a or cadherin-11 blocking antibody (SYN0012)

Expression of IL-6 has been shown to be enhanced in a mixed population of fibroblasts and MΦs [213], which motivated us to look at MΦ markers and localization in the infarct after MI. Transcription of F4/80 was significantly reduced at day seven *in vivo*, suggesting a decreased number of MΦs present at this time, though there was no significant difference in transcription at day three or 21 (**Figure 5.7A**). Immunostaining of hearts at day three after infarct show an apparent reduction in the colocalization of (and hence the likely interactions between) activated MyoFBs (α-SMA) and MΦs (F4/80) in the infarct and border zone (**Figure 5.7B**).

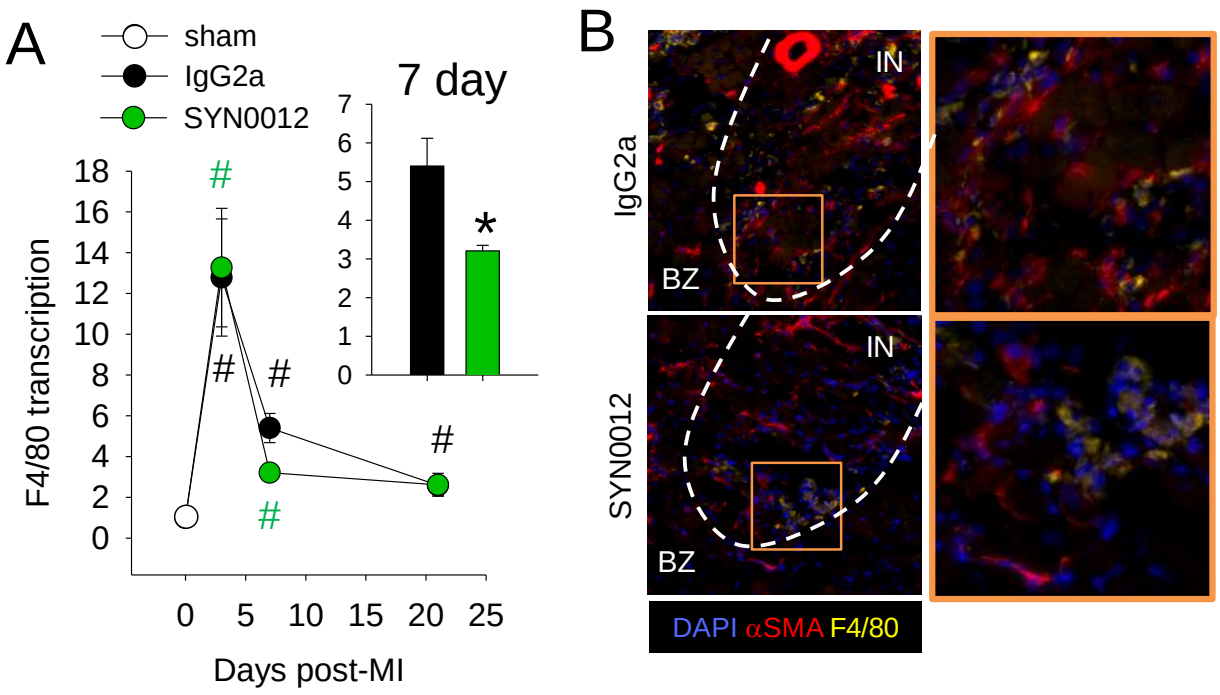

Figure 5.7 Reduction of F4/80 observed three days post-MI *in vivo* with SYN0012 treatment. Transcription of F4/80 over time, with the relative fold change at seven days called out for clarity (A). #

indicates significant ($p > 0.05$) difference from sham, and * indicates significant difference ($p > 0.05$) between IgG2a and SYN0012 samples.

Transcriptional changes of inflammatory and fibrotic signaling factors

Expression of other inflammatory markers was not changed significantly over this time course by SYN0012 treatment (**Figure 5.8**), but the average transcription of MMP13 in control animals at day seven was significantly enhanced relative to sham, whereas the expression of MMP13 had dropped back to baseline levels by day seven in the SYN0012 treated case (**Figure 5.8D**). Profibrotic/myofibroblastic markers, including TGF-β1, cadherin-11, α-SMA, and collagen-1 were also not dramatically changed by treatment (**Figure 5.9**). Of the profibrotic markers, note that TGF-β1 transcription is no longer significantly enhanced in the SYN0012 treated group, at seven days after MI, in contrast to the control group (**Figure 5.9A**). Furthermore, it may be noted that cadherin-11 transcription is more slowly upregulated with SYN0012 treatment, which may indicate a positive feedback effect of signaling downstream of cadherin-11 engagement (**Figure 5.9B**). Also, this confirms that cadherin-11 transcription is significantly increased above sham over the three weeks of myocardial remodeling, but does appear to peak at seven days. Finally, while there is no significant difference in transcription of either collagen-1 (**Figure 5.9C**) or α-SMA (**Figure 5.9D**), transcription of both was moderately reduced by SYN0012 treatment over the time course of the experiment.

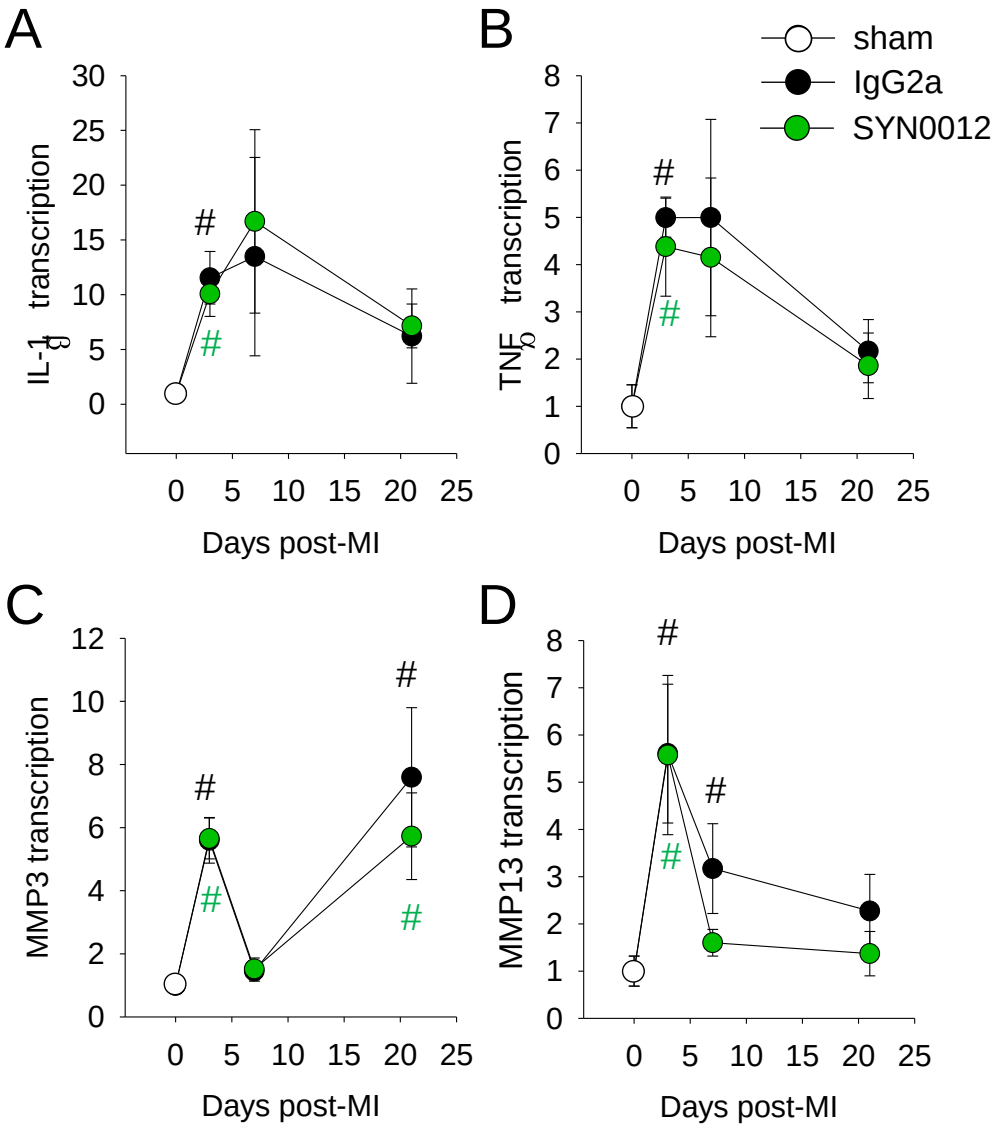

Figure 5.8 Transcriptional changes of inflammatory proteins after MI. IL-1β (A), TNF-a (B), MMP3 (C), and MMP13 (D). # indicates significant difference ($p < 0.05$) from sham. $n \geq 3$ animals.

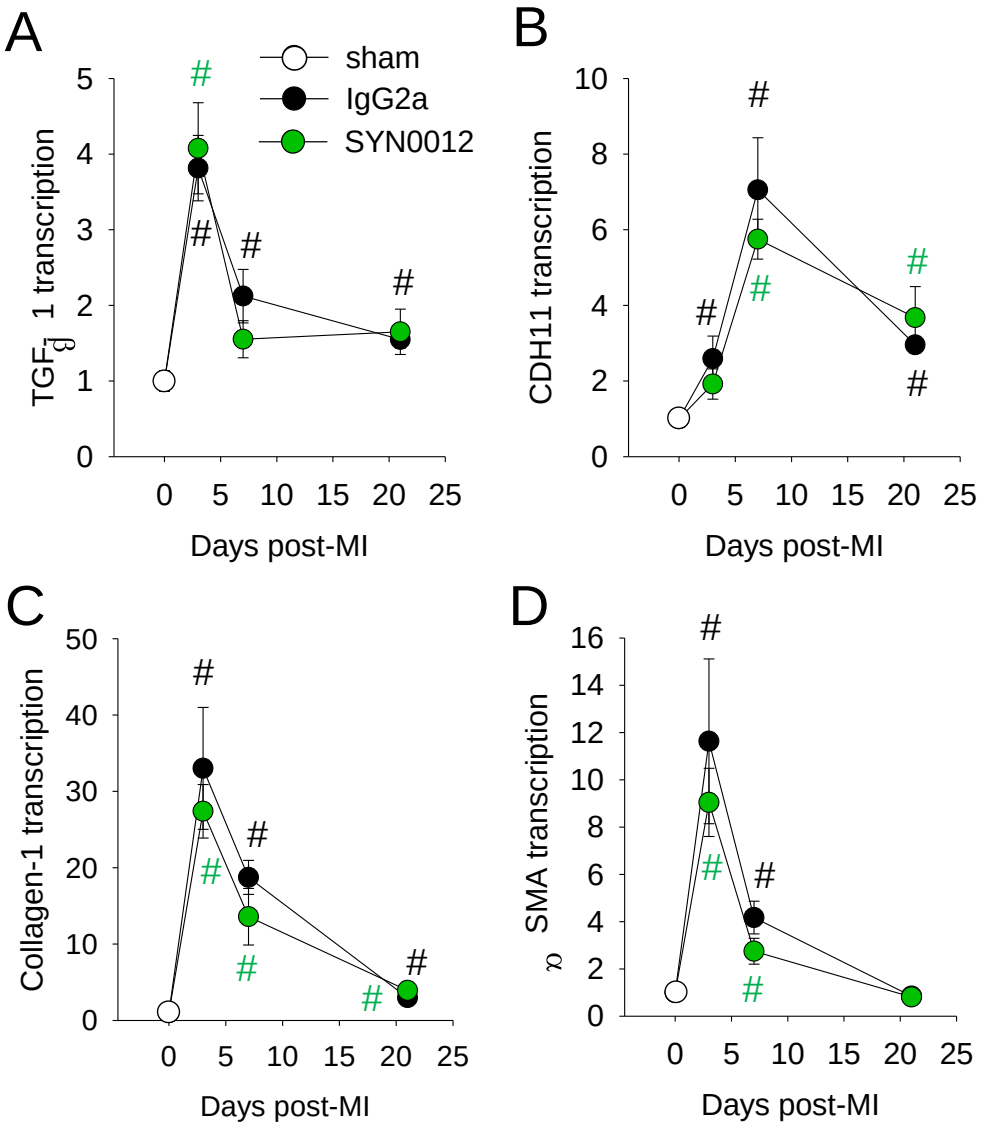

Figure 5.9 Transcriptional changes of pro-fibrotic proteins after MI. TGF-β1 (A), cadherin-11 (B), Collagen-1(C), and α-SMA (D). # indicates significant difference ($p < 0.05$) from sham. $n \geq 3$ animals.

Transcriptional changes of pro-angiogenic signaling factors

We also measured transcription of known pro-angiogenic signaling factors FGF2, VEGF-a and the VEGF receptor Flk-1 (**Figure 5.10A-C**) and were surprised to observe decreased expression of all three across all timepoints, which were significant at twenty-one days in the case of VEGF-a. FGF2 was significantly enhanced relative to sham at all time points in control, but only at day three in the SYN0012 treated group. Despite a marked reduction in angiogenic signaling, we did not observe a reduction in vascular density *in vivo*, and in fact observed increased numbers of muscularized vessels and fewer MyoFBs in the SYN0012 treated infarct at twenty-one days (**Figure 5.10D**). This observed reduction in MyoFBs in the infarct corresponds well with the reduction in α-SMA and reduced scar compaction (**Figure 5.4B-E**).

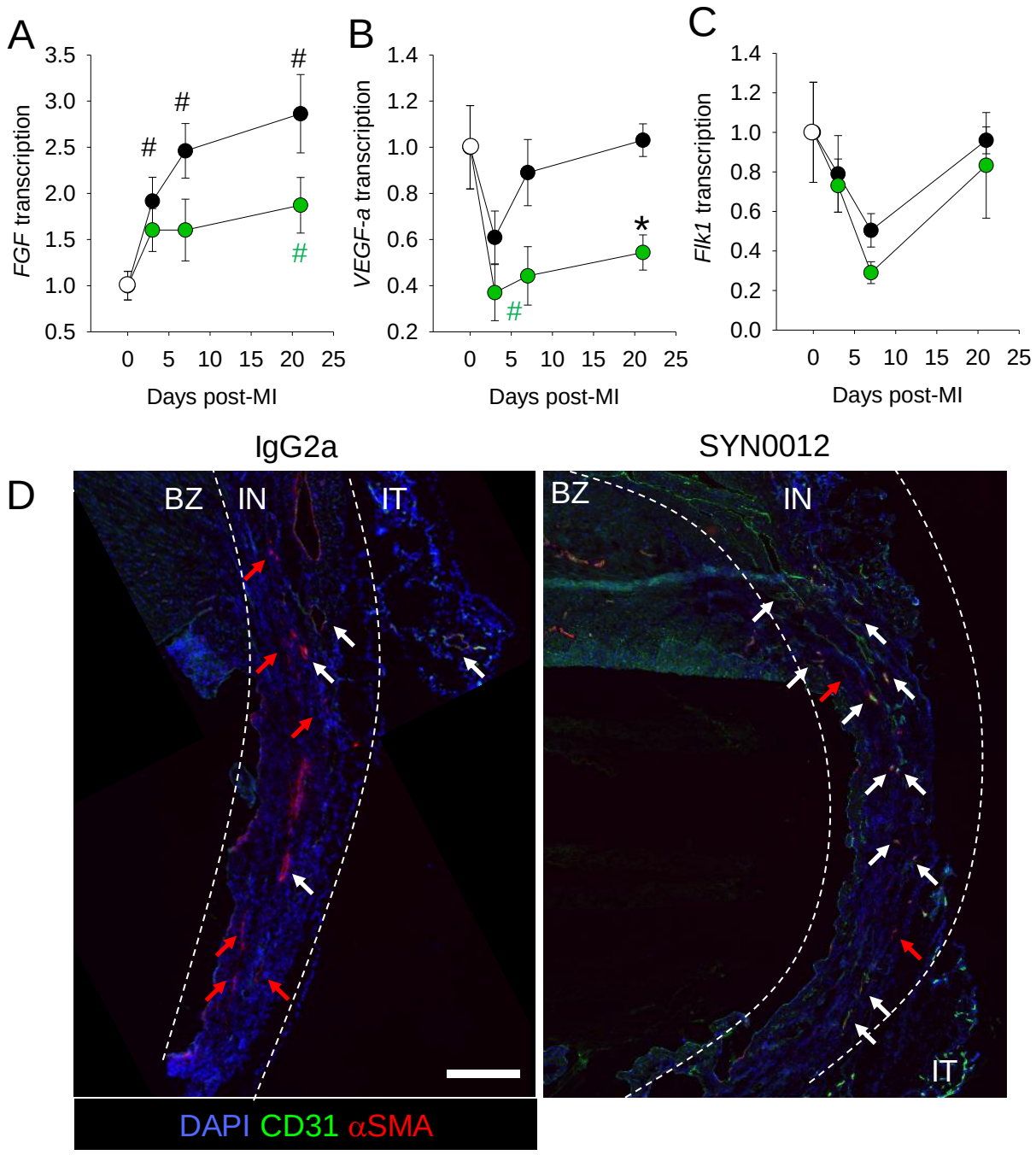

Figure 5.10 Transcriptional changes of pro-angiogenic proteins after MI. Relative fold change from sham for FGF2 (A), VEGF-a (B), and Flk-1 (C) reduced by SYN0012 treatment *in vivo*. n ≥ 3 animals. # indicates significant ($p > 0.05$) difference from sham, and * indicates significant difference ($p > 0.05$) between IgG2a and SYN0012 samples. Immunostained hearts isolated twenty-one days after infarct, stained for endothelial cells (CD31) and smooth muscle cells or MyoFBs (α-SMA). IN indicates the infarct area, BZ indicates border zone, and IT indicates inflammation tissue. White arrows indicate the location of muscularized arterioles and arteries, while red arrows indicate locations of MyoFBs (α-SMA without CD31).

Co-culture of CFs and MΦs increase expression of inflammatory signals

Given the changes we observed in IL-6 and F4/80 we observed in vivo, we hypothesized that SYN0012 treatment might be preventing MΦ/CF interactions reported to promote IL-6 transcription, either by blocking direct cadherin-11 bonds between cell types or by preventing their interactions in vivo. To test this hypothesis, we used a co-culture system of CFs and intraperitoneal MΦs. Co-culture of fifty thousand CFs with zero to fifty thousand MΦs showed significant increases in IL-6 expression with addition of MΦs, with all CF containing samples producing significantly more IL-6 than MΦs alone (**Figure 5.11A**). qPCR of these samples confirmed that transcription of F4/80 closely corresponds to the number of MΦs present (**Figure 5.11B**), and furthermore that transcription of MMP13 was significantly increased over CFs alone by co-culture with MΦs (**Figure 5.11C**). Transcription of MMP13 was roughly two-fold higher in MΦs alone than in a 1:1 coculture in a previous experiment, so this increase is likely due mostly to the increased number of MΦs. The addition of IgG2a to this *in vitro* co-culture environment did not significantly alter the secretion of IL-6 from the non-treated controls, but SYN0012 treatment did significantly lower IL-6 production in the 1:1 co-culture condition (**Figure 5.11D**). Comparison of F4/80 transcription indicated that the blocking antibody had no significant effect on the relative proportion of MΦs in the co-culture system (**Figure 5.11E**) or on the co-cultured production of MMP13 (**Figure 5.11F**).

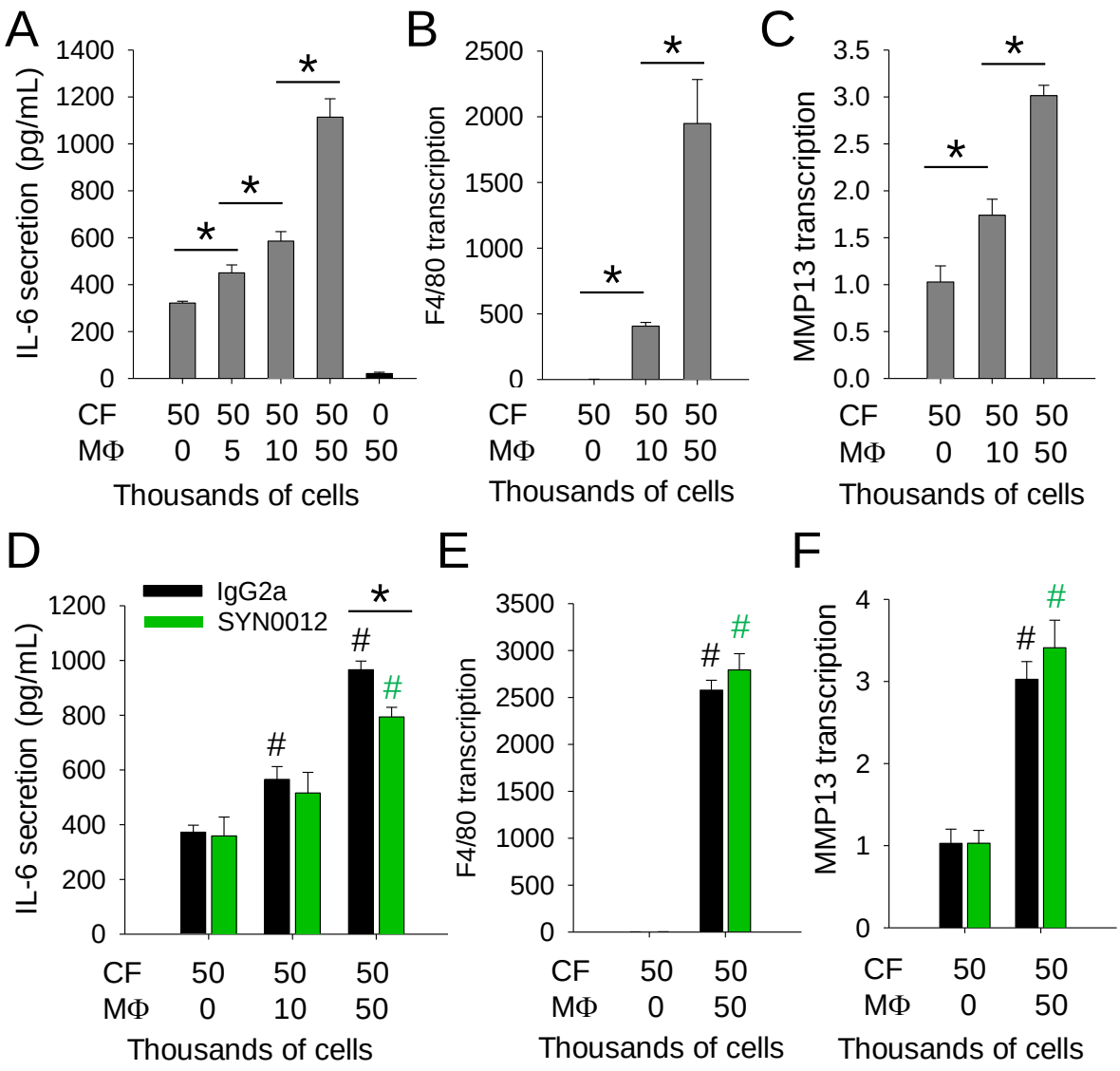

Figure 5.11 Co-culture of MΦs and fibroblasts increase expression of IL-6 and MMP13. # indicates significant ($p > 0.05$) difference from sham, and * indicates significant difference ($p > 0.05$) between IgG2a and SYN0012 samples. n = 3.

Further analysis of the transcription in the co-culture setting indicates that TGF-β1 transcription was significantly enhanced by co-culture and, somewhat surprisingly, was also significantly enhanced by SYN0012 in the co-culture setting (**Figure 5.12A**). MMP3, FGF2 and VEGF-a transcription were not affected by either addition of antibody

or by co-culture (**Figure 5.12B,C,F**), indicating that different cellular mechanisms must be regulating their expression *in vivo*. Transcription of both α-SMA and Collagen-1 were significantly reduced in the co-culture system, likely because these proteins are not expressed by MΦs, so the relative transcription was reduced by the same proportion of relative CF decrease (50%) (**Figure 5.12D,E**).

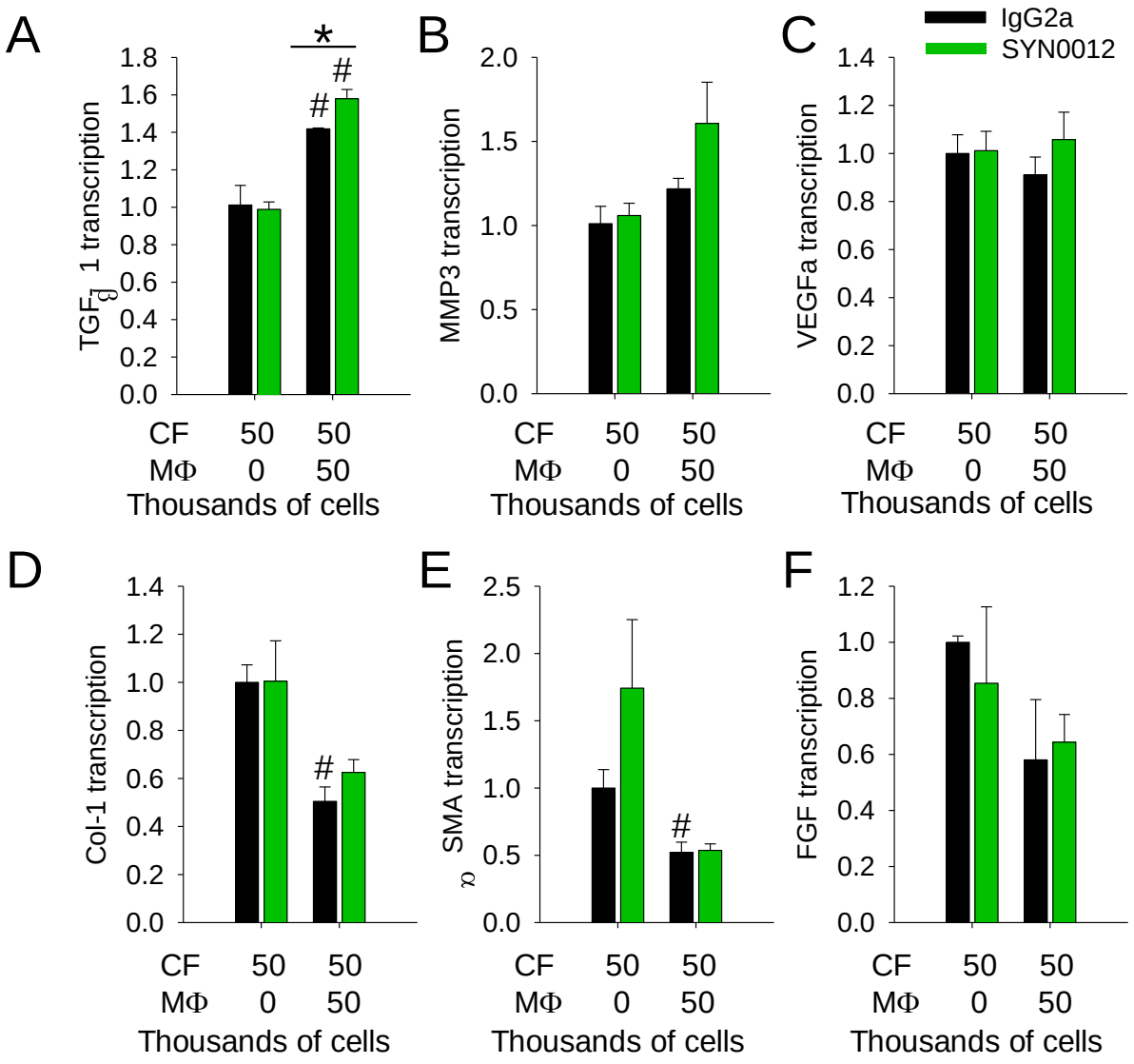

Figure 5.12 Co-culture effects on other aspects of inflammatory/remodeling cascade. Transcriptional levels of TGF-β1 (A), MMP3 (B), VEGF-a (C), Collagen-I (D), αSMA (E), and FGF (D) in CF/ MΦ co-culture. # indicates significant ($p > 0.05$) difference from sham, and * indicates significant difference ($p > 0.05$) between IgG2a and SYN0012 samples. n = 3.

Comparison of MΦ polarization in vivo and in vitro

Given the recent rise in interest in the role of MΦs and MΦ polarization in remodeling after infarcts, we measured the transcription of three markers of MΦ phenotype in both our *in vivo* time course and *in vitro* co-culture system to see whether it would be effected by SYN0012 treatment. CD14 is associated with the proinflammatory M1 MΦ phenotype, while mannose receptor 1 (Mnr1) and arginase-1 (Arg1) are associated with the reparative M2 phenotype. The M2 phenotype is associated with scarring and remodeling, as well as the resolution of inflammation. We observed no significant differences between the treatments *in vitro*, though all three proteins had a larger relative reduction in the SYN0012 treated group between day three and day seven (**Figure 5.13A-C**). In the co-culture setting, there was no change with SYN0012 for either CD14 or Mnr1, but we did observe a significant increase in transcription of Arg1 with SYN0012 treatment (**Figure 5.13D-F**).

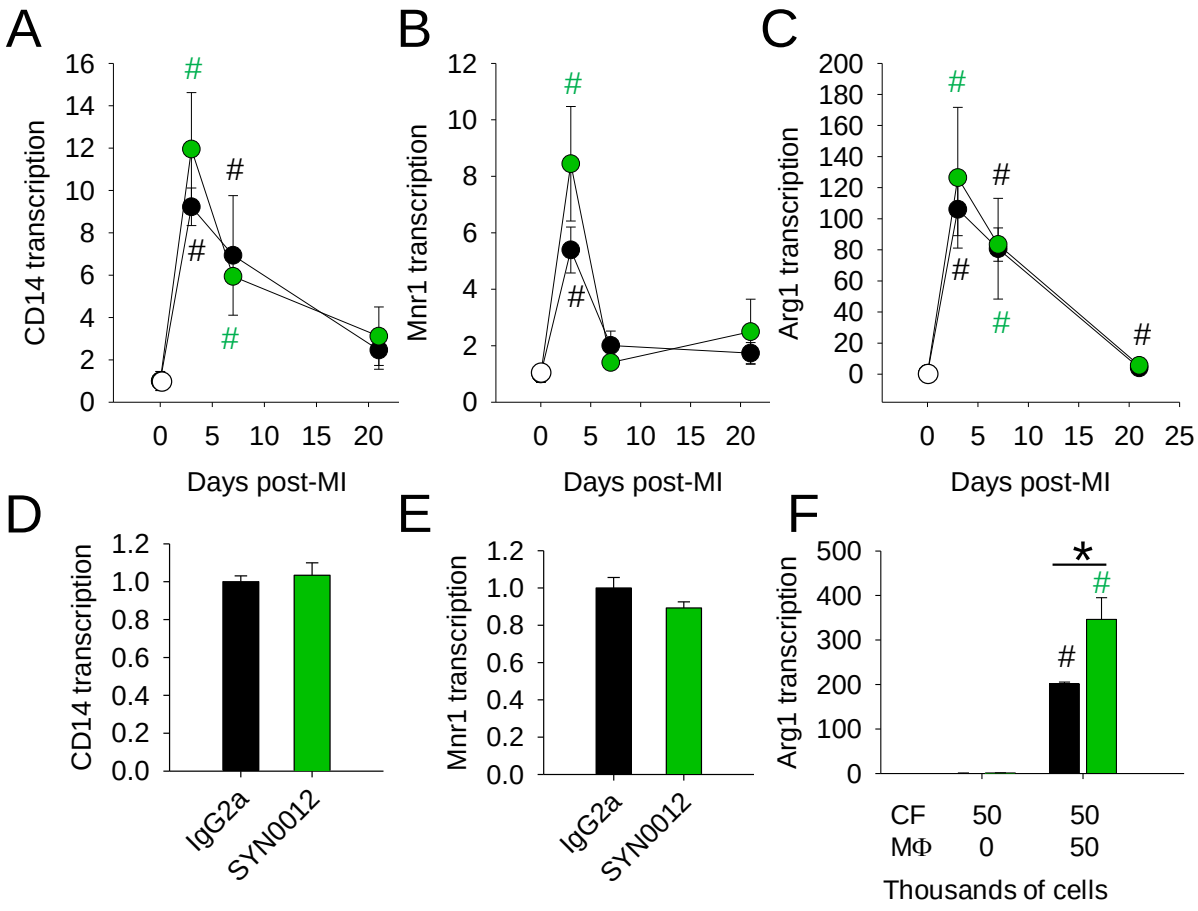

Figure 5.13 Transcriptional changes of markers of MΦ polarization. Transcription of MΦ polarization markers *in vivo* (A-C) n > 3 animals, an *in vitro* (D-F) n=3. # indicates significant (p > 0.05) difference from sham, and * indicates significant difference (p > 0.05) between IgG2a and SYN0012 samples.

Discussion

Our findings confirm that cadherin-11 is highly expressed in primarily non-CM cells after MI and furthermore plays a functional role promoting tissue breakdown and myocardial remodeling. A peak of cadherin-11 expression at seven days suggests a prominent role for MyoFBs, which are particularly active between weeks two and three following MI when the bulk of scar formation occurs [79]. However, the fact that cadherin-11 is already significantly enhanced at day three, suggests that other cell types, especially cells derived from inflammatory monocytes, including MΦs, are also relevant. Immunostaining revealed that a subset of MΦs, endothelial cells, smooth muscle cells and MyoFBs in the infarct region seven days after MI all express cadherin-11. This is the first reported evidence that cadherin-11 plays a functional role after MI.

To better understand how this protein may be functioning in the heart, we compared the response of littermate control WT and global CDH11-/- animals. Results indicated that cadherin-11 may be playing a functional role increasing LV remodeling after MI in the first seven days. The null mice had significantly improved EF and LV systolic volume relative to WT, but these changes do not persist to day 21. Immunostaining confirmed that much of the increase in cadherin-11 expression observed in overall transcription is localized to the infarct. Trichrome staining shows less collagen compaction in the null animals, which is likely due to contractile deficiencies in cadherin-11 null cells, as reported elsewhere [169]. We confirmed intrinsic differences in contractile ability of WT and CDH11-/- CFs that are likely relevant to infarct healing. Insufficient scar compaction can lead to increased wall strain and remodeling. Additionally, there may be compensatory mechanisms in the null mice,

whereby a permanent deletion of cadherin-11 leads to overexpression of related adhesion and signaling proteins. In any case, a genetic deletion is less relevant to clinical applications, since there are no known connections between cadherin-11 mutations and cardiac disease.

We next moved onto a therapeutic model using a blocking antibody against cadherin-11 that has proven to be effective in the contexts of pulmonary fibrosis and rheumatoid arthritis, two conditions characterized by excessive, inflammation-driven fibrotic remodeling. Our treatment strategy did not require pretreatment or acute application to achieve significant benefits *in vivo*. While we did not observe a significant increase in survival (**Figure 5.3A**), twice as many mice died in the control group relative to the treated cohort during the highest risk period for cardiac rupture (days 3-7). This is likely a consequence of the tissue breakdown and subsequent softening of the myocardial wall mediated by the inflammatory response. The control animals had more consistently softer infarcts at seven days (**Figure 5.4A**). SYN0012 treatment caused significant improvement of ejection fraction relative to IgG2a treated controls by seven days after infarct, which was maintained up to 5 weeks past the end of treatment (**Figure 5.3B**). This result indicates that cadherin-11 is in some way contributing to the loss of functional contractile cardiomyocytes during the inflammatory and proliferative phases in the first week of remodeling. Treatment with a blocking antibody more effectively preserves cardiac function within the first week, and prevents the continued worsening of function from day seven to day fifty-six that occurs in the IgG2a treated animals. Furthermore, while the left ventricular volume was not significantly altered by treatment at seven days, the dramatic increases in both diastolic and systolic volumes

between days seven and twenty-one, and again between days twenty-one and fifty-six, observed in controls were completely prevented in mice who received SYN0012 treatment (**Figure 5.3C,D**). This combined with the peak of cadherin-11 expression occurring near day seven seems to suggest that cadherin-11 expressing cells play an active role in LV remodeling and expansion during the fibrotic phase of infarct healing. LV expansion is a common, generally irreversible feature in the eventual progression to heart failure, which is a factor in 1 in 9 deaths in the United States [1]. A treatment that effectively limits this remodeling could have profound impacts on patient outcomes after MI.

Using AFM, we observed changes in the mechanical environment of the infarct over the time course of infarct healing. The initial drop in tissue stiffness in response to the inflammatory response observed at seven days is necessary to clear dead cells but contributes to risk of cardiac rupture (**Figure 5.4A**). While it has often been assumed, there are very few direct measurements of decreased stiffness after infarct. Our system allows for a quantitative assessment of regional tissue stiffness changes through the time course of healing. The stiffening of the developing scar we measured between days seven and twenty-one preserves the mechanical integrity of the LV, but also increases substrate stiffness in the infarct itself, as well as potentially increasing local strains in the microenvironment of the infarct and border zone. This increases mechanical activation of fibroblasts (see chapters 3-4) and can lead to progressive fibrotic remodeling especially at the vulnerable border zone. Indeed, our technique of AFM of fresh frozen tissue gives a more accurate representation of the microenvironment experienced by the cells, which may be much more variable than

bulk tissue measurements would indicate. By day 56, we observed that while the control infarcts were still highly variable, across a large range of medium and high stiffness, the treated hearts have much more consistent measured stiffnesses that correspond well to the original myocardial stiffness (**Figure 5.4A**). Trichrome analysis of the infarct size confirms that the fractional length of the infarct continues to increase from day twenty-one to day 56 and is significantly larger than the corresponding scar size in SYN0012 treated animals (**Figure 5.4B**). Significant scar thinning in the radial direction observed in controls is also not seen in the treated animals. This compaction is likely mediated by α-SMA expressing MyoFBs, which are not enhanced in SYN0012 treated hearts at twenty-one days (**Figure 5.4D**). A recent analysis of the mechanics of infarct expansion an remodeling based on a review of a number of published *in vivo* studies concluded that limiting radial scar thinning was an attractive target for improving functional outcomes [214]. Maintaining relatively high scar thickness was found to reduce LV expansion during diastole and, by consequence, increase the ejection fraction and function of the hearts in a finite element model. Our functional data corresponds well to this report, showing that limiting scar thinning (potentially through targeting cadherin-11 expressing MyoFBs) better preserves cardiac function.

We next measured the contractility of CFs embedded in a 3D-collagen matrix after incubation with either IgG2a or SYN0012 (**Figure 5.5**). Given the profound reduction in gel contraction in CDH11-/- CFs (**Figure 5.2 E**), the absence of a SYN0012-mediated effect in the collagen gel assay was initially surprising. The genetic deletion of cadherin, and subsequent cellular adaptation, must be mediating a dramatic change in CF contractile machinery that is not triggered by blocking cadherin-11

adhesion. The blocking antibody does not prevent transcription of cadherin-11 or localization at the cell membrane, so it is likely that cadherin-11 is still acting to assemble adherens junction proteins and link the cell membrane to the cytoskeleton. The blocking antibody prevents a large portion of the cadherin bonds between cells, which can interfere with transmission of both force and mechanotransductive signals. Using the novel I-wire system, an ECTC that allows for CF contraction of 3D collagen under tension, we were able to detect a difference in intrinsic longitudinal stress created in the construct after 7 days of SYN0012 treatment. This finding supports the hypothesis that blocking cadherin-11 bonds between cells may effectively prevent mechanosensing and cellular reinforcement of environmental mechanical stress.

Having determined a clear functional effect of cadherin-11 blockade in limiting myocardial remodeling and infarct expansion after MI, we set out to determine the cellular mechanisms mediating this effect. We used real time qPCR, which allowed for an examination of transcriptional changes of many signaling factors and cellular markers over the range of infarct healing. Our first measurable change was a significant reduction in IL-6 expression at three days following infarct (**Figure 5.6**). This reduction was most evident in the non-CM cells. IL-6 has been shown to have a multifaceted role in cardiovascular disease, and there is evidence that blocking IL-6 leads to CM loss and worsened outcomes [215], [216]. However, IL-6 has also been shown to promote the infiltration, migration, and polarization of MΦs, as well as MyoFB activation [217]–[220]. It seems likely that by specific targeting of the non-CM cell population of the heart, our treatment effectively limits the negative cell activating effects of IL-6, without interfering with its function in CMs. The decrease in IL-6 was evident at three days, which is a time

point associated with a high number of MΦs and the beginning of the transition from inflammatory to proliferative phase of healing.

In addition to a direct decrease of IL-6 expression early in the healing process, our data also suggest that blocking cadherin-11 limits the persistence or proliferation of MΦs in the heart between day three and day seven (**Figure 5.7**), perhaps contributing to the increasing infarct size and remodeling observed in controls between day seven and day fifty-six (**Figure 5.3-4**). There has been an increased interest in the role of MΦs in the process of healing and remodeling after MI [4], [15], [16]. It has been reported that interactions between fibroblasts and MΦs promote increased expression of IL-6, though the mechanisms of this interaction had not been completely described. We hypothesized that cadherin-11 might regulate the interactions between fibroblasts and MΦs, and observed that three days after MI, there appears to be more interactions between MΦs and MyoFBs in the IgG2a treated hearts than the SYN0012 treated. This indicates that while there may not have been a significant difference in the number of MΦs (indicated by F4/80 transcription), blocking cadherin-11 adhesion may prevent the migration of MΦs throughout the infarct and border zone, minimizing their subsequent interaction with resident MyoFBs. By day seven after infarct, we measured a significant reduction in F4/80, indicating that there are significantly fewer MΦs present in the heart by this time. Regardless of their particular phenotype, MΦs are significant drivers of tissue remodeling, especially when interacting with MyoFBs.

We also measured a number of other inflammatory, fibrotic, and angiogenic signals and proteins over the time course of healing (**Figure 5.8-9**). While none of these

were significantly altered by SYN0012 in the first week after infarct, we did observe a faster return to baseline values by day seven for MMP13 and TGF-β1, which are associated with tissue breakdown and fibrosis, respectively. We also observed a reduction in transcription of both FGF2, VEGF-a, and Flk-1 that are often associated with improved revascularization and improved outcomes [74], [94] (**Figure 5.10**). However, we observed increases numbers of arterioles in the treated groups at twenty-one days, corresponding to a time of reduced angiogenic markers. VEGF-a transcription has been shown to peak in the border zone within 12 hours of MI, but be reduced overall in the infarct area, especially in later stages of remodeling [221]. It is possible that SYN0012 allows for more preservation of the native vasculature or faster restoration/maturation of new vasculature, so that the hypoxic conditions that typically drive angiogenic signaling are reduced. Blocking cadherin-11 adhesion in endothelial cells may also be limiting the number of endothelial cells driven to undergo EndMT, which may help preserve vascularization and limit numbers of MyoFBs in the infarct. Future studies will more fully explore the role of cadherin-11 in vasculogenesis and endothelial cell behavior after MI.

We decided to investigate the MΦ/CF interaction and how it contributes to the inflammatory and remodeling signaling observed *in vivo*. Specifically, interactions between MΦs and fibroblasts have been reported to regulate IL-6 expression, response to TGF-β1 signaling and fibrosis [213]. To this end, we performed co-culture experiments to determine whether cadherin-11 may mediate interactions between MΦs and MyoFBs in the regulation of inflammatory and fibrotic signaling. Our *in vitro* findings confirm that co-culture of these cells promotes significant expression of inflammatory

compounds like IL-6 and MMP13, and suggest that cadherin-11 is partially responsible mediating the fibroblast/MΦ interaction that promotes IL-6 expression by fibroblasts (**Figure 5.11D**). Preliminary immunostaining of MΦs and MyoFBs in vitro shows potential evidence for direct cadherin-11 bonds between these cells, but more work is needed to characterize the specific effect of SYN0012 on the formation of such adhesions (**Figure 5.14**).

We were initially surprised to see a significant increase in TGF-β1 transcription with SYN0012 (**Figure 5.12A**) *in vitro*, given the generally pro-fibrotic role of this growth factor. However, upon reflection, TGF-β1 is a necessary cue for the resolution of inflammation [76], [81], [222]. SYN0012 treatment may be promoting enhanced TGF-β1 expression between days three and six that speeds the resolution of inflammation, contributing to the reduction of F4/80, TGF-β1 and MMP13 expression observed *in vivo* at days seven and twenty-one. Future experiments are necessary to further investigate this finding. Because TGF-β1 is released in an inactive form, mere transcriptional changes are not sufficient to determine the actual role of TGF-β1 signaling in the heart.

This study led us to develop the following potential cellular mechanism for the role of cadherin-11 in the remodeling infarct (**Figure 5.14**). Interactions between MΦs and CFs, in part mediated by cadherin-11, promote the expression of IL-6, as well as MMP13 and TGF-β1. The intracellular signaling that mediates these transcriptional changes is not well understood, but given reports in the literature (Chapter 3), it is likely that p120 catenin is involved in the transmission of signals through Rac1, and β-catenin is involved in signaling with significant crosstalk with MAPKs and Smads. Expression of

these proteins promotes inflammation, tissue breakdown, and myofibroblast differentiation. Cadherin-11 may also be involved in mechanosensing of increased strain in this low stiffness environment, and in sensing increased substrate stress in fibrotic environments. Future studies will clarify the specifics of mechanotransductive signaling downstream of cadherin-11 adhesion in both CFs and the other cell types of the heart.

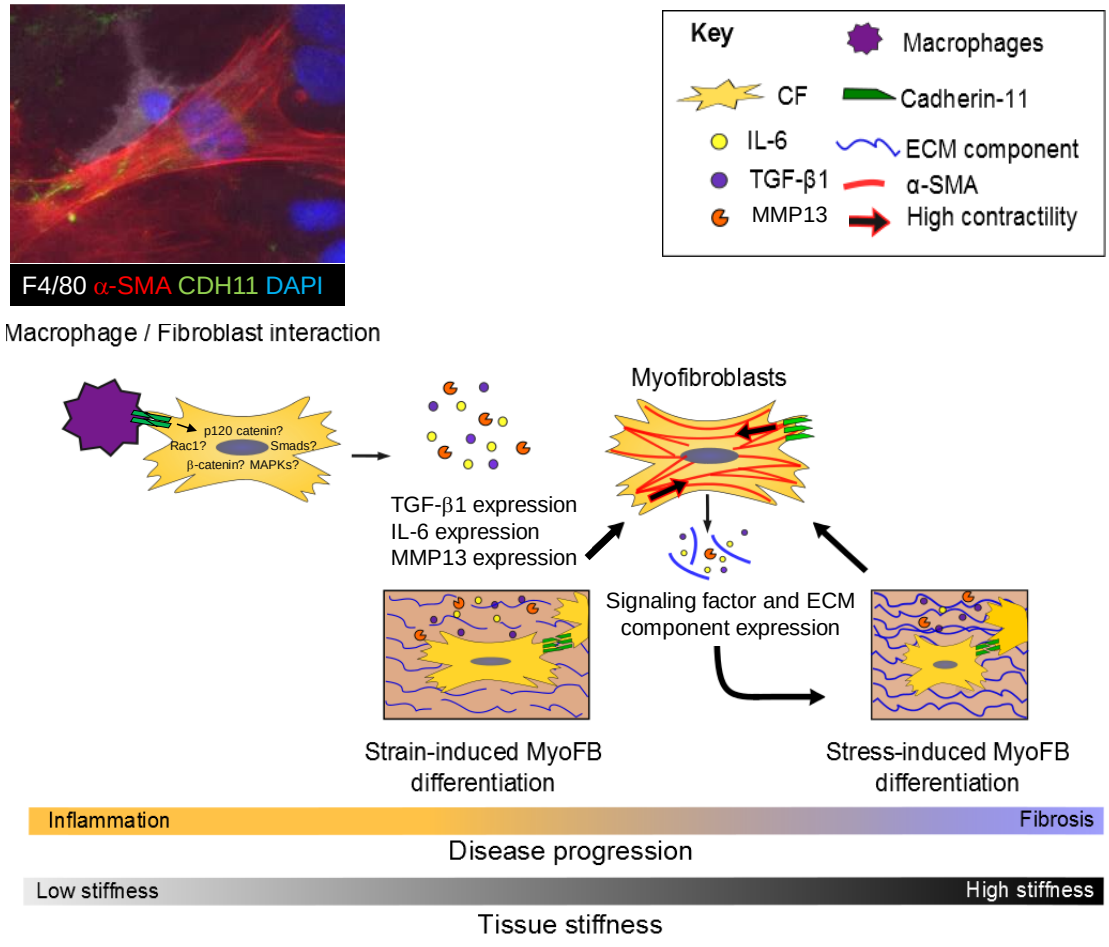

Figure 5.14 Proposed cellular roles of cadherin-11 on MΦs and CFs.

MΦ polarization has been much discussed as a critical regulator of inflammation and remodeling, but we did not observe any differences in MΦ markers *in vivo* (**Figure**

5.13A-C). More recent work has highlighted the incompleteness of an M1/M2 paradigm, so more work would be needed to understand the alterations to MΦ phenotype induced by this treatment [223], [224]. One telling result is the significant increase in Arg1 expression induced by SYN0012 treatment *in vitro*. Arg1 is typically associated with M2 MΦs, the reparative phenotype. Arg1 inhibits nitric oxide synthesis, and promotes cell proliferation and tissue repair [219], [225], [226]. It is possible that SYN0012 is also promoting a relative increase in Arg1 expression *in vivo*, but the concurrent reduction in overall MΦs is masking the effect.

Overall, we believe that cadherin-11 is expressed by and mediates activation of multiple non-CM cell types to promote the persistence of active remodeling in the infarct and border zone after MI. Treatment with SYN0012 does not prevent the necessary inflammatory and reparative response, but does facilitate a faster and more complete resolution of inflammation and active remodeling, resulting in a stable, smaller scar and less myocardial remodeling. We believe that this effect is mediated in large part by reducing the interactions between MΦs and fibroblasts in the healing infarct area, both directly by preventing cadherin-11 bonds, and indirectly by limiting the migration, proliferation and persistence of MΦs in the tissue (**Figure 5.15**).

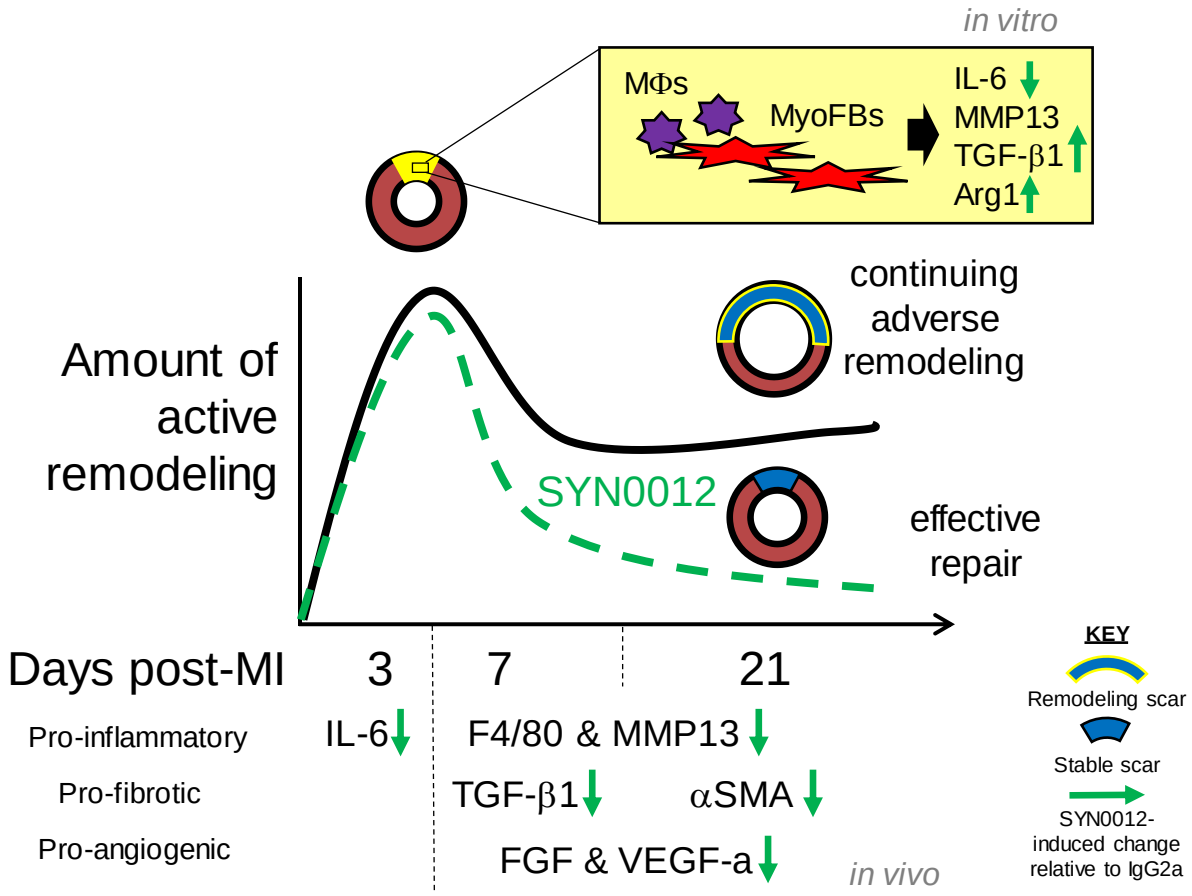

Figure 5.15 Summary of proposed mechanism. SYN0012 mediates improvement after MI by reducing the intensity and duration of active remodeling in the infarct and border zone throughout the time course of healing. We propose that SYN0012 limits the *in vivo* interactions between MyoFBs and MΦs that promote pro-remodeling protein expression, and further, that SYN0012 directly effects some of these expression effects.

While our functional results reveal both a profound role for cadherin-11 and a clear and beneficial effect of SYN0012 treatment, our evidence for the cellular mechanisms of this effect is somewhat limited in scope. Transcriptional activity can give a broad view of cellular behavior over time, but does not provide full insight into either the specific cells responsible for the observed changes or the actual functional protein that is available after various post-transcriptional modifications and trafficking. Using transcription of F4/80 as a proxy measurement of the MΦ population may not fully

represent the range of MΦ subtypes found *in vivo* after MI, or how those populations change in response to treatment. Future studies using flow cytometry and a broader range of *in vivo* and *in vitro* techniques will strengthen and help clarify the cellular mechanisms we have described in this work.

This aim characterizes phenotypic changes and tissue remodeling throughout the course of infarct healing and highlights a potential new treatment strategy for improving outcomes after myocardial infarction: an antibody blockade of cadherin-11. Importantly, the administration of this functional blocking antibody did not need to be acute (within 12 hours of injury) to have demonstrative and multifaceted, positive effects on healing and cardiac function. These data suggest that targeting cadherin-11-expressing MΦs and MyoFBs limits inflammation-driven remodeling while preserving cardiac function.

CHAPTER 6

AIM 3: QUANTIFYING CARDIOMYOCYTE MECHANICS

Text for Chapter 6 adapted in part from:

[227] Manalo, A., **Schroer, A.K.**, Fenix, A., Coogan, J., Brolsma, T., Burnette, D., Bader, D., *The loss of protein CENP-F disrupts cardiomyocyte architecture and function.* Circulation Research, 2016. **(in preparation).**

[228] **Schroer, A.K.,** Shotwell, M., Sidorov, V.Y., Wikswo, J.P., Merryman, W.D., *I-Wire Heart-on-a-Chip II: Biomechanical analysis of contractile, three-dimensional cardiomyocyte tissue constructs.* Acta Biomaterialia, 2016. **(in press)**.

Introduction to CM biology and relevance to disease

CMs are the cellular source of the mechanical forces that determine both heart function and the mechanical environment experienced by all the non-CM cells described in the previous chapters. CMs have complex internal and junctional machinery, which allows for the coordinated contraction of the myocardial wall and effective pumping of blood throughout the body. However, a host of clinically relevant mutations and pharmacological compounds can negatively affect this function and lead to detrimental cardiomyopathies. Altered demands on the heart, in response to either pressure overload or ischemic disease, can also trigger CM remodeling and pathologic cardiomyopathy.

Despite a large range of etiologies, many of these CM-originating pathologies are also associated with interstitial fibrosis and increased risk of heart failure. This is likely in

response to disruption of the mechanical and chemical signaling occurring in the heart between native CMs and non-CM cells, especially CFs. Recently developed biological and biomedical tools can be used to investigate the function and structure of CMs *in vitro* to identify structural and functional changes associated with disease and dysfunction *in vivo*.

CENP-F mutation alters cardiac cell structure and mechanics

There are many mutations that are known to cause CM dysfunction, and subsequent cardiomyopathies, cardiac fibrosis, and heart failure. While many of the most commonly studied directly affect the sarcomeric structure, which is responsible for contraction, other proteins associated with the sarcolemma and cell adhesion have also been linked to cardiomyopathies [229]–[231]. Deficiency for both integrin linked kinase and N-cadherin lead to the development of dilated cardiomyopathies in mice [232], [233]. Another cytoskeletal accessory protein that causes dilated cardiomyopathy is centromere protein F (CENP-F), which participates in the regulation of microtubules. Mutations of this protein have been linked to human cardiomyopathies, and the development of the dilated cardiomyopathy phenotype with substantial interstitial cardiac fibrosis has been reported in mice with a CM specific knock out [234], but the particular effect of the mutation on both fibroblast and CM structure and function was largely unknown.

As part of a collaboration with the Bader lab, specifically with Annabelle Manalo, I was able to use both image processing in MATLAB and AFM to clarify the effect of this mutation in isolated MEFs, CFs, and CMs. First, CMs were isolated from WT and KO mice and were subsequently fixed and stained for alpha actinin, or β-catenin and actin.

Cells were imaged on a high magnification confocal microscope, whereupon I assessed their sarcomeric structure using Fast Fourier analysis of the spatial frequency of the cells. After rotating to a consistent, horizontal axis, a trace of pixel intensity was taken along the length of the cell at regular intervals, and a FFT was performed on that trace allowing for the calculation of the average sarcomere length per slice (calculated from the first peak spatial frequency from a plot of FFT magnitude) (**Figure 6.1**). While there was no significant difference in sarcomere length between WT and KO cells (**Figure 6.1D**), the 2D power spectrum show significantly fewer defined peaks in the KO cell images, corresponding to a loss of sharp edges in the z-disks with the mutation (**Figure 6.1E**).

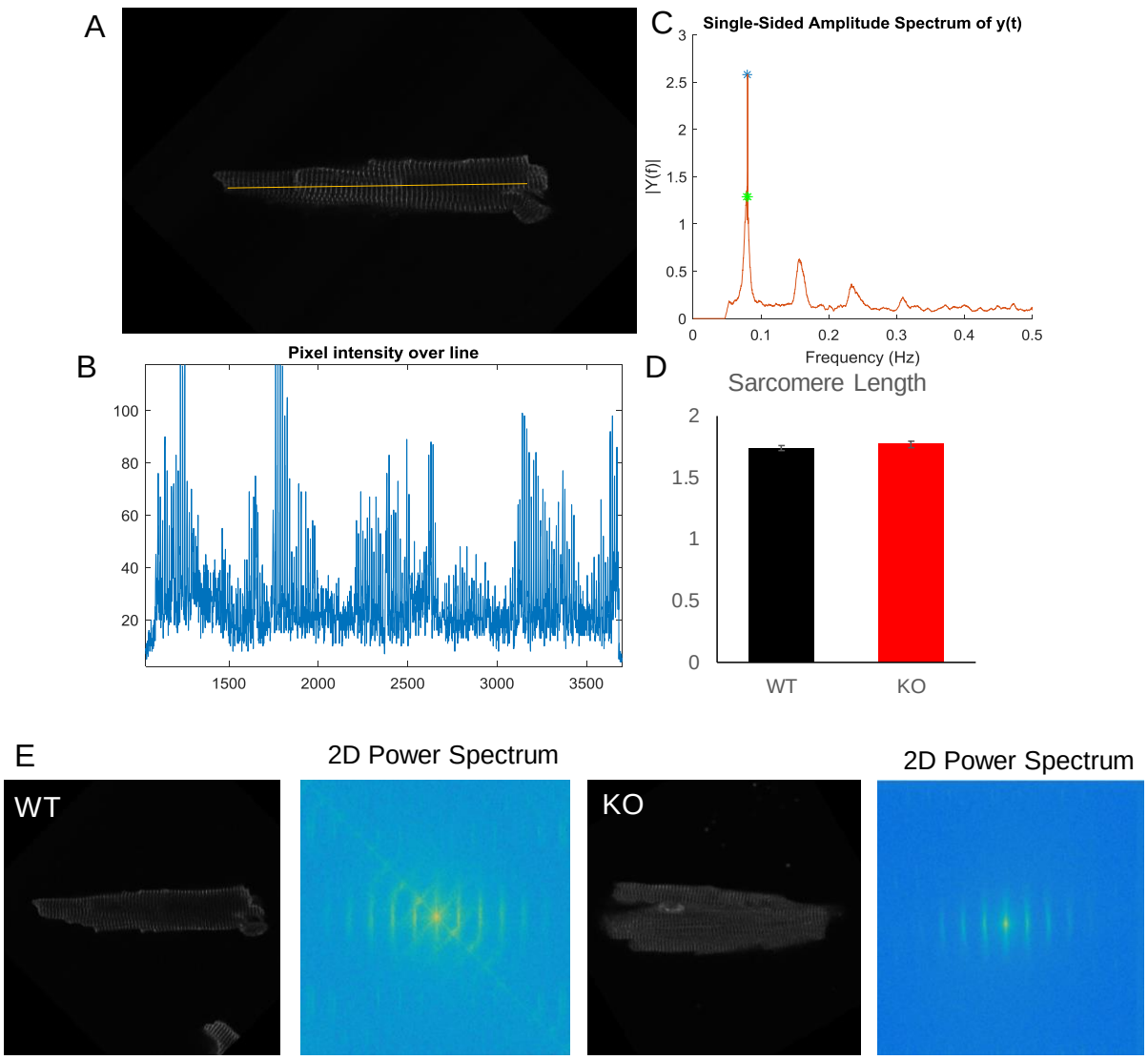

Figure 6.1 Quantification of sarcomere length. Confocal images of individual CMs stained for alpha-actinin were rotated to align the cell horizontally (A) and a horizontal traces (representative trace shown by yellow line) at 10 pixel vertical spacing gave a vector of intensity (B), and a smoothed amplitude spectrum of the FFT transform of this intensity signal (C) was used to find the primary peak frequency. The inverse of this frequency gives a measure of sarcomere length per slice and these were averaged together (D) to reveal consistent sarcomere lengths between groups (N=3 cells per group). 2D FFT in MATLAB allows for visualization of the overall frequency power spectrum (E).

I further characterized the amount of β-catenin present at adherens junctions in several slices of a WT and KO CM. By thresholding the intensity of the β-catenin image

and eliminating isolated pixels, I could identify the adherens junctions and quantify their overall area and average intensity (**Figure 6.2**).

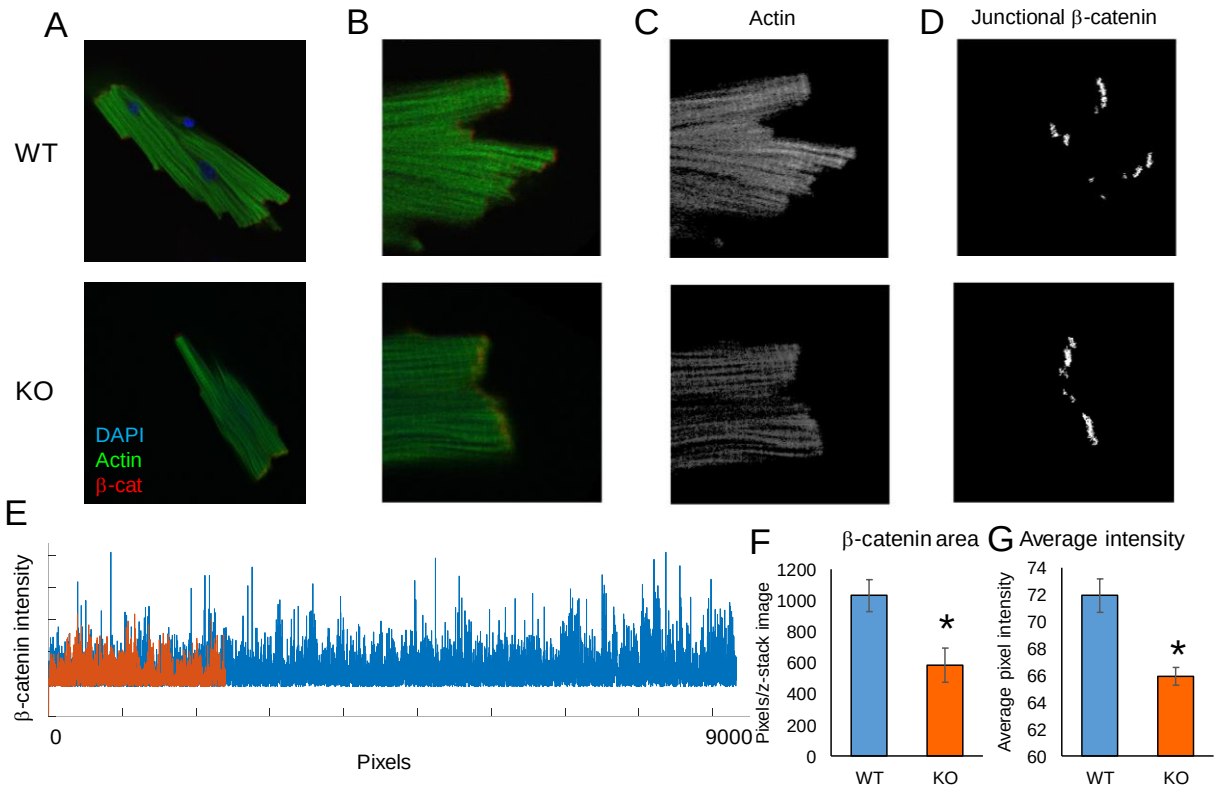

Figure 6.2 Quantification of adheren junction β-catenin. Confocal images of individual CMs stained for actin and β-catenin were rotated to align the cell horizontally (A) and a horizontal traces (representative trace shown by yellow line) at 10 pixel vertical spacing gave a vector of intensity (B), and a smoothed amplitude spectrum of the FFT transform of this intensity signal (C) was used to find the primary peak frequency. The inverse of this frequency gives a measure of sarcomere length per slice and these were averaged together (D) to reveal consistent sarcomere lengths between groups (N=1 cell).

Finally, I used a Bruker biocatalyst atomic force microscope (AFM) system to measure the stiffness of live isolated cardiomyocytes, MEFs, and CFs. The quantitative nano-mechanical mapping mode was used to assess both the topography and elastic modulus of WT and KO cells. We used a blunted pyramidal tip to indent and gather mechanical information from about a micron below the cell surface. The system was calibrated on a 40kPa polyacrylamide gel. Between four and ten cells were scanned per group and the median elastic modulus calculated from approximately 10x10 micron

scans for each cell (≥10,000 measurements per scan). The average median cell stiffness was calculated and compared between WT and KO cells with a student t-test. AFM assessment revealed that the elastic modulus of the KO CM was significantly less than the WT cells. Conversely, KO MEFs were significantly stiffer (**Figure 6.3**). Additionally, scanning CFs isolated from adult WT and KO hearts revealed that many of the KO cells had loss of detectable intracellular fibers, and instead had stiff, round protrusions, predominantly near the cell nucleus (**Figure 6.4**). These features may correspond to the whorls of over-stabilized microtubules observed in immunostaining of these cells [227].

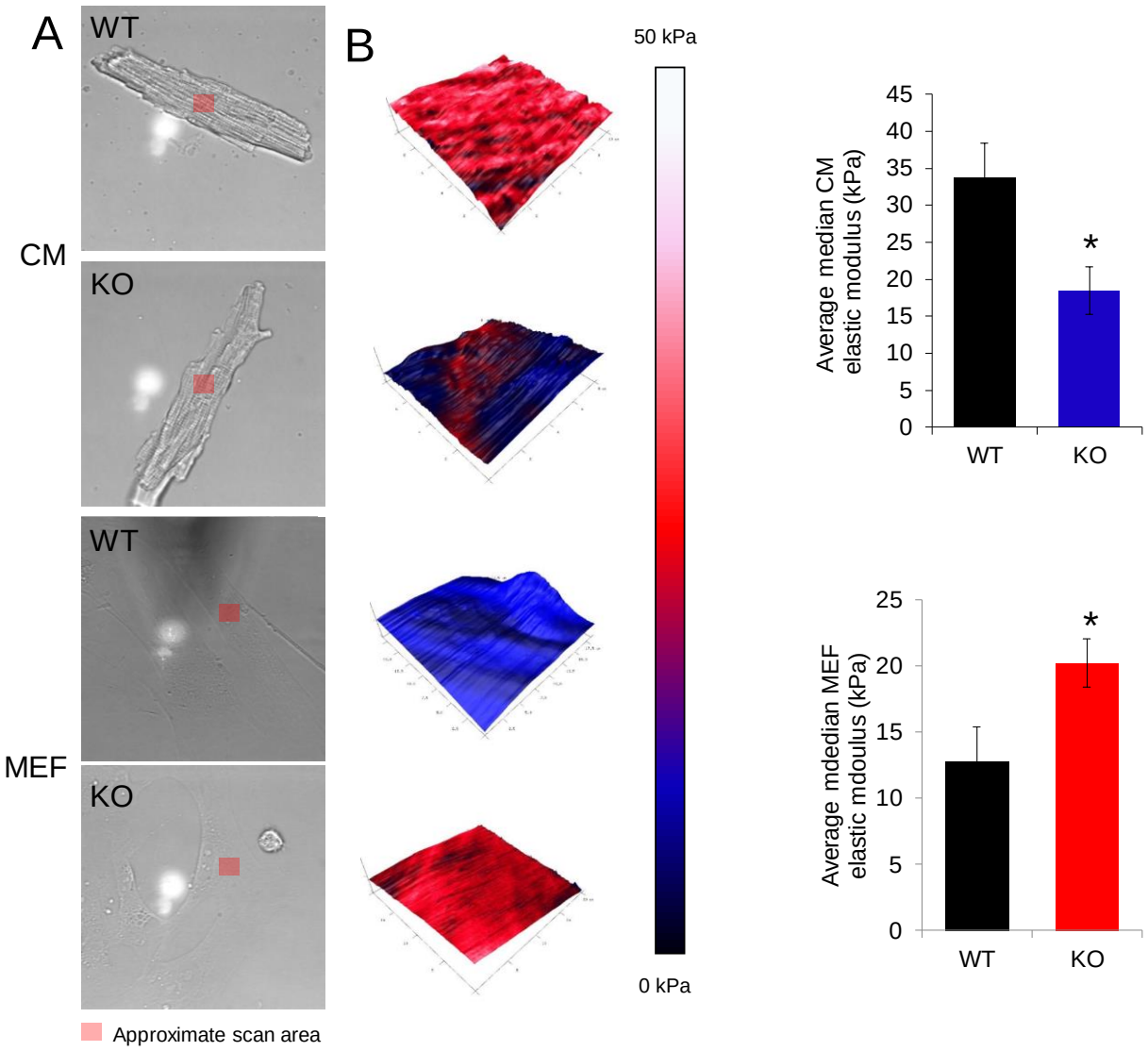

Figure 6.3 Quantification of cardiac cell stiffness. AFM of WT and CENP-F KO CMs and MEFs. Bright field images of representative cells with approximate scan area highlighted in red. Next a colormap of the elastic modulus of an approximately 10x10 μm scan, overlayed on a 3D rendering of the topography of the cell surface. Finally the average median elastic modulus of each cell type is presented. * indicated $p < 0.05$ relative to WT. $N \leq 11$ for CM, $N \leq 5$ for MEFs.

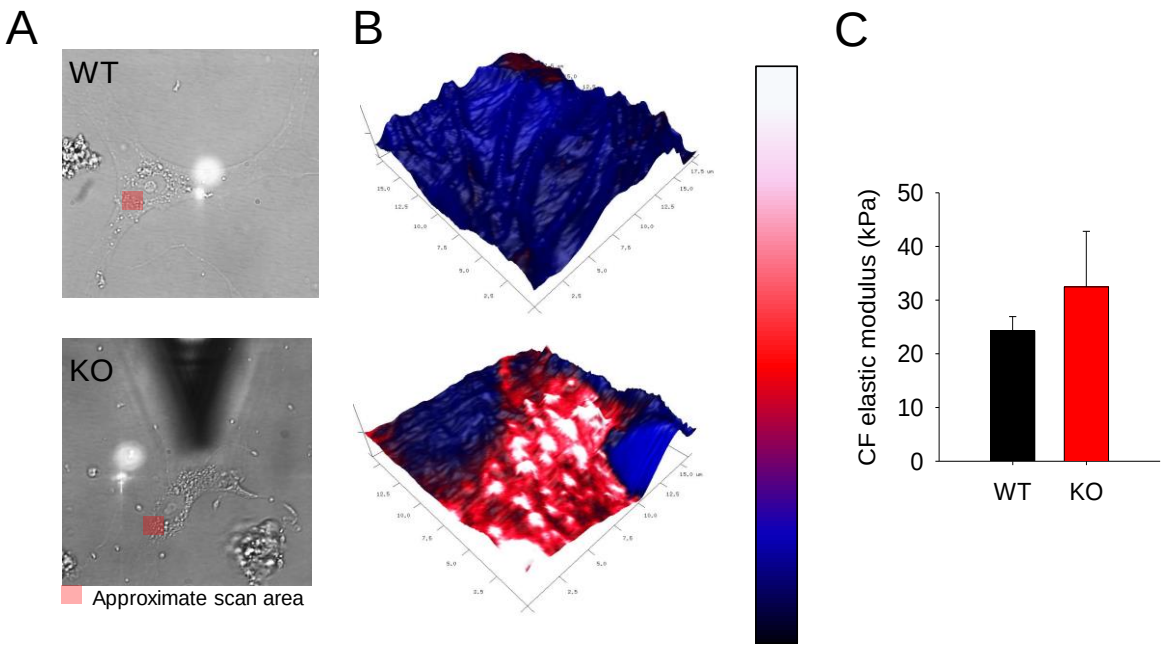

Figure 6.4 Quantification of CF stiffness. Atomic force microscopy of WT and KO cardiac fibroblasts. Bright field images of representative cells with approximate scan area highlighted in red. Next a colormap of the elastic modulus of an approximately 10x10 μm scan, overlayed on a 3D rendering of the topography of the cell surface. Finally the average median elastic modulus of each cell type is presented.

These findings suggest that the CENP-F mutation is disrupting the internal mechanical structure of both CMs and fibroblasts by altering microtubule structure and stability. It also highlights a distinct role and function for microtubules in CMs, which is relatively undefined. Specifically, while the loss of CENP-F on average increases stiffness of fibroblasts, it functionally decreases the stiffness of CMs in the region just proximal to the membrane. This area contains both costamere structures and the sarcolemma, both of which are involved in mechanotransductive signaling in the CM, as well as transmitting forces generated in the myofibrils to neighboring cells and the ECM. When this structure is disrupted (as occurs with CENP-F mutation), the effects extend internally to overall sarcomere alignment (measured by both TEM and quantification of

immunostaining (**Figure 6.2**)), and externally to reduced heart function and the development of dilated cardiomyopathy [234].

The organ level effects of this mutation, especially the observable interstitial fibrosis, are likely due to alteration of CF behavior. In the original study of this CENP-F mutation in mice, a CM specific deletion caused significant interstitial fibrosis, mediated by the genetically normal CFs. Given the natural sensitivity of fibroblasts to dysregulated mechanical environments and their *in vivo* localization interspersed among CMs, it is not then surprising that evidence of profibrotic MyoFB activity is evident *in vivo*. With an observable decrease in stiffness near the cell membrane and dysregulated junctions and sarcomeres, the CENP-F knock-out CMs likely exert irregular force profile on interstitial CFs *in vivo*, leading to the observed cardiomyopathy. While this study has been limited to investigation of the internal structure of individual cardiac cells, it is expected that the complex, 3D interactions of CMs and CFs direct the progression of this disease, along with many cardiac diseases. Future study is needed to observe and characterize these cellular interactions and their relative effects on contractile function and ECM remodeling.

Introduction of engineered cardiac tissue constructs

One class of tools that has been developed to better characterize cardiac cell function *in vitro* is engineered cardiac tissue constructs (ECTCs), which allow for recreation of some of the cellular components of cardiac tissue, but also for more precise measurement of physiological properties, including mechanical function.

Cardiac thin films have been used in many applications, and are attractive for their ease of production and adaptability for use in different contexts [18], [235], [236]. However, they are limited by a two-dimensional frame. There are some three-dimensional constructs, but many of these, like most traditional muscle measurement techniques, rely on either isometric or isotonic setups, whereas in the heart, the muscle is contracting against an applied transverse load in an auxotonic manner.

To address some of the limitations of existing ECTCs, a team at Vanderbilt developed the I-wire construct, which consists of a linear cellular construct suspended in media in a PDMS channel and mounted on conductive wires at each end. The construct is formed from a suspension of cells in an ECM solution (either collagen or fibrin) which is poured into the channel and allowed to compact over the course of a week. A calibrated probe can then be brought into contact with the side of the construct, and displacement of the stage used to stretch the construct. The system is mounted on an inverted microscope, so the deflection of the probe can be measured optically, both at static equilibrium at different stage positions and, in the case of CM containing constructs, with the addition of electrical stimulation. An initial study was conducted to describe the creation of these constructs using neonatal rat CMs and the ability of the system to replicate relevant parameters in CM biology. In tandem with this work, I worked with the original creators of the I-wire platform, as well as Matthew Shotwell, to develop a mathematical modeling strategy to describe the construct mechanics using a Hill-type model.

The following study presents the biomechanical analysis of the “I-Wire” platform using a modified Hill model of muscle mechanics that allows for further characterization

of construct function and response to perturbation. The I-Wire engineered cardiac tissue construct (ECTC) is a novel experimental platform to investigate cardiac cell mechanics during auxotonic contraction. Whereas passive biomaterials often exhibit nonlinear and dissipative behavior, active tissue equivalents, such as ECTCs, also expend metabolic energy to perform mechanical work that presents additional challenges in quantifying their properties. The I-Wire model uses the passive mechanical response to increasing applied tension to measure the inherent stress and resistance to stretch of the construct before, during, and after treatments. Both blebbistatin and isoproterenol reduced prestress and construct stiffness; however, blebbistatin treatment abolished subsequent force-generating potential while isoproterenol enhanced this property. We demonstrate that the described model can replicate the response of these constructs to intrinsic changes in force-generating potential in response to both increasing frequency of stimulation and decreasing starting length. This analysis provides a useful mathematical model of the I-Wire platform, increases the number of parameters that can be derived from the device, and serves as a demonstration of quantitative characterization of nonlinear, active biomaterials. We anticipate that this quantitative analysis of I-Wire constructs will prove useful for qualifying patient-specific cardiomyocytes and fibroblasts prior to their utilization for cardiac regenerative medicine.

Three-dimensional engineered cardiac tissue constructs (ECTCs) fill an important gap in understanding cardiomyocyte (CM) function, fibroblasts, and the extracellular matrix (ECM) they produce in a physiologically relevant, *in vitro* context. ECTCs exemplify the challenges associated with characterizing a nonlinear, dissipative, active biomaterial with a mathematical model. We developed the “I-Wire” ECTC

platform to probe the function of CMs while both the applied force and length are changing during auxotonic contraction [237]. This ECTC design better approximates the environment *in vivo*, since CMs contract against the changing load of ventricular pressure in their native environment. While the I-Wire offers useful insights into CM mechanics and function, the dynamically changing length and force can make analysis more complex than a simple isometric or isotonic contraction. Here we have developed an analysis strategy that permits extraction of different CM and ECTC properties and physiologic responses.

The force-generating capacity of cardiac muscle is inherently dependent on length, passive stiffness, and velocity of contraction [238]–[240]. A simple model for muscle mechanics that includes damped parallel and series elastic springs was originally proposed by Hill, and it has been used to describe striated muscle mechanics in many contexts [238], [241]–[245]. Although the Hill model has limitations, it has been used and modified in numerous applications, such as predictions of the relevant mechanics involved in heart failure and interventional treatment strategies [246]–[250]. The objective of this work is to use a modified Hill model to predict changes in CM mechanics in the I-Wire construct to gain insight into clinically relevant mechanical effects, and to demonstrate the detailed characterization of an active tissue equivalent of significant clinical interest.

Methods of I-wire development and analysis

ECTC creation and measurement

ECTCs were formed and their mechanical response to increasing, perpendicularly applied tension was measured as described [237]. Neonatal rat ventricular cells were obtained from 2-day-old neonatal Sprague-Dawley [91] rats using a trypsin digestion protocol with agitation overnight at 4˚C [251]. The population of isolated cells used to form the construct was heterogeneous, including CMs, CFs, ECs, and vascular smooth muscle cells [19]. The isolated cells were mixed with fibrinogen (5 mg/mL, Sigma-Aldrich, St. Louis, MO, USA) / Matrigel™ (100 μL/mL, BD Biosciences, San Jose, CA, USA) plus thrombin (30μL/mL, Sigma-Aldrich, St. Louis, MO, USA) [54], and pipetted in a casting mold (**Figure 6.5A**). The construct polymerized for one hour at 37˚C, then 2 mL of cell culture media was added per well. Over time, the preparation contracted to form an elongated construct roughly 350-400 μm in diameter and 7 mm long. After 13-15 days of culturing, the contractility and stiffness of the engineered cardiac tissue construct (ECTC) (Fig. 1B, C) could be measured using a microscope-based optical setup.

To create longitudinal tension in the construct, a translatable stage applies transverse force to the construct with a flexible probe, and the deformation of the probe allows for precise measurement of both the tensile properties and the developed force in the construct over the course of a contraction (**Figure 6.6B**). Contraction was stimulated by a 5 ms pulse (six times threshold) delivered through the anchoring wires, and probe position was recorded at 200 frames per second. For each contraction condition, seven successive contractions were averaged.

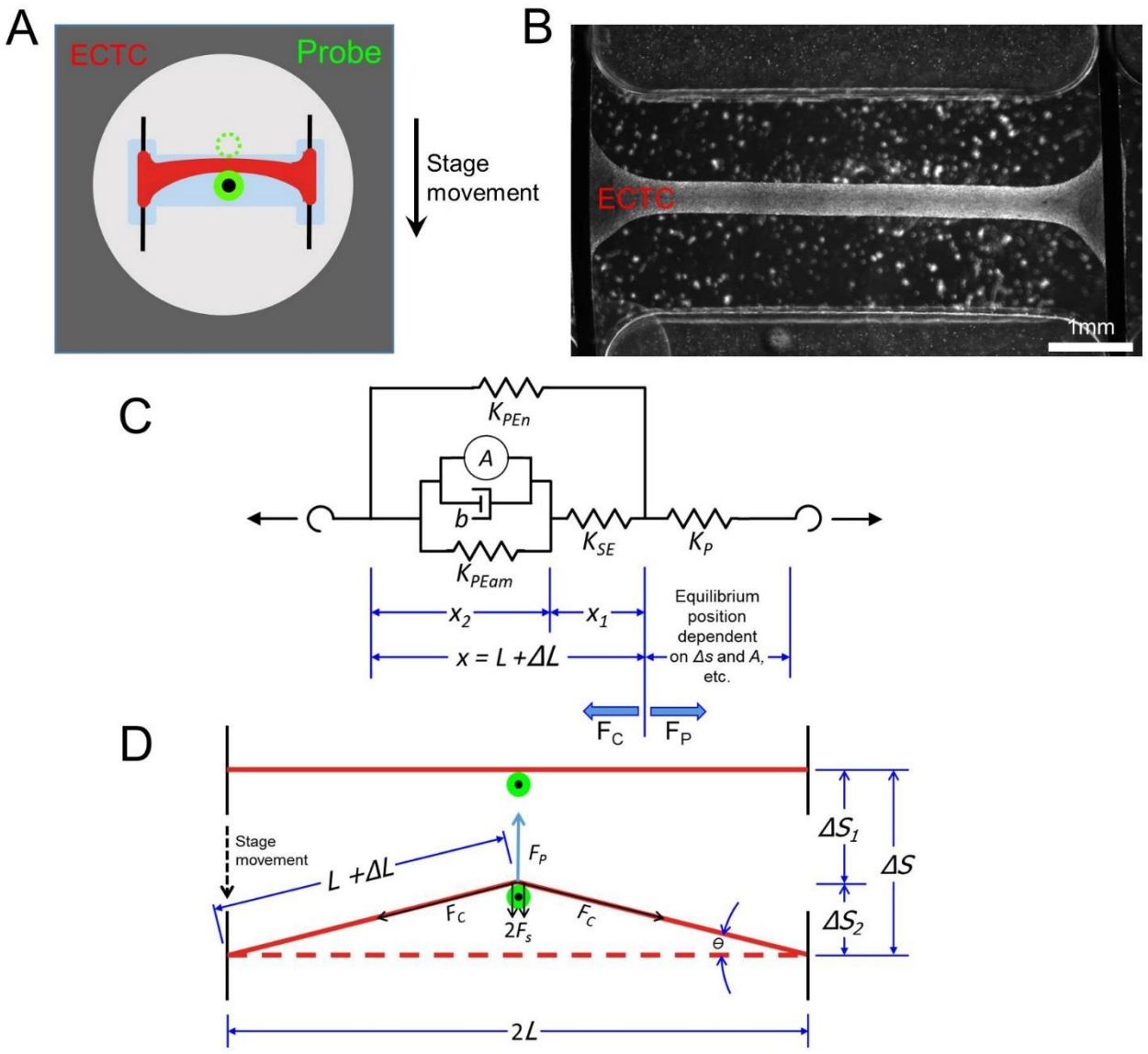

Figure 6.5. Platform description and model schematic. (A) Representation of the I-Wire construct from above, with the unloaded position of the probe indicated by the dotted green circle. (B) Image of I-wire construct. (C) Schematic simplified to highlight relevant measurements. See text for variable names. (D) Diagram of the relevant mechanical model (a modified, Hill type model), consisting of the muscle mechanics components (left side of dashed line) linked to a nonlinear (with respect to L) spring representing the probe (right side of dashed line).

The passive and peak developed force, as presented in the companion paper, were calculated as the transverse force exerted on the probe by the construct (F_P) and were proportional to the deflection of the probe from center (Δs_1) multiplied by the stiffness of the probe (K_P); (Figure 1F of [237]) and Equation 6.1. The following equations describe how to transform a transverse force applied by the probe by stage displacement to a longitudinal force along the length of the construct (F_C). We start with Hooke's law

$$F_P = K_P \Delta s_1 \ . \qquad \text{Equation 6.1}$$

The lateral deflection of the probe tip (Δs_1) and the lateral displacement of the construct midpoint (Δs_2) sum to the total deflection of the stage (Δs):

$$\Delta s_1 = \Delta s - \Delta s_2 \ . \qquad \text{Equation 6.2}$$

Δs_2 can be calculated from the extension of the construct (ΔL) according to the Pythagorean Theorem

$$\Delta s_2 = \sqrt{(L + \Delta L)^2 - L^2} = \sqrt{\Delta L(2L + \Delta L)} \ , \qquad \text{Equation 6.3}$$

which in turn can be substituted into Equation 6.2, and further into Equation 6.1 to yield

$$\Delta s_1 = \Delta s - \sqrt{\Delta L(2L + \Delta L)} \ , \qquad \text{Equation 6.4}$$

$$F_P = K_P(\Delta s - \sqrt{\Delta L(2L + \Delta L)}) \ , \qquad \text{Equation 6.5}$$

which describes the transverse force in terms of construct stretch along its length and initial stage displacement. Finally, F_P is balanced by the lateral component of force developed along the construct direction in both halves of the construct. Simple trigonometry shows that

$$F_C = \frac{F_P(L+\Delta L)}{2\Delta s_2} = \frac{F_P(L+\Delta L)}{2\sqrt{\Delta L(2L+\Delta L)}} \ , \qquad \text{Equation 6.6}$$

as derived in Appendix B.

Table 6.1. Model variables

Variable	Description (units)
Δs	Distance I-Wire frame is moved laterally to apply force with the probe (m)
Δs_1	Distance the end of the cantilever probe is deflected (m)
Δs_2	$\Delta s - \Delta s_1$ (m)
F_P	Transverse force delivered by the cantilever probe (N)
F_C	Longitudinal force within the ECTC in response to F_P (N)
L	Half-length of unstretched I-Wire construct, in practice 3.5 mm (m)
L_{int}	Intrinsic half-length of the ECTC were its end wires released (m)
ΔL	Change in ECTC half-length as the probe stretches the ECTC (m)
ΔL_{offset}	Estimated difference between L and L_{int} int. (m)
$prestress$	Estimated tension in unstretched construct at length L (N)
K_M	Steady-state stiffness of muscle construct (Nm^{-1})
K_P	Cantilever probe spring constant (Nm^{-1})
K_{PEam}	Spring constant of actin/myosin parallel element (Nm^{-1})
K_{SE}	Spring constant of series element (Nm^{-1})
K_{PEn}	Spring constant of non-actin/myosin parallel element (Nm^{-1})

Action potentials in ECTC were recorded by using floating micropipettes filled with 3-M KCl [252]. The micropipettes were pulled from borosilicate glass capillaries (WPI, Sarasota, FL) by a micropipette puller (P80/PC, Sutter Instruments, Novato, CA, USA). The tips of the micropipettes were mounted on a platinum wire of 50 µm diameter. The reference Ag/AgCl electrode (EP8, WPI, Sarasota, FL, USA) was placed in the well next to the PDMS insert. The electrodes were connected with a dual differential electrometer (Duo 773, WPI, Sarasota, FL, USA) and signals were digitized, visualized, and recorded by a digital oscilloscope (TDS5034B, Tektronix, Beaverton, OR, USA). The sampling rate was 25 kHz. The recorded data were processed with a

Savitzky-Golay digital filter (OriginLab, Northampton, MA, USA). To inhibit contractility, the excitation-contraction uncoupler blebbistatin (Sigma-Aldrich, St. Louis, MO, USA) was applied at a concentration of 6 μM.

Model development

In recognition of the complexity of cardiac tissue as a biomaterial, we divided the parallel elastic resistance term in the traditional Hill model to differentiate the passive contributions of actin myosin interactions and other passive mechanical linkages, including microtubules, z-discs, and extracellular matrix. The second passive element (K_{Pn}) (**Figure 6.5D**) was not responsive to treatment with blebbistatin or isoproterenol. Blebbistatin is a reversible specific inhibitor of the actin-myosin interaction [253]. Particularly, it binds to the myosin-ADP-P_i complex, impedes phosphate release, and thereby stabilizes the metastable state of myosin [254]. Whereas isoproterenol is a known β-adrenergic stimulator, which affects both contractility and heart rate [255].

When transformed from passive transverse force exerted on the probe to passive tension along the construct length (Equation 5.6), the resultant forces have a linear relationship with respect to the steady-state relative passive length change with a non-zero prestress y-intercept (**Figure 6.6A,B**) as follows:

$$F_C = K_M * \left(\Delta L + \Delta L_{offset}\right) = K_M * \Delta L + prestress \ , \qquad \text{Equation 6.7}$$

with K_M serving as a lumped parameter of the three elastic elements,

$$K_M = \frac{K_{PEam} + K_{PEn} + K_{PEn} * \frac{K_{PEam}}{K_{SE}}}{1 + \frac{K_{PEam}}{K_{SE}}} \ . \qquad \text{Equation 6.8}$$

This muscle mechanics model is linked to a nonlinear (with respect to ΔL) spring (**Figure 6.5C**; right side) that represents the force applied by the probe to the construct

(Equation 6.9), which should be equivalent to the value of the force in the construct (Equation 6.7),

$$F_C = \frac{1}{2} K_P \left(\frac{\Delta s}{\sqrt{\Delta L(2L+\Delta L)}} - 1 \right) (L + \Delta L) \ . \qquad \text{Equation 6.9}$$

The passive resistance of the muscle was used to estimate model parameters K_M, *prestress*, and ΔL_{off} (**Figure 6.5**) for each construct, before and after different perturbations (blebbistatin treatment: 6 μM; isoproterenol treatment: 1 μM; the incubation time for blebbistatin and isoproterenol was 10 min; shortening the construct: ~20 percent of original length).

The final step in the analysis, described in detail in Appendix B, is to derive the differential equation that relates ΔL to its rate of change of $\dot{\Delta L}$

$$\dot{\Delta L} = \frac{\left(1+\frac{K_{PEam}}{K_{SE}}\right) f_1(\Delta L) - K_M(\Delta L + \Delta L_{offset}) - F_A}{b\left(1-\frac{f_2(\Delta L)-K_{PEn}}{K_{SE}}\right)}, \qquad \text{Equation 6.10}$$

which can be used to predict the contraction traces by solving it in MATLAB using ode15s.

Study design statistical analysis

Five independent constructs were treated with blebbistatin and changes in K_M were quantified from the mean of the constructs' passive tension before and after treatment over a range of stage displacements (0-1300 μm). Experimental measurements are presented as means ± SEM, and force measurements were compared at each stage position using an unpaired t-test. Seven constructs were treated with isoproterenol, and their passive mechanics and dynamic contraction were

fit independently over a range of stage displacements (0-2000 μm), which correspond to increasing applied transverse loads.

The passive model parameters were estimated for each construct using linear least squares analysis of the passive force measurements. Active contraction was then simulated in the model by an activation force function originating in the contractile element with a magnitude of around 1.4 mN (within a physiological range for a construct with 0.1 mm^2 area [256]) and a duration of 250 ms (the measured length of an action potential in these constructs [237]). Three active parameters (K_{SE}, K_{PEam}, and b) were estimated using a nonlinear least squares optimization technique in MATLAB. More information about the model formulation and optimization techniques can be found in the supplemental materials. The confidence intervals of parameter estimates were approximated using the observed information method [257]. The effects of pharmacologic treatment on the model parameters conserved across constructs were assessed using paired t-tests. One construct was shortened to assess the model's accuracy at different lengths.

Results of I-wire analysis

Chemically induced changes in passive mechanics and developed force

We transformed the measured data from the transverse-force and transverse-deflection I-Wire coordinate system into longitudinal force and length changes along the construct. This allowed us to demonstrate a significant reduction in passive tension after treatment with blebbistatin over all applied transverse loads (**Figure 6.6A**). Our model framework assumed that blebbistatin treatment would abolish the actin-myosin

contribution to passive stiffness (represented by K_{PEam}), causing the overall passive parameter K_M to be equal to K_{PEn} (Equation 6.8). A linear fit to the passive force measurements both before and after introduction of blebbistatin revealed that the non-actin myosin passive stiffness element contributes approximately 67% percent of the total passive force in the muscle and about 73% of the prestress (**Figure 6.6A**). We also measured the effect of isoproterenol treatment, a β-adrenergic agonist known to increase the rate of calcium cycling and muscle contractility while reducing muscle tension [258]. There was a significant reduction in passive force at every applied load after isoproterenol treatment (**Figure 6.6B**). When analyzing these data using our passive mechanics model, we observed a slight, insignificant decrease in the overall K_M as well as a significant reduction of both *prestress* and ΔL_{offset} values (**Table 6.2**). We also observed a significant increase in the developed force generated by the constructs (**Figure 6.6C**).

Table 6.2. Passive mechanic metrics for control and isoproterenol-treated ECTCs

	Control	**Isoproterenol**	p-value
K_M	0.7 ± 0.05 Nm^{-1}	0.6 ± 0.05 Nm^{-1}	0.054
prestress	0.22 ± 0.02 mN	0.12 ± 0.01 mN	<0.001
ΔL_{offset}	311 ± 14 μm	210 ± 25 μm	0.003

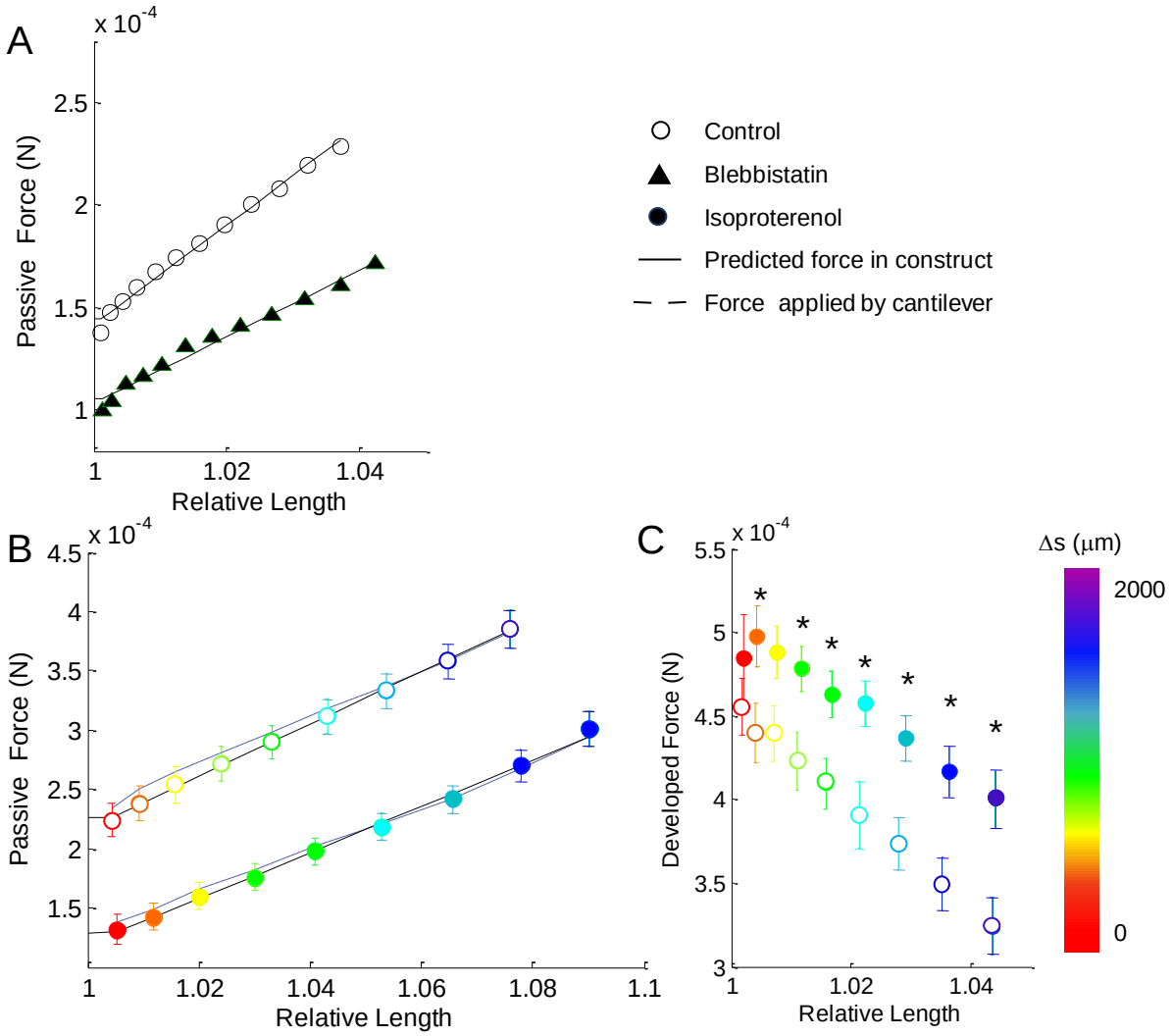

Figure 6.6. Passive and developed forces in constructs are affected by pharmacological perturbations. (A) Passive force in constructs treated with blebbistatin was significantly reduced ($p < 0.01$) for all samples. (B) Passive force was significantly reduced ($p < 0.01$) between all isoproterenol treated samples, and the predicted and calculated force in the ECTC had relatively close agreement with experimental data. (C) Peak developed force was significantly increased ($p < 0.05$) in the isoproterenol-treated constructs at most applied tensions (* indicates $p < 0.5$). Experimental data presented as mean ± SEM.

Simulation of active contraction

Once we estimated the passive muscle stiffness, prestress, and offset for each construct, active contraction was simulated at a variety of starting tensions corresponding experimental range of stage displacement. An idealized biexponential curve was used to simulate the activation force generated by the CMs in response to electrical stimulation (**Figure 6.7A**) [244]. We simulated muscle inactivation by setting K_{SE} to zero, and the model predicted no muscle shortening, as was observed with blebbistatin treatment of the constructs. Three active parameters (K_{SE}, K_{PEam}, and b) were estimated using a nonlinear least squares optimization technique in MATLAB. Regardless of starting conditions or relative elastic element contributions, this procedure consistently found that the isoproterenol-treated constructs had a significant reduction (50%; $p < 0.05$) in the estimated viscosity parameter of the contractile element (b). Independent optimization of K_{SE} and K_{PEam} also found a significant reduction ($p < 0.05$) of K_{SE} in the isoproterenol groups relative to control. In general, this optimization reduced the overall mean squared error of the model fit by between two- and five-fold across the seven constructs. Using these techniques, the model successfully predicted the experimentally measured developed force (**Figure 6.7B-C**) and length changes of individual constructs (**Figure 6.7D-E**). Furthermore, averaging the estimated parameters across constructs gave a robust fit of the average developed force (**Figure 6.7F**).

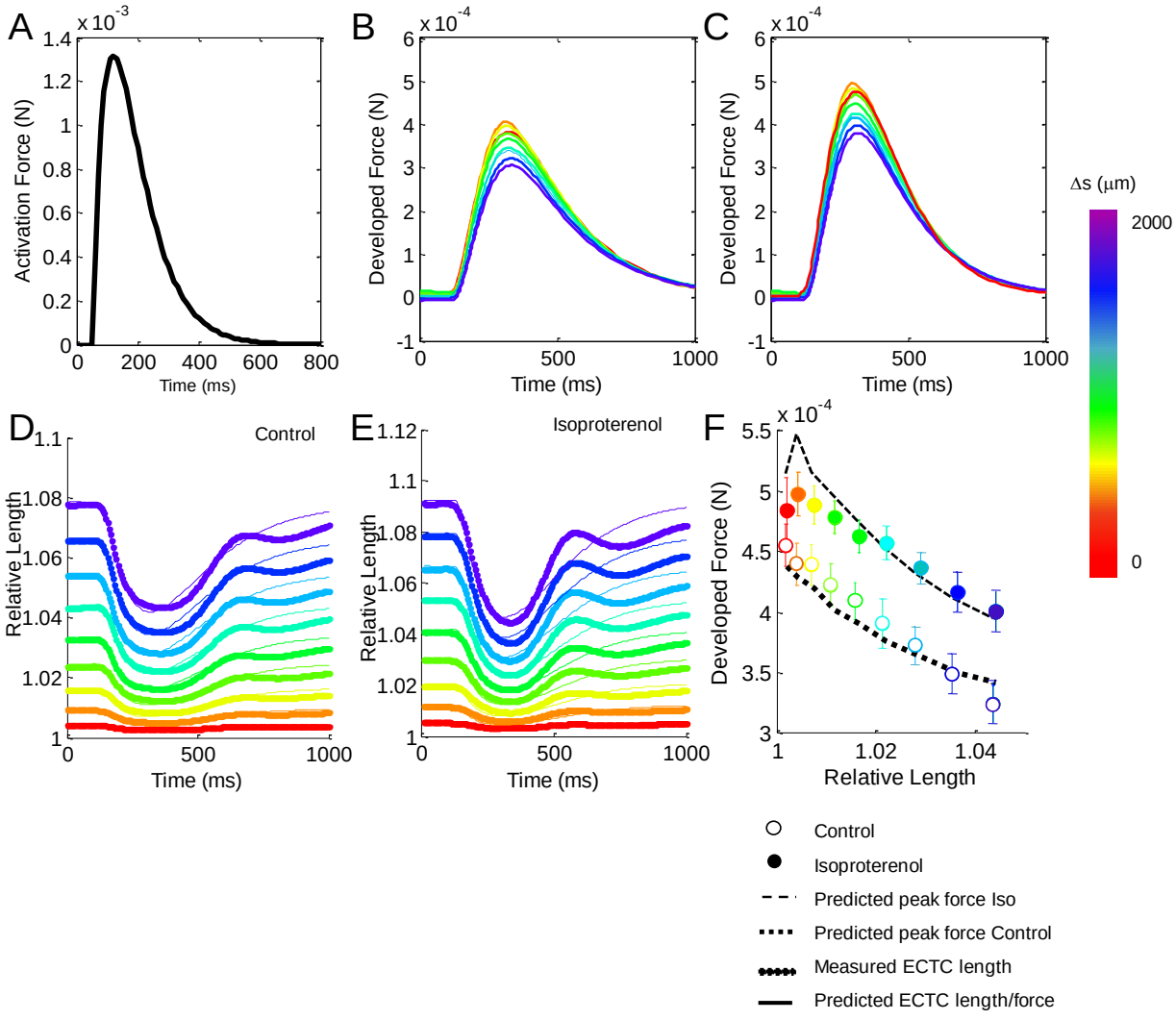

Figure 6.7. Predicted active force in ECTCs. (A) Biexponential activation force input used. (B,C) Predicted developed force and (D,E) relative predicted length compared to measured data for representative construct. (F) Predicted model fit to average data using average of best fit parameters. Experimental data presented as mean ± SEM.

Simulating active contraction with microelectrode trace

After characterizing the fidelity of our model fit using an idealized biexponential function, we repeated these analyses using data from a microelectrode trace of the action potential as the activation force (**Figure 6.8A**). The estimated model parameters using this alternative activation force function confirmed a reduction of the viscosity parameter (*b*) with isoproterenol treatment, and the experimental data were well fitted by visual inspection. However, the mean squared error was approximately two- to four-fold higher, relative to that associated with the biexponential activation force function (**Figure 6.8B-E**). Next, we modified the width of the activation force trace to attempt to recreate the mechanical restitution curve described in the original paper describing the I-wire device [237]. By varying the action potential duration from 150 ms to 250 ms (**Figure 6.8F**), the model predicted increasing force traces (**Figure 6.8G**) and peak forces (**Figure 6.8H**) that greatly resembled the experimental data presented in Figures. 2 and 4 of the companion paper [237].

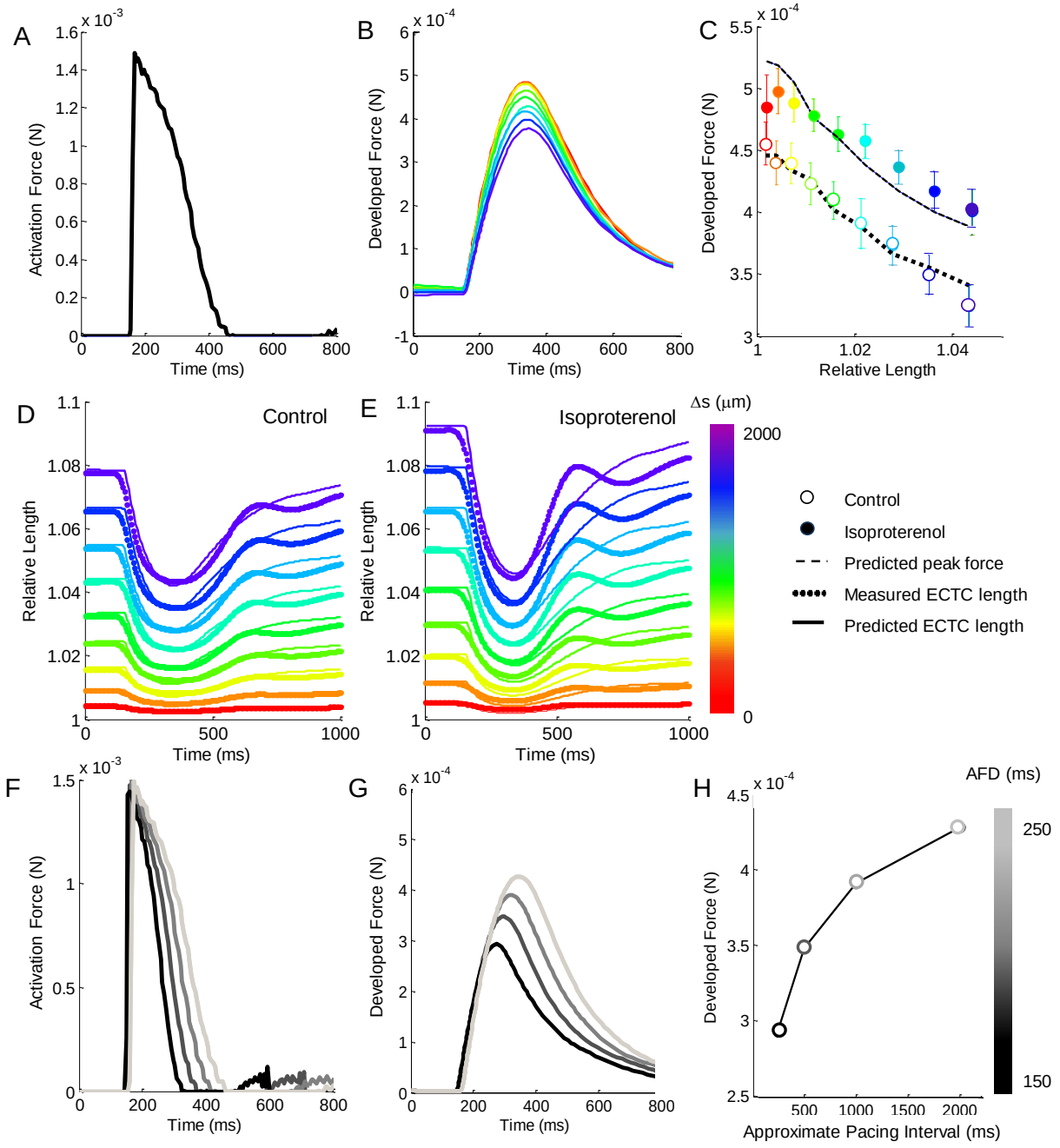

Figure 6.8. Simulation of active contraction using construct action potential. (A) Activation force shape taken from a measurement of the action potential voltage (1) scaled similarly to idealized biexponential function. (B) Developed force traces, (C) peak forces, and (D,E) relative length fit in a representative construct. (F) Horizontal scaling of activation force traces to match measured values at different pacing frequencies. (G) Predicted model response to these inputs for the construct at a tension 0.54 mN, and (H) the peak developed force plotted over the estimated pacing frequency.

Shortening construct to predict length-related effects

We tested the model's response to reducing the length of a preformed construct by ~20% by moving one of the anchoring wires to a new groove in the PDMS mold (**Figure 6.9A**). The experimental results revealed an overall decrease in the peak developed force, as well as a flattening of the downward trend of force generation (**Figure 6.9B**). This experiment was simulated in the model first by assuming that the measured mechanical stiffness of the construct would remain unchanged by the release of tension, merely shifting over to have an offset and prestress of 0 (**Figure 6.9C**, black line). This manipulation resulted in a large mismatch with the experimental passive force data and a poor fit to the peak developed force data (**Figure 6.9D** black line). Next, the K_M was estimated using the passive force measurements in the shortened constructs (45% reduction from original), but prestress was still defined as 0 (**Figure 6.9C**, dark grey line). This correction improved the fit of the passive and developed force (**Figure 6.9D**, dark grey line) but the data were still mismatched. Next, both the K_M and prestress were fit to the experimental data, giving a much better fit of the passive force (**Figure 6.9C**, light grey line), but significantly under-predicting the peak force (**Figure 6.9D**, light grey line). Finally, the ratio of K_{SE} to K_{PEam} was changed to restore the value of the series element stiffness to that of the K_{SE} original construct length, and the results showed significant improvement of developed force fit (**Figure 6.9D**, dashed light grey line), as well as overall fit.

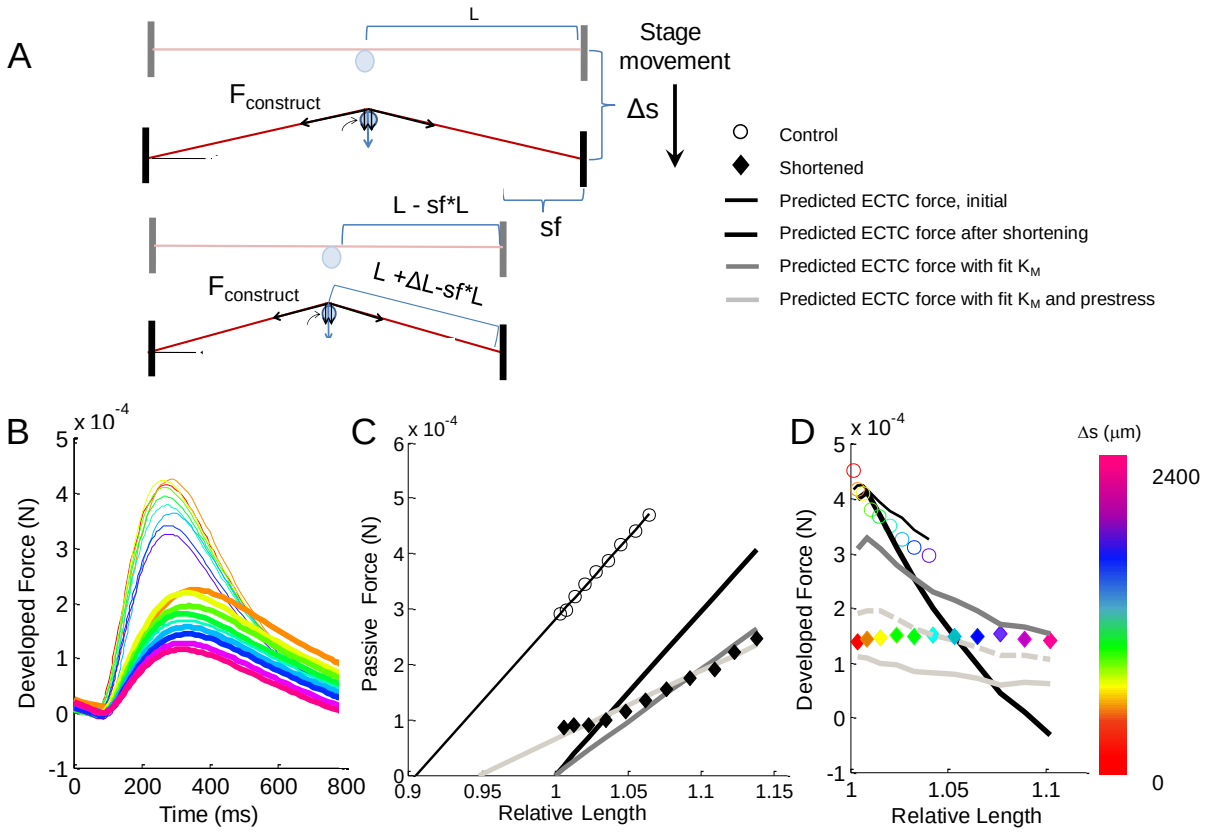

Figure 6.9. **Shortening construct to predict length-related effects.** (A) Schematic of construct shortening. (B) Traces of developed force in the original and shortened configurations. The thicker lines represent the shortened configuration. (C,D) Experimental and model fits of passive force and peak developed force in construct before and after shortening.

Discussion

CMs are a specialized and complex cells whose function is integrally linked to their internal structure and external environment. They are also key contributors to the progression of fibrotic disease in the heart, generating the forces that surround all cardiac cells. Novel bioengineered devices and analysis techniques like the ones described above can help clarify CM mechanics and their implications for the development of cardiac fibrosis. Our investigation of CENP-F mutant CMs and

fibroblasts highlights the uniqueness of the CM intracellular structure, and the impact that internal structure can have on organ level disease. The rest of the chapter focuses on the development of a ECTC and a strategy for analysis that can be used to study cardiac cell mechanics in response to a host of perturbations, including clinically relevant mutations.

We have presented a model-based method to quantify the passive elasticity and active contractility of an ECTC that is extremely useful to the biomedical, bioengineering and physiology communities. This analysis allows an in-depth characterization of the mechanics of a 3D cardiac muscle construct that is able to dynamically contract while subjected to a range of applied transverse forces, and it complements the presentation of the data in the original paper [237]. The analysis strategy presented here allows for translation from force generated in the construct applied as a perpendicular load (F_P) to the longitudinal tension internal to and along the length of the construct (F_C). The peak force developed along the construct following contraction consistently decreased with increasing applied tension and applied stretch (**Figure 6.6C**). This was likely a result of the intrinsic force-length relationship of striated muscle cells, including CMs, in which the force-generating potential rapidly declines past the optimal length [238], [239]. This construct-focused analysis also makes it possible to estimate the prestress generated by CMs as well as fibroblasts during the process of construct formation and compaction. We demonstrated that this stress is significantly reduced by both blebbistatin and isoproterenol treatments. Blebbistatin is known to disrupt actin/myosin interactions within CM sarcomeres and has been shown to disrupt traction forces generated by fibroblasts [259], [260].

This model also enables simulation of active muscle contraction. The comparisons in Figures 6.7 and 6.8 demonstrate that either a biexponential curve or that resembling an action potential can be used as activation force inputs to drive the model, although the biexponential activation force trace delivers consistently better fits to the experimental measurements. In the future, microelectrode trace measurements could be used to predict altered mechanics in response to genetic mutations or drug effects. Parameter estimation using either activation force function revealed a significant decrease in effective contractile element viscosity (*b*), and suggests a potential decrease in K_{SE} after treatment with isoproterenol. Both effects are likely related to the increase in calcium availability and turnover mediated by isoproterenol, which decreases the short-term stiffening effect of actin-myosin interactions [247], [258], [261]. Future experiments to image intracellular calcium transients during contraction should make it possible to quantify these changes.

The collection of experimental data examined here was not sufficient to definitively differentiate the relative contributions of the model parameters and the active force function using the nonlinear least squares estimation method. The dynamic nature of the modified Hill model, however, allows prediction of mechanical responses to differing mechanical and electrical stimuli. Thus, it is possible to consider hypothetical experiments *in silico*, and to design experiments that are more highly informative about the underlying model components. For example, in order to distinguish the model parameters from the active force function, a natural next step experimentally would be to vary the rate and shape of mechanical loading in the absence of electrical stimuli (i.e., no active force). Supplemental Figure B4 illustrates the mechanical stimuli and

resulting passive changes in construct length for two such hypothetical experiments. These findings would permit independent assessment of the contributions of K_{PEam}, K_{SE} and b, which in turn would enable an inverse analysis of the data to estimate the activation force traces. Further development of the model should benefit from additional measurements that record the calcium transients associated with CM contraction and that image the differences in both transmembrane calcium potential between simultaneous field stimulation of the entire construct and the response that propagates from a bipolar stimulating electrode at one end of the fiber. It is likely that these calcium traces will correspond with the predicted activation force traces, improving the model fit and providing insight into electromechanical coupling.

This model is also able to recreate changes in muscle mechanics in response to changing electrical and physical inputs. Recreating the pacing frequency restitution curve confirms that using action potential traces is a viable input for predicting contractile response. Furthermore, the shortening experiments provided an interesting opportunity to test and refine the model. The peak force developed by the shortened ECTC was significantly lower than that for the original length, which suggests that the construct length has been reduced below some optimal length, thus reducing force-generating capacity. Our initial assumption that construct stiffness would be preserved with a large reduction in length proved to be a poor fit to the data. Subsequent trials revealed that at the reduced length, the construct has a much lower linear passive stiffness and retains some prestress even at low initial stretch. These results indicate that the stiffness that appeared linear at the original length is actually part of an

exponential or partially nonlinear stiffness function common in biological tissues [247], [262].

The I-Wire platform and these measurements and estimates of intrinsic muscle properties (K_M, *prestress*, and viscosity *b*) provide a powerful new tool for quantifying the effects of pharmacological strategies on CM function *in vitro*. Of particular importance, the constructs have a uniform cross-sectional area over most of their length, in contrast to animal papillary and trabecular muscles. In addition, it is feasible to study 3D ECTCs formed with CMs that are derived from human induced pluripotent stem cells. The I-Wire platform and our model-based analysis will also inform more complex models of heart function for interventional planning purposes [248]–[250] [246], [263]–[266].

With the advancement of induced pluripotent stem cell (iPSC) technologies specific to the heart [267], there is the possibility of being able to use cell-based technologies to support cardiac regeneration [26], [268]. This would then present the challenge of qualifying the cells that will be used to repair an ailing heart – one must be able to assess the mechanical, electrical, and metabolic potential of the cells prior to their use in a patient, particularly if those cells were derived from the patient's own iPSCs. The I-Wire platform in the accompanying paper [237] in combination with the modeling described in this one may provide this capability: prior to the utilization of the cardiomyocytes, fibroblasts, and other cells for regenerative therapy, these same cells could be used to create an *in vitro* I-Wire construct whose performance could be evaluated using a standardized protocol. Given such a protocol, one then might be able

to further refine the process by which these cells are derived to better optimize their performance *in vivo.*

Overall, we believe that this new technique will improve our understanding of the complex interplay between CM mechanics and function, and will also serve as a demonstration of model-based quantification of mechanically active tissue equivalents. Furthermore, we have in this paper outlined a computational procedure that should be applicable to many other active, contractile biomaterials and their mimics [269]–[271]. This platform, in addition to the single cell analysis techniques used to characterized the CENP-F KO cells, will provide valuable insight into the CM contributions to disease and cardiac mechanobiology.

CHAPTER 7

Impact and Future Directions

Summary and impact of results

This work approaches the pressing clinical issue of cardiac fibrosis from several perspectives, with the aim of developing better understanding of the cellular players and their respective roles in the complex biomechanical environment of the heart (**Figure 7.1**). Mechanobiology is particularly relevant in the heart because of the unique mechanical demands of cardiac function, and the dynamic process of tissue remodeling (and subsequent alteration of mechanical cues) that occurs during disease. Cadherin-11 is a mechanosensitive protein that mediates cell-cell interactions and transmission of force, so it was a natural focus of interest. We confirmed an important role for cadherin-11 in regulating both inflammation and fibrotic remodeling after myocardial infarction.

The first part of this dissertation focuses on a portion of the complex crosstalk between growth factor signaling and mechanosensing in fibroblasts. I primarily investigated the crosstalk between TGF-β1, FGF2, and integrin signaling in the regulation of MyoFB phenotype. TGF-β1 and FGF2 oppose one another in the regulation of both α-SMA and cadherin-11 expression, but both are active during the proliferative and fibrotic phases of myocardial remodeling. While these two cytokines lead to opposite end-points of fibroblast differentiation, they signal through similar intracellular mechanisms. Specifically, both cytokines cause phosphorylation of both MAPK p38 and ERK. Substrate stiffness is also a key modulator of MyoFB phenotype

and is transduced through integrins via p38 and ERK as well. In this case, we found that different dynamic signaling through Src, FAK, p38 and ERK could explain the inverse effects of TGF-β1 and FGF2 on α-SMA expression [139]. We also observed a decrease in expression of MyoFB markers α-SMA and cadherin-11 when plating on a softer, fibronectin-coated PDMS substrate. While α-SMA and cadherin-11 were similarly regulated by TGF-β1, FGF2, and stiffness, the absence of FAK had inverse effects on the expression of these two MyoFB proteins. Indeed, recent investigation of cadherin-11 has revealed that there is complex and in some ways inverse relationship between the expression of cadherin-11, α-SMA, and other MyoFB markers. In addition to MAPK signaling, GSK-3β and β-catenin signaling also play roles in signaling through growth factors in the regulation of MyoFB markers. In addition, β-catenin associates with cadherins and participates in mechanotransduction downstream of cadherins, including cadherin-11. This work can inform future studies into the regulation of the MyoFB phenotype, which has important implications for wound healing and fibrosis in both the heart and other organ systems. There is still much to be learned about heterogeneity within MyoFB populations, and how this heterogeneity can affect the relative accumulation and remodeling of ECM during development and disease. This study identified some of the common and distinct mechanism that regulate expression of two important MyoFB markers, cadherin-11 and α-SMA. Understanding the different signals that control generation vs. transmission of intracellular forces may clarify how fibroblasts coordinate large ECM remodeling efforts.

The next portion of my doctoral work expanded the focus to examine the population of non-CM cells that are relevant to cardiac fibrosis after MI, with a particular

focus on the cell-cell adhesion protein cadherin-11. We identified and described a critical role for cadherin-11 in the process of inflammation and fibrotic remodeling after MI. We discovered that cadherin-11 is expressed in non-CM cells in the heart and is highly expressed after MI in inflammatory cells, endothelial cells, smooth muscle cells, and MyoFBs. *In vivo* comparisions of wild type and cadherin-11-/- mice indicated that cadherin-11 functions to promote and increase initial inflammatory remodeling after MI. Next we tested a potential therapeutic blocking antibody against cadherin-11 (SYN0012) and found dramatic improvement in function, corresponding to a reduction in remodeling, measured by echocardiography, histological assessment, and atomic force microscopy. Mechanical and histological assessment of the hearts would suggest that the control hearts would experience higher amounts of strain due to tissue breakdown and remodeling, which would likely increase strain induced MyoFB differentiation. While CDH11-/- CFs have significantly impaired contractility, we observed no difference in CF contractility after treatment with SYN0012 in a free-floating gel environment *in vitro*. However, using the I-wire platform we were able to detect a significant reduction in intrinsic stress generated in a linearized, tensioned construct. This suggests that the dynamic mechanical environment of an infarct is important for SYN0012-mediated effects on MyoFB differentiation. It also highlights the functional difference between a mutation and a blocking antibody treatment. The former removes cadherin-11 from all of its potential roles interacting with other proteins in the cell membrane or adherens junction, while the latter specifically prevents cell-cell cadherin bonds.

After extensive screening of transcriptional changes due to SYN0012 treatment over time, we concluded that the beneficial effect is mediated by an overall reduction in

the inflammatory/remodeling program. This effect begins with a reduction in IL-6 expression in the non-CM cell population at day three post-MI, followed by a significant decrease in MΦs present at seven days post-MI. According to the results of an *in vitro* co-culture study, reduced interaction between fibroblasts and MΦs *in vivo* would decrease IL-6 expression and MMP13 expression. IL-6 expression was also directly reduced by SYN0012 treatment in the co-culture system, indicating that the mechanism for MΦ induced stimulation of IL-6 expression by CFs is partially dependent on cadherin-11. TGF-β1 was increased by SYN0012 treatment in the *in vitro* co-culture system, but the overall TGF-β1 *in vivo* was reduced at seven days. This is likely due to a faster and more effective resolution of inflammation with treatment, mediated by decreased IL-6 and increased TGF-β1 in the first week. We also observed a decrease in FGF2 and VEGF-a, that surprisingly did not seem to correlate with decreased vascularization. To conclude, we discovered that cadherin-11 promotes an overall increase in cellular activity and inflammation-driven remodeling and presents an attractive therapeutic target for improving outcomes after MI. Targeting cadherin-11 has several advantages: targeting the extracellular portion of a protein expressed by activated cell types simplifies effective drug delivery, blocking cadherin-11 modulates but does not eliminate the necessary components of inflammation and fibrotic remodeling, and studies using a similar strategy in other organs have not revealed any significant side-effects. This study also highlights the significance of proteins like cadherin-11 that mediate cellular interactions and force transmission.

Finally, I developed tools to investigate CM mechanics, which can provide additional information to understand cardiac function during disease and the mechanical

microenvironment experienced by cardiac cells. I first quantitatively analyzed the effects of a cytoskeletal structuring protein (CENP-F) on the internal structure of CM, as well as the mechanical properties of both CMs and fibroblasts. We observed that the loss of CENP-F reduces sarcomeric regularity and integrity. It also decreases the amount of β-catenin in the junctions between CMs, which potentially indicates insufficient transfer of force between CMs. Disrupted structural and specifically junctional integrity of CMs has been shown to drive the development of dilated cardiomyopathy in several papers, and this is also the main tissue phenotype that occurs as a result of the CENP-F mutation. Furthermore, microtubule disruption similar to the effects of the CENP-F mutation is a key method of action for several chemotherapeutics with known cardiotoxic effects. Cardiomyopathies in general are often associated with an increase in interstitial fibrosis that can be attributed to a disrupted mechanical environment between CMs, the natural location of interstitial fibroblasts and MΦs. Understanding how such intracellular changes affect cellular interactions and function could have a large impact on cardiac health.

Another important experimental tool that can bridge the gap between single cell studies of structural and mechanical changes and organ level changes is engineered cardiac tissue constructs. The final piece of my doctoral work focused on improving the mechanical analysis of one such construct, the I-wire construct. I developed a Hill-based modeling strategy that allowed for the quantification and comparison of mechanical properties including passive construct elasticity and initial prestress with pharmacological treatments including blebbistatin and isoproterenol. Both of these treatments decreased prestress in the constructs, and blebbistatin significantly

decreased the overall passive construct stiffness by disrupting the contributions of the actin-myosin interactions. We further used the model to estimate best-fit values for the dynamic mechanical parameters by comparing measured and simulated force traces in response to idealized and measured microelectrode activation traces. We observed a significant decrease in the functional viscosity of the constructs in response to isoproterenol treatment. We were also able to replicate the measured pacing restitution curves using measured activation traces, reinforcing that microelectrode traces could be a reasonable input for predicting mechanical tissue outputs. Finally, by shortening the construct, we were able to determine that our assumptions of linear mechanic components, not surprisingly, are not able to fully capture the mechanics of muscle tissue constructs at significantly reduced lengths. This may very well translate to the dramatically reduced function observed *in vivo* after dramatic LV expansion and remodeling. This construct platform can also be used for investigation of non-CM cell remodeling. Our initial test with CFs treated with or without SYN0012 revealed a difference in intrinsic stress generated by CFs that was not quantifiable with a traditional contractility assay. This finding highlights the need for platforms like I-wire to advance our ability to quantify cellular mechanics.

Overall, this doctoral project approaches the mechanobiology of cardiac fibrosis from the perspective of multiple cell types, covering a range of molecular sources of signaling and disruption. Given its critical role in fibroblast force transmission and regulation of signaling, I focused on cadherin-11 in the context of MyoFB differentiation, heterotypic cellular interactions, and remodeling after MI. My findings relating to regulation of the MyoFB phenotype will inform future studies into integrin signaling and

MyoFB population heterogeneity. Furthermore, I have determined and described a significant role for cadherin-11 in promoting inflammation and remodeling in the heart after MI and present it as a viable therapeutic target for improving outcomes. Finally, the techniques for quantifying CM structure and mechanics presented in this work will allow for better understanding of the cardiac mechanobiology throughout development and disease.

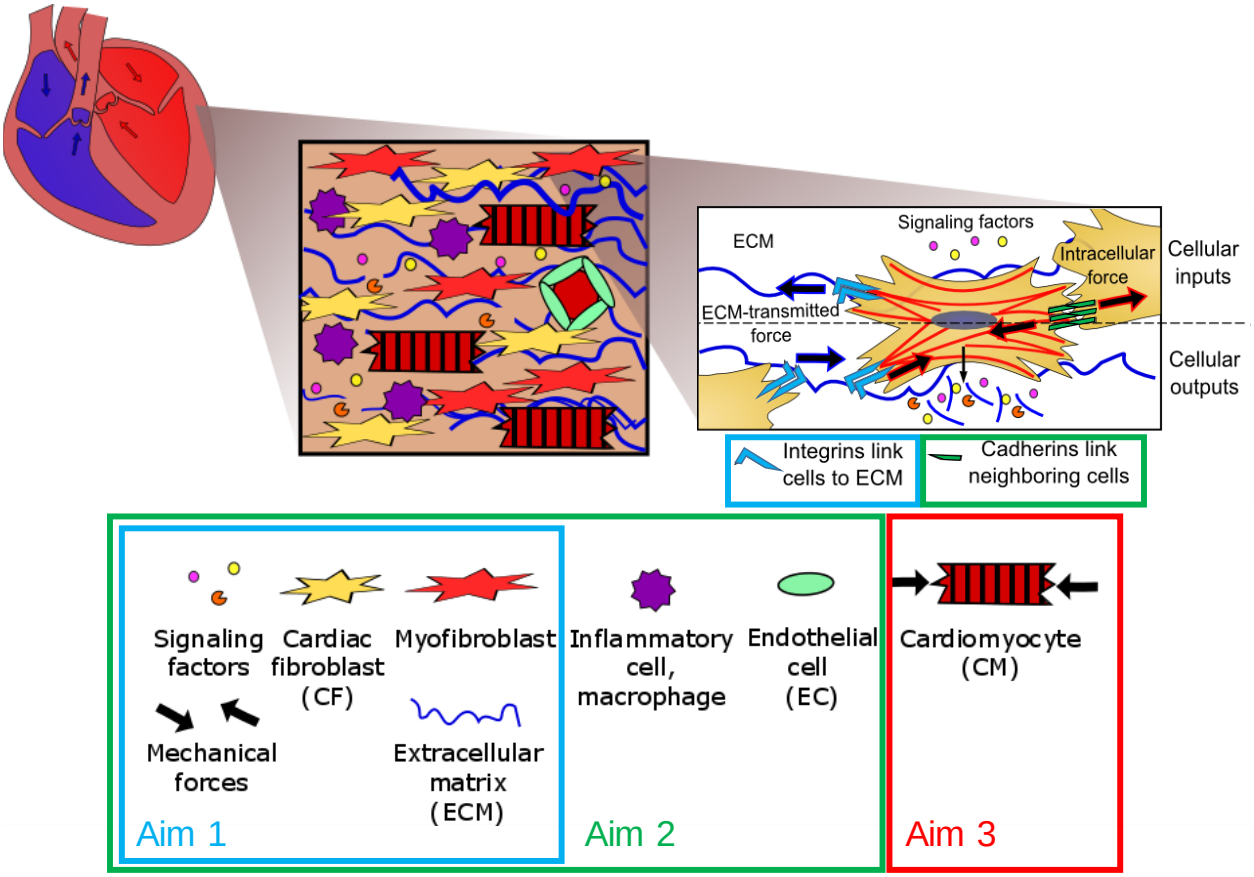

Figure 7.1 Graphical summary of dissertation topic and aims. The work described in this dissertation contributed to several publications, which will, along with this dissertation, distribute these insights and findings to a broader audience. Ch. 1-3 [19], Ch. 4 [139], Ch. 5 [208], Ch. 6 [227], [228]

Future directions

This work makes some important steps forward to understand the cellular components of cardiac fibrosis and mechanobiology, and can be used to inform new hypotheses and experimental directions. More study into the intracellular signaling both upstream and downstream of cadherin-11 expression and engagement will be very helpful for clarifying its specific place in the cellular regulatory network. Two of the most likely candidates for signaling downstream of cadherin-11 are β-catenin and p120 catenin. Both of these proteins associate with the intracellular domain of the cadherin-11 protein to form components of the adherens junction complex which mechanically link cadherins to the cytoskeleton. They have also both been shown to participate in or overlap with signaling downstream of TGF-β1 and Wnt signaling. Both participate in some degree of signaling downstream of cadherin-11 expression and engagement, but their particular roles in cadherin-11 mechanotransduction of applied strain, substrate stiffness, and intercellular tension has not been fully explored. β-catenin has been shown to participate in strain induced signaling downstream of cadherin-1 and -2, but the distinctions between these different cadherins as it affects mechanotransduction has yet to be explored [188, 189]. *In vitro* techniques including the application of exogenous strain with a Flexcell system, AFM, or 3D tissue construct system could all be utilized in pursuit of this knowledge. Each of these experimental systems has distinct advantages and disadvantages, but used together they can provide a clearer picture of cadherin-11 mechanobiology.

These studies can be performed in multiple cell-types to better understand the multifaceted role of cadherin-11 in complex cardiac remodeling. The work presented in

this dissertation primarily focused on CFs, as they are the main cell type responsible for ECM synthesis during fibrosis. However, our results revealed potentially important functions for cadherin-11 in both MΦs and ECs in the context of healing after MI. In the case of MΦs, future studies are needed to clarify the specific roles cadherin-11 play in MΦ recruitment, migration, proliferation, and polarization. Flow cytometry and MRI studies could be used to great effect to observe alterations in MΦ subpopulations and their recruitment in hearts after infarction, or in different cardiovascular disease models. More work is also needed to clarify the role of cadherin-11 in EC function in disease, specifically as it relates to EndMT, angiogenesis, and arteriogenesis. Cadherin-11 has been reported in ECs, and has been shown to promote EndMT, but whether there is a specific mechanobiological cue for that transformation has not been determined. Angiogenesis and arteriogenesis are both important and complex cellular processes that are correlated with improved outcomes after MI. Investigation of these *in vivo* processes and related cellular assays *in vitro* with and without cadherin-11 perturbations will clarify what role cadherin-11 might play in promoting cell differentiation and migration. All of these studies will clarify the mechanisms of SYN0012 effects.

High resolution imaging modalities like MRI could also allow for more complete characterization of the dynamic mechanical strain environment of both the infarct and the border zone during the time course of remodeling. Finite element inverse modeling from high resolution images could be used to estimate mechanical properties throughout the myocardium from measured strain profiles, and our AFM measurement technique could be used to validate and gain a more complete understanding of the spatial heterogeneity of tissue stiffness. Combining this technique with immunostaining

of tissue sections could allow for direct assessment of how microenvironmental mechanics effect cell phenotype and migration.

Future studies altering the specific timing and volume of SYN0012 treatments, targeting only the first week or later weeks of remodeling, will also clarify both the role of cadherin-11 in disease and the suitability of a blocking antibody therapeutic strategy. It would also be a natural next step to investigate whether cadherin-11 plays a role in cardiac fibrosis downstream of other sources of cardiac disease, including pressure overload, dilated or hypertrophic cardiomyopathies.

Finally, the tools developed in Aim 3 can be used to better understand CM structure and mechanics in multiple applications and disease models. Both single cell assessment and larger tissue construct systems allow for more complete functional characterization of CMs derived from human induced pluripotent stem cells. These cells have been developed as a useful model system to understand the etiology of human disease and consequences of specific mutations and drugs [11]. The ability to quantify intracellular organization and stiffness along with multicellular functionality will prove very helpful to these ends. Future work with the I-wire system will be used to more conclusively distinguish between the different dynamic parameters (**Figure B6**). This model will also be used to design optimal experiments to most efficiency optimize the information gleaned from the I-wire construct system. The I-wire system can also be used to investigate the relative contributions of different ECM components, integrin signaling, cadherin blockade, and the effect of co-culture in 3D in a more physiologically relevant, tunable system.

To conclude, my doctoral work has advanced the field of mechanobiology and cardiac fibrosis, identifying a critical role for the mechano-sensitive junctional protein cadherin-11 in cardiac remodeling after myocardial infarction. These studies have centered on the focal role of mechanosensing in cardiac cell activation and progressive tissue remodeling. I have also identified a viable therapeutic target for limiting adverse remodeling and improving outcomes after MI: cadherin-11. Future development and testing of the blocking antibody treatment described herein will hopefully have a large beneficial impact on the millions who suffer from myocardial infarction and cardiac fibrosis each year.

APPENDIX A

Model of Myofibroblast Differentiation

Model Development

The model is a system of ODEs describing the dynamics of relative protein activation and α-SMA production in fibroblasts. To simplify the model, a normalized closed system was assumed, wherein the total amount of each protein species in the signaling pathway is conserved at a value of 1. While many of these proteins have multiple phosphorylation states and conformations which affect their enzyme activity, most protein species were simplified to 2 activation states, “on” or “off”. Src, FAK, and TβR2 were given 3 activation states to capture more system interactions. In total, the model contains nine active variables (Table A1), 27 kinetic rate coefficients (Table A2), and 12 inputs and boundary conditions which can be varied experimentally and *in silico.* Figure 1B shows a general descriptive schematic of the interactions and protein species represented in the model. First order activation rates proportional to the relative activation of the upstream species were used to model signaling cascades, unless more specific interactions were known. Michaelis-Menten kinetics was used in cases of direct phosphorylation, as with Src activation of FAK tyrosines in the 400-900 range and Src phosphorylation of TGFβ receptor 2 (TβR2).

Table A1 List of Active Variables.

Variable name	Description
B1on	amount of activated β1 integrin as a fraction of total
B3on	amount of activated β3 integrin as a fraction of total
TBRT	TGF-β1 receptor (TβR2) with TGF-β1 ligand attached
pTBR2	phosphorylated and ligand bound TGF-β1 receptor (TβR2)
pS	activated Src kinase
pFAK	FAK phosphorylated on tyrosine 397
3pF	FAK phosphorylated on tyrosines in 400-900 range with active kinase activity
pP	active p38
pE	active ERK

The total amount of each protein is conserved and given a value of 1, so the inactive species fraction is calculated at each time point as 1 - Σ (active protein species).

Regulation of α-SMA production

In the simplification of this system, we focused on p38 and ERK as the sole regulators of α-SMA production. Phosphorylated p38 (pp38) promotes the production of α-SMA while pERK inhibits α-SMA accumulation by slowing the rate of production. According the model proposed by Kawai-Kowase et. al, ERK activated by FGF2 signaling prevents smooth muscle gene expression by interfering with serum response factor (SRF) function via an unknown mechanism [140]. We represented this in the model with the following equation:

$$\alpha SMA\ production = \frac{d[\alpha SMA]}{dt} = \frac{kaSMAf * [pp38]}{(kaSMAi * [pERK] + 1)} \qquad \text{Equation 4.1}$$

This equation was chosen assuming that the rate of production of α-SMA at any given moment would be roughly proportional to the amount of active p38, but also decreased by increasing activation of ERK. Because cells always express a baseline level of α-SMA, the reduction by ERK was limited by the addition of a +1 term, so that the initially low amount of active ERK would not cause an unstable increase in α-SMA.

After initial experimental results showed a dramatically lower amount of α-SMA in SYF-/- cells despite comparable levels of p38 phosphorylation, a modified equation for α-SMA production was devised.

$$\alpha SMA\ production = \frac{d[\alpha SMA]}{dt} = \frac{kaSMAf * [pp38] * (0.01 + pS)}{(kaSMAi * [pERK] + 1)} \qquad \text{Equation 4.2}$$

This equation somewhat artificially delivers a dramatic reduction in α-SMA expression when Src is absent, without requiring a subsequent decrease in p38 activation. We assume that p38 in this case is roughly proportional to SRF activity, and this additional Src term may represent downstream activation of MRTF, which works in concert with SRF to regulate α-SMA production. The addition of the 0.01 term within the Src activated expression similarly allows for some, diminished quantity of α-SMA expression even in the absence of Src.

Parameter Estimation

Parameters were estimated by comparison with previously published models and by calculating the maximum relative activation changes in relevant experimental contexts. Both p38 and ERK are activated via cascades of signaling events downstream of growth factor receptors, Src, and FAK [96, 190], but these cascades are approximated as a single step with a lump parameter for the sake of model simplicity. To estimate values for these lump parameters, we measured α-SMA expression and relative ERK and p38 phosphorylation in MEFs after 24 hours of treatment with 1 or 10 ng/ml TGF-β1 and FGF2. We also tuned our model's sensitivity to changes in mechanical stiffness by measuring α-SMA in cells plated on PDMS of stiffnesses ranging from 230 kPa to 2.14 MPa and on TCP (stiffness ~ 3 GPa [275]). The MATLAB optimization function *lsqnonlin* was used to vary up to three parameters at once to find the set of parameters which minimized the mean squared error (MSE) of the model fit to the growth factor sensitivity curves or the stiffness curve. While comparing candidate

models, two parameters (kTpP and kα-SMAf) were optimized to fit the growth factor calibration data set for each model.

Table A2: List of parameter values

Parameter	Description	Value [hr^{-1}]	Source
k1f	rate of β1 integrin adhesion and activation	23	Estimated from [273]
k1r	rate of β1 integrin deactivation	0.567	Estimated from [273]
k2f	rate of β3 integrin adhesion and activation	23	Estimated from [273]
k2f	rate of β3 integrin deactivation	0.567	Estimated from [273]
k3f	rate of TGF-β1 ligand attachment to TBR2 receptor	60	[193]
k3r	rate of TGF-β1 disassociation	15	Estimated from [193]
kIpF	rate of β1 integrin activation of FAK	0.454	estimated from [179], [273]
kIpS	rate of β3 integrin activation of Src	20.15	estimated from [273], [276]
kTpS	rate of TGFβ receptor activation of Src	120	estimated from [137], [177], [178]
kSpF	rate of Src association with FAK and activation of secondary phosphorylation sites	29	estimated from [180], [192], [273]
KmSF	Michaelis Menten constant for Src activation of FAK	0.1	estimated from [192]
kFAKpE	rate of FAK activation of ERK	240	estimated from [273], [277]
kFGFpERK*	rate of FGF activation of ERK	40	estimated from [89], [140]
kSpT	rate of Src phosphorylation of TBR2	40	estimated from [177], [178]
KmST	Michaelis Menten constant for Src activation of TBR2	0.1	estimated from [177], [178]
kTpP*	rate of TGF-β1 activation of pp38	130.4-1076	estimated from [177], [178]
kIpP*	rate of β1 integrin activation of p38	50	estimated from [42], [185]
kPr	rate of p38 dephosphorylation	579.6	[278]
kEr	rate of ERK dephosphorylation	210	estimated from [273]
kSr	rate of Src dephosphorylation	432	estimated from [273]
kFr	rate of FAK dephosphorylation	48.35	estimated from [273]
kTr	rate of ligand induced TBR2 deactivation	15	[193]
kE	intrinsic rate of ERK activation	10	estimated and optimized
kP	intrinsic rate of p38 activation	10	estimated and optimized
kαSMAf*	rate of p38 promotion of αSMA	1.1-11	estimated and optimized for each model
kαSMAi*	rate of ERK inhibition of αSMA production	20	estimated and optimized
kαSMAr	rate of αSMA degredation	1.03	estimated from [279]

Initial estimates of values were calculated from literature and varied to find the optimal parameter set. Parameters that were optimized to calibration data set indicated by *

Model derivation:

This ODE model was developed and analyzed in MATLAB. The initial conditions of all active protein species were set at 0.001, the environmental conditions were matched to experimental levels, and the model was allowed to equilibrate by simulation of 24 hours of culture, resulting in a steady state values for each parameter. Using these steady state variable values as a starting point, the dynamic response of the system to treatments like addition of TGF-β1 or FGF2 was simulated. For the sake of model stability and parsimony the total quantity for each of the protein species was set to 1 and the quantity of the inactive species was calculated within the ODE expression per the following conservation equations. In other words, the variables for active protein species were calculated and processes as a fraction of the total protein pool.

An ODE function was assembled containing the conservation equations (Table A3) and all the rate equations outlined below (Table A4-A10). This function was called within an ode solver in MATLAB, and the following conservation equations and current value for the active variables (Table A1) – another input into the solver - were used to calculate the amount of inactive or unphosphorylated species for each protein. These variables were used to calculate the rate of change of each active species from each biological source. The rate equations are listed in Tables A4-A10, divided by the region of the signaling network.

Table A3: Table of active protein species conservation equations. The prefix 'p' indicates a phosphorylated species and the suffix 'tot' indicates the total value of the protein species.

	Protein	Conservation equation
1	β1 integrin	B1tot = B1off + 2*(B1on)
2	β3 integrin	B3tot = B3off + 2*(B3on)
3	FAK	Ftot = F + pF + 3pF
4	Src	Stot = S + pS + 3pF
5	p38	Ptot = P + pP
6	ERK	ERKtot = ERK + pERK
7	TGF-β1 receptor	TBR2 = TBR2off + TBR2T + pTBR2

More details on the specific activation steps can be found below. Net rate of change equations for each species are bolded.

Integrin activation and clustering

Both intracellular and extracellular cues can lead to and strengthen integrin activation, but this model focuses on “outside-in” signaling linked to adhesion to ECM proteins collagen and fibronectin. Integrins with a β1 subunit can adhere to both fibronectin and collagen and are known to stimulate the activation of the autophosphorylation site on FAK (y397) [123], [179], [273]. Integrins containing the β3 subunit are activated by adhesion to the RGD subunit of fibronectin and can directly activate Src [276], [280]. In both cases, integrin clustering reinforces integrin activation and allows greater signaling to downstream targets like Src and FAK. In the model, dynamic clustering is approximated by a simple dimerization step whereby ECM adhesion leads to a pair of activated β1 or β3 integrins which in turn stimulate FAK or Src activation at a proportional rate. Hammer et al. made a similar assumption in their model of integrin signaling through integrin to FAK and ERK, and the rate constants k1f, k2f, k1r and k2r were calculated from the referenced model parameters. The active dimerized pair is accounted as B1on or B3on variables and is regulated by a second order equation (see table A4). Since the formation of this pair requires 2 inactive integrins, the conservation equation for both integrin species includes a scaling factor of 2 (See table A3) so that the total amount of integrin remains constant. The rate of integrin activation was made proportional to the availability of fibronectin (Fn) or collagen (Cl). Again, these are assumed to have a maximal value of 1, equivalent to a coated surface. Since MEFs are known to excrete fibrullar collagen and fibronectin in culture [40], [123], especially on stiff substrates, we assumed that cells plated on plastic had the equivalent of 20 percent of fibronectin present on a fibronectin coated surface (assumed to be a maximum value of 1) and 10 percent collagen of maximum collagen.

Taking the rate of change of activated β1 integrin dimers as an example, the first step is to calculate the amount of unengaged integrin subunits B1off, using equation A3.1.

$$B1tot = B1off + 2*(B1on) = 1 \qquad \text{equation A3.1}$$

$$B1off = 1 - 2*(B1on)$$

This value is then used to calculate the rate of new activated dimerization resulting from interaction with fibronectin according at a rate proportional to Fn, the fraction of available unengaged β1 integrin subunits (squared since two subunits are needed for each reaction), and the rate constant k1f:

$$B1on\_rate\_Fn = k1f * Fn * B1off * B1off \quad .$$

A similar expression gives the rate of dimerization due to collagen (Cl), which was assumed to have the same rate constant k1f

$$B1on\_rate\_Fn = k1f * Cl * B1off * B1off \quad .$$

Finally, these dimers (B1on) disassociate at a rate proportional to k1r:

B1on_rate_diss = B1on*k1r .

Combining these expressions gives the net rate of active β1 integrin dimer (B1on) formation, as follows:

B1on_rate = k1f *Fn*B1off*B1off + k1f *Cl*B1off*B1off – k1r *B1on.Equation A4.1

This equation, and a similar expression for β3 integrin is presented below.

Table A4: Equations describing integrin activation and clustering.

	Description	Equation
1	**β1 integrin activation and clustering**	B1on_rate = k1f * Fn * B1off *B1off + k1f *Cl*B1off*B1off – k1r *B1on
2	**β3 integrin activation and clustering**	B3on_rate = k2f * Fn * B3off *B3off – k2r *B3on

This activation is also modulated by the log of the substrate stiffness, since β1 integrin subunits are known to activate the autophosphorylation site tyrosine 397 of FAK proportionally to the log of substrate stiffness [179]. p38 phosphorylation is sensitive to stiffness, and since β1 integrin is known to activate p38, all candidate models besides model 5 contain a stiffness dependent activation of p38 [42], [281]. These reactions are proportional to both the (normalized) number of active integrin dimers, and the amount of the unphosphorylated species of FAK, Src, and p38 (F, S, and P, respectively) as calculated from the conservation equations in Table A3. These equations are also contain a rate contant (kIpF, kIpS, kIpP) estimated from literature as described above. These equations will be included in the net rate of phosphorylation for FAK, Src, and p38, as described with more detail below.

Table A5: Equations describing integrin based activation intracellular kinases via force sensitive mechanisms

	Description	Equation
1	β1 integrin activation of FAK	IpFrate = kIpF * log10(10*stiffness)*B1on*F
2	β3 integrin activation of Src	IpSrate = kIpS * log10(10*stiffness)*B3on*S
3	β1 integrin activation of p38	IpPrate = kIpP * log10(10*stiffness)*B1on*P
4	β1 integrin activation of p38 (model 5)	IpPrate = kIpP * B1on*P

TGF-β1 signaling and Src based regulation

Src has an important role in non-canonical TGF-β1 signaling to p38 in the regulation of MyoFB differentiation. After TGF-β1 ligand binding, the 284 tyrosine residue on TGF-β1 receptor 2 (TβR2) must be phosphorylated by Src for TGF-β1 induced activation of p38 to occur [177]. This two-step activation is accounted for by the inclusion of an intermediate activation state for the TβR2 receptor (TBR2T) which is associated with a TGF-β1 ligand and able to activate Src kinase activity, but unable to activate p38. The net rate of change for this species is given in equation A6.1, with a forward rate proportional to the amount of available TGF-β1 (Tgfb), the amount of unbound TβR2 (TBR2off) and a forward rate constant k3f and a reverse rate proportional to the amount of bound receptors (TBR2T) and a reverse rate constant.

Both bound (TBR2T) and bound, phosphorylated TβR2 (pTBR2) can lead to Src phosphorylation, so the rate of TGF-β1 receptor activation of Src is proportional to the sum of these two species and inactive Src (Equation A6.2). Since Src is known to directly phosphorylate bound TβR2, the equation for this activation step follows classic Michaelis Menten kinetics, with a forward rate equation and a Michaelis Menten constant (Equation A6.3).

The phosphorylated form of the receptor (pTBR2) is able to induce p38 phosphorylation and Src activation [177] (Equation A6.4).

Half of the TBR2 becomes recycled to a ligand free state after dephosphorylation, which can be seen in the last component of the net rate of change TBR2T.

Table A6: Equations describing TGF-β1 signaling and receptor activation

	Description	**Equation**
1	TGF-β1 binding to receptor	TBRTrate = k3f * Tfgb * TBR2off – k3r * TBR2T
2	TGF-β1 based activation of Src	TpSrate = kTpS * S * (pTBR2 + TBR2T)
3	Src phosphorylation of TβR2	SpTrate = kSpT * TBR2T * pS/(KmST + TBR2T)
4	TGF-β1 based activation of p38	TpSrate = kTpP * P * pTBR2
5	Dephosphorylation of TβR2	dpT= - kTr * pTBR2
6	**Net rate of change of TBR2T**	dTBR2 = TBRTrate – SpTrate – 0.5*dpT
7	**Net rate of change of pTBR2**	dpTBR2 = SpTrate - dpT

FGF2 signaling

Since there are no known activation or regulatory steps for the FGF receptor by the proteins in this network, we used a more simplified set of equations to reflect FGF activation of both FAK and ERK, with a direct forward reaction proportional to the relative amount of FGF present, and the amount of inactive FAK and ERK (F, and ERK, respectively).

Table A7: Equations describing FGF2 signaling

	Description	**Equation**
1	FGF2 activation of FAK	FGFpFrate = FGF2 * kFGFpF *F
2	FGF2 induced activation of ERK	pERKrate = FGF2 * kFGFpERK*ERK

Src-FAK interactions

Src and FAK have a complex series of interactions and cross-phosphorylation which require special attention in the model. FAK is a large scaffolding protein with several phosphorylation sites and interactions with a large number of other proteins. β1 integrin activation leads to phosphorylation of the autophosphorylation site of FAK, tyrosine 397 [123]. An association of the SH2 domain of the Src protein with the phosphorylated tyrosine 397 promotes the open conformation of Src that prevents deactivation by phosphorylation of tyrosine 527 and allows for more phosphorylation of tyrosine 416, increasing in Src kinase activity [282], [283]. When Src is associating with FAK in this manner, it can also cause the phosphorylation of FAK at tyrosines 576, 577, 861, 925, and others. This secondary phosphorylation activates the kinase activity of FAK and allows for signaling to downstream targets like ERK and p38. It also promotes FAK autophosphorlyation of y397 of surrounding FAK proteins [180]. This complex relationship is represented in the model by a 3 step activation scheme for FAK: inactive (FAK), phosphorylated on 397 (pFAK), and in a complex with Src with the additional tyrosine residues of FAK phosphorylated (3pF). Src also has 3 active states: inactive (Src), active (pSrc), and in the Src/FAK complex. Src phosphorylation of FAK creates this complex (Equation A8.1) and primarily follows Michaelis Menten kinetics, but a subset follows a standard rate equation format. Autophosphorylation of inactive FAK by the activated kinase form also follows Michaelis Menten kinetics. Dephosphorylation of both proteins follows a fairly straightforward first ord A similar Src/FAK activation model was used in a model developed by Caron-Lormier et. al in 2004 [192]. Whether or not Src in complex with FAK is able to phosphorylate pp38 or perform other roles is one of the questions investigated by model comparisons.

Table A8: Equations describing Src and FAK activation

	Description	Equation
1	Src phosphorylation of FAK	SpFrate = kSpF * S * pF + 10 * kSpF * pS * pF/(KmSF+pF)
2	FAK autophosphorylation	FpFrate = kFpF * F * p3F /(KmFF + F)
3	Dephosphorylation of Src	dppS = kSr * pS
4	Dephosphorylation of pFAK	dppF = kFr * pF
5	**Net changes in Src activation**	dpS = IpSrate + TpSrate - dppS –SpFrate +kFr * p3F/10
6	**Net changes in FAK y397 phosphorylation**	dpF = IpFrate + FpFrate - dppF – SpFrate +FGFpFrate + kFr*p3F
7	**Net changes in FAK-Src complex with phosphorylated kinase domain**	dp3F = SpFrate – kFr * p3F

Ten percent of the complex returns to pS phase after dissolution of the 3pF state, and all of it returns to the pF state.

Remaining activations and dephosphorylation of p38 and ERK

These equations follow standard forward and reverse kinetics.

Table A9: Regulation of p38 and ERK

	Description	Equation
1	Src phosphorylation of p38	SpPrate = kSpP * (pS) * P
2	FAK phosphorylation of ERK	FpErate = kFakpE * p3F *ERK
3	Dephosphorylation of p38	dppP = - kPr * pP
4	Dephosphorylation of ERK	dppERK = - kEr * pERK
5	**Net changes in p38 activation**	dpP = IpPrate + TpPrate + SpPrate + dppS
6	**Net changes in ERK phosphorylation**	dpERK = FpErate + pERKrate + dppERK + kE*ERK

Dynamic feedback loops

A major goal of this study was to understand the crosstalk between direct TGF-β1 and FGF2 signaling to p38 and ERK. To account for the transient nature of signaling to both p38 and ERK, some of the candidate models included negative feedback to Src and ERK. The Src feedback loop approximates the role of Csk to limit Src kinase activity as focal adhesions mature over time. Src and FAK activation signal through Cas and cause an accumulation of paxillin in focal adhesions roughly proportional to the accumulation of α-SMA [284]. Paxillin recruits Csk, which lowers Src activity [197, 202]. Another potentially relevant feedback mechanism is calpain, which is activated by ERK and degrades FAK and β3 integrin [286]. Finally, we simulated a positive feedback loop by which p38 stimulates β3 integrin expression [135]. These mechanisms add complexity to the model but also make the model more relevant to the biological system and provide closer matching with the dynamic phosphorylation events.

Table A10: Equations describing potential feedback loops

	Description	**Equation**
1	Time dependent negative feedback to Src	dppS = - kSr * pS –kSr *100*α-SMA * pS
2	Time dependent feedback to ERK	dppE = - kEr * pERK -10 *pERK/α-SMA
3	β3 integrin activation and clustering (model 6)	B3on_rate = k2f * Fn * B3off *B3off – k2r *B1on + kPB3 * B3off * B3off
4	Accumulation of active calpain (model 7)	calrate = kEaC*pERK – cal *kcaldeg
5	β3 integrin activation and clustering (model 7)	B3on_rate = k2f * Fn * B3off *B3off – k2r *B1on –kcaldeg*cal*B3on
6	Dephosphorylation of pFAK (model 7)	dppF = - kFr * pF – kcaldeg *cal*B3on

The final step of the ODE function assembled all of the expressions for net change of phosphorylation events, combining the net equations given above as the output of the ODE function.

Sensitivity Analysis

Both the initial conditions and rate constants were varied over two decades around the primary estimation, and the relative change in output (α-SMA concentration) and sensitivity coefficients S (relative change in output per relative change in parameter (P)) were calculated and ordered. This analysis provides insight into the bottlenecks and critical junctions where the system is more or less sensitive to perturbations.

$$Sensitivity\ Parameter\ S = \frac{\Delta\ \alpha SMA/\alpha SMA_0}{\Delta\ P/P_0}$$

Equation 3

Candidate Model Development and Statistical Comparison

We developed a set of candidate models which contain modified signaling mechanisms, reflecting different hypotheses. A data set independent from the calibration curves used to refine the model was used to evaluate model fit and quantitatively assess the likelihood of certain interaction mechanisms. After simulating the set of 8 experiments with each candidate model, we calculated the χ^2 statistic for the set of experimental results. The χ^2 statistic is a metric for measuring model fit while accounting for variability in experimental measurements.

$$\chi^2 = \sum_{i=1}^{N} \frac{(y\_exp_i - y\_model_i)}{\sigma_i}$$

Equation 4

When χ^2 is minimized, the agreement between the model prediction and the data is optimized.

Model evaluation using the Using the Akaike Information Criterion (AIC)

The Akaike information criterion (AIC) is a metric for comparing models with different numbers of independent parameters (K), to attempt to optimize both the accuracy and the model simplicity, or parsimony, of different models variants [205, 206].

$$AIC = 2K + 2((N/2) * \log(2\pi * MSE + 1))$$

Equation 5

N reflects the number of experimental data points and MSE is the mean squared error. This criterion can be used to great effect in determining the relative likelihood of multiple models.

A.2 - Results

TGF-β1, FGF2, and stiffness modulate α-SMA in a predictable manner

We conducted calibration experiments to correlate growth factor concentration and stiffness to internal signaling and regulation of α-SMA and refine our initial estimates of lump parameters. Our first calibration experiment (**Figure 3A-C**) clarified the relationship between growth factor concentration, equilibrium p38 and ERK phosphorylation, and α-SMA expression in MEF+/+ cells. At 24 hours, there is no significant change in pp38 with treatment with 1 or 10 ng/mL FGF2, but there is a significant log-linear increase proportional to TGF-β1 concentration (Figure 3A). There is significant ERK phosphorylation after 24 hours treatment with TGF-β1 that is independent of TGF-β1 concentration. There is also a significant increase in ERK activation with FGF2 treatment, which is highly dependent on FGF2 concentration (Figure 3B). These data were used to refine estimates of kTpP, kFGFpE, and kα-SMAf (Table 3). The variability of the experimental measurements was considered in the optimization protocol; we selected the set of parameters which gave the minimum χ^2 statistic for each candidate model. By this technique, we achieved good agreement with our calibration curves, with χ^2 values as low as 8.12 (p = 0.7) for the set of 15 growth factor measurements, indicating that the model is a good fit to the data.

We measured α-SMA production over a range of substrate stiffness (Figure 3D) and found a statistically significant interaction between cell type and substrate stiffness (p = 0.009). α-SMA production was significantly reduced when cells were cultured on PDMS, with the lowest α-SMA expression corresponding to a PDMS stiffness of 900 kPa. There was no significant difference between α-SMA expression on fibronectin coated TCP and uncoated TCP in either cell type. α-SMA in FAK-/- cells is significantly higher than in MEF+/+ (p < 0.001) on TCP (stiffness = 3E6 kPa) but is not statistically different at lower stiffness, indicating that FAK-/- are more sensitive to changes in stiffness than MEF+/+ cells. These data were also used to refine model fit and parameter estimation, especially in determining kIpP. χ^2 values as low as 2.9 (p = 0.96) were calculated for the set of 11 substrate measurements. After quantifying MAPK phosphorylation and α-SMA expression at 24 hours, we directed our focus to the details of dynamic signaling.

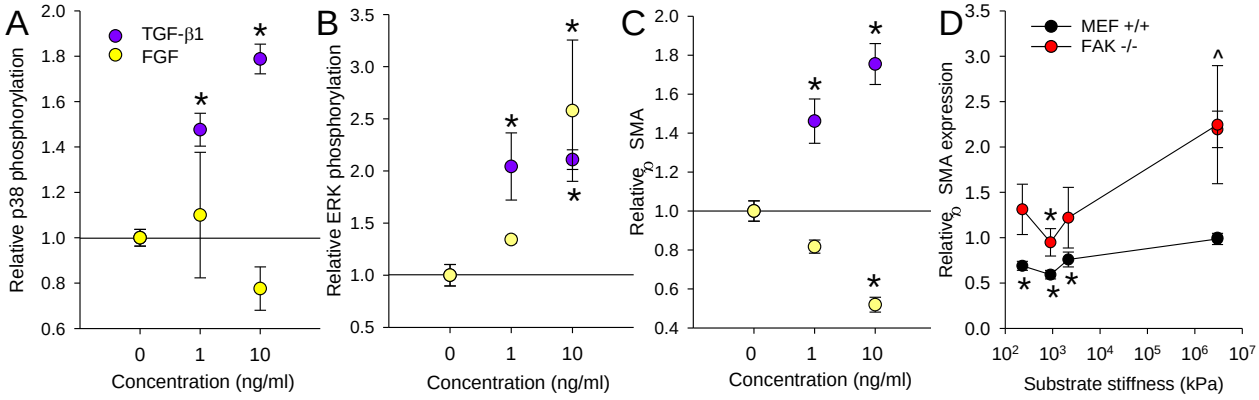

Figure A.1. Calibration curves for reaction to growth factors and stiffness. A-C. Concentration dependent changes to p38 and ERK activation and α-SMA expression in response to TGF-β1 and FGF2. D. Sensitivity to stiffness in production of α-SMA in MEF+/+ and FAK-/- cells. * indicates significant difference from the no treatment/TCP condition within each cell type. ^ indicates significant difference from MEF+/+ sample within substrate. Active p38 and pERK data from densitometry of western blots (A-B) and α-SMA determined from indirect ELISA (C-D). Average results are presented (n=4-12). These data were used to refine model parameters.

The dynamic ERK and p38 trends produced by model simulations share the same general shape as the experimental results, but the relative values are lower (Figure 4G-L). In this model, FGF2 does not directly activate p38, since the short duration and relatively low level of activation would not have a significant enough effect on α-SMA content to justify the addition of model complexity. The model does predict a slight rise in p38 activation in MEFs following FGF2 stimulation that is transduced through FAK enhanced Src activation (Figure 4G).

Experimental Results

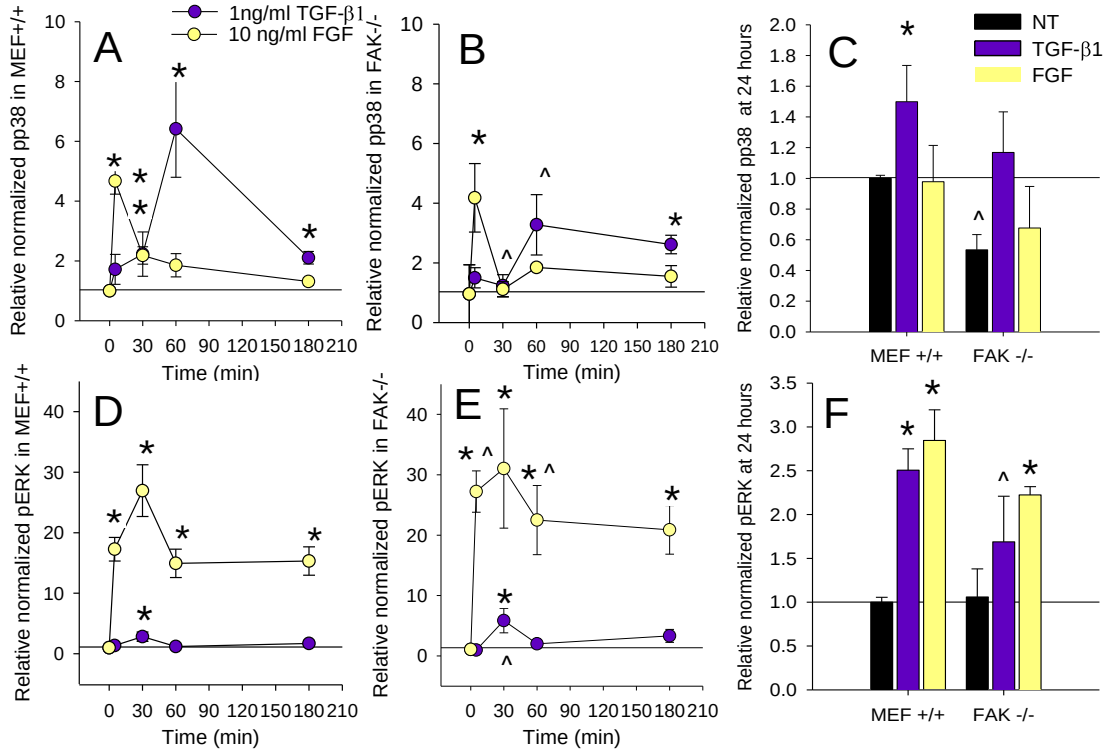

Model Predictions

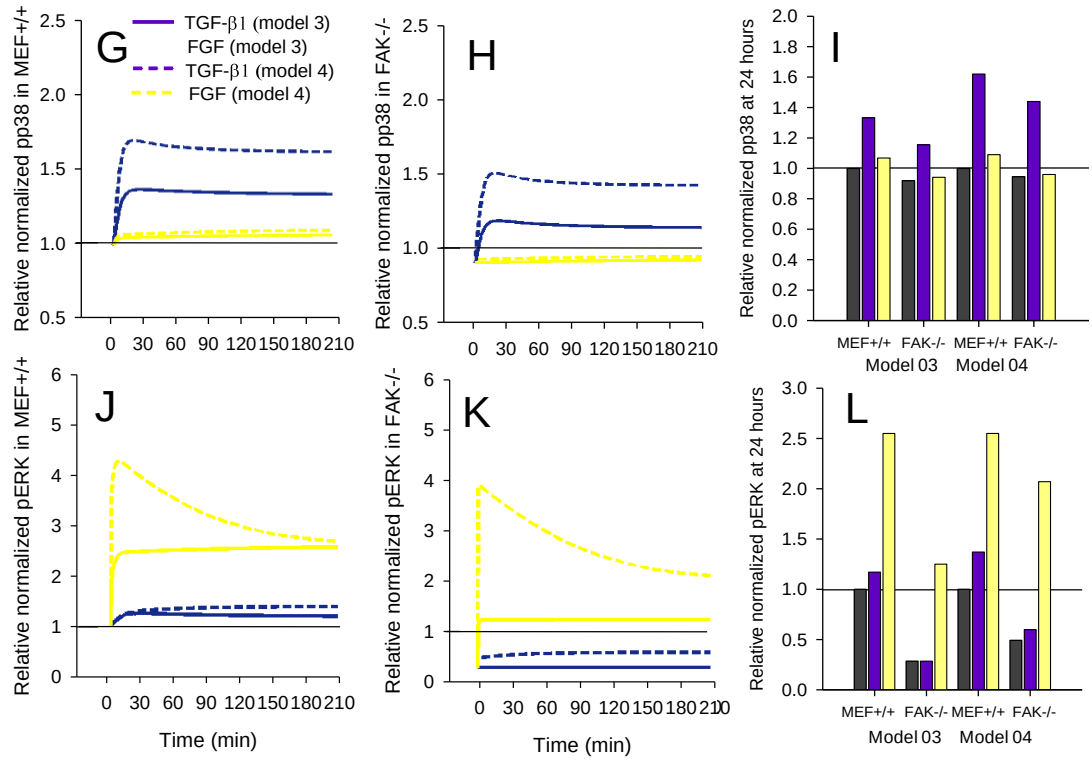

Figure A.2. Different dynamic activation profiles for activation of ERK and p38. Averaged results of western blot densitometry analysis for pp38 (A-C) and ERK (D-F) activation over a 3 hour time course in MEF+/+ (A,D) and FAK -/- (B,E) cells treated with 1ng/ml TGF-β1 or 10 ng/ml FGF. Average p38 and ERK activity after 24 hours of treatment (C,F). * indicates significant difference ($p < 0.05$) from average no treatment within cell type and time course. ^ indicates significant difference ($p < 0.05$) from the MEF+/+ sample within treatment and time point. G-L are the model output values for the same quantities at the same time points.

Sensitivity Analysis

Sensitivity analysis of the model with optimized parameters predicted that FAK-/- cells would be more sensitive to TGF-β1, FGF2, and stiffness relative to MEF+/+ cells. Sensitivity analysis indicates that the model's response to TGF-β1 stimulation is most sensitive to changes in rate constants controlling the activation and deactivation of p38, Src, and TβR2. Of the boundary constraints and initial conditions, the total amount of β1 integrin has the largest effect on relative α-SMA in MEF+/+ and FAK-/- models, with sensitivity coefficients of -0.34 and -0.29, respectively. While the rank and sign of sensitivities is conserved between MEF+/+ and FAK-/- models, the magnitude of the parameters is often higher in FAK-/- models. One interesting exception is kTpP, which is slightly lower in FAK-/- models (0.152 vs. 0.176). In MEF+/+ simulations, the response to FGF2 is most sensitive to the rate of FGF2 activation of ERK, the deactivation rate of FAK, and the rate of FAK based activation by integrins. SYF-/- models have no reaction to TGF-β1, and their reaction to FGF2 is less sensitive to stiffness, FGF2, and the rate of ERK activation by FGF2 than the MEF+/+ model. Sensitivity to both TGF-β1 and FGF2 was predicted to increase on fibronectin coated PDMS (stiffness 900 kPa) relative to TCP.

Model can predict results across substrate and cell type

With optimized model parameters, we tested our model's ability to predict the effect of growth factor treatment on cells lacking Src and FAK that we observed *in vitro*. Figure 5A shows the model results plotted over the experimental results (same as Figure 2). We also measured the combined effects of treatment and substrate stiffness by treating cells plated on fibronectin coated PDMS (Figure 5B) and found a statistically significant interaction between substrate and treatment ($p = 0.004$). Further, there is a significant difference ($p < 0.05$) between TCP and PDMS for NT and TGF-β1 treated cells, but not for FGF2 treated cells. Within each substrate, both FGF2 and TGF-β1 treatment cause a significant ($p < 0.05$) change in α-SMA expression. The model predictions are plotted over the experimental results, and were within a standard deviation for all but the TGF-β1 treated sample on PDMS.

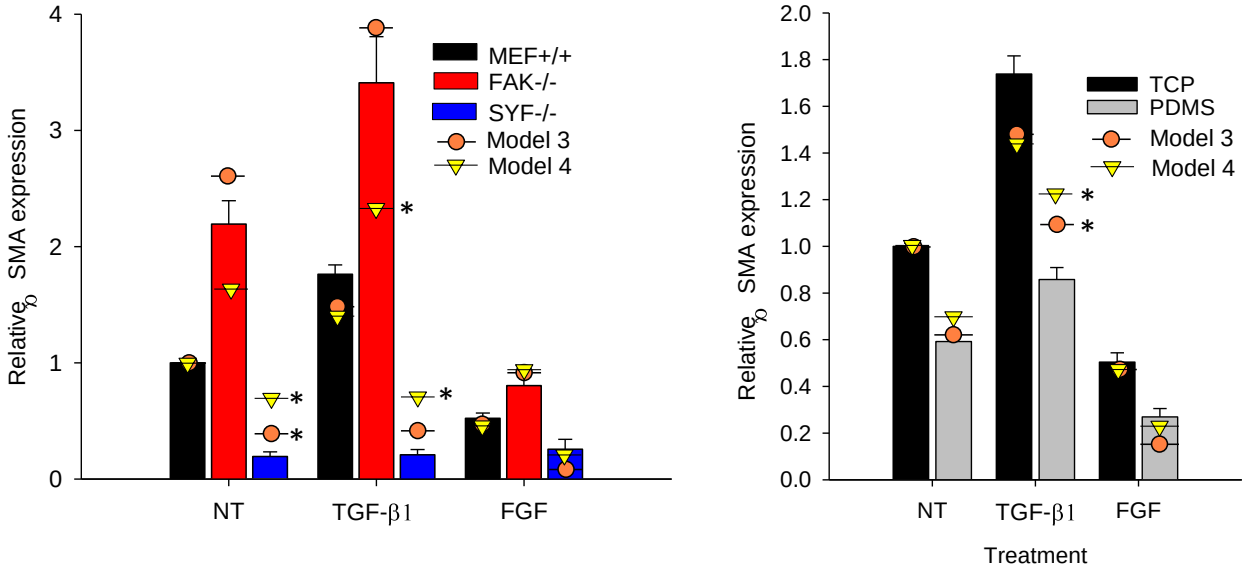

Figure A.3. Model fit to TGF-β1 and FGF2 treatment across cell types and substrates. Average values of α-SMA in MEF+/+ and FAK-/- cells (A) after 24 hour treatments and (B) in MEFs on TCP or fibronectin coated PDMS. Model predictions from model 04 with optimized parameters are plotted as triangles.

Model comparisons

Eight candidate models were developed and evaluated to find the most ideal fit to both steady state protein activation and dynamic protein phosphorylation events. The relative AIC (calculated as the difference between a given models AIC and the minimum AIC) provides a useful criterion for eliminating inferior models and improving model parsimony. After parameter optimization of kα-SMAf and kTpP for each model, simulated α-SMA outputs were compared against the validation data set (Figure A.3) and the MSE, χ^2 statistic, AIC, and ΔAIC were calculated (Table A4). The relative strength of evidence for any model (in comparison) can be estimated as $e^{-\Delta AIC/2}$. In other words, a model with ΔAIC > 10 is 148.4 times less likely than the best model [205, 206]. We found that the model with the lowest AIC also had a very low MSE and χ^2 while maintaining close agreement with the dynamic pp38 and pERK curves observed experimentally. Model 03 contained the modified α-SMA production equation (Equation 2) which has a Src dependent term and negative feedback to Src but did not contain negative feedback to ERK. ΔAIC for the equivalent model (02) with the unmodified equation for α-SMA production (Equation 1) was 5.91, giving strong support that the Src dependent term is supported by the data. Model 15 does not have a negative feedback loop for ERK, which means that the observed change in relative ERK phosphorylation from 3 hours to 24 hours (Figure 4D-F) could not be replicated by this model. The equivalent model with negative feedback to ERK (model 04) had an ΔAIC of 1, so it is reasonably close to the optimal model. Furthermore, after optimization model 04 was able to achieve lower χ^2 values and better matching to the calibration data. Model 04

simulations are presented in Figures 4 and 5. Model 07 had the lowest MSE and best fit to the experimental data set via the addition of a calpain feedback loop which degrades β3 integrin and FAK , but this addition of model complexity increased the AIC score above the simpler models 03 and 04. These data indicate that the features of the model presented above have reasonable support from the data. Our model comparison revealed that a direct dependency on active Src greatly enhanced the quality of model fit. It also indicated that including more complex network interactions like calpain based negative feedback can improve model accuracy, but not enough to justify additional model complexity.

Table A11. Model comparison and statistical analysis

Model	Features	MSE	χ^2	ΔAIC
01	No Src dependency or Src feedback or ERK feedback	0.768	541.96	6.66
02	No Src dependency term, but Src and ERK feedback	0.499	278.9	6.03
04*	Src dependency, Src and ERK feedback	0.090	24.79	0.93
05	Model 04 without stiffness dependence of IpP	0.163	51.23	1.96
06*	Model 04 with β3 integrin positive feedback	0.083	19.14	2.82
07*	Model 03 with Calpain negative feedback to ERK	0.019	16.46	3.85
08	More direct αSMA dependence on ERK	0.052	44.47	0.35
03*	Src dependency and Src feedback	0.029	18.64	0

* Indicates that the χ^2 value for the given model has a $p < 0.05$ for a χ^2 distribution with 15 degrees of freedom, indicating that the model predictions are not significantly different from the experimental data set.

A.3 - Discussion

Using genetically modified MEFs, we have highlighted the importance of Src family kinases and FAK in the regulation of myofibroblast differentiation. Our results demonstrate a profound inhibitory effect of removing Src on αSMA production and stress fiber assembly. Densitometry revealed comparable levels of p38 and ERK phosphorylation in SYF-/- cells relative to MEF+/+ cells (data not shown), so the effect is likely operating through a different mechanism. This prompted the addition of a Src dependent term to the αSMA production equation to capture the significant αSMA reduction in SYF-/- cells (Equation A2). Without the addition of that term, SYF-/- cells *in silico* behave similarly to FAK-/-, since the absence of Src prevents the activation of FAK kinase ability. It is likely that signaling downstream of Cas and other Src substrates is necessary for proper αSMA synthesis. TGF-β1 signals to TGF-β activated kinase 1 and subsequent αSMA production is significantly reduced with Src inhibition and the

removal of FAK [199]. This result is consistent with recent reports of Src's prominent role in non-canonical TGF-β1 signaling in the context of myofibroblast differentiation [137].

Our model uses an activation function proportional to the log of stiffness to simulate integrin activation of FAK, Src, and p38, which gives good agreement with experimental results (Figure 3D). We further showed the combinatorial effect of substrate changes and growth factor treatments and found a significant interaction, justifying the development of an integrated signaling model (Figure 5B). All the data in Figure 5 were well matched by a model whose parameters had been optimized to an independent data set (Figure 3), which strengthens our proposed model on the roles on p38 and pERK. The largest discrepancy between model prediction and experimental results, response to TGF-β1 in cells on PDMS, highlights an area needing more detailed investigation: the effect of stiffness and integrin signaling on TGF-β1 pathways.

We developed a computational model of these overlapping signaling pathways and a set of tools for network analysis and hypothesis generation. Sensitivity analysis of the model predicted higher sensitivity to FGF2 and stiffness in FAK-/- cells relative to MEF+/+. Experimentally, FAK-/- cells demonstrated a larger relative change in response to FGF2 than in wild type cells (63% or 49% decrease, respectively), but a smaller relative response to TGF-β1 (55% or 73% increase, respectively) (Figure 4A). According to the constituitive equation for α-SMA activation, the sensitivity of equilibrium α-SMA to both p38 and pERK is inversely proportional to ERK activation, so lower basal ERK activation, as found in FAK-/- cells, should cause higher sensitivity to all parameters which affect ERK and p38 activation. Functionally, equations 1 and 2 mean that the presence of active ERK dampens the sensitivity of the system to changes in MAPK activation. Since the growth factors present in serum can cause a significant increase in ERK activation, we performed all of our ELISA and western blot experiments in serum free conditions. Sensitivity to both TGF-β1 and FGF2 was predicted to increase with decreasing stiffness according to the model prediction, and was observed in the case of FGF2 (54.5% vs. 49.5% decrease) though the reverse is true for TGF-β1 (45% vs. 73% increase) (Figure 5B). Further investigation into altered signaling on softer substrates could help clarify this discrepancy. Future analysis of the model using larger calibration and validation data sets will give more insight into the dynamics of MyoFB regulation. Overall, this study demonstrates the feasibility of p38/ERK/Src based regulation of α-SMA production during fibroblast differentiation.

In this study we have demonstrated that an ODE-based computational model of relative protein expression can capture a subset of the dynamic and steady-state events observed during fibroblast differentiation. We have further shown that the mechanism of Src/p38/ERK based regulation of α-SMA as described herein is a feasible model for regulation of MyoFB differentiation. Model simulations were able to replicate some of the dynamic features of TGF-β1 and FGF2 signaling to p38 and pERK and show that despite the fact that it increases with TGF-β1 treatment, ERK may still be acting primarily as a negative regulator of α-SMA.

APPENDIX B

Additional Information About I-wire Model

B1. Model details and derivation

The geometry of the model is described in Figure B1, and our implementation of the Hill Model in Figure B2, both from Figure 1 of the main paper. All parameters are listed in Table B1.

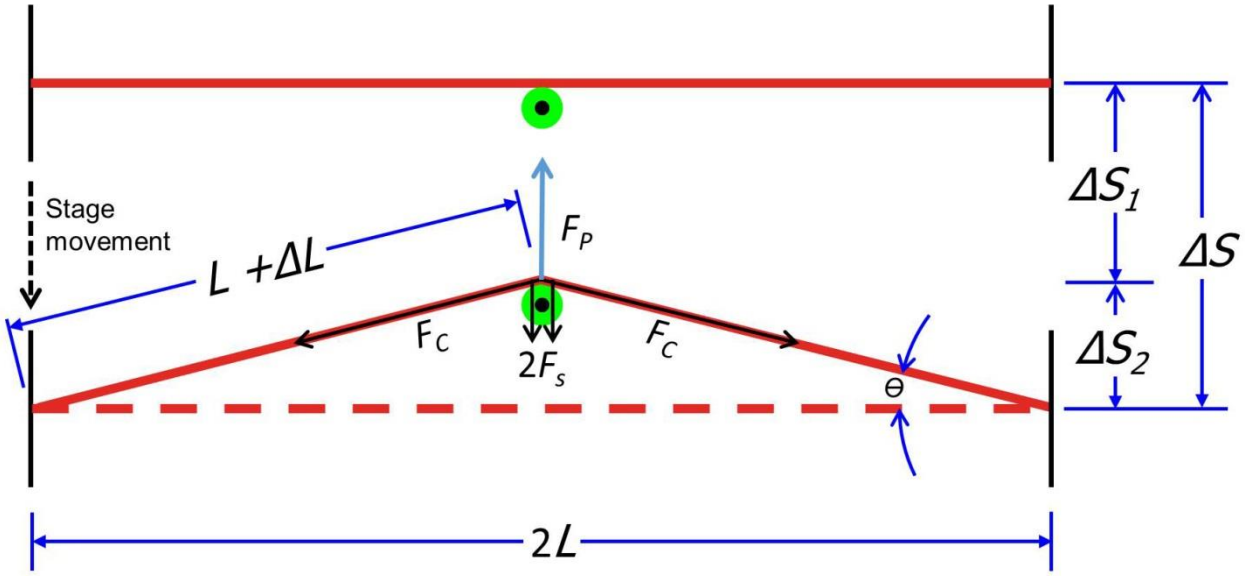

Figure B1: The geometry of an I-Wire measurement of the elastic and contractile properties of an engineered cardiac tissue construct.

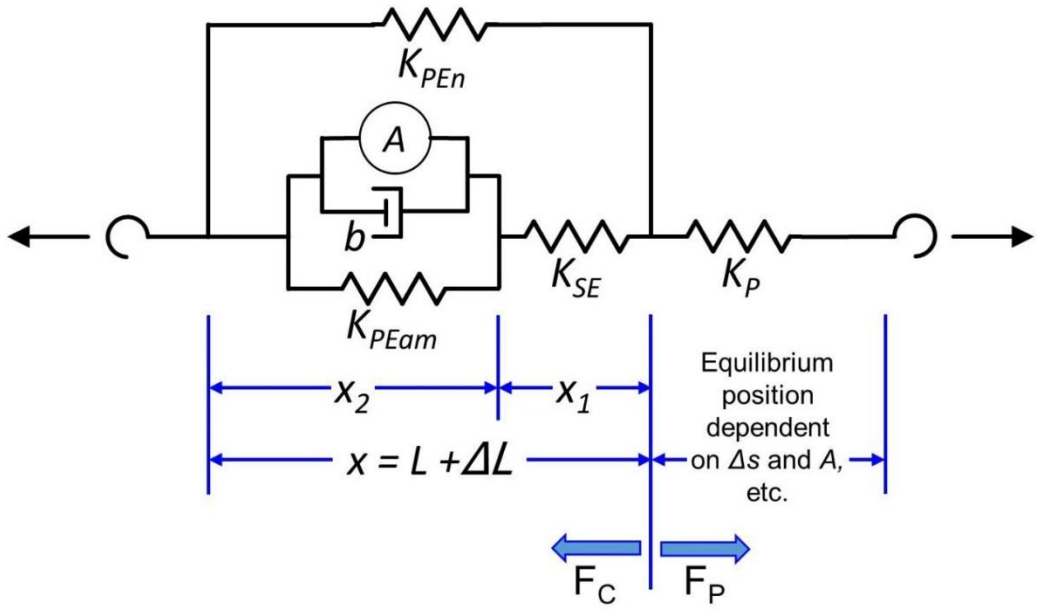

Figure B2: The Hill model and key distances as adapted to an I-Wire measurement of the elastic and contractile properties of an engineered cardiac tissue construct.

Table B1: Model variables

Variable	Description (units)
L	Half-length of unstretched I-Wire construct (m)
Δs	Distance I-Wire frame is moved (m)
Δs_1	Distance cantilever (probe) is moved (m)
Δs_2	$\Delta s - \Delta s_1$ (m)
ΔL	Distance I-Wire construct is stretched (m)
ΔL_{offset}	Distance unstretched I-Wire construct is from resting (m)
θ	Angle between hypotenuse and parallel leg of stretched I-Wire (rad)
F_P	Force delivered by the cantilever (probe) (N)
F_C	Force of the I-Wire construct in response to F_P (N)
prestress	Estimated tension in unstretched construct (N)
K_M	Steady-state stiffness of muscle construct (Nm^{-1})
K_C	Cantilever (probe) spring constant (Nm^{-1})
K_{PEam}	Spring constant of actin/myosin parallel element (Nm^{-1})
K_{SE}	Spring constant of series element (Nm^{-1})
K_{PEn}	Spring constant of non-actin/myosin parallel element (Nm^{-1})
b	Dashpot stiffness ($Nm^{-1}s$) (Note data reported in Nm^{-1}milliseconds)
F_A	Active force (N)

Derivation

B1.1 Construct extension and the force on the probe,

We begin with the Pythagorean Theorem

$L^2 + \Delta s_2{}^2 = (L + \Delta L)^2$,

which can be solved for Δs_2

$\Delta s_2 = \sqrt{(L + \Delta L)^2 - L^2} = \sqrt{L^2 + 2L\Delta L + \Delta L^2 - L^2} = \sqrt{\Delta L(2L + \Delta L)}$

and ΔL

$\Delta L = \sqrt{L^2 + \Delta s_2{}^2} - L = \sqrt{L^2 + (\Delta s - \Delta s_1)^2} - L$.

Given the spring constant K_P and displacement Δs_1 of the probe, the transverse force applied to the construct by the probe, F_P, is given by Hooke's law, $F_P = K_P \Delta s_1$. This allows us to write

$$\Delta L = \sqrt{L + \left(\Delta s - \frac{F_P}{K_P}\right)^2} - L \, .$$

The longitudinal force within each half of the construct is F_C. From the drawing, we see that F_P is balanced by the components F_S of each of the two forces F_C that are antiparallel to F_P, *i.e.* $F_P = 2F_S$ (We ignore the minus sign). The geometry of the problem allows us to relate F_P and F_S directly

$$F_P = K_P \, \Delta s_1 = K_P(\Delta s - \Delta s_2) = 2F_C \sin(\theta) = 2F_C \, \frac{\Delta s_2}{L + \Delta L} \, .$$

We can use our expression for Δs_2 to eliminate it from both sides of the equation

$$F_P = K_P \left(\Delta s - \sqrt{\Delta L(2L + \Delta L)}\right) = 2F_C \, \frac{\sqrt{\Delta L(2L + \Delta L)}}{L + \Delta L} \, .$$

Solving this for F_C, we obtain

$$F_C = \frac{1}{2} \, K_P \frac{\Delta s - \sqrt{\Delta L(2L + \Delta L)}}{\sqrt{\Delta L(2L + \Delta L)}} (L + \Delta L) = \frac{1}{2} \, K_P \left(\frac{\Delta s}{\sqrt{\Delta L(2L + \Delta L)}} - 1\right)(L + \Delta L) \, . \text{(S1)}$$

We note for future use that F_C is simply a function of ΔL, which we can write as

$F_C = f_1(\Delta L)$.

We now need to compute the time derivative of F_C during a muscle contraction

$$\dot{F}_C \stackrel{\text{def}}{=} \frac{\mathrm{d}}{\mathrm{d}t} F_C = \frac{1}{2} K_P \frac{\mathrm{d}}{\mathrm{d}t} \left\{ \left(\frac{\Delta s}{\sqrt{\Delta L(2L + \Delta L)}} - 1 \right) (L + \Delta L) \right\}.$$

We note that

$$\frac{\mathrm{d}\Delta L}{\mathrm{d}t} = \dot{x}\,.$$

By the chain rule, we find that

$$\begin{aligned} &\dot{F}_C \\ &= \frac{1}{2} K_P \left\{ (L + \Delta L) \left(-\frac{1}{2} \Delta s \left(\Delta L(2L + \Delta L) \right)^{-3/2} (2L\dot{x} + 2\Delta L\dot{x}) \right) \right. \\ &\left. + \left(\Delta s \left(\Delta L(2L + \Delta L) \right)^{-1/2} - 1 \right) \dot{x} \right\}, \end{aligned}$$

which simplifies to

$$\dot{F}_C = \frac{1}{2} K_P \left\{ (L + \Delta L) \left(-\Delta s \left(\Delta L(2L + \Delta L) \right)^{-3/2} (L + \Delta L) \right) + \left(\Delta s \left(\Delta L(2L + \Delta L) \right)^{-1/2} - 1 \right) \right\} \dot{x}\,,$$

$$\dot{F}_C = \frac{1}{2} K_P \left\{ -\Delta s \left(\Delta L(2L + \Delta L) \right)^{-3/2} (L + \Delta L)^2 + \Delta s \left(\Delta L(2L + \Delta L) \right)^{-1/2} - 1 \right\} \dot{x}\,,$$

$$\begin{aligned} &\dot{F}_C \\ &= \frac{1}{2} K_P \left\{ -\Delta s \left(\Delta L(2L + \Delta L) \right)^{-1} \left(\Delta L(2L + \Delta L) \right)^{-1/2} (L + \Delta L)^2 \right. \\ &\left. + \Delta s \left(\Delta L(2L + \Delta L) \right) \left(\Delta L(2L + \Delta L) \right)^{-1} \left(\Delta L(2L + \Delta L) \right)^{-1/2} - 1 \right\} \dot{x}\,, \end{aligned}$$

$$\dot{F}_C = \frac{1}{2} K_P \left\{ \frac{\Delta s \left(-(L + \Delta L)^2 + \Delta L(2L + \Delta L) \right)}{\Delta L(2L + \Delta L) \sqrt{\Delta L(2L + \Delta L)}} - 1 \right\} \dot{x}\,,$$

$$\dot{F}_C = \frac{1}{2} K_P \left\{ \frac{\Delta s \left(-L^2 - 2L\Delta L - \Delta L^2 + 2L\Delta L + \Delta L^2 \right)}{\Delta L(2L + \Delta L) \sqrt{\Delta L(2L + \Delta L)}} - 1 \right\} \dot{x}\,,$$

$$\dot{F}_C = -\frac{1}{2} K_P \left\{ \frac{\Delta s L^2}{\Delta L(2L + \Delta L) \sqrt{\Delta L(2L + \Delta L)}} + 1 \right\} \dot{x}\,.$$

This too is a function of ΔL, which we can write as

$$\dot{F}_C = f_2(\Delta L)\, \dot{x}\,.$$

B1.3 Hill model

We now analyze the Hill model components in Figure B2 to interpret the response of the I-wire construct in terms of its elastic and contractile properties.

The force in the I-wire construct is the sum of the forces in non-actin/myosin passive elements (F_N), associated with the extracellular matrix, and in the myocytes themselves (F_M)

$F_C = F_N + F_M$.

The non-actin/myosin contribution, the uppermost component in Figure S2, obeys Hooke's law

$F_N = K_{PEn}\, x$.

The lower components describe the contractile properties of the myocytes. The same force F_M is passed through the left (parallel) and right (serial) components of the myocyte contribution. We have for the series elastic component Hooke's law

$F_M = K_{SE}\, x_1$.

For the parallel components, three terms, the active contractile element, the velocity-dependent dashpot, and the parallel elastic element, contribute to F_M

$F_M = F_A + b\dot{x_2} + K_{PEam} x_2$.

We can eliminate x_2 and its temporal derivative $\dot{x_2}$to obtain

$F_M = F_A + b(\dot{x} - \dot{x_1}) + K_{PEam}(x - x_1)$.

We can use Hooke's law for the series elastic element to eliminate x_1 and $\dot{x_1}$

$$F_M = F_A + b(\dot{x} - \frac{\dot{F_M}}{K_{SE}}) + K_{PEam}(x - \frac{F_M}{K_{SE}})$$

$$F_M = F_A + b(\dot{x} - \frac{\dot{F}_C - \dot{F}_N}{K_{SE}}) + K_{PEam} x - \frac{K_{PEam} F_M}{K_{SE}}$$

$$(1 + \frac{K_{PEam}}{K_{SE}}) F_M = F_A + b(\dot{x} - \frac{\dot{F}_C - \dot{F}_N}{K_{SE}}) + K_{PEam} x$$.

We next replace F_M

$$(1+\frac{K_{PEam}}{K_{SE}})(F_C-F_N)=F_A+b(\dot{x}-\frac{\dot{F}_C-\dot{F}_N}{K_{SE}})+K_{PEam}x$$

and then F_N and $\dot{F}_N$ to obtain

$$(1+\frac{K_{PEam}}{K_{SE}})(F_C-K_{PEn}\,x)=F_A+b(\dot{x}-\frac{\dot{F}_C-\dot{F}_N}{K_{SE}})+K_{PEam}x\,.(1)$$

We collect terms such that all time-dependence is on the right side of the equation

$$\left(1+\frac{K_{PEam}}{K_{SE}}\right)F_C-\left(K_{PEam}+K_{PEn}+\frac{K_{PEn}\,K_{PEam}}{K_{SE}}\right)x=F_A+b\left(\dot{x}-\frac{\dot{F}_C-K_{PEn}\,\dot{x}}{K_{SE}}\right).$$

At steady-state equilibrium, there is no active force and both temporal derivatives are zero

$$\left(1+\frac{K_{PEam}}{K_{SE}}\right)F_C-\left(K_{PEam}+K_{PEn}+\frac{K_{PEn}\,K_{PEam}}{K_{SE}}\right)x=0\,,$$

which allows us to solve for F_C

$$F_C=\frac{\left(K_{PEam}+K_{PEn}+\frac{K_{PEn}\,K_{PEam}}{K_{SE}}\right)}{1+\frac{K_{PEam}}{K_{SE}}}x=K_M x\,,$$

where

$$K_M=\frac{K_{PEam}+K_{PEn}+\frac{K_{PEn}\,K_{PEam}}{K_{SE}}}{1+\frac{K_{PEam}}{K_{SE}}}.$$

We can use this to simplify the preceding equation (1) when there is time dependence, *i.e.,* during a contraction of the muscle

$$\left(1+\frac{K_{PEam}}{K_{SE}}\right)(F_C-K_M\,x)=F_A+b\left(\dot{x}-\frac{\dot{F}_C-K_{PEn}\,\dot{x}}{K_{SE}}\right).(2)$$

In order to explicitly identify and collect time- and length-dependent terms, we first replace F_C and $\dot{F}_C$ with their previously derived functions

$$\left(1+\frac{K_{PEam}}{K_{SE}}\right)f_1(\Delta L)-K_M\,x=F_A+b\left(\dot{x}-\frac{f_2(\Delta L)\dot{\Delta L}-K_{PEn}\,\dot{x}}{K_{SE}}\right).(3)$$

Recognizing the equivalence of $\dot{x}$ and $\dot{\Delta L}$, this becomes

$$\left(1+\frac{K_{PEam}}{K_{SE}}\right)f_1(\Delta L)-K_M\,x=F_A\;+b\left(1-\frac{f_2(\Delta L)-K_{PEn}}{K_{SE}}\right)\dot{\Delta L}.\,(4)$$

We can now solve this for $\dot{\Delta L}$

$$\dot{\Delta L}=\frac{\left(1+\frac{K_{PEam}}{K_{SE}}\right)f_1(\Delta L)-K_M\,x-F_A}{b\left(1-\frac{f_2(\Delta L)-K_{PEn}}{K_{SE}}\right)}\,.(5)$$

We introduce ΔL_{offset}, the predicted distance from true resting length based on the prestress tension in the unstretched construct assuming a linear passive kM,

$\Delta L_{offset}+\Delta L=x=x_1+x_2$
to obtain our final differential equation

$$\dot{\Delta L}=\frac{\left(1+\frac{K_{PEam}}{K_{SE}}\right)f_1(\Delta L)-K_M(\Delta L+\Delta L_{offset})-F_A}{b\left(1-\frac{f_2(\Delta L)-K_{PEn}}{K_{SE}}\right)}\,.(6)$$

This differential equation was used to predict the contraction traces and was solved in MATLAB using *ode15s*. Data were given as force applied on the probe, and the construct length change ΔL was calculated as described above (**B1.1**). This calculated ΔL was used to calculate the force in the construct during steady-state stretching and active contraction (**B1.2-3**).

To accommodate the new starting length of the shortened construct, Equation 6 was modified to include a shortening factor (*sf*) which represented the relative change to the starting length of the construct:

$$F_{construct}=\frac{F_{probe}*(L(1-sf)+\Delta L)}{2\Delta s_2}=\frac{F_{probe}*(L(1-sf)+\Delta L)}{2\sqrt{\Delta L^2+2L\Delta L*(1-sf)}}.$$

S2. Parameter estimation details

The first step of parameter estimation for each independent construct is a linear best fit through the passive force over relative length changes. Linear least squares fit the experimental trend to estimate stiffness (K_M; slope) and prestress (intercept) in the construct (**Figure B3** and **Table B2**), and this linear model projects down to the relative length where the construct would have no prestress (the offset of length change).

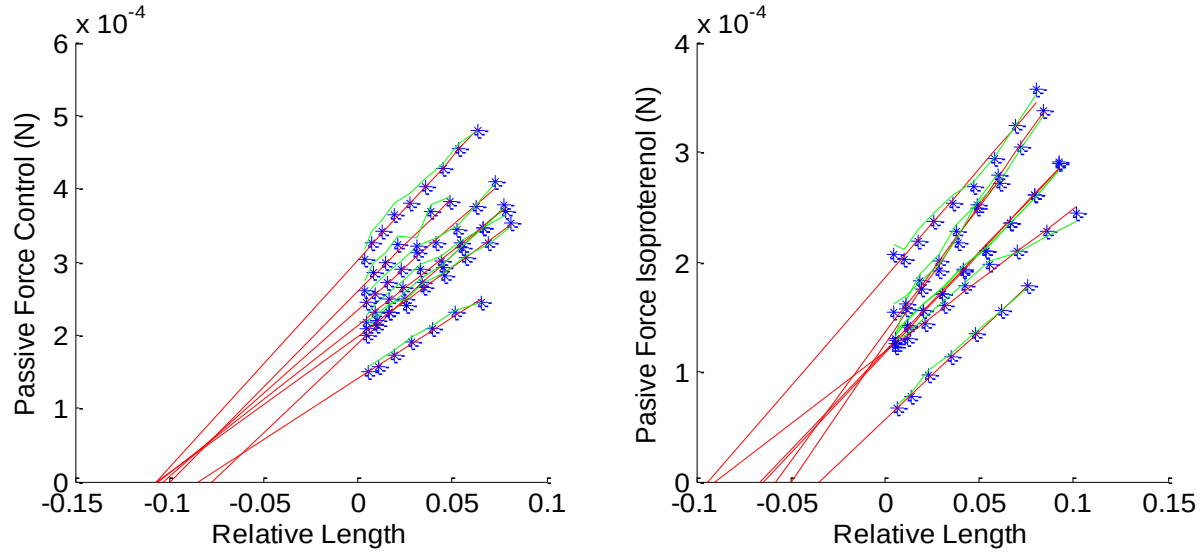

Figure B3: Passive model fits for all isoproterenol treated constructs. Experimental data is represented by blue asterisks, force applied by the probe (Eq. 7) is represented by the green lines, and the passive model fit (Eq. 5) is represented by red lines.

Table B2: Individual passive model fits

Construct	1	2	3	4	5	6	7
K_M (control)	6.37E-01	7.60E-01	5.87E-01	7.19E-01	5.24E-01	8.17E-01	8.90E-01
K_M (iso)	5.74E-01	5.68E-01	4.10E-01	7.92E-01	5.08E-01	7.29E-01	6.25E-01
prestress (control)	2.14E-04	1.88E-04	1.99E-04	2.36E-04	1.41E-04	2.59E-04	3.02E-04
prestress (iso)	1.17E-04	1.19E-04	1.18E-04	1.26E-04	5.68E-05	1.34E-04	1.86E-04
ΔL_{offset} (control)	3.36E-04	2.47E-04	3.39E-04	3.30E-04	2.71E-04	3.17E-04	3.39E-04
ΔL_{offset} (iso)	2.04E-04	2.09E-04	2.88E-04	1.59E-04	1.12E-04	1.84E-04	2.98E-04

The passive parameters (K_m, *prestress,* and ΔL_{offset}) were used as a starting point for parameter estimation for each construct. The *lsqnonlin* function in MATLAB was used to estimate the set of parameters that minimized the residual sum of squared errors (RSS) between the predicted and measured relative length over time for all applied tension conditions. The residuals and Jacobian matrix (i.e., the matrix of partial derivatives of the predicted lengths with respect to the model parameters, evaluated at the estimated model parameters) outputs from the *lsqnonlin* function were input into the *nlparci* function to calculate the confidence intervals for the estimated parameters. Active parameters (K_{SE}, K_{PEam}) were initially set at values which followed the equation $K_{PEam} = (K_M - K_{PEn})(1 - \frac{1}{ratio})$, where $ratio = \frac{K_{SE}}{K_{PEam}}$, and has a value of 2 [244]. The viscosity parameter (b) was originally set to 0.315 for all samples. The initial simulations with these parameters fit the experimental data relatively poorly (**Figure B4** and **Table**

B3.1). After the initial simulations, the parameters (K_{SE}, $K_{PE,}$ *b)* were estimated with the *lsqnonlin* function. This optimization dramatically improved the quality of fit (**Figure B4** and **Table B3.2**). Comparing the estimated parameters before and after isoproterenol treatment with a paired t-test indicated a significant decrease ($p = 0.037$) in *b* (mean decreases from 0.66 to 0.33). We also performed an optimization using the traditional Hill model by setting K_{PEn} to zero and found that the model was able to fit the data very similarly (**Table B3.3**), and that the stiffness previously associated with K_{PEn} was represented among the remaining (stiffness) parameters. Two of the samples that ran into a lower bound (0.013) for optimization for the b parameter with $K_{PEn} = 0.67^* K_M$ were more stably fit when K_{PEn} was set to 0. Taking $K_{PEn} = 0$, both K_{SE} and b were significantly reduced ($p < 0.05$) after isoproterenol. The parameters were also estimated by varying the initial ratio between K_{SE} and K_{PEam} and using an action potential trace as the active force model input. In both cases the quality of fit decreased (**Table B3.4-5**) and *b* was always significantly decreased after isoproterenol.

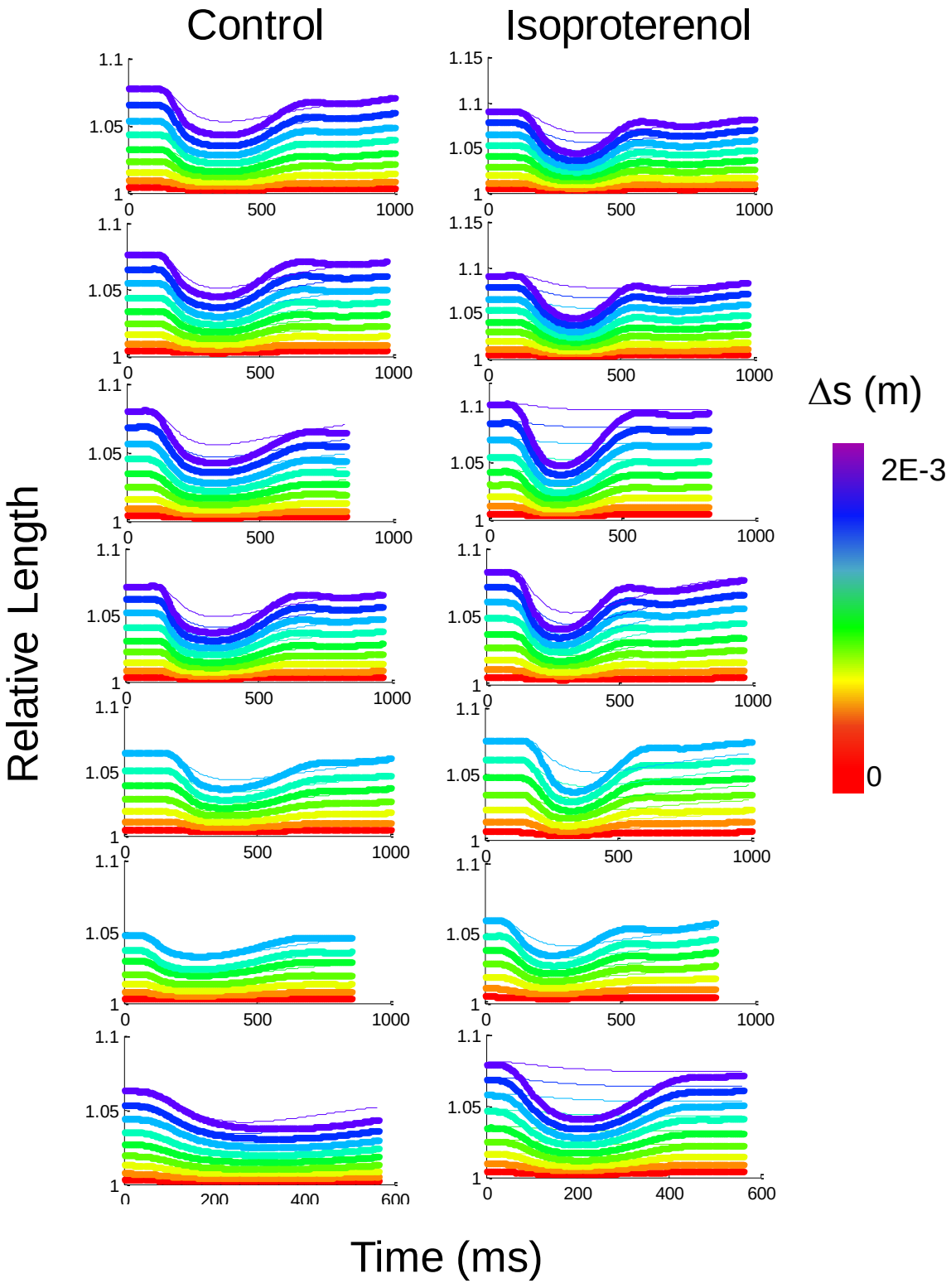

Figure B4: Original model predictions of position with ratio = 2. Experimental data plotted with thicker lines, and model prediction shown with thin lines.

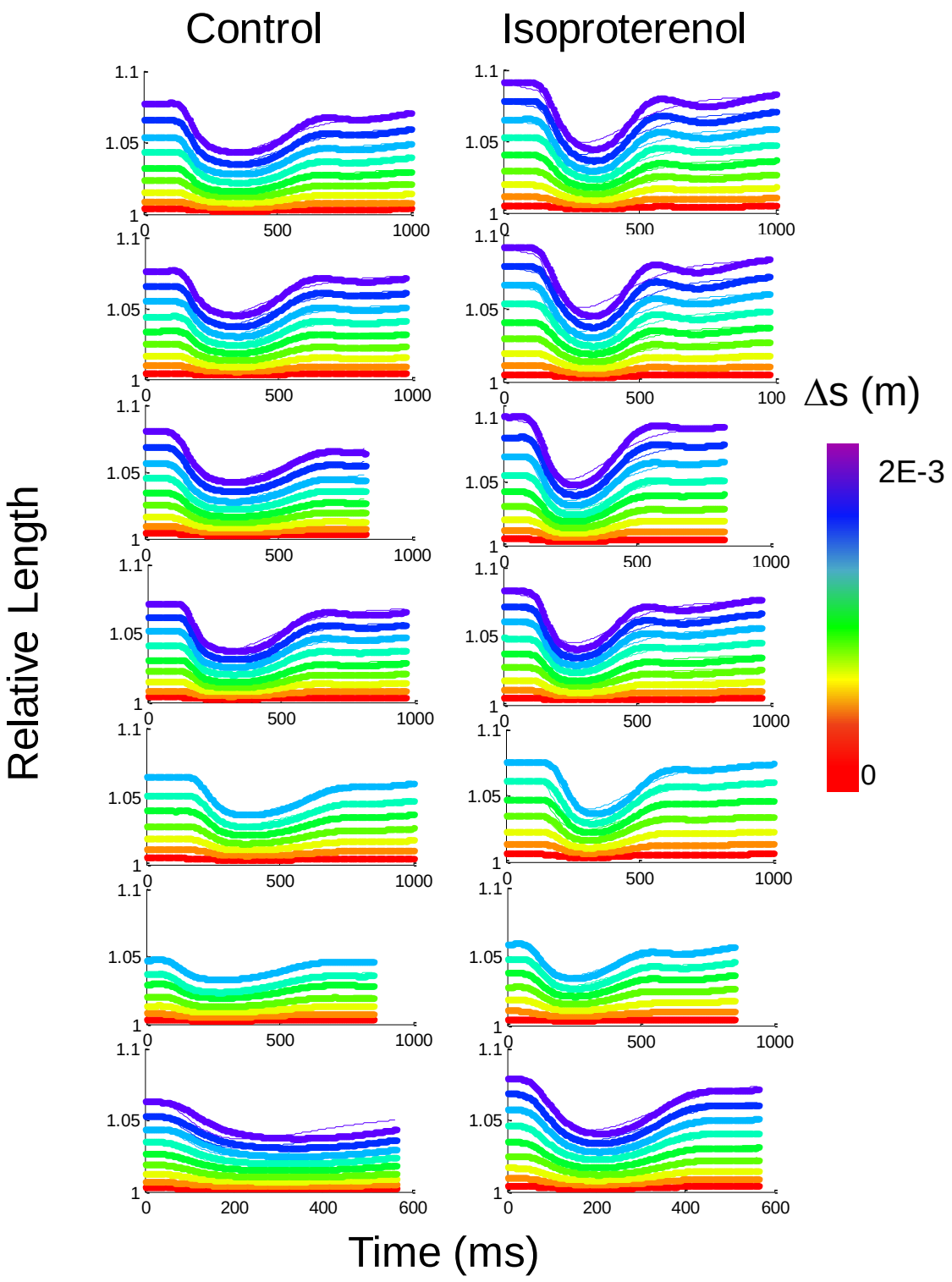

Figure B5: Model predictions with estimated best fit parameter. Experimental data plotted with thicker lines, and model prediction shown with thin lines.

Table S3: Summary of parameter estimates (confidence intervals), and mean squared error (MSE)

	KPEn	KPE	KSE	b	MSE	KPEn	KPE	KSE	b	MSE
Table S3.1: Original values with ratio = 2, KPEn = KM*0.67										
1	4.26E-01	3.15E-01	6.31E-01	3.15E-01	1.55E-05	3.85E-01	2.22E-01	4.45E-01	3.15E-01	5.27E-05
2	5.08E-01	3.75E-01	7.51E-01	3.15E-01	1.21E-05	3.82E-01	8.80E-02	1.76E-01	3.15E-01	1.12E-04
3	3.94E-01	2.91E-01	5.80E-01	3.15E-01	2.90E-05	2.75E-01	2.51E-02	5.02E-02	3.15E-01	2.64E-04
4	4.83E-01	3.56E-01	7.10E-01	3.15E-01	2.03E-05	5.30E-01	4.64E-01	9.31E-01	3.15E-01	2.03E-05
5	3.50E-01	2.59E-01	5.17E-01	3.15E-01	9.40E-06	3.41E-01	2.35E-01	4.70E-01	3.15E-01	5.20E-05
6	5.49E-01	4.04E-01	8.08E-01	3.15E-01	3.89E-06	4.89E-01	2.72E-01	5.43E-01	3.15E-01	1.34E-05
7	5.96E-01	4.42E-01	8.80E-01	3.15E-01	8.44E-06	4.16E-01	4.16E-02	8.33E-02	3.15E-01	1.97E-04
Table S3.2: Best parameter fit, KPEn = KM*0.67										
1	4.26E-01	4.98E-01 (4.86E-01, 5.11E-01)	8.30E-01 (8.17E-01, 8.42E-01)	2.08E-01 (2.05E-01, 2.12E-01)	2.31E-06	3.85E-01	6.56E-01 (6.25E-01, 6.88E-01)	6.28E-01 (6.15E-01, 6.40E-01)	1.43E-01 (1.38E-01, 1.48E-01)	9.72E-06
2	5.08E-01	6.94E-01 (6.78E-01, 7.10E-01)	6.75E-01 (6.66E-01, 6.85E-01)	1.68E-01 (1.64E-01, 1.72E-01)	3.07E-06	3.82E-01	4.48E-01 (4.32E-01, 4.64E-01)	4.01E-01 (3.91E-01, 4.10E-01)	1.00E-01 (9.65E-02, 1.04E-01)	1.01E-05
3	3.94E-01	3.97E-01 (3.94E-01, 4.01E-01)	1.21E+00 (1.18E+00, 1.23E+00)	3.03E-01 (2.98E-01, 3.08E-01)	1.57E-06	2.75E-01	2.08E-01 (1.97E-01, 2.19E-01)	1.60E-01 (1.54E-01, 1.66E-01)	3.15E-02 (3.00E-02, 3.31E-02)	9.38E-06
4	4.83E-01	5.36E-01 (5.27E-01, 5.49E-01)	8.90E-01 (8.74E-01, 9.02E-01)	1.61E-01 (1.58E-01, 1.64E-01)	2.65E-06	5.30E-01	1.02E+00 (1.00E+00, 1.05E+00)	9.81E-01 (9.65E-01, 9.97E-01)	1.83E-01 (1.78E-01, 1.87E-01)	5.50E-06
5	3.50E-01	4.70E-01 (4.64E-01, 4.73E-01)	4.95E-01 (4.89E-01, 4.98E-01)	1.68E-01 (1.67E-01, 1.70E-01)	1.24E-06	3.41E-01	5.33E-01 (5.24E-01, 5.46E-01)	3.79E-01 (3.75E-01, 3.85E-01)	8.17E-02 (7.89E-02, 8.45E-02)	4.70E-06
6	5.49E-01	4.89E-01 (4.57E-01, 5.21E-01)	5.11E-01 (5.02E-01, 5.21E-01)	2.01E-01 (1.97E-01, 2.05E-01)	9.16E-07	4.89E-01	8.93E-01 (8.61E-01, 9.21E-01)	5.49E-01 (5.43E-01, 5.58E-01)	1.61E-01 (1.56E-01, 1.64E-01)	1.95E-06
7	5.96E-01	1.22E+00 (1.21E+00, 1.24E+00)	1.01E+00 (1.00E+00, 1.02E+00)	2.55E-01 (2.52E-01, 2.58E-01)	1.50E-07	4.16E-01	2.32E-01 (2.19E-01, 2.45E-01)	1.97E-01 (1.89E-01, 2.05E-01)	3.15E-02 (3.00E-02, 3.28E-02)	2.40E-06
Table S3.3: Best parameter fit, KPEn = 0										
1	0	1.01E+00 (1.01E+00, 1.01E+00)	2.27E+00 (2.25E+00, 2.29E+00)	4.92E-01 (4.86E-01, 4.95E-01)	2.58E-06	0	1.46E+00 (1.42E+00, 1.51E+00)	1.50E+00 (1.47E+00, 1.53E+00)	3.08E-01 (3.00E-01, 3.15E-01)	9.55E-06
2	0	1.21E+00 (1.20E+00, 1.21E+00)	1.92E+00 (1.91E+00, 1.93E+00)	4.13E-01 (4.10E-01, 4.16E-01)	4.71E-06	0	1.46E+00 (1.43E+00, 1.49E+00)	1.38E+00 (1.36E+00, 1.41E+00)	3.15E-01 (3.09E-01, 3.25E-01)	9.96E-06
3	0	8.11E-01 (8.04E-01, 8.14E-01)	3.31E+00 (3.25E+00, 3.41E+00)	6.34E-01 (6.28E-01, 6.44E-01)	1.85E-06	0	8.04E-01 (7.92E-01, 8.17E-01)	8.36E-01 (8.23E-01, 8.49E-01)	1.34E-01 (1.32E-01, 1.37E-01)	7.48E-06
4	0	1.06E+00 (1.06E+00, 1.06E+00)	2.70E+00 (2.67E+00, 2.72E+00)	4.04E-01 (3.94E-01, 4.10E-01)	3.36E-06	0	1.84E+00 (1.80E+00, 1.87E+00)	1.94E+00 (1.91E+00, 1.97E+00)	3.28E-01 (3.22E-01, 3.34E-01)	5.99E-06
5	0	8.39E-01 (8.36E-01, 8.42E-01)	1.29E+00 (1.28E+00, 1.30E+00)	3.85E-01 (3.82E-01, 3.91E-01)	1.62E-06	0	1.19E+00 (1.18E+00, 1.19E+00)	9.43E-01 (9.43E-01, 9.43E-01)	1.98E-01 (1.97E-01, 1.99E-01)	4.47E-06
6	0	1.56E+00 (1.50E+00, 1.61E+00)	1.64E+00 (1.62E+00, 1.67E+00)	5.62E-01 (5.52E-01, 5.74E-01)	9.23E-07	0	1.97E+00 (1.95E+00, 1.99E+00)	1.44E+00 (1.43E+00, 1.46E+00)	4.20E-01 (4.10E-01, 4.29E-01)	2.21E-06
7	0	2.71E+00 (2.68E+00, 2.74E+00)	2.08E+00 (2.07E+00, 2.09E+00)	5.08E-01 (5.02E-01, 5.11E-01)	1.47E-07	0	1.21E+00 (1.21E+00, 1.22E+00)	1.31E+00 (1.30E+00, 1.32E+00)	1.85E-01 (1.82E-01, 1.87E-01)	2.27E-06
Table S3.4: Best ratio/b fit, KPEn = KM*0.67										
1	4.26E-01	2.71E-01	9.27E-01	2.53E-01 (2.45E-01, 2.62E-01)	3.62E-06	3.85E-01	2.94E-01	5.30E-01	1.15E-01 (1.11E-01, 1.20E-01)	1.77E-05

2	5.08E-01	4.35E-01	5.93E-01	1.78E-01 (1.75E-01, 1.80E-01)	4.69E-06	3.82E-01	3.11E-01	4.70E-01	4.42E-02 (4.26E-02, 4.54E-02)	1.61E-05
3	3.94E-01	2.30E-01	1.22E+00	3.34E-01 (3.22E-01, 3.47E-01)	2.84E-06	2.75E-01	1.70E-01	6.62E-01	3.15E-02 (2.59E-02, 3.72E-02)	8.37E-05
4	4.83E-01	3.34E-01	8.17E-01	1.68E-01 (1.63E-01, 1.74E-01)	4.71E-06	5.30E-01	4.16E-01	7.03E-01	2.20E-01 (2.13E-01, 2.26E-01)	1.41E-05
5	3.50E-01	3.15E-01	3.79E-01	1.47E-01 (1.44E-01, 1.50E-01)	1.99E-06	3.41E-01	3.97E-01	2.88E-01	7.00E-02 (6.91E-02, 7.10E-02)	5.34E-06
6	5.49E-01	5.30E-01	5.49E-01	2.21E-01 (2.16E-01, 2.25E-01)	9.74E-07	4.89E-01	5.27E-01	4.42E-01	1.26E-01 (1.24E-01, 1.29E-01)	4.24E-06
7	5.96E-01	4.98E-01	7.13E-01	1.50E-01 (1.47E-01, 1.53E-01)	8.49E-07	4.16E-01	2.84E-01	7.44E-01	3.15E-02 (2.78E-02, 3.50E-02)	3.36E-05

Table S3.5: Best parameter fit, AP curve, KPEn = KM*0.67

1	4.26E-01	8.86E-01 (8.86E-01, 8.86E-01)	2.25E+00 (2.25E+00, 2.25E+00)	3.72E-01 (3.72E-01, 3.72E-01)	9.54E-06	3.85E-01	7.67E-01 (7.67E-01, 7.67E-01)	2.30E+00 (2.30E+00, 2.30E+00)	3.15E-01 (3.15E-01, 3.15E-01)	2.08E-05
2	5.08E-01	1.06E+00 (1.06E+00, 1.06E+00)	2.68E+00 (2.68E+00, 2.68E+00)	3.72E-01 (3.72E-01, 3.72E-01)	8.28E-06	3.82E-01	7.57E-01 (7.57E-01, 7.57E-01)	2.27E+00 (2.27E+00, 2.27E+00)	3.15E-01 (3.15E-01, 3.15E-01)	2.06E-05
3	3.94E-01	8.23E-01 (8.20E-01, 8.26E-01)	2.00E+00 (1.98E+00, 2.02E+00)	4.10E-01 (4.07E-01, 4.13E-01)	1.14E-05	2.75E-01	5.46E-01 (5.46E-01, 5.46E-01)	1.64E+00 (1.64E+00, 1.64E+00)	3.15E-01 (3.15E-01, 3.15E-01)	4.96E-05
4	4.83E-01	1.01E+00 (1.01E+00, 1.01E+00)	2.51E+00 (2.51E+00, 2.51E+00)	3.79E-01 (3.79E-01, 3.79E-01)	5.93E-06	5.30E-01	1.05E+00 (1.05E+00, 1.06E+00)	3.15E+00 (3.15E+00, 3.15E+00)	3.15E-01 (3.15E-01, 3.15E-01)	2.31E-05
5	3.50E-01	7.32E-01 (7.32E-01, 7.32E-01)	1.83E+00 (1.83E+00, 1.83E+00)	3.79E-01 (3.79E-01, 3.79E-01)	4.81E-06	3.41E-01	6.75E-01 (6.75E-01, 6.75E-01)	2.03E+00 (2.02E+00, 2.03E+00)	3.15E-01 (3.15E-01, 3.15E-01)	2.73E-05
6	5.49E-01	1.15E+00 (1.15E+00, 1.15E+00)	2.87E+00 (2.87E+00, 2.87E+00)	3.75E-01 (3.75E-01, 3.75E-01)	1.31E-05	4.89E-01	9.72E-01 (9.72E-01, 9.72E-01)	2.91E+00 (2.91E+00, 2.91E+00)	3.15E-01 (3.15E-01, 3.15E-01)	2.64E-05
7	5.96E-01	1.25E+00 (1.25E+00, 1.25E+00)	3.14E+00 (3.14E+00, 3.14E+00)	3.66E-01 (3.66E-01, 3.66E-01)	4.49E-06	4.16E-01	8.33E-01 (8.33E-01, 8.33E-01)	2.49E+00 (2.49E+00, 2.49E+00)	3.15E-01 (3.15E-01, 3.15E-01)	3.65E-05

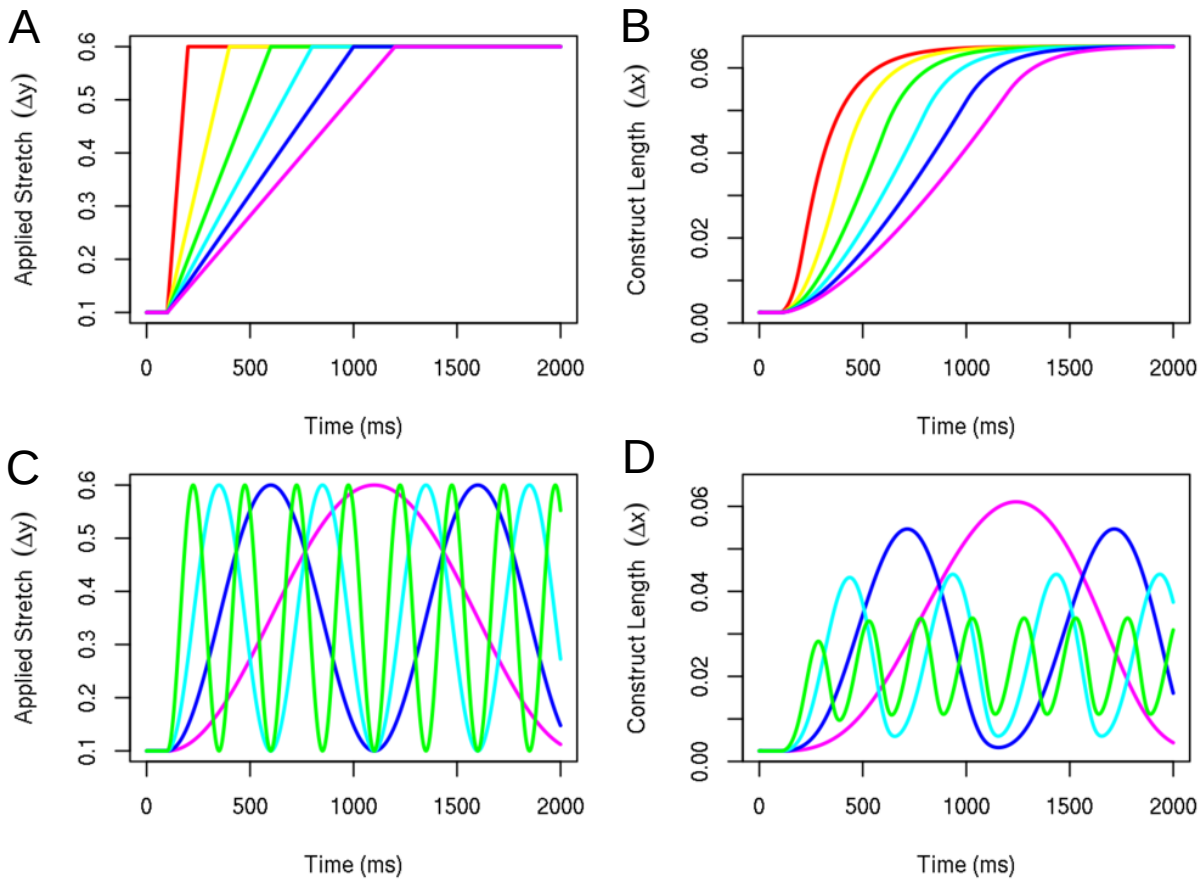

Figure B6: Panels A and C: Simulated experimental mechanical inputs (Δy is equivalent to Δs; cf. Figure B1). Panels B and D: Passive stretch in I-wire construct as predicted by modified Hill model (Δx is equivalent to ΔL; cf. Figure 1).

REFERENCES

[1] D. Mozaffarian *et al.*, “Heart Disease and Stroke Statistics—2016 Update,” *Circulation*, vol. 133, no. 4, pp. e38–e360, 2016.

[2] A. Takawale, M. Shen, D. Fan, and Z. Kassiri, “Cardiac Fibrosis and Heart Failure: Cause or Effect?,” *Adv. Biochem. Heal. Dis.*, vol. 13, pp. 219–235, 2015.

[3] R. G. Gourdie, S. Dimmeler, and P. Kohl, “Novel Therapeutic Strategies Targeting Fibroblasts and Fibrosis in Heart Disease,” *Nat. Rev. Drug Discov.*, vol. In press, no. 9, pp. 620–638, 2016.

[4] N. G. Frangogiannis, “The inflammatory response in myocardial injury, repair, and remodelling,” *Nat Rev Cardiol*, vol. 11, no. 5, pp. 255–265, 2014.

[5] M. Evans *et al.*, “Angiotensin-Converting Enzyme Inhibitors and Angiotensin Receptor Blockers in Myocardial Infarction Patients With Renal Dysfunction,” *J. Am. Coll. Cardiol.*, vol. 67, no. 14, pp. 1687–1697, 2016.

[6] J. Riegler *et al.*, “Human Engineered Heart Muscles Engraft and Survive Long Term in a Rodent Myocardial Infarction Model,” *Circ. Res.*, vol. 117, no. 8, pp. 720–730, 2015.

[7] D. M. Clifford *et al.*, “Stem cell treatment for acute myocardial infarction.,” *Cochrane Database Syst. Rev.*, vol. 2, no. 2, p. CD006536, 2012.

[8] L. Ye *et al.*, “Cardiac repair in a porcine model of acute myocardial infarction with human induced pluripotent stem cell-derived cardiovascular cells.,” *Cell Stem Cell*, vol. 15, no. 6, pp. 750–61, 2014.

[9] F. van den Akker, J. C. Deddens, P. a Doevendans, and J. P. G. Sluijter, “Cardiac stem cell therapy to modulate inflammation upon myocardial infarction.,” *Biochim. Biophys. Acta*, vol. 1830, no. 2, pp. 2449–58, 2013.

[10] C. M. Howard and T. A. Baudino, “Dynamic cell-cell and cell-ECM interactions in the heart,” *J Mol Cell Cardiol*, vol. 70, pp. 19–26, 2014.

[11] A. J. Ribeiro *et al.*, “Contractility of single cardiomyocytes differentiated from pluripotent stem cells depends on physiological shape and substrate stiffness,” *Proc Natl Acad Sci U S A*, vol. 112, no. 41, pp. 12705–12710, 2015.

[12] I. Banerjee, K. Yekkala, T. K. Borg, and T. A. Baudino, “Dynamic interactions between myocytes, fibroblasts, and extracellular matrix,” *Ann N Y Acad Sci*, vol. 1080, pp. 76–84, 2006.

[13] S. R. Ali *et al.*, “Developmental Heterogeneity of Cardiac Fibroblasts Does Not Predict Pathological Proliferation and Activation,” *Circ. Res.*, vol. 115, no. 7, pp. 625-U81, 2014.

[14] O. Aisagbonhi, M. Rai, S. Ryzhov, N. Atria, I. Feoktistov, and A. K. Hatzopoulos, “Experimental myocardial infarction triggers canonical Wnt signaling and endothelial-to-mesenchymal transition,” *Dis Model Mech*, vol. 4, no. 4, pp. 469–483, 2011.

[15] H. B. Sager *et al.*, “Proliferation and Recruitment Contribute to Myocardial Macrophage Expansion in Chronic Heart Failure,” *Circ Res*, vol. 119, no. 7, pp. 853–864, 2016.

[16] N. G. Frangogiannis, “Emerging roles for macrophages in cardiac injury: cytoprotection, repair, and regeneration,” *J Clin Invest*, vol. 125, no. 8, pp. 2927–2930, 2015.

[17] D. E. Conway and M. A. Schwartz, “Flow-dependent cellular mechanotransduction in atherosclerosis,” *J Cell Sci*, vol. 126, no. Pt 22, pp. 5101–5109, 2013.

[18] R. E. Horton *et al.*, “Angiotensin II Induced Cardiac Dysfunction on a Chip,” *PLoS One*, vol. 11, no. 1, p. e0146415, 2016.

[19] A. K. Schroer and W. D. Merryman, “Mechanobiology of myofibroblast adhesion in fibrotic cardiac disease,” *J Cell Sci*, vol. 128, pp. 1865–1875, 2015.

[20] S. K. Agarwal, “Integrins and cadherins as therapeutic targets in fibrosis,” *Front Pharmacol*, vol. 5, p. 131, 2014.

[21] R. S. Ross, “Molecular and mechanical synergy: cross-talk between integrins and growth factor receptors,” *Cardiovasc. Res.*, vol. 63, no. 3, pp. 381–390, 2004.

[22] M. L. Valencik, D. Zhang, B. Punske, P. Hu, J. A. McDonald, and S. E. Litwin, “Integrin activation in the heart: a link between electrical and contractile dysfunction?,” *Circ Res*, vol. 99, no. 12, pp. 1403–1410, 2006.

[23] S. K. Chang *et al.*, “Cadherin-11 regulates fibroblast inflammation,” *Proc Natl Acad Sci U S A*, vol. 108, no. 20, pp. 8402–8407, 2011.

[24] D. M. Lee *et al.*, “Cadherin-11 in synovial lining formation and pathology in arthritis.,” *Science*, vol. 315, no. 5814, pp. 1006–10, 2007.

[25] D. J. Schneider *et al.*, “Cadherin-11 contributes to pulmonary fibrosis: potential role in TGF-beta production and epithelial to mesenchymal transition,” *FASEB J*, vol. 26, no. 2, pp. 503–512, 2012.

[26] G. Vunjak Novakovic, T. Eschenhagen, and C. Mummery, “Myocardial tissue engineering: in vitro models,” *Cold Spring Harb Perspect Med*, vol. 4, no. 3, 2014.

[27] M. L. McCain and K. K. Parker, “Mechanotransduction: the role of mechanical stress, myocyte shape, and cytoskeletal architecture on cardiac function,” *Pflugers Arch*, vol. 462, no. 1, pp. 89–104, 2011.

[28] M. K. Sewell-Loftin *et al.*, “Myocardial contraction and hyaluronic acid mechanotransduction in epithelial-to-mesenchymal transformation of endocardial cells,” *Biomaterials*, vol. 35, no. 9, pp. 2809–2815, 2014.

[29] M. G. Monaghan, M. Linneweh, S. Liebscher, B. Van Handel, S. L. Layland, and K. Schenke-Layland, “Endocardial-to-mesenchymal transformation and mesenchymal cell colonization at the onset of human cardiac valve development,” *Dev.*, vol. 143, no. 3, pp. 473–482, 2016.

[30] T. Haack and S. Abdelilah-Seyfried, “The force within: endocardial development, mechanotransduction and signalling during cardiac morphogenesis.,” *Development*, vol. 143, no. 3, pp. 373–86, 2016.

[31] H. E. Olivey, N. A. Mundell, A. F. Austin, and J. V Barnett, “Transforming growth factor-beta stimulates epithelial-mesenchymal transformation in the proepicardium,” *Dev Dyn*, vol. 235, no. 1, pp. 50–59, 2006.

[32] J. Wylie-Sears, R. A. Levine, and J. Bischoff, “Losartan inhibits endothelial-to-mesenchymal transformation in mitral valve endothelial cells by blocking transforming growth factor-beta-induced phosphorylation of ERK,” *Biochem Biophys Res Commun*, vol. 446, no. 4, pp. 870–875, 2014.

[33] J. G. Jacot, J. C. Martin, and D. L. Hunt, “Mechanobiology of cardiomyocyte development,” *J Biomech*, vol. 43, no. 1, pp. 93–98, 2010.

[34] K. E. Porter and N. A. Turner, “Cardiac fibroblasts: at the heart of myocardial remodeling,” *Pharmacol Ther*, vol. 123, no. 2, pp. 255–278, 2009.

[35] J. M. C. Ngu *et al.*, “Human cardiac fibroblast extracellular matrix remodeling: dual effects of tissue inhibitor of metalloproteinase-2.,” *Cardiovasc. Pathol.*, vol. 23, no. 6, pp. 335–343, 2014.

[36] W. David Merryman, “Mechano-potential etiologies of aortic valve disease,” *J. Biomech.*, vol. 43, no. 1, pp. 87–92, 2010.

[37] W. Chen and N. G. Frangogiannis, “Fibroblasts in post-infarction inflammation and cardiac repair,” *Biochim. Biophys. Acta-Molecular Cell Res.*, vol. 1833, no. 4, pp. 945–953, 2013.

[38] G. J. Mahler and J. T. Butcher, “Inflammatory regulation of valvular remodeling: the good(?), the bad, and the ugly,” *Int J Inflam*, vol. 2011, p. 721419, 2011.

[39] L. A. Cuniberti, P. G. Stutzbach, E. Guevara, G. G. Yannarelli, R. P. Laguens, and R. R. Favaloro, “Development of mild aortic valve stenosis in a rabbit model of hypertension,” *J. Am. Coll. Cardiol.*, vol. 47, no. 11, pp. 2303–2309, 2006.

[40] W. D. Merryman *et al.*, “Correlation between heart valve interstitial cell stiffness and transvalvular pressure: implications for collagen biosynthesis,” *Am J Physiol Hear. Circ Physiol*, vol. 290, no. 1,

pp. H224-31, 2006.

[41] H. Zhao *et al.*, “Microengineered in vitro model of cardiac fibrosis through modulating myofibroblast mechanotransduction.,” *Biofabrication*, vol. 6, no. 4, p. 45009, 2014.

[42] T. Meyer-ter-Vehn, H. Han, F. Grehn, and G. Schlunck, “Extracellular matrix elasticity modulates TGF-beta-induced p38 activation and myofibroblast transdifferentiation in human tenon fibroblasts,” *Invest Ophthalmol Vis Sci*, vol. 52, no. 12, pp. 9149–9155, 2011.

[43] X. Huang *et al.*, “Matrix stiffness-induced myofibroblast differentiation is mediated by intrinsic mechanotransduction,” *Am J Respir Cell Mol Biol*, vol. 47, no. 3, pp. 340–348, 2012.

[44] B. Hinz, P. Pittet, J. Smith-Clerc, C. Chaponnier, and J. J. Meister, “Myofibroblast development is characterized by specific cell-cell adherens junctions,” *Mol Biol Cell*, vol. 15, no. 9, pp. 4310–4320, 2004.

[45] A. D. Doyle and K. M. Yamada, “Mechanosensing via cell-matrix adhesions in 3D microenvironments,” *Experimental Cell Research*, vol. 343, no. 1. pp. 60–66, 2016.

[46] J. S. Harunaga and K. M. Yamada, “Cell-matrix adhesions in 3D,” *Matrix Biology*, vol. 30, no. 7–8. pp. 363–368, 2011.

[47] E. L. Baker and M. H. Zaman, “The biomechanical integrin,” *J Biomech*, vol. 43, no. 1, pp. 38–44, 2010.

[48] L. Li *et al.*, “The human cadherin 11 is a pro-apoptotic tumor suppressor modulating cell stemness through Wnt/beta-catenin signaling and silenced in common carcinomas,” *Oncogene*, vol. 31, no. 34, pp. 3901–3912, 2012.

[49] J. Heuberger and W. Birchmeier, “Interplay of cadherin-mediated cell adhesion and canonical Wnt signaling,” *Cold Spring Harb Perspect Biol*, vol. 2, no. 2, p. a002915, 2010.

[50] S. A. Thompson *et al.*, “Acute slowing of cardiac conduction in response to myofibroblast coupling to cardiomyocytes through N-cadherin,” *J. Mol. Cell. Cardiol.*, vol. 68, pp. 29–37, 2014.

[51] J. D. Hutcheson *et al.*, “Cadherin-11 regulates cell-cell tension necessary for calcific nodule formation by valvular myofibroblasts,” *Arter. Thromb Vasc Biol*, vol. 33, no. 1, pp. 114–120, 2013.

[52] D. E. Leckband and J. de Rooij, “Cadherin adhesion and mechanotransduction,” *Annu Rev Cell Dev Biol*, vol. 30, pp. 291–315, 2014.

[53] A. K. Barry *et al.*, “alpha-catenin cytomechanics--role in cadherin-dependent adhesion and mechanotransduction,” *J Cell Sci*, vol. 127, no. Pt 8, pp. 1779–1791, 2014.

[54] S. Y. Xu, A. C. Liu, H. Kim, and A. I. Gotlieb, “Cell density regulates in vitro activation of heart valve interstitial cells,” *Cardiovasc. Pathol.*, vol. 21, no. 2, pp. 65–73, 2012.

[55] E. Charbonney, P. Speight, A. Masszi, H. Nakano, and A. Kapus, “beta-catenin and Smad3 regulate the activity and stability of myocardin-related transcription factor during epithelial-myofibroblast transition,” *Mol Biol Cell*, vol. 22, no. 23, pp. 4472–4485, 2011.

[56] F. Caraci *et al.*, “TGF-beta1 targets the GSK-3beta/beta-catenin pathway via ERK activation in the transition of human lung fibroblasts into myofibroblasts,” *Pharmacol Res*, vol. 57, no. 4, pp. 274–282, 2008.

[57] E. de Marchena *et al.*, “Respective prevalence of the different carpentier classes of mitral regurgitation: a stepping stone for future therapeutic research and development,” *J Card Surg*, vol. 26, no. 4, pp. 385–392, 2011.

[58] J. D. Hutcheson, E. Aikawa, and W. D. Merryman, “Potential drug targets for calcific aortic valve disease,” *Nat Rev Cardiol*, vol. 11, no. 4, pp. 218–231, 2014.

[59] A. Geirsson *et al.*, “Modulation of transforming growth factor-beta signaling and extracellular matrix production in myxomatous mitral valves by angiotensin II receptor blockers,” *Circulation*, vol. 126, no. 11 Suppl 1, pp. S189-97, 2012.

[60] W. D. Merryman and F. J. Schoen, “Mechanisms of calcification in aortic valve disease: role of

mechanokinetics and mechanodynamics," *Curr Cardiol Rep*, vol. 15, no. 5, p. 355, 2013.

[61] H. Aupperle and S. Disatian, "Pathology, protein expression and signaling in myxomatous mitral valve degeneration: Comparison of dogs and humans," *J. Vet. Cardiol.*, vol. 14, no. 1, pp. 59–71, 2012.

[62] M. A. Hagler *et al.*, "TGF-?? signalling and reactive oxygen species drive fibrosis and matrix remodelling in myxomatous mitral valves," *Cardiovasc. Res.*, vol. 99, no. 1, pp. 175–184, 2013.

[63] E. R. Mohler 3rd, F. Gannon, C. Reynolds, R. Zimmerman, M. G. Keane, and F. S. Kaplan, "Bone formation and inflammation in cardiac valves," *Circulation*, vol. 103, no. 11, pp. 1522–1528, 2001.

[64] J. B. L. de Waroux *et al.*, "Functional anatomy of aortic regurgitation - Accuracy, prediction of surgical repairability, and outcome implications of transesophageal echocardiography," *Circulation*, vol. 116, no. 11, pp. I264–I269, 2007.

[65] A. C. Liu, V. R. Joag, and A. I. Gotlieb, "The emerging role of valve interstitial cell phenotypes in regulating heart valve pathobiology," *Am J Pathol*, vol. 171, no. 5, pp. 1407–1418, 2007.

[66] S. M. Dusenbery *et al.*, "Myocardial extracellular remodeling is associated with ventricular diastolic dysfunction in children and young adults with congenital aortic stenosis," *J. Am. Coll. Cardiol.*, vol. 63, no. 17, pp. 1778–1785, 2014.

[67] B. S. Burlew and K. T. Weber, "Cardiac fibrosis as a cause of diastolic dysfunction," *Herz*, vol. 27, no. 2, pp. 92–98, 2002.

[68] C. F. Azevedo *et al.*, "Prognostic Significance of Myocardial Fibrosis Quantification by Histopathology and Magnetic Resonance Imaging in Patients With Severe Aortic Valve Disease," *J. Am. Coll. Cardiol.*, vol. 56, no. 4, pp. 278–287, 2010.

[69] J. G. Travers, F. A. Kamal, J. Robbins, K. E. Yutzey, and B. C. Blaxall, "Cardiac fibrosis: The fibroblast awakens," *Circulation Research*, vol. 118, no. 6. pp. 1021–1040, 2016.

[70] X. R. Huang *et al.*, "Smad3 Mediates Cardiac Inflammation and Fibrosis in Angiotensin II-Induced Hypertensive Cardiac Remodeling," *Hypertension*, vol. 55, no. 5, pp. 1165-U153, 2010.

[71] L. Gullestad, T. Ueland, L. E. Vinge, A. Finsen, A. Yndestad, and P. Aukrust, "Inflammatory Cytokines in Heart Failure: Mediators and Markers," *Cardiology*, vol. 122, no. 1, pp. 23–35, 2012.

[72] B. Chen and N. G. Frangogiannis, "Macrophages in the Remodeling Failing Heart," *Circ Res*, vol. 119, no. 7, pp. 776–778, 2016.

[73] Y. G. Ma *et al.*, "Matrix Metalloproteinase-28 Deletion Exacerbates Cardiac Dysfunction and Rupture After Myocardial Infarction in Mice by Inhibiting M2 Macrophage Activation," *Circ. Res.*, vol. 112, no. 4, p. 675–+, 2013.

[74] J. A. Virag, M. L. Rolle, J. Reece, S. Hardouin, E. O. Feigl, and C. E. Murry, "Fibroblast growth factor-2 regulates myocardial infarct repair: effects on cell proliferation, scar contraction, and ventricular function," *Am J Pathol*, vol. 171, no. 5, pp. 1431–1440, 2007.

[75] K. H. Schuleri *et al.*, "Cardiovascular magnetic resonance characterization of peri-infarct zone remodeling following myocardial infarction," *J Cardiovasc Magn Reson*, vol. 14, p. 24, 2012.

[76] M. Ikeuchi *et al.*, "Inhibition of TGF-beta signaling exacerbates early cardiac dysfunction but prevents late remodeling after infarction," *Cardiovasc. Res.*, vol. 64, no. 3, pp. 526–535, 2004.

[77] M. Ersboll *et al.*, "Early diastolic strain rate in relation to systolic and diastolic function and prognosis in acute myocardial infarction: a two-dimensional speckle-tracking study," *Eur. Heart J.*, vol. 35, no. 10, p. 648–+, 2014.

[78] J. H. Wang *et al.*, "Hypoxia-stimulated cardiac fibroblast production of IL-6 promotes myocardial fibrosis via the TGF-beta1 signaling pathway," *Lab Invest*, vol. 96, no. 8, pp. 839–852, 2016.

[79] K. D. Boudoulas and A. K. Hatzopoulos, "Cardiac repair and regeneration: the Rubik's cube of cell therapy for heart disease," *Dis Model Mech*, vol. 2, no. 7–8, pp. 344–358, 2009.

[80] J. Davis and J. D. Molkentin, "Myofibroblasts: trust your heart and let fate decide," *J Mol Cell*

Cardiol, vol. 70, pp. 9–18, 2014.

[81] M. Bujak and N. G. Frangogiannis, “The role of TGF-beta signaling in myocardial infarction and cardiac remodeling,” *Cardiovasc Res*, vol. 74, no. 2, pp. 184–195, 2007.

[82] Y. Yang *et al.*, “Modified VEGF targets the ischemic myocardium and promotes functional recovery after myocardial infarction,” *J. Control. Release*, vol. 213, pp. 27–35, 2015.

[83] D. A. Svystonyuk *et al.*, “Fibroblast growth factor-2 regulates human cardiac myofibroblast-mediated extracellular matrix remodeling,” *J. Transl. Med.*, vol. 13, no. 1, p. 147, 2015.

[84] C. M. Yu, G. L. Tipoe, K. Wing-Hon Lai, and C. P. Lau, “Effects of combination of angiotensin-converting enzyme inhibitor and angiotensin receptor antagonist on inflammatory cellular infiltration and myocardial interstitial fibrosis after acute myocardial infarction,” *J. Am. Coll. Cardiol.*, vol. 38, no. 4, pp. 1207–1215, 2001.

[85] G. A. Walker, K. S. Masters, D. N. Shah, K. S. Anseth, and L. A. Leinwand, “Valvular myofibroblast activation by transforming growth factor-beta: implications for pathological extracellular matrix remodeling in heart valve disease,” *Circ Res*, vol. 95, no. 3, pp. 253–260, 2004.

[86] W. D. Merryman, H. D. Lukoff, R. A. Long, G. C. Engelmayr Jr., R. A. Hopkins, and M. S. Sacks, “Synergistic effects of cyclic tension and transforming growth factor-beta1 on the aortic valve myofibroblast,” *Cardiovasc Pathol*, vol. 16, no. 5, pp. 268–276, 2007.

[87] P. Kong, P. Christia, and N. G. Frangogiannis, “The pathogenesis of cardiac fibrosis,” *Cellular and Molecular Life Sciences*, vol. 71, no. 4. pp. 549–574, 2014.

[88] J. J. Tomasek, G. Gabbiani, B. Hinz, C. Chaponnier, and R. a Brown, “Myofibroblasts and mechano-regulation of connective tissue remodelling.,” *Nat. Rev. Mol. Cell Biol.*, vol. 3, no. 5, pp. 349–63, 2002.

[89] R. S. Greenberg, A. M. Bernstein, M. Benezra, I. H. Gelman, L. Taliana, and S. K. Masur, “FAK-dependent regulation of myofibroblast differentiation,” *FASEB J*, vol. 20, no. 7, pp. 1006–1008, 2006.

[90] A. M. Kloxin, J. A. Benton, and K. S. Anseth, “In situ elasticity modulation with dynamic substrates to direct cell phenotype,” *Biomaterials*, vol. 31, no. 1, pp. 1–8, 2010.

[91] A. von Gise and W. T. Pu, “Endocardial and Epicardial Epithelial to Mesenchymal Transitions in Heart Development and Disease,” *Circ. Res.*, vol. 110, no. 12, pp. 1628–1645, 2012.

[92] A. Akhmetshina *et al.*, “Activation of canonical Wnt signalling is required for TGF-beta-mediated fibrosis,” *Nat. Commun.*, vol. 3, 2012.

[93] K. Balachandran, P. Sucosky, H. Jo, and A. P. Yoganathan, “Elevated cyclic stretch alters matrix remodeling in aortic valve cusps: implications for degenerative aortic valve disease,” *Am J Physiol Hear. Circ Physiol*, vol. 296, no. 3, pp. H756-64, 2009.

[94] D. T. Paik *et al.*, “Wnt10b Gain-of-Function Improves Cardiac Repair by Arteriole Formation and Attenuation of Fibrosis,” *Circ. Res.*, vol. 117, no. 9, pp. 804–816, 2015.

[95] A. P. Dalla Costa, C. F. M. Z. Clemente, H. F. Carvalho, J. B. Carvalheira, and K. G. Franchini, “FAK mediates the activation of cardiac fibroblasts induced by mechanical stress through regulation of mTOR complex,” *Faseb J.*, vol. 24, 2010.

[96] X. Wang *et al.*, “Meshless Deformable Models for 3D Cardiac Motion and Strain Analysis from Tagged MRI,” *Magn Reson Imaging*, 2014.

[97] K. E. Smith, S. A. Metzler, and J. N. Warnock, “Cyclic strain inhibits acute pro-inflammatory gene expression in aortic valve interstitial cells,” *Biomech Model Mechanobiol*, vol. 9, no. 1, pp. 117–125, 2010.

[98] P. J. Wipff, D. B. Rifkin, J. J. Meister, and B. Hinz, “Myofibroblast contraction activates latent TGF-beta1 from the extracellular matrix,” *J Cell Biol*, vol. 179, no. 6, pp. 1311–1323, 2007.

[99] V. Sarrazy *et al.*, “Integrins alpha v beta 5 and alpha v beta 3 promote latent TGF-beta 1 activation

by human cardiac fibroblast contraction," *Cardiovasc. Res.*, vol. 102, no. 3, pp. 407–417, 2014.

[100] J. J. Santiago *et al.*, "Cardiac fibroblast to myofibroblast differentiation in vivo and in vitro: expression of focal adhesion components in neonatal and adult rat ventricular myofibroblasts," *Dev Dyn*, vol. 239, no. 6, pp. 1573–1584, 2010.

[101] C. I. Fisher, J. Chen, and W. D. Merryman, "Calcific nodule morphogenesis by heart valve interstitial cells is strain dependent," *Biomech. Model. Mechanobiol.*, vol. 12, no. 1, pp. 5–17, 2013.

[102] C. Y. Y. Yip, J. H. Chen, R. G. Zhao, and C. A. Simmons, "Calcification by Valve Interstitial Cells Is Regulated by the Stiffness of the Extracellular Matrix," *Arterioscler. Thromb. Vasc. Biol.*, vol. 29, no. 6, pp. 936-U417, 2009.

[103] M. C. Cushing, M. P. Jaeggli, K. S. Masters, L. A. Leinwand, and K. S. Anseth, "Serum deprivation improves seeding and repopulation of acellular matrices with valvular interstitial cells," *J Biomed Mater Res A*, vol. 75, no. 1, pp. 232–241, 2005.

[104] A. Petersen, P. Joly, C. Bergmann, G. Korus, and G. N. Duda, "The impact of substrate stiffness and mechanical loading on fibroblast-induced scaffold remodeling," *Tissue Eng Part A*, vol. 18, no. 17–18, pp. 1804–1817, 2012.

[105] B. D. Southern *et al.*, "Matrix-driven myosin II mediates the pro-fibrotic fibroblast phenotype," *J. Biol. Chem.*, vol. 291, no. 12, pp. 6083–6095, 2016.

[106] M. Ieda *et al.*, "Cardiac fibroblasts regulate myocardial proliferation through beta1 integrin signaling," *Dev Cell*, vol. 16, no. 2, pp. 233–244, 2009.

[107] K. Fujiu and R. Nagai, "Fibroblast-mediated pathways in cardiac hypertrophy," *J Mol Cell Cardiol*, vol. 70, pp. 64–73, 2014.

[108] S. Y. Shai *et al.*, "Cardiac myocyte-specific excision of the ??1 integrin gene results in myocardial fibrosis and cardiac failure," *Circ. Res.*, vol. 90, no. 4, pp. 458–464, 2002.

[109] D. Fan *et al.*, "A Disintegrin and Metalloprotease-17 Regulates Pressure Overload–Induced Myocardial Hypertrophy and Dysfunction Through Proteolytic Processing of Integrin β1," *Hypertension*, vol. 68, pp. 937–948, 2016.

[110] H. Okada *et al.*, "Integrins protect cardiomyocytes from ischemia/reperfusion injury," *J Clin Invest*, vol. 123, no. 10, pp. 4294–4308, 2013.

[111] C. Penna *et al.*, "Overexpression of the muscle-specific protein, melusin, protects from cardiac ischemia/reperfusion injury," *Basic Res Cardiol*, vol. 109, no. 4, p. 418, 2014.

[112] J. R. Gershlak and L. D. Black 3rd, "Beta 1 integrin binding plays a role in the constant traction force generation in response to varying stiffness for cells grown on mature cardiac extracellular matrix," *Exp Cell Res*, 2014.

[113] J. H. Chen and C. A. Simmons, "Cell-Matrix Interactions in the Pathobiology of Calcific Aortic Valve Disease Critical Roles for Matricellular, Matricrine, and Matrix Mechanics Cues," *Circ. Res.*, vol. 108, no. 12, pp. 1510–1524, 2011.

[114] T. Fujimura, S. Moriwaki, G. Imokawa, and Y. Takema, "Crucial role of fibroblast integrins alpha2 and beta1 in maintaining the structural and mechanical properties of the skin," *J Dermatol Sci*, vol. 45, no. 1, pp. 45–53, 2007.

[115] S. X. Liu and A. Leask, "Integrin beta 1 Is Required for Dermal Homeostasis," *J. Invest. Dermatol.*, vol. 133, no. 4, pp. 899–906, 2013.

[116] T. Riikonen, J. Westermarck, L. Koivisto, A. Broberg, V. M. Kahari, and J. Heino, "Integrin Alpha-2-Beta-1 Is a Positive Regulator of Collagenase (Mmp-1) and Collagen Alpha-1(I) Gene-Expression," *J. Biol. Chem.*, vol. 270, no. 22, pp. 13548–13552, 1995.

[117] Y. Zhang *et al.*, "Disentangling the multifactorial contributions of fibronectin, collagen and cyclic strain on MMP expression and extracellular matrix remodeling by fibroblasts," *Matrix Biol*, 2014.

[118] C. F. Krieglstein *et al.*, "Collagen-binding integrin alpha1beta1 regulates intestinal inflammation in experimental colitis.," *J. Clin. Invest.*, vol. 110, no. 12, pp. 1773–82, 2002.

[119] A. Rodriguez, J. Karen, H. Gardner, B. Gerdin, K. Rubin, and C. Sundberg, “Integrin alpha(1)beta(1) is involved in the differentiation into myofibroblasts in adult reactive tissues in vivo,” *J. Cell. Mol. Med.*, vol. 13, no. 9B, pp. 3449–3462, 2009.

[120] K. K. Kim *et al.*, “Epithelial cell alpha3beta1 integrin links beta-catenin and Smad signaling to promote myofibroblast formation and pulmonary fibrosis,” *J Clin Invest*, vol. 119, no. 1, pp. 213–224, 2009.

[121] J. E. Naugle *et al.*, “Type VI collagen induces cardiac myofibroblast differentiation: implications for postinfarction remodeling,” *Am. J. Physiol. Circ. Physiol.*, vol. 290, no. 1, pp. H323–H330, 2006.

[122] M. Aragno *et al.*, “Oxidative stress triggers cardiac fibrosis in the heart of diabetic rats,” *Endocrinology*, vol. 149, no. 1, pp. 380–388, 2008.

[123] Z. Wang *et al.*, “RGD-independent cell adhesion via a tissue transglutaminase-fibronectin matrix promotes fibronectin fibril deposition and requires syndecan-4/2 and {alpha}5{beta}1 integrin co-signaling,” *J Biol Chem*, vol. 285, no. 51, pp. 40212–40229, 2010.

[124] M. C. Cushing, J. T. Liao, and K. S. Anseth, “Activation of valvular interstitial cells is mediated by transforming growth factor-beta1 interactions with matrix molecules,” *Matrix Biol*, vol. 24, no. 6, pp. 428–437, 2005.

[125] H. J. Zhang *et al.*, “Deletion of Soluble Epoxide Hydrolase Attenuates Cardiac Hypertrophy via Down-Regulation of Cardiac Fibroblasts-Derived Fibroblast Growth Factor-2,” *Crit. Care Med.*, vol. 42, no. 5, pp. E345–E354, 2014.

[126] F. Bouzeghrane, C. Mercure, T. L. Reudelhuber, and G. Thibault, “Alpha8beta1 integrin is upregulated in myofibroblasts of fibrotic and scarring myocardium,” *J Mol Cell Cardiol*, vol. 36, no. 3, pp. 343–353, 2004.

[127] M. L. Burgess, L. Terracio, T. Hirozane, and T. K. Borg, “Differential integrin expression by cardiac fibroblasts from hypertensive and exercise-trained rat hearts,” *Cardiovasc Pathol*, vol. 11, no. 2, pp. 78–87, 2002.

[128] S. X. Liu *et al.*, “Expression of integrin beta 1 by fibroblasts is required for tissue repair in vivo,” *J. Cell Sci.*, vol. 123, no. 21, pp. 3674–3682, 2010.

[129] P. Roca-Cusachs, N. C. Gauthier, A. Del Rio, and M. P. Sheetz, “Clustering of alpha(5)beta(1) integrins determines adhesion strength whereas alpha(v)beta(3) and talin enable mechanotransduction,” *Proc Natl Acad Sci U S A*, vol. 106, no. 38, pp. 16245–16250, 2009.

[130] Y. P. Luo, Y. Sun, Z. H. Zhu, and F. Li, “Is the Change of Integrin alpha(v)beta(3) Expression in the Infarcted Myocardium Related to the Clinical Outcome?,” *Clin. Nucl. Med.*, vol. 39, no. 7, pp. 655–657, 2014.

[131] X. Gu and K. S. Masters, “Regulation of valvular interstitial cell calcification by adhesive peptide sequences,” *J Biomed Mater Res A*, vol. 93, no. 4, pp. 1620–1630, 2010.

[132] J. A. Benton, B. D. Fairbanks, and K. S. Anseth, “Characterization of valvular interstitial cell function in three dimensional matrix metalloproteinase degradable PEG hydrogels,” *Biomaterials*, vol. 30, no. 34, pp. 6593–6603, 2009.

[133] S. Balasubramanian *et al.*, “beta3 integrin in cardiac fibroblast is critical for extracellular matrix accumulation during pressure overload hypertrophy in mouse,” *PLoS One*, vol. 7, no. 9, p. e45076, 2012.

[134] A. M. Manso *et al.*, “Talin1 has unique expression versus talin 2 in the heart and modifies the hypertrophic response to pressure overload,” *J Biol Chem*, vol. 288, no. 6, pp. 4252–4264, 2013.

[135] D. V Pechkovsky *et al.*, “Transforming growth factor beta1 induces alphavbeta3 integrin expression in human lung fibroblasts via a beta3 integrin-, c-Src-, and p38 MAPK-dependent pathway,” *J Biol Chem*, vol. 283, no. 19, pp. 12898–12908, 2008.

[136] T. Watanabe *et al.*, “Adaptor protein Crk induces Src-dependent activation of p38 MAPK in regulation of synovial sarcoma cell proliferation,” *Mol Cancer Res*, vol. 7, no. 9, pp. 1582–1592,

2009.

[137] J. D. Hutcheson, L. M. Ryzhova, V. Setola, and W. D. Merryman, “5-HT(2B) antagonism arrests non-canonical TGF-beta1-induced valvular myofibroblast differentiation,” *J Mol Cell Cardiol*, vol. 53, no. 5, pp. 707–714, 2012.

[138] G. Elberg, L. Chen, D. Elberg, M. D. Chan, C. J. Logan, and M. A. Turman, “MKL1 mediates TGF-beta1-induced alpha-smooth muscle actin expression in human renal epithelial cells,” *Am J Physiol Ren. Physiol*, vol. 294, no. 5, pp. F1116-28, 2008.

[139] A. K. Schroer, L. M. Ryzhova, and W. D. Merryman, “Network Modeling Approach to Predict Myofibroblast Differentiation,” *Cell. Mol. Bioeng.*, vol. 7, no. 3, pp. 446–459, 2014.

[140] K. Kawai-Kowase *et al.*, “Basic fibroblast growth factor antagonizes transforming growth factor-beta1-induced smooth muscle gene expression through extracellular signal-regulated kinase 1/2 signaling pathway activation,” *Arter. Thromb Vasc Biol*, vol. 24, no. 8, pp. 1384–1390, 2004.

[141] A. Grella, D. Kole, W. Holmes, and T. Dominko, “FGF2 Overrides TGFβ1-Driven Integrin ITGA11 Expression in Human Dermal Fibroblasts,” *J. Cell. Biochem.*, vol. 117, no. 4, pp. 1000–1008, 2016.

[142] S. K. Verma *et al.*, “Rac1 and RhoA differentially regulate angiotensinogen gene expression in stretched cardiac fibroblasts,” *Cardiovasc Res*, vol. 90, no. 1, pp. 88–96, 2011.

[143] K. E. Michael, D. W. Dumbauld, K. L. Burns, S. K. Hanks, and A. J. Garcia, “Focal adhesion kinase modulates cell adhesion strengthening via integrin activation,” *Mol Biol Cell*, vol. 20, no. 9, pp. 2508–2519, 2009.

[144] A. Katsumi, A. W. Orr, E. Tzima, and M. A. Schwartz, “Integrins in mechanotransduction,” *J Biol Chem*, vol. 279, no. 13, pp. 12001–12004, 2004.

[145] C. Grashoff *et al.*, “Measuring mechanical tension across vinculin reveals regulation of focal adhesion dynamics,” *Nature*, vol. 466, no. 7303, pp. 263–266, 2010.

[146] A. Carisey *et al.*, “Vinculin regulates the recruitment and release of core focal adhesion proteins in a force-dependent manner,” *Curr. Biol.*, vol. 23, no. 4, pp. 271–281, 2013.

[147] J. D. Humphries, P. Wang, C. Streuli, B. Geiger, M. J. Humphries, and C. Ballestrem, “Vinculin controls focal adhesion formation by direct interactions with talin and actin,” *J Cell Biol*, vol. 179, no. 5, pp. 1043–1057, 2007.

[148] G. Kaushik *et al.*, “Vinculin network-mediated cytoskeletal remodeling regulates contractile function in the aging heart.,” *Sci. Transl. Med.*, vol. 7, no. 292, p. 292ra99, 2015.

[149] E. J. Arnsdorf, P. Tummala, and C. R. Jacobs, “Non-canonical Wnt signaling and N-cadherin related beta-catenin signaling play a role in mechanically induced osteogenic cell fate,” *PLoS One*, vol. 4, no. 4, p. e5388, 2009.

[150] B. Cha *et al.*, “Mechanotransduction activates canonical Wnt/β-catenin signaling to promote lymphatic vascular patterning and the development of lymphatic and lymphovenous valves.,” *Genes Dev*, 2016.

[151] M. Yao *et al.*, “Force-dependent conformational switch of alpha-catenin controls vinculin binding,” *Nat. Commun.*, vol. 5, p. 4525, 2014.

[152] S. Huveneers *et al.*, “Vinculin associates with endothelial VE-cadherin junctions to control force-dependent remodeling,” *J Cell Biol*, vol. 196, no. 5, pp. 641–652, 2012.

[153] S. Yonemura, Y. Wada, T. Watanabe, A. Nagafuchi, and M. Shibata, “alpha-Catenin as a tension transducer that induces adherens junction development,” *Nat. Cell Biol.*, vol. 12, no. 6, pp. 533–542, 2010.

[154] Q. le Duc *et al.*, “Vinculin potentiates E-cadherin mechanosensing and is recruited to actin-anchored sites within adherens junctions in a myosin II-dependent manner,” *J Cell Biol*, vol. 189, no. 7, pp. 1107–1115, 2010.

[155] M. Yanagisawa and P. Z. Anastasiadis, “p120 catenin is essential for mesenchymal cadherin-

mediated regulation of cell motility and invasiveness," *J Cell Biol*, vol. 174, no. 7, pp. 1087–1096, 2006.

[156] A. Kourtidis, S. P. Ngok, and P. Z. Anastasiadis, "P120 catenin: An essential regulator of cadherin stability, adhesion-induced signaling, and cancer progression," *Prog. Mol. Biol. Transl. Sci.*, vol. 116, pp. 409–432, 2013.

[157] Y. Kudo-Sakamoto *et al.*, "Calpain-dependent Cleavage of N-cadherin Is Involved in the Progression of Post-myocardial Infarction Remodeling," *J Biol Chem*, vol. 289, no. 28, pp. 19408–19419, 2014.

[158] A. Vreeker, L. van Stuijvenberg, T. J. Hund, P. J. Mohler, P. G. J. Nikkels, and T. A. B. van Veen, "Assembly of the Cardiac Intercalated Disk during Pre- and Postnatal Development of the Human Heart," *PLoS One*, vol. 9, no. 4, 2014.

[159] A. Chopra, E. Tabdanov, H. Patel, P. A. Janmey, and J. Y. Kresh, "Cardiac myocyte remodeling mediated by N-cadherin-dependent mechanosensing," *Am J Physiol Hear. Circ Physiol*, vol. 300, no. 4, pp. H1252-66, 2011.

[160] J. H. King, C. L. Huang, and J. A. Fraser, "Determinants of myocardial conduction velocity: implications for arrhythmogenesis," *Front Physiol*, vol. 4, p. 154, 2013.

[161] M. Okazaki *et al.*, "Molecular cloning and characterization of OB-cadherin, a new member of cadherin family expressed in osteoblasts," *J Biol Chem*, vol. 269, no. 16, pp. 12092–12098, 1994.

[162] Z. M. Deng, G. F. Niu, L. Cai, R. X. Wei, and X. L. Zhao, "The Prognostic Significance of CD44V6, CDH11, and beta-Catenin Expression in Patients with Osteosarcoma," *Biomed Res. Int.*, 2013.

[163] S. Assefnia *et al.*, "Cadherin-11 in poor prognosis malignancies and rheumatoid arthritis: common target, common therapies," *Oncotarget*, vol. 5, no. 6, pp. 1458–1474, 2014.

[164] M. H. Wu *et al.*, "Identification of Cadherin 11 as a Mediator of Dermal Fibrosis and Possible Role in Systemic Sclerosis," *Arthritis Rheumatol.*, vol. 66, no. 4, pp. 1010–1021, 2014.

[165] P. Pittet, K. Lee, A. J. Kulik, J. J. Meister, and B. Hinz, "Fibrogenic fibroblasts increase intercellular adhesion strength by reinforcing individual OB-cadherin bonds," *J Cell Sci*, vol. 121, no. Pt 6, pp. 877–886, 2008.

[166] R. P. Langhe *et al.*, "Cadherin-11 localizes to focal adhesions and promotes cell-substrate adhesion," *Nat. Commun.*, vol. 7, p. 10909, 2016.

[167] H. Wang, L. A. Leinwand, and K. S. Anseth, "Roles of transforming growth factor-beta1 and OB-cadherin in porcine cardiac valve myofibroblast differentiation," *FASEB J*, 2014.

[168] J. J. Zhou *et al.*, "Cadherin-11 Expression Patterns in Heart Valves Associate with Key Functions during Embryonic Cushion Formation, Valve Maturation and Calcification," *Cells Tissues Organs*, vol. 198, no. 4, pp. 300–310, 2013.

[169] S. Alimperti, H. You, T. George, S. K. Agarwal, and S. T. Andreadis, "Cadherin-11 regulates both mesenchymal stem cell differentiation into smooth muscle cells and the development of contractile function in vivo," *J Cell Sci*, vol. 127, no. Pt 12, pp. 2627–2638, 2014.

[170] M. Dobaczewski *et al.*, "Smad3 signaling critically regulates fibroblast phenotype and function in healing myocardial infarction," *Circ Res*, vol. 107, no. 3, pp. 418–428, 2010.

[171] N. H. Kim, S. H. Choi, T. R. Lee, C. H. Lee, and A. Y. Lee, "Cadherin 11, a miR-675 target, induces N-cadherin expression and epithelial-mesenchymal transition in melasma," *J Invest Dermatol*, vol. 134, no. 12, pp. 2967–2976, 2014.

[172] J. J. Tomasek, G. Gabbiani, B. Hinz, C. Chaponnier, and R. a Brown, "Myofibroblasts and mechano-regulation of connective tissue remodelling.," *Nat. Rev. Mol. Cell Biol.*, vol. 3, no. 5, pp. 349–63, 2002.

[173] J. Wang, H. Chen, a Seth, and C. a McCulloch, "Mechanical force regulation of myofibroblast differentiation in cardiac fibroblasts.," *Am. J. Physiol. Heart Circ. Physiol.*, vol. 285, no. 5, pp. H1871–H1881, 2003.

[174] M. R. Junttila, S. P. Li, and J. Westermarck, “Phosphatase-mediated crosstalk between MAPK signaling pathways in the regulation of cell survival,” *FASEB J*, vol. 22, no. 4, pp. 954–965, 2008.

[175] G. E. Plopper, H. P. McNamee, L. E. Dike, K. Bojanowski, and D. E. Ingber, “Convergence of integrin and growth factor receptor signaling pathways within the focal adhesion complex,” *Mol Biol Cell*, vol. 6, no. 10, pp. 1349–1365, 1995.

[176] S. K. Mitra and D. D. Schlaepfer, “Integrin-regulated FAK-Src signaling in normal and cancer cells,” *Curr Opin Cell Biol*, vol. 18, no. 5, pp. 516–523, 2006.

[177] A. J. Galliher and W. P. Schiemann, “Src phosphorylates Tyr284 in TGF-beta type II receptor and regulates TGF-beta stimulation of p38 MAPK during breast cancer cell proliferation and invasion,” *Cancer Res*, vol. 67, no. 8, pp. 3752–3758, 2007.

[178] A. J. Galliher and W. P. Schiemann, “Beta3 integrin and Src facilitate transforming growth factor-beta mediated induction of epithelial-mesenchymal transition in mammary epithelial cells,” *Breast Cancer Res*, vol. 8, no. 4, p. R42, 2006.

[179] J. C. Friedland, M. H. Lee, and D. Boettiger, “Mechanically activated integrin switch controls alpha5beta1 function,” *Science (80-.).*, vol. 323, no. 5914, pp. 642–644, 2009.

[180] J. W. Thomas *et al.*, “CELL BIOLOGY AND METABOLISM : SH2- and SH3-mediated Interactions between Focal Adhesion Kinase and Src SH2- and SH3-mediated Interactions between Focal Adhesion Kinase and Src *,” vol. 273, no. 1, pp. 577–583, 1998.

[181] S. Rohr, “Cardiac fibroblasts in cell culture systems: myofibroblasts all along?,” *J Cardiovasc Pharmacol*, vol. 57, no. 4, pp. 389–399, 2011.

[182] M. Bujak and N. G. Frangogiannis, “The role of TGF-beta signaling in myocardial infarction and cardiac remodeling,” *Cardiovasc Res*, vol. 74, no. 2, pp. 184–195, 2007.

[183] H. Hanafusa *et al.*, “Involvement of the p38 mitogen-activated protein kinase pathway in transforming growth factor-beta-induced gene expression,” *J Biol Chem*, vol. 274, no. 38, pp. 27161–27167, 1999.

[184] P. Maher, “p38 mitogen-activated protein kinase activation is required for fibroblast growth factor-2-stimulated cell proliferation but not differentiation,” *J Biol Chem*, vol. 274, no. 25, pp. 17491–17498, 1999.

[185] J. Ivaska, H. Reunanen, J. Westermarck, L. Koivisto, V. M. Kahari, and J. Heino, “Integrin alpha2beta1 mediates isoform-specific activation of p38 and upregulation of collagen gene transcription by a mechanism involving the alpha2 cytoplasmic tail,” *J Cell Biol*, vol. 147, no. 2, pp. 401–416, 1999.

[186] T. Eubanks, J. Greenberg, P. Dobrin, F. Harford, and R. Gamelli, “The effects of different corticosteroids on the healing colon anastomosis and cecum in a rat model.,” *Am Surg.*, vol. 63, no. 3, pp. 266–269, 1997.

[187] M. C. Cushing, P. D. Mariner, J. T. Liao, E. A. Sims, and K. S. Anseth, “Fibroblast growth factor represses Smad-mediated myofibroblast activation in aortic valvular interstitial cells,” *FASEB J*, vol. 22, no. 6, pp. 1769–1777, 2008.

[188] M. W. Chan, P. D. Arora, P. Bozavikov, and C. A. McCulloch, “FAK, PIP5KIgamma and gelsolin cooperatively mediate force-induced expression of alpha-smooth muscle actin,” *J Cell Sci*, vol. 122, no. Pt 15, pp. 2769–2781, 2009.

[189] D. Faust *et al.*, “Differential p38-dependent signalling in response to cellular stress and mitogenic stimulation in fibroblasts,” *Cell Commun Signal*, vol. 10, p. 6, 2012.

[190] S. S. Bajikar and K. A. Janes, “Multiscale models of cell signaling,” *Ann Biomed Eng*, vol. 40, no. 11, pp. 2319–2327, 2012.

[191] K. L. Yee, V. M. Weaver, and D. A. Hammer, “Integrin-mediated signalling through the MAP-kinase pathway,” *Iet Syst. Biol.*, vol. 2, no. 1, pp. 8–15, 2008.

[192] G. Caron-Lormier and H. Berry, “Amplification and oscillations in the FAK/Src kinase system

during integrin signaling," *J Theor Biol*, vol. 232, no. 2, pp. 235–248, 2005.

[193] J. M. Vilar, R. Jansen, and C. Sander, "Signal processing in the TGF-beta superfamily ligand-receptor network," *PLoS Comput Biol*, vol. 2, no. 1, p. e3, 2006.

[194] K. a Janes, J. G. Albeck, S. Gaudet, P. K. Sorger, D. a Lauffenburger, and M. B. Yaffe, "A systems model of signaling identifies a molecular basis set for cytokine-induced apoptosis.," *Science*, vol. 310, no. 5754, pp. 1646–1653, 2005.

[195] K. A. Janes, H. C. Reinhardt, and M. B. Yaffe, "Cytokine-induced signaling networks prioritize dynamic range over signal strength," *Cell*, vol. 135, no. 2, pp. 343–354, 2008.

[196] D. Ilic *et al.*, "Reduced cell motility and enhanced focal adhesion contact formation in cells from FAK-deficient mice," *Nature*, vol. 377, no. 6549, pp. 539–544, 1995.

[197] X. Q. Brown, K. Ookawa, and J. Y. Wong, "Evaluation of polydimethylsiloxane scaffolds with physiologically-relevant elastic moduli: interplay of substrate mechanics and surface chemistry effects on vascular smooth muscle cell response," *Biomaterials*, vol. 26, no. 16, pp. 3123–3129, 2005.

[198] M. K. Sewell-Loftin, C. B. Brown, H. S. Baldwin, and W. D. Merryman, "A novel technique for quantifying mouse heart valve leaflet stiffness with atomic force microscopy," *J Hear. Valve Dis*, vol. 21, no. 4, pp. 513–520, 2012.

[199] X. Shi-wen *et al.*, "Requirement of transforming growth factor beta-activated kinase 1 for transforming growth factor beta-induced alpha-smooth muscle actin expression and extracellular matrix contraction in fibroblasts," *Arthritis Rheum*, vol. 60, no. 1, pp. 234–241, 2009.

[200] Q. Ding, C. L. Gladson, H. Wu, H. Hayasaka, and M. A. Olman, "Focal adhesion kinase (FAK)-related non-kinase inhibits myofibroblast differentiation through differential MAPK activation in a FAK-dependent manner," *J Biol Chem*, vol. 283, no. 40, pp. 26839–26849, 2008.

[201] F. Caraci *et al.*, "TGF-beta 1 targets the GSK-3 beta/beta-catenin pathway via ERK activation in the transition of human lung fibroblasts into myofibroblasts," *Pharmacol. Res.*, vol. 57, no. 4, pp. 274–282, 2008.

[202] X. Gu and K. S. Masters, "Role of the MAPK/ERK pathway in valvular interstitial cell calcification," *Am J Physiol Hear. Circ Physiol*, vol. 296, no. 6, pp. H1748-57, 2009.

[203] S. Liu *et al.*, "FAK is required for TGFbeta-induced JNK phosphorylation in fibroblasts: implications for acquisition of a matrix-remodeling phenotype," *Mol Biol Cell*, vol. 18, no. 6, pp. 2169–2178, 2007.

[204] G. C. Blobe, W. P. Schiemann, and H. F. Lodish, "Role of transforming growth factor beta in human disease," *N Engl J Med*, vol. 342, no. 18. pp. 1350–1358, 2000.

[205] A. K. Farina, Y. S. Bong, C. M. Feltes, and S. W. Byers, "Post-transcriptional regulation of cadherin-11 expression by GSK-3 and beta-catenin in prostate and breast cancer cells," *PLoS One*, vol. 4, no. 3, p. e4797, 2009.

[206] H. Lal *et al.*, "Cardiac fibroblast glycogen synthase kinase-3beta regulates ventricular remodeling and dysfunction in ischemic heart," *Circulation*, vol. 130, no. 5, pp. 419–430, 2014.

[207] E. H. Noss, S. K. Chang, G. F. Watts, and M. B. Brenner, "Modulation of matrix metalloproteinase production by rheumatoid arthritis synovial fibroblasts after cadherin 11 engagement," *Arthritis Rheum*, vol. 63, no. 12, pp. 3768–3778, 2011.

[208] A. K. Schroer, C. Clark, Q. Zhang, H. Lal, T. Force, and W. D. Merryman, "Cadherin-11 exacerbates inflammation and maladaptive remodeling after myocardial infarction," *Circ. Res.*, vol. (in prepar, 2016.

[209] N. G. Frangogiannis, "Regulation of the inflammatory response in cardiac repair," *Circ Res*, vol. 110, no. 1, pp. 159–173, 2012.

[210] X. Ding, Y. Huang, S. Liu, H. Lv, J. Lin, and T. Sun, "[Expression of cadherin-11 in rheumatoid arthritis synovium and its correlation with inflammation]," *Xi Bao Yu Fen Zi Mian Yi Xue Za Zhi*, vol.

30, no. 12, pp. 1295–1299, 2014.

[211] H. B. Golden *et al.*, “Isolation of cardiac myocytes and fibroblasts from neonatal rat pups,” *Methods Mol Biol*, vol. 843, pp. 205–214, 2012.

[212] X. Zhang, R. Goncalves, and D. M. Mosser, “The isolation and characterization of murine macrophages,” *Curr Protoc Immunol*, vol. Chapter 14, p. Unit 14 1, 2008.

[213] F. Ma *et al.*, “Macrophage-stimulated cardiac fibroblast production of IL-6 is essential for TGF beta/Smad activation and cardiac fibrosis induced by angiotensin II,” *PLoS One*, vol. 7, no. 5, p. e35144, 2012.

[214] W. J. Richardson and J. W. Holmes, “Why Is Infarct Expansion Such an Elusive Therapeutic Target?,” *Journal of Cardiovascular Translational Research*, vol. 8, no. 7. pp. 421–430, 2015.

[215] J. Muller *et al.*, “Interleukin-6-dependent phenotypic modulation of cardiac fibroblasts after acute myocardial infarction,” *Basic Res Cardiol*, vol. 109, no. 6, p. 440, 2014.

[216] M. Huang, D. Yang, M. Xiang, and J. Wang, “Role of interleukin-6 in regulation of immune responses to remodeling after myocardial infarction,” *Hear. Fail Rev*, vol. 20, no. 1, pp. 25–38, 2015.

[217] M. Fuchs *et al.*, “Role of interleukin-6 for LV remodeling and survival after experimental myocardial infarction,” *FASEB J*, vol. 17, no. 14, pp. 2118–2120, 2003.

[218] C. Zhang, Y. Li, Y. Wu, L. Wang, X. Wang, and J. Du, “Interleukin-6/signal transducer and activator of transcription 3 (STAT3) pathway is essential for macrophage infiltration and myoblast proliferation during muscle regeneration,” *J Biol Chem*, vol. 288, no. 3, pp. 1489–1499, 2013.

[219] M. R. Fernando, J. L. Reyes, J. Iannuzzi, G. Leung, and D. M. McKay, “The pro-inflammatory cytokine, interleukin-6, enhances the polarization of alternatively activated macrophages,” *PLoS One*, vol. 9, no. 4, p. e94188, 2014.

[220] G. C. Melendez, J. L. McLarty, S. P. Levick, Y. Du, J. S. Janicki, and G. L. Brower, “Interleukin 6 mediates myocardial fibrosis, concentric hypertrophy, and diastolic dysfunction in rats,” *Hypertension*, vol. 56, no. 2, pp. 225–231, 2010.

[221] T. Zhao, W. Zhao, Y. Chen, R. A. Ahokas, and Y. Sun, “Vascular endothelial growth factor (VEGF)-A: role on cardiac angiogenesis following myocardial infarction,” *Microvasc Res*, vol. 80, no. 2, pp. 188–194, 2010.

[222] D. Y. Nah and M. Y. Rhee, “The inflammatory response and cardiac repair after myocardial infarction,” *Korean Circ J*, vol. 39, no. 10, pp. 393–398, 2009.

[223] M. Nahrendorf and F. K. Swirski, “Abandoning M1/M2 for a Network Model of Macrophage Function,” *Circ Res*, vol. 119, no. 3, pp. 414–417, 2016.

[224] M. L. Lindsey, J. J. Saucerman, and K. Y. DeLeon-Pennell, “Knowledge gaps to understanding cardiac macrophage polarization following myocardial infarction,” *Biochim Biophys Acta*, 2016.

[225] V. Briken and D. M. Mosser, “Editorial: switching on arginase in M2 macrophages,” *J Leukoc Biol*, vol. 90, no. 5, pp. 839–841, 2011.

[226] Z. Yang and X. F. Ming, “Functions of arginase isoforms in macrophage inflammatory responses: impact on cardiovascular diseases and metabolic disorders,” *Front Immunol*, vol. 5, p. 533, 2014.

[227] A. Manalo *et al.*, “The loss of protein CENP-F disrupts cardiomyocyte architecture and function,” *Circ. Res.*, 2016.

[228] A. K. Schroer, M. Shotwell, V. Y. Sidorov, J. P. Wikswo, and W. D. Merryman, “I-Wire Heart-on-a-Chip II: Biomechanical analysis of contractile, three-dimensional cardiomyocyte tissue constructs,” *Acta Biomater.*, vol. (under rev, 2016.

[229] S. Nag *et al.*, “Contractility parameters of human beta-cardiac myosin with the hypertrophic cardiomyopathy mutation R403Q show loss of motor function,” *Sci Adv*, vol. 1, no. 9, p. e1500511, 2015.

[230] J. A. Spudich *et al.*, “Effects of hypertrophic and dilated cardiomyopathy mutations on power output by human beta-cardiac myosin,” *J. Exp. Biol.*, vol. 219, no. Pt 2, pp. 161–167, 2016.

[231] J. A. Spudich, “Hypertrophic and dilated cardiomyopathy: four decades of basic research on muscle lead to potential therapeutic approaches to these devastating genetic diseases,” *Biophys J*, vol. 106, no. 6, pp. 1236–1249, 2014.

[232] M. C. Ferreira-Cornwell, Y. Luo, N. Narula, J. M. Lenox, M. Lieberman, and G. L. Radice, “Remodeling the intercalated disc leads to cardiomyopathy in mice misexpressing cadherins in the heart,” *J Cell Sci*, vol. 115, no. Pt 8, pp. 1623–1634, 2002.

[233] A. Traister *et al.*, “Integrin-linked kinase mediates force transduction in cardiomyocytes by modulating SERCA2a/PLN function,” *Nat. Commun.*, vol. 5, p. 4533, 2014.

[234] E. Dees *et al.*, “Cardiac-specific deletion of the microtubule-binding protein CENP-F causes dilated cardiomyopathy,” *Dis Model Mech*, vol. 5, no. 4, pp. 468–480, 2012.

[235] M. L. McCain, S. P. Sheehy, A. Grosberg, J. A. Goss, and K. K. Parker, “Recapitulating maladaptive, multiscale remodeling of failing myocardium on a chip,” *Proc Natl Acad Sci U S A*, vol. 110, no. 24, pp. 9770–9775, 2013.

[236] J. Shim, A. Grosberg, J. C. Nawroth, K. K. Parker, and K. Bertoldi, “Modeling of cardiac muscle thin films: pre-stretch, passive and active behavior,” *J Biomech*, vol. 45, no. 5, pp. 832–841, 2012.

[237] V. Y. Sidorov, P. C. Samson, T. N. Sidorova, J. M. Davidson, C. C. Lim, and J. P. Wikswo, “I-Wire cardiac tissue construct for cardiac physiology and pharmacology,” 2016.

[238] A. V Hill and R. S. Sec, “The heat of shortening and the dynamic constants of muscle,” *Sect. Biophys. Dep. Physiol. Univ. Coll. London*, pp. 612–745, 1938.

[239] K. B. Campbell, M. Chandra, R. D. Kirkpatrick, B. K. Slinker, and W. C. Hunter, “Interpreting cardiac muscle force-length dynamics using a novel functional model,” *Am J Physiol Hear. Circ Physiol*, vol. 286, no. 4, pp. H1535-45, 2004.

[240] H. A. Shiels and E. White, “The Frank-Starling mechanism in vertebrate cardiac myocytes,” *J. Exp. Biol.*, vol. 211, no. 13, pp. 2005–2013, 2008.

[241] A. V Hill, “Mechanics of the contractile element of muscle,” *Nature*, vol. 166, no. 4219, pp. 415–419, 1950.

[242] A. V Hill, “First and Last Experiments in Muscle Mechanics,” Cambridge University Press, 1970.

[243] T. A. McMahon, *Muscles, reflexes and locomotion*. Princeton University Press, 1984.

[244] R. Shadmehr and S. P. Wise, “A simple muscle model,” in *Computational Neurobiology of Reaching and Pointing*, Cambridge: MIT Press, 2005.

[245] D. Chapelle, F. Clement, F. Genot, P. Le Tallec, M. Sorin, and J. Urquiza, “A Physiologically-Based Model for the Active Cardiac Muscle Contraction,” in *Functional Imaging and Modeling of the Heart*, vol. 2230, 2001, pp. 128–133.

[246] M. Sermesant *et al.*, “Cardiac function estimation from MRI using a heart model and data assimilation: Advances and difficulties,” *Funct. Imaging Model. Hear. Proc.*, vol. 3504, pp. 325–337, 2005.

[247] J. M. Winters and S. .-Y. Woo, “Hill-based muscle models: A systems engineering perspective,” in *Multiple Muscle Systems: Biomechanics and Movement Organization*, Springer-Verlag, 1990, pp. 69–93.

[248] K. D. Costa, J. W. Holmes, and A. D. McCulloch, “Modelling cardiac mechanical properties in three dimensions,” *Philos. Trans. R. Soc. London Ser. a-Mathematical Phys. Eng. Sci.*, vol. 359, no. 1783, pp. 1233–1250, 2001.

[249] V. Y. Wang, H. I. Lam, D. B. Ennis, B. R. Cowan, A. A. Young, and M. P. Nash, “Modelling passive diastolic mechanics with quantitative MRI of cardiac structure and function,” *Med. Image Anal.*, vol. 13, no. 5, pp. 773–784, 2009.

[250] K. L. Sack, N. H. Davies, J. M. Guccione, and T. Franz, “Personalised computational cardiology: Patient-specific modelling in cardiac mechanics and biomaterial injection therapies for myocardial infarction,” *Hear. Fail Rev*, 2016.

[251] E. J. Farrar and J. T. Butcher, “NFkB activation drives mesenchymal transformation and susceptibility to calcification in aortic valve endothelial cells.,” *FASEB J*, vol. 27, 2013.

[252] V. Y. Sidorov, M. C. Woods, and J. P. Wikswo, “Effects of elevated extracellular potassium on the stimulation mechanism of diastolic cardiac tissue.,” *Biophys. J.*, vol. 84, no. 5, pp. 3470–9, 2003.

[253] A. F. Straight, “Dissecting Temporal and Spatial Control of Cytokinesis with a,” vol. 1743, no. 2003, 2011.

[254] M. Kovacs, J. Toth, C. Hetenyi, A. Malnasi-Csizmadia, and J. R. Sellers, “Mechanism of blebbistatin inhibition of myosin II,” *J Biol Chem*, vol. 279, no. 34, pp. 35557–35563, 2004.

[255] O. E. Brodde and M. C. Michel, “Adrenergic and muscarinic receptors in the human heart,” *Pharmacol Rev*, vol. 51, no. 4, pp. 651–690, 1999.

[256] L. B. Hazeltine *et al.*, “Effects of substrate mechanics on contractility of cardiomyocytes generated from human pluripotent stem cells,” *Int J Cell Biol*, vol. 2012, p. 508294, 2012.

[257] V. V Fedorov and S. L. Leonov, “No Title,” in *Optimal Design for Nonlinear Response Models*, CRC Press, 2013.

[258] I. Suard, N. Pery-Man, C. Coirault, J. C. Pourny, Y. Lecarpentier, and D. Chemla, “Relaxant effects of isoproterenol in isolated cardiac muscle: influence of loading patterns,” *Am J Physiol*, vol. 267, no. 5 Pt 2, pp. H1814-23, 1994.

[259] K. A. Beningo, K. Hamao, M. Dembo, Y. L. Wang, and H. Hosoya, “Traction forces of fibroblasts are regulated by the Rho-dependent kinase but not by the myosin light chain kinase,” *Arch Biochem Biophys*, vol. 456, no. 2, pp. 224–231, 2006.

[260] J. S. Allingham, R. Smith, and I. Rayment, “The structural basis of blebbistatin inhibition and specificity for myosin II,” *Nat Struct Mol Biol*, vol. 12, no. 4, pp. 378–379, 2005.

[261] F. I. Malik *et al.*, “Cardiac myosin activation: a potential therapeutic approach for systolic heart failure,” *Science (80-.).*, vol. 331, no. 6023, pp. 1439–1443, 2011.

[262] E. S. Grood, R. E. Mates, and H. Falsetti, “A Model of cardiac muscle dynamics,” *Circ. Res.*, vol. 35, pp. 184–196, 1974.

[263] L. C. Lee, Z. Zhihong, A. Hinson, and J. M. Guccione, “Reduction in left ventricular wall stress and improvement in function in failing hearts using Algisyl-LVR,” *J Vis Exp*, no. 74, 2013.

[264] J. F. Wenk *et al.*, “A coupled biventricular finite element and lumped-parameter circulatory system model of heart failure,” *Comput Methods Biomech Biomed Engin*, vol. 16, no. 8, pp. 807–818, 2013.

[265] J. F. Wenk *et al.*, “Biventricular finite element modeling of the Acorn CorCap Cardiac Support Device on a failing heart,” *Ann Thorac Surg*, vol. 95, no. 6, pp. 2022–2027, 2013.

[266] J. F. Wenk *et al.*, “Regional Left Ventricular Myocardial Contractility and Stress in a Finite Element Model of Posterobasal Myocardial Infarction,” *J. Biomech. Eng. Asme*, vol. 133, no. 4, 2011.

[267] T. Fujiwara *et al.*, “Nicorandil suppresses the increases in plasma level of matrix metalloproteinase activity and attenuates left ventricular remodeling in patients with acute myocardial infarction,” *Hear. Vessel.*, vol. 22, no. 5, pp. 303–309, 2007.

[268] M. A. Laflamme and C. E. Murry, “Heart regeneration,” *Nature*, vol. 473, no. 7347, pp. 326–335, 2011.

[269] H. Stoyanov, M. Kollosche, S. Risse, R. Wache, and G. Kofod, “Soft conductive elastomer materials for stretchable electronics and voltage controlled artificial muscles,” *Adv. Mater.*, vol. 25, no. 4, pp. 578–583, 2013.

[270] M. Ma, L. Guo, D. G. Anderson, and R. Langer, “Bio-inspired polymer composite actuator and

generator driven by water gradients," *Science (80-.).*, vol. 339, no. 6116, pp. 186–189, 2013.

[271] B. K. Juluri *et al.*, "A mechanical actuator driven electrochemically by artificial molecular muscles," *ACS Nano*, vol. 3, no. 2, pp. 291–300, 2009.

[272] B. W. Benham-Pyle, B. L. Pruitt, and W. J. Nelson, "Cell adhesion. Mechanical strain induces E-cadherin-dependent Yap1 and beta-catenin activation to drive cell cycle entry," *Science (80-.).*, vol. 348, no. 6238, pp. 1024–1027, 2015.

[273] K. L. Yee, V. M. Weaver, and D. A. Hammer, "Integrin-mediated signalling through the MAP-kinase pathway," *Iet Syst. Biol.*, vol. 2, no. 1, pp. 8–15, 2008.

[274] B. S. Hendriks, F. Hua, and J. R. Chabot, "Analysis of mechanistic pathway models in drug discovery: p38 pathway," *Biotechnol. Prog.*, vol. 24, no. 1, pp. 96–109, 2008.

[275] P. M. Gilbert *et al.*, "Substrate elasticity regulates skeletal muscle stem cell self-renewal in culture," *Science (80-.).*, vol. 329, no. 5995, pp. 1078–1081, 2010.

[276] E. G. Arias-Salgado, S. Lizano, S. Sarkar, J. S. Brugge, M. H. Ginsberg, and S. J. Shattil, "Src kinase activation by direct interaction with the integrin beta cytoplasmic domain.," *Proc. Natl. Acad. Sci. U. S. A.*, vol. 100, no. 23, pp. 13298–13302, 2003.

[277] J. G. Wang, M. Miyazu, E. Matsushita, M. Sokabe, and K. Naruse, "Uniaxial cyclic stretch induces focal adhesion kinase (FAK) tyrosine phosphorylation followed by mitogen-activated protein kinase (MAPK) activation," *Biochem Biophys Res Commun*, vol. 288, no. 2, pp. 356–361, 2001.

[278] P. Khanna, E. Weidert, F. Vital-Lopez, A. Armaou, C. D. Maranas, and C. Dong, "Model Simulations Reveal VCAM-1 Augment PAK Activation Rates to Amplify p38 MAPK and VE-Cadherin Phosphorylation," *Cell. Mol. Bioeng.*, vol. 4, no. 4, pp. 656–669, 2011.

[279] H. J. Hsu, C. F. Lee, A. Locke, S. Q. Vanderzyl, and R. Kaunas, "Stretch-induced stress fiber remodeling and the activations of JNK and ERK depend on mechanical strain rate, but not FAK," *PLoS One*, vol. 5, no. 8, p. e12470, 2010.

[280] A. Obergfell *et al.*, "Coordinate interactions of Csk, Src, and Syk kinases with ??IIb??3 initiate integrin signaling to the cytoskeleton," *J. Cell Biol.*, vol. 157, no. 2, pp. 265–275, 2002.

[281] N. A. Bhowmick, R. Zent, M. Ghiassi, M. McDonnell, and H. L. Moses, "Integrin beta 1 signaling is necessary for transforming growth factor-beta activation of p38MAPK and epithelial plasticity," *J Biol Chem*, vol. 276, no. 50, pp. 46707–46713, 2001.

[282] K. B. Kaplan, J. R. Swedlow, D. O. Morgan, and H. E. Varmus, "c-Src enhances the spreading of src-/- fibroblasts on fibronectin by a kinase-independent mechanism," *Genes Dev*, vol. 9, no. 12, pp. 1505–1517, 1995.

[283] R. Roskoski Jr., "Src kinase regulation by phosphorylation and dephosphorylation," *Biochem Biophys Res Commun*, vol. 331, no. 1, pp. 1–14, 2005.

[284] B. Hinz, V. Dugina, C. Ballestrem, B. Wehrle-Haller, and C. Chaponnier, "alpha-smooth muscle actin is crucial for focal adhesion maturation in myofibroblasts," *Mol Biol Cell*, vol. 14, no. 6, pp. 2508–2519, 2003.

[285] D. McGarrigle, D. Shan, S. Yang, and X. Y. Huang, "Role of tyrosine kinase Csk in G protein-coupled receptor- and receptor tyrosine kinase-induced fibroblast cell migration," *J Biol Chem*, vol. 281, no. 15, pp. 10583–10588, 2006.

[286] M. P. Playford and M. D. Schaller, "The interplay between Src and integrins in normal and tumor biology," *Oncogene*, vol. 23, no. 48, pp. 7928–7946, 2004.

[287] K. A. Burnham D., "Model Selection and Multi-Model Inference: A Practical Information-Theoretic Approach." Springer, 2002.

[288] H. Shankaran, Y. Zhang, W. B. Chrisler, J. A. Ewald, H. S. Wiley, and H. Resat, "Integrated experimental and model-based analysis reveals the spatial aspects of EGFR activation dynamics," *Mol Biosyst*, vol. 8, no. 11, pp. 2868–2882, 2012.